

~~TOP SECRET~~ G

BIF-008-W-C-019839-RI-80

This document contains 128 classified sheets including the front and back cover.

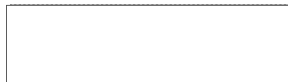


PHOTOGRAPHIC SYSTEM REFERENCE HANDBOOK
FOR
GAMBIT RECONNAISSANCE SYSTEM
WITH
EXTENDED ALTITUDE CAPABILITY
(EAC)

VOLUME 2

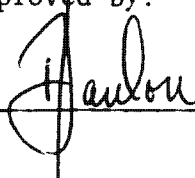
Prepared by
BIF-008

Under Contract



25X1

Approved by:



1 July 1980

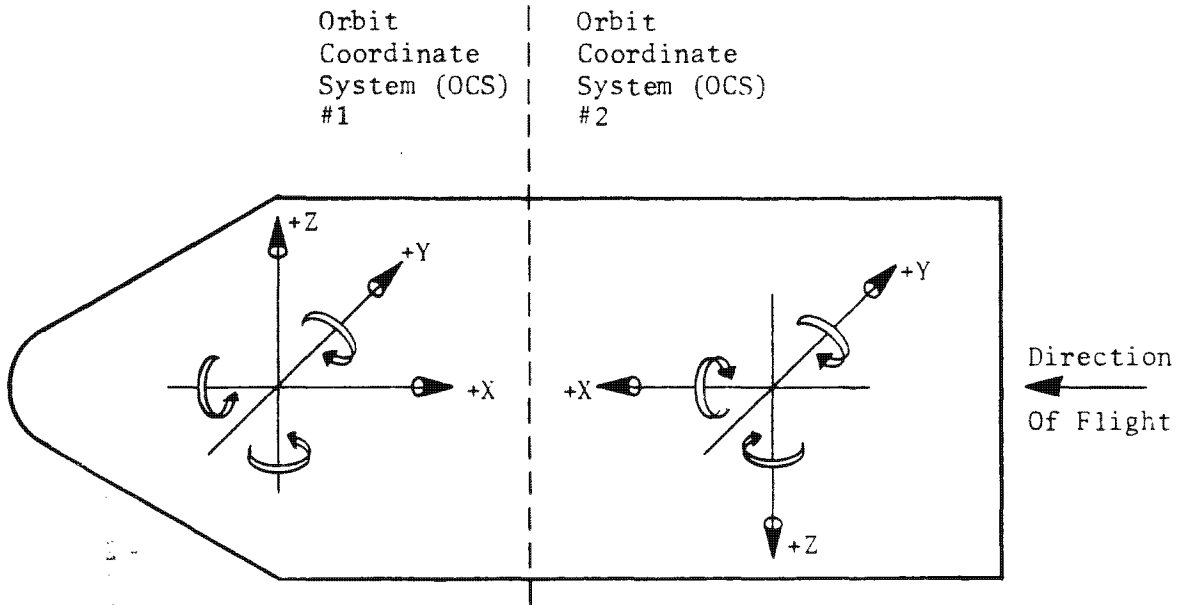
"WARNING - THIS DOCUMENT SHALL NOT BE USED AS A SOURCE FOR DERIVATIVE CLASSIFICATION"

~~TOP SECRET~~ G

Handle via **BYEMAN**
Control System Only

~~TOP SECRET~~ G

BIF-008- W-C-019839-RI-80



BIF-008 Uses OCS #1

OCS #1 Is Used In This Document

Orbit Coordinate Systems Sign Convention

FRONTISPIECE

"WARNING - THIS DOCUMENT SHALL NOT BE USED AS A SOURCE FOR DERIVATIVE CLASSIFICATION"

~~TOP SECRET~~ G

Handle via **BYEMAN**
Control System Only

~~TOP SECRET~~ G

BIF-008- W-C-019839-RI-80

TABLE OF CONTENTS

	<u>Page</u>
VOLUME 2	
PART 2 ANALYSIS	
11.0 SCENE LUMINANCE	2.11-1
11.1 Solar Irradiance at the Target	2.11-3
11.1.1 Sun Angle	2.11-3
11.1.2 Insolation and Atmospheric Transmission	2.11-3
11.2 Target Reflectance	2.11-7
11.3 Atmospheric Transmission	2.11-11
11.4 Haze	2.11-13
11.5 Radiation Effect	2.11-13
11.6 Summary	2.11-13
12.0 OPTICAL ANALYSIS	2.12-1
12.1 Analytic Tools	2.12-1
12.1.1 Spread Functions	2.12-1
12.1.2 Test Objects	2.12-3
12.1.3 Modulation	2.12-6
12.2 Modulation Transfer Function (MTF)	2.12-8
12.2.1 Linear System	2.12-9
12.2.2 Nonlinear System	2.12-11
12.2.3 System MTF	2.12-15
12.3 Threshold Modulation	2.12-16
12.3.1 Measurement	2.12-17
12.3.2 Assumptions	2.12-18

~~TOP SECRET~~ G

~~TOP SECRET~~ G

BIF-008-W-C-019839-RI-80

TABLE OF CONTENTS (Continued)

	<u>Page</u>
VOLUME 2	
12.4 Optical Quality Factor (OQF)	2.12-19
12.4.1 Calculation	2.12-19
12.4.2 Contributors to OQF Reduction	2.12-21
12.5 Lens Performance	2.12-26
12.5.1 Lens MTF and OQF	2.12-26
12.5.2 Resolution Predictions	2.12-28
12.6 Through-Focus Characteristics	2.12-31
12.6.1 Heterochromatic, Off-Axis, Through-Focus Characteristics	2.12-31
12.6.2 Monochromatic, Through-Focus Characteristics	2.12-34
12.7 Thermally Induced Focus Changes	2.12-34
12.7.1 Isothermal Analysis	2.12-34
12.7.2 Transient Thermal Analysis	2.12-36
13.0 VENTING ANALYSIS	2.13-1
13.1 Shipment	2.13-1
13.2 Venting Model	2.13-1
13.3 Ascent Venting	2.13-2
13.4 Conditioned Air Flow	2.13-5
14.0 THERMAL ANALYSIS	2.14-1
14.1 Prelaunch	2.14-1
14.1.1 Cold Environment	2.14-2
14.1.2 Hot Environment	2.14-4
14.2 Ascent	2.14-5
14.2.1 Design Requirements	2.14-5
14.2.2 Design Predictions	2.14-6

~~TOP SECRET~~ G

~~TOP SECRET G~~

BIF-008-W-C-019839-RI-80

TABLE OF CONTENTS (Continued)

	<u>Page</u>
VOLUME 2	
14.3 Orbital	2.14-10
14.3.1 Design Parameters	2.14-10
14.3.2 Design Requirements	2.14-10
14.3.3 Orbital Design	2.14-14
14.4 PPS/DP EAC Overage Analysis	2.14-42
14.5 Thermal Analysis	2.14-44
14.6 Recovery	2.14-46
14.6.1 Nose-Aft Flight	2.14-49
14.6.2 Pitchdown	2.14-49
14.6.3 PPS/DP EAC Recovery	2.14-50
14.7 Additional Considerations	2.14-53
14.7-1 Tumbling	2.14-53
14.7-2 Hotdogging	2.14-56
15.0 EJECTION ANALYSIS	2.15-1
15.1 Main Hatch	2.15-1
15.2 Dual Recovery Module (DRM) Ejectable Components	2.15-1
15.2.1 SRV 1 and SRV 2	2.15-3
15.2.2 Ejectable Adapter (EA)	2.15-3
15.3 Ejection Model	2.15-3
15.3.1 General Free-Body Equations	2.15-4
15.3.2 Spring Ejectors	2.15-5
15.3.3 Mass Properties	2.15-8
15.3.4 Monte Carlo Approach	2.15-9
15.4 Application of the Model	2.15-10
15.4.1 Ejectable Adapter Geometry	2.15-10
15.4.2 SRV 2 Geometry	2.15-14
15.5 Results	2.15-14

25X1

~~TOP SECRET G~~

~~TOP SECRET~~ G

BIF-008- W-C-019839-RI-80

TABLE OF CONTENTS (Continued)

	<u>Page</u>
VOLUME 2	
15.6 Conclusions	2.15-18
15.6.1 SRV 1	2.15-18
15.6.2 Ejectable Adapter	2.15-18
15.6-3 SRV 2	2.15-18
16.0 CONSUMABLES MANAGEMENT	2.16-1
16.1 Photographic Film	2.16-1
16.1.1 Film Usage Control	2.16-1
16.1.2 Film Usage Influences	2.16-2
16.2 Electrical Power	2.16-2
16.2.1 Power Usage Control	2.16-2
16.2.2 Power Usage Influences	2.16-2
16.3 Attitude Control Gas	2.16-3
16.3.1 Control Gas Usage Control	2.16-3
16.3.2 Control Gas Usage Influences	2.16-3
16.4 Orbit Maintenance Fuel	2.16-4
16.4.1 Orbit Maintenance Fuel Usage Control	2.16-4
16.4.2 Orbit Maintenance Fuel Usage Influences	2.16-4
 PART 3 HARDWARE DESCRIPTION	
1.0 PHOTOGRAPHIC PAYLOAD SECTION/DUAL PLATEN EXTENDED ALTITUDE CAPABILITY	3.1-1
1.1 PPS/DP EAC General Description	3.1-1
1.1.1 PPS/DP EAC Assembly Modules	3.1-1
1.1.2 PPS/DP EAC External Finish	3.1-6
1.2 Dual Recovery Module	3.1-6
1.2.1 DRM Access Panels	3.1-11
1.2.2 DRM Structure and Internal Components	3.1.11

v
~~TOP SECRET~~ G

Handle via BYEMAN
Control System Only

~~TOP SECRET~~ G

BIF-008-W-C-019839-RI-80

TABLE OF CONTENTS (Continued)

VOLUME 2		<u>Page</u>
1.3	Supply and Electronics	3.1-26
1.3.1	Supply Electronics Structure	3.1-26
1.3.2	SEM Components	3.1-39
1.3.3	SEM/COM Mating	3.1-44
1.4	Camera Optics Module	3.1-44
1.4.1	Camera Optics Module - External Sources	3.1-46
1.4.2	Camera Optics Assembly (Internal Structure)	3.1-59
1.4.3	PPS/DP EAC - SCS Interface	3.1-73

~~TOP SECRET~~ G

~~TOP SECRET~~ G

BIF-008-W-C-019839-RI-80

This page intentionally blank

vii

~~TOP SECRET~~ G

Handle via BYEMAN
Control System Only

~~TOP SECRET G~~

BIF-008- W-C-019839-RI-80

LIST OF ILLUSTRATIONS

<u>VOLUME 2</u> <u>Figure</u>	<u>Title</u>	<u>Page</u>
2.11-1	Radiance Parameters	2.11-2
2.11-2	Sun Angle Geometry	2.11-4
2.11-3	Sun Angle vs Latitude	2.11-5
2.11-4	Sun Angle vs Latitude	2.11-6
2.11-5	Solar Spectral Irradiance	2.11-8
2.11-6	Relative Irradiance vs Sun Angle	2.11-9
2.11-7	Spectral Reflectance of Ground Scenes	2.11-10
2.11-8	Zenith Angle and Obliquity	2.11-11
2.11-9	Atmospheric Transmission	2.11-12
2.11-10	Haze Radiance	2.11-14
2.11-11	Radiation-Induced Fog	2.11-15
2.12-1	Point-Spread Function	2.12-2
2.12-2	Light Scattering by the Emulsion	2.12-2
2.12-3	Actual and Geometric Image Distributions	2.12-4
2.12-4	Image Distributions of Sinusoidal Object	2.12-5
2.12-5	Low-Frequency Modulation	2.12-7
2.12-6	High-Frequency Modulation	2.12-8
2.12-7	MTF Concept	2.12-8
2.12-8	Transfer Characteristics of a Linear System	2.12-9
2.12-9	Nonlinear Transfer Concept	2.12-11
2.12-10	Transfer Characteristics of a Nonlinear System	2.12-12
2.12-11	Typical Lens MTF	2.12-15
2.12-12	Typical TM Curve	2.12-16
2.12-13	OQF vs RMS Wavefront Error	2.12-20
2.12-14	R-5 Lens MTF	2.12-29
2.12-15	AIM Illustration	2.12-30
2.12-16	Limiting Resolution	2.12-32

~~TOP SECRET G~~

~~TOP SECRET~~ G

BIF-008- W-C-019839-RI-80

LIST OF ILLUSTRATIONS (Continued)

<u>VOLUME 2</u> <u>Figure</u>	<u>Title</u>	<u>Page</u>
2.12-17	Heterochromatic Off-Axis Through-Focus Curve	2.12-35
2.12-18	Monochromatic Through-Focus Curves	2.12-35
2.12-19	Thermal Focus Shift	2.12-37
2.13-1	Venting Model Illustration	2.13-3
2.13-2	Recommended Operating Limits for Clean Room	2.13-7
2.14-1	Time vs Temperature, +Z FSE Panel	2.14-3
2.14-2	Ascent Maximum Longitudinal Skin Temperature Distribution	2.14-7
2.14-3	Ascent Maximum Longitudinal Skin Temperature Distribution EAC Finish Patterns	2.14-8
2.14-4	Ascent Pinpuller Temperatures	2.14-9
2.14-5	Film Temperature vs Time Limits	2.14-12
2.14-6	Fixed Adapter Skin Temperature Minimum Altitude 67 nmi, Beta Angle: 0 Degrees	2.14-16
2.14-7	Fixed Adapter Skin Temperature Minimum Altitude 85 nmi, Beta Angle: 0 Degrees	2.14-17
2.14-8	Fixed Adapter Skin Temperature Minimum Altitude 85 nmi, Beta Angle: 60 Degrees	2.14-18
2.14-9	IBS Blanket Temperature Minimum Altitude 65 nmi	2.14-20
2.14-10	Orbit Average Heat Fluxes, Cylindrical Section	2.14-22
2.14-11	SEM Orbital Average Skin Temperature Distributions	2.14-23
2.14-12	COM Skin Temperature vs Orbit Position Angle ($\beta=0^\circ$, Roll= 0°) for Pattern $-60^\circ \leq \beta \leq 60^\circ$	2.14-26
2.14-13	COM Paint Pattern Temperature Range	2.14-27
2.14-14	COM Environmental Energy Requirements, 60-Degree Pattern	2.14-28
2.14-15	COM Environmental Energy Requirement, 48-Degree Pattern	2.14-29
2.14-16	COM Environmental Energy Requirement, 30-Degree Pattern	2.14-30

~~TOP SECRET~~ G

~~TOP SECRET~~ G

BIF-008-W-C-019839-RI-80

LIST OF ILLUSTRATIONS (Continued)

<u>VOLUME 2</u> <u>Figure</u>	<u>Title</u>	<u>Page</u>
2.14-17	COM Environmental Energy Requirement, Sun-Synchronous Pattern	2.14-31
2.14-18	COM Environmental Energy Requirements (Watt-Hours/Day) EAC Symmetric Pattern	2.14-32
2.14-19	COM Environmental Energy Requirements (Watt-Hours/Day) EAC Asymmetric Pattern (0 to +40, or 0 to -40 Degrees)	2.14-33
2.14-20	Predicted COM Curvature	2.14-36
2.14-21	Predicted COM Curvature	2.14-37
2.14-22	Predicted COM Curvature	2.14-38
2.14-23	Rotation of COA Optical Axis	2.14-39
2.14-24	Operating Constraint EAC Symmetric Finish Pattern	2.14-43
2.14-25	Operating Constraint EAC Asymmetric Finish Pattern	2.14-45
2.14-26	Lens Tube Constraints on Viewport Door Open Time	2.14-47
2.14-27	Ross Corrector Constraints on Viewport Door Open Time	2.14-48
2.14-28	COM Predictions for 68 nmi Recovery	2.14-51
2.14-29	COM Predictions for 65 nmi Recovery	2.14-52
2.14-30	COM Skin Temperatures, Tumbling Rev 3	2.14-54
2.14-31	COM Curvature, Tumbling Rev 3	2.14-55
2.14-32	Pinpuller Temperature, Tumbling Rev	2.14-57
2.14-33	COM Curvature Derivation	2.14-58
2.14-34	COA Suspension System Geometry	2.14-61
2.14-35	COA Suspension System Model	2.14-62
2.14-36	External Structure Centerline Deflection Model	2.14-63
2.14-37	Angular Rotation of COA Axis with Respect to SCS Axis	2.14-70
2.14-38	Operating and Nonoperating Curvature Constraints	2.14-73

x

~~TOP SECRET~~ GHandle via BYEMAN
Control System Only

~~TOP SECRET~~ G

BIF-008- W-C-019839-RI-80

LIST OF ILLUSTRATIONS (Continued)

<u>VOLUME 2</u> <u>Figure</u>	<u>Title</u>	<u>Page</u>
2.15-1	PPS/DP EAC Ejectable Components	2.15-2
2.15-2	Free-Body Reference Plane	2.15-4
2.15-3	Theoretical Force-Displacement Curve	2.15-5
2.15-4	Spring Ejector Assembly	2.15-7
2.15-5	Ejection Force Geometry, Ejectable Adapter	2.15-11
2.15-6	Free-Body Diagram, Ejectable Adapter	2.15-12
2.15-7	Ejectable Adapter Configuration	2.15-13
2.15-8	Ejection Force Geometry, SRV	2.15-15
2.15-9	Free-Body Diagram, SRV	2.15-16
3.1-1	PPS/DP EAC Assembly	3.1-2
3.1-2	PPS/DP EAC Major Components	3.1-3
3.1-3	DRM Internal Components	3.1-7
3.1-4	DRM Film Path Details (Internal SRV)	3.1-9
3.1-5	Dual Recovery Module Access Panels	3.1-13
3.1-6	Ejectable Adapter (-X View)	3.1-16
3.1-7	Ejectable Adapter (-Z View)	3.1-17
3.1-8	Fixed Adapter (-Z View)	3.1-21
3.1-9	Fixed Adapter (+X View, EA Attached)	3.1-23
3.1-10	Supply Electronics Module (+Y Side)	3.1-27
3.1-11	SEM Access Panels	3.1-29
3.1-12	FSE Internal Components	3.1-31
3.1-13	SEM Internal Temperature Monitors (-Y Side)	3.1-35
3.1-14	SEM Internal Temperature Monitors (+Y Side)	3.1-36
3.1-15	SEM Aft Bulkhead	3.1-37
3.1-16	SEM Electronic Unit Locations (-Y Side)	3.1-40
3.1-17	SEM Electronic Unit Locations (+Y Side)	3.1-41

~~TOP SECRET~~ G

~~TOP SECRET~~ G

BIF-008- W-C-019839-RI-80

LIST OF ILLUSTRATIONS (Continued)

<u>VOLUME 2</u> <u>Figure</u>	<u>Title</u>	<u>Page</u>
3.1-18	SEM/COM Interface	3.1-45
3.1-19	COM Access Panels	3.1-48
3.1-20	COM Forward Barrel	3.1-49
3.1-21	COM Forward Barrel Structure	3.1-51
3.1-22	COM Aft Barrel Structure	3.1-57
3.1-23	Camera Optics Assembly	3.1-61
3.1-24	COA Structural Cylinder (-Y Side)	3.1-63
3.1-25	COA (-Y Side) Showing Adjustable A-Frame	3.1-65
3.1-26	Primary Mirror Mount(-X View)	3.1-67
3.1-27	COA Internal Structure	3.1-69
3.1-28	Stereo Mirror Yoke Assembly	3.1-71
3.1-29	COA Double Bulkhead (-X View)	3.1-74
3.1-30	PPS/SCS Alignment Scheme	3.1-76

~~TOP SECRET~~ G

~~TOP SECRET~~ G

BIF-008-W-C-019839-RI-80

LIST OF TABLES

<u>VOLUME 2</u> <u>Table</u>	<u>Title</u>	<u>Page</u>
2.11-1	Cloud Cover Multiplier	2.11-7
2.11-2	Total Integrated Irradiance and Approximate Illumination	2.11-16
2.12-1	Ross Lens Surface Contributions to Wavefront Error	2.12-21
2.12-2	Summary of Tolerances and Distributions	2.12-24
2.12-3	Lens Inhomogeneity OQF Contribution	2.12-25
2.12-4	OQF Summary	2.12-27
2.13-1	Venting Model Parameters	2.13-4
2.13-2	Maximum Differential Pressures	2.13-6
2.14-1	COM Curvature Equations	2.14-41
2.15-1	Center of Gravity Offsets (\bar{Z})	2.15-8
2.15-2	Mass Properties (1/78 Estimate)	2.15-9
2.15-3	Distribution Parameters	2.15-10
2.15-4	Estimated Range of Miss-Distances	2.15-14
2.15-5	Analysis Result for Mass Properties	2.15-17
3.1-1	DRM Access Panels	3.1-15
3.1-2	COM Access Panels	3.1-47

~~TOP SECRET~~ G

~~TOP SECRET~~ GBIF-008- W-C-019839-RI-80

11.0 SCENE LUMINANCE

Apparent scene luminance is a function of the spectral nature of the illumination, target spectral reflectance characteristics, and atmospheric haze and spectral transmittance. Since the PPS/DP EAC optics and film spectral sensitivity extend beyond the visible portion of the electromagnetic spectrum, a discussion of scene "luminance" as it relates to exposure determination must be radiometrically rather than photometrically based. Figure 2.11-1 illustrates the factors involved. Total illumination (photometric) or total irradiance (radiometric) on the entrance pupil of the PPS/DP EAC is concerned with those scene elements radiating directly toward the PPS/DP EAC, and is given by:

$$H_I(\lambda) = H_O(\lambda) R_T(\lambda) T_A(\lambda) + H_Z(\lambda)$$

where: $H_O(\lambda)$ = Solar irradiance at surface of the earth

$R_T(\lambda)$ = Target spectral reflectance

$T_A(\lambda)$ = Atmospheric spectral transmittance

$H_Z(\lambda)$ = Atmospheric haze radiance

$H_I(\lambda)$ = Total irradiance = radiant energy incident on the entrance pupil of the PPS/DP EAC

The integrated irradiance H_I is the integral of $H_I(\lambda)$ taken over the spectral bandpass of the system:

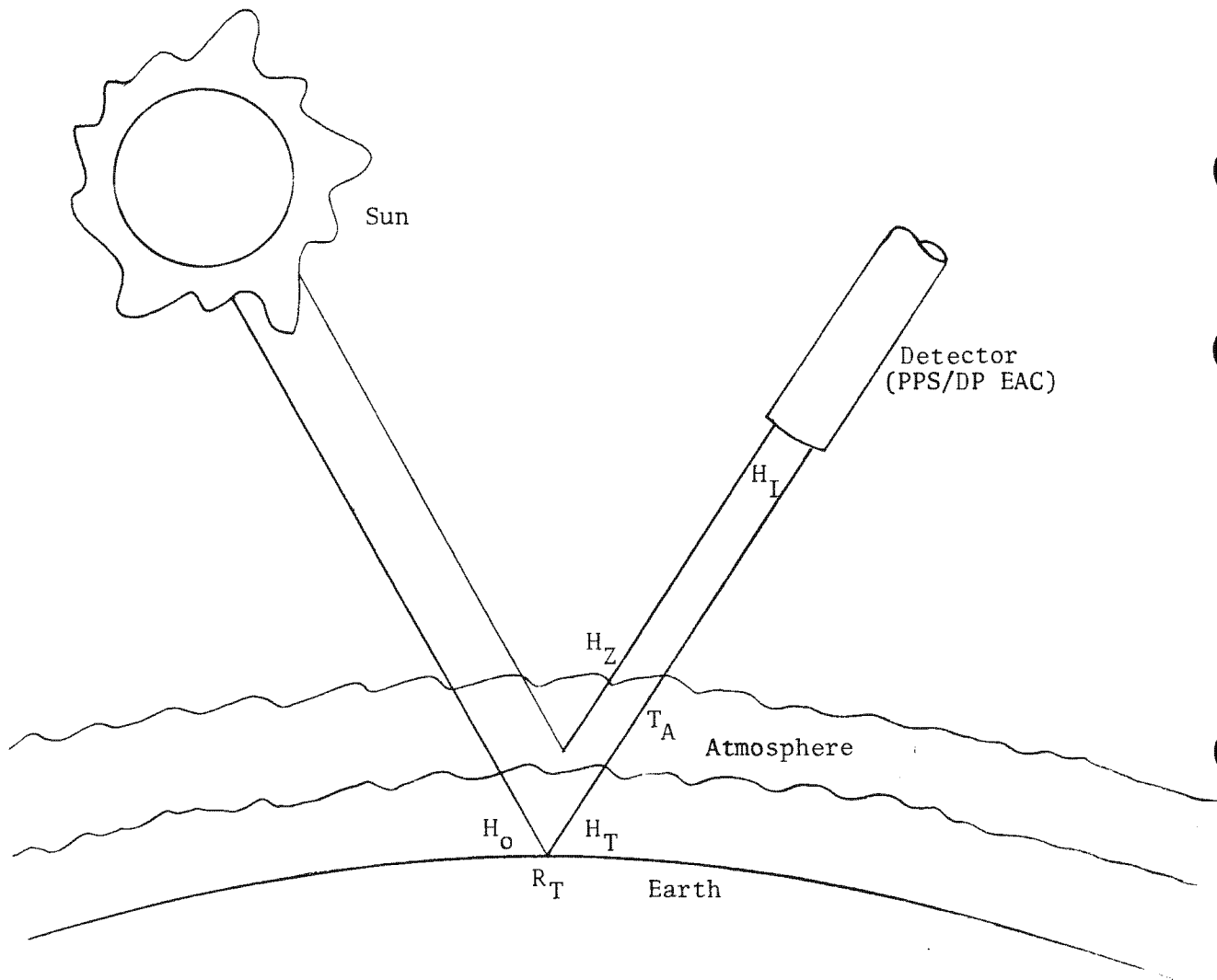
$$H_I = \int_{\lambda_1}^{\lambda_2} H_I(\lambda) d\lambda = \int_{\lambda_1}^{\lambda_2} [H_O(\lambda) R_T(\lambda) T_A(\lambda) + H_Z(\lambda)] d\lambda$$

2.11-1

~~TOP SECRET~~ GHandle via BYEMAN
Control System Only

~~TOP SECRET~~ G

BIF-008- W-C-019839-RI-80



- H_O = Solar Irradiance On The Surface Of The Earth
- $H_O R_T = H_T$ = Target Radiance = Radiance Reflected From The Surface Of The Earth
- T_A = Atmospheric Transmission
- H_Z = Haze Radiance = Energy Radiated By The Atmosphere
- H_I = Integrated Irradiance

Figure 2.11-1. Radiance Parameters

2.11-2

~~TOP SECRET~~ G

Handle via **BYEMAN**
Control System Only

~~TOP SECRET~~ GBIF-008- W-C-019839-RI-8011.1 Solar Irradiance at The Target

11.1.1 Sun Angle

The principal factor influencing target irradiance is solar altitude or sun angle. Sun angle is defined as the apparent elevation of the sun relative to a plane tangent to the earth at the target. Figure 2.11-2 illustrates the sun angle parameters. The equation for sun angle may be written by applying the law of cosines for spherical triangles to the triangle SPN.

$$\alpha = \sin^{-1} (\cos \phi \cos \Delta T \cos \delta + \sin \phi \sin \delta)$$

where: α = Sun angle
 ϕ = Geocentric latitude of target
 ΔT = Angle between earth-sun line and target meridian plane
 δ = Solar declination

The inclination which will provide a sun-synchronous orbit varies with altitude. Figure 2.11-3 shows typical sun-angle vs latitude curves for Day 1 and Day 120 for a sun-synchronous orbit. Figure 2.11-4 illustrates the result when a Gambit vehicle is placed in a high-altitude orbit having an inclination associated with a low-altitude mission.

11.1.2 Insolation and Atmospheric Transmission

The amount of energy reaching the target plane per unit area is determined by the solar energy per unit area at the earth-sun distance, the sun angle, and the spectral transmittance of the atmosphere along the target-sun line.

2.11-3

~~TOP SECRET~~ GHandle via BYEMAN
Control System Only

~~TOP SECRET~~ G

BIF-008- W-C-019839-RI-80

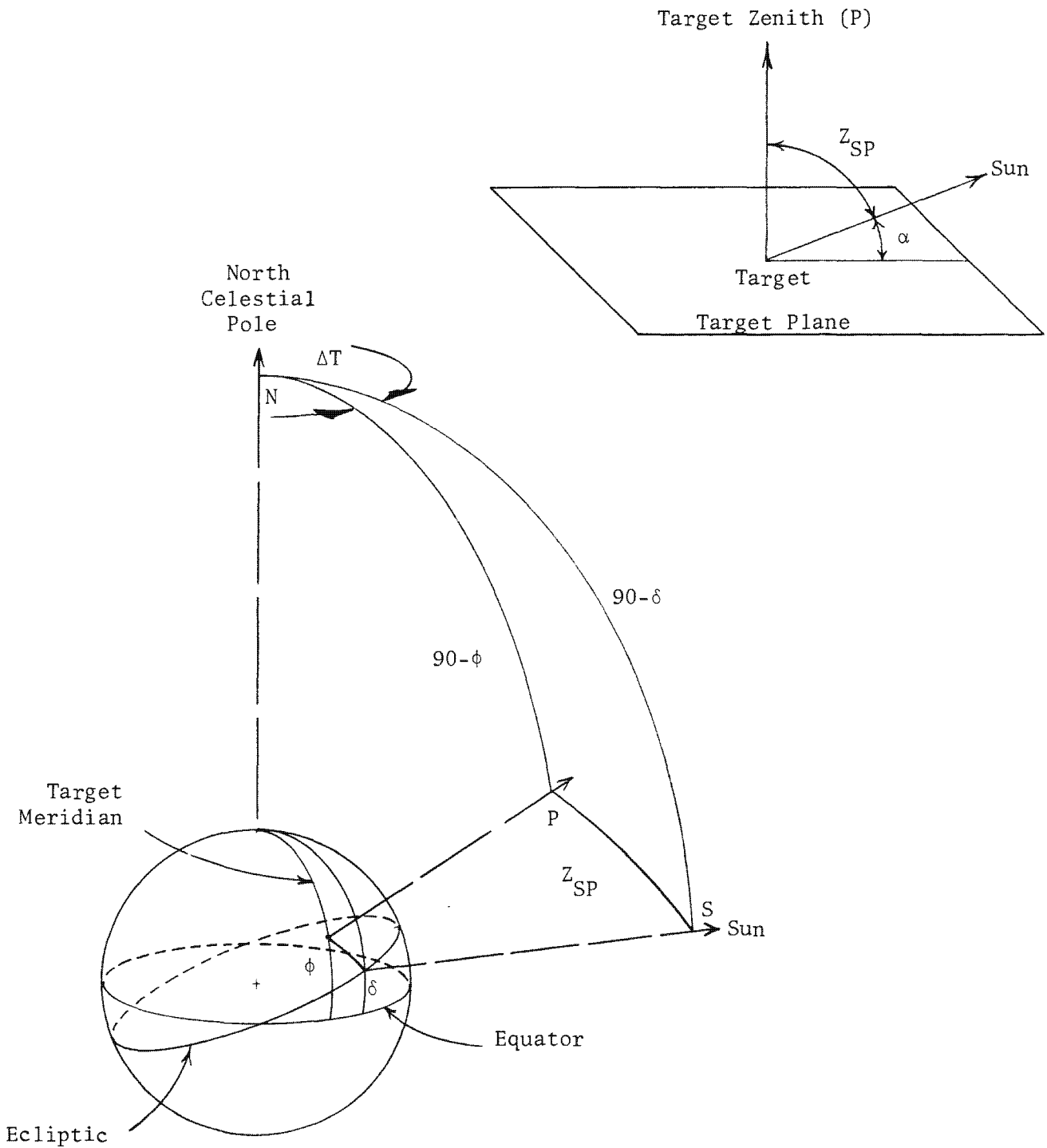


Figure 2.11-2. Sun Angle Geometry

2.11-4

~~TOP SECRET~~ G

Handle via BYEMAN
Control System Only

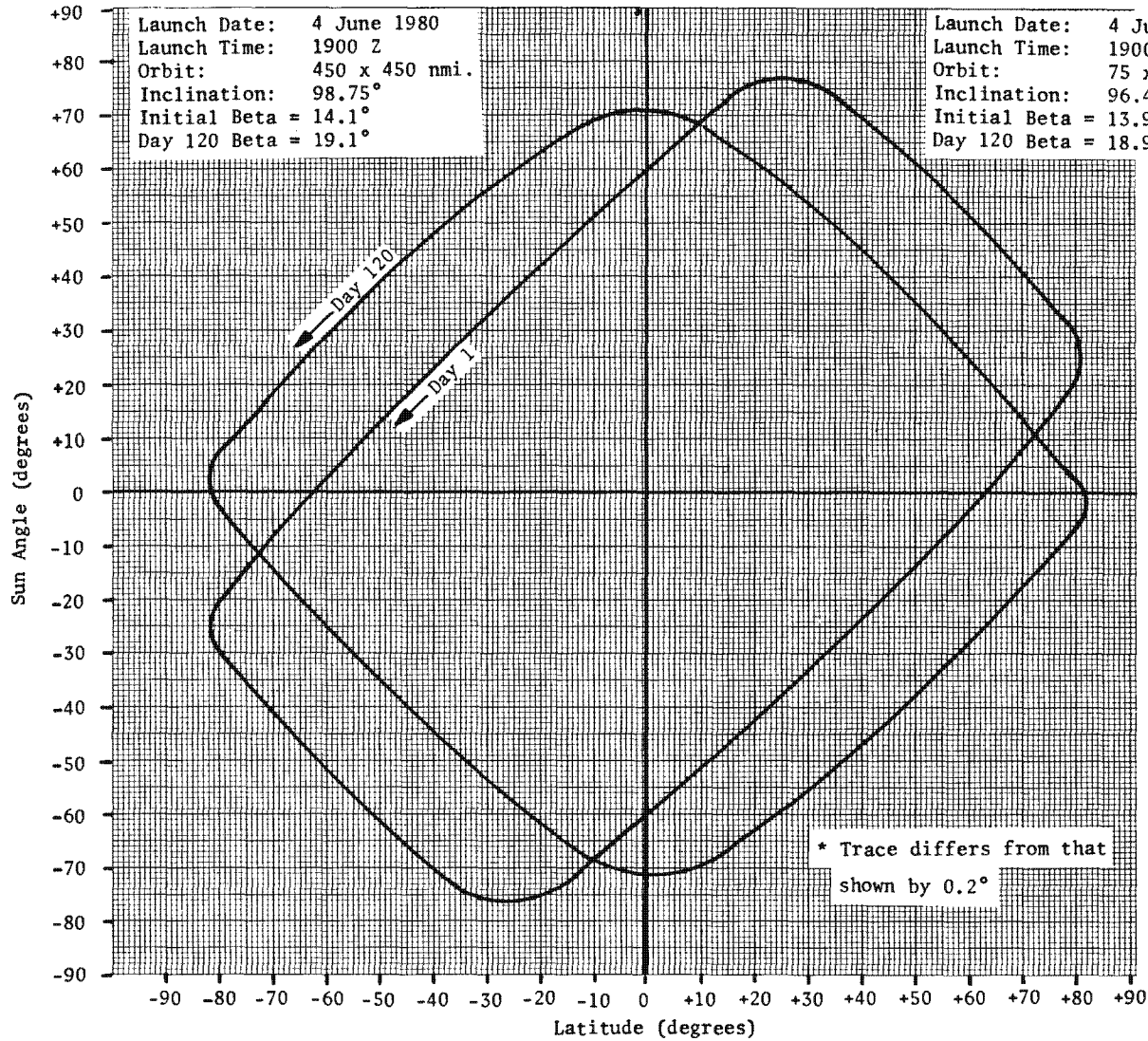


Figure 2.11-3. Sun Angle vs Latitude

Approved for Release: 2017/02/14 C05097220

2.11-5

Approved for Release: 2017/02/14 C05097220

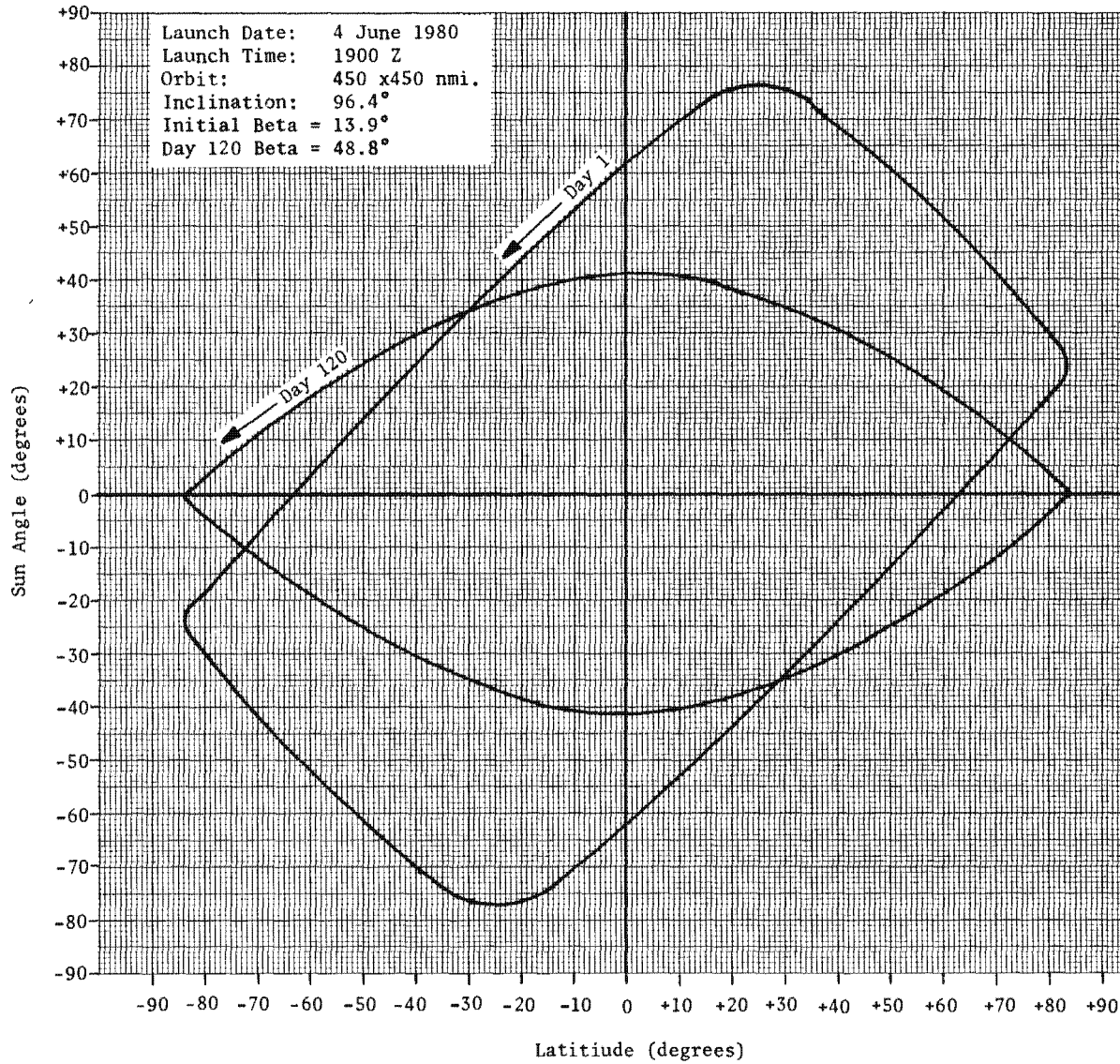


Figure 2.11-4. Sun Angle vs Latitude

2.11-6

~~TOP SECRET~~ GBIF-008-W-C-019839-RI-80

Figure 2.11-5 shows the solar spectral irradiance between 350 and 750 nm outside the atmosphere, at the mean earth-sun distance. The curve applies for a quiet sun and represents a solar constant of 1390 W/m^2 .

Figure 2.11-6 depicts the dependence of target irradiance on sun angle. This curve takes into account the increasing atmospheric path with decreasing sun angle. Cloud cover may be accounted for by multiplication by the appropriate constant, shown in Table 2.11-1.

TABLE 2.11-1
CLOUD COVER MULTIPLIER

<u>Cloud Cover</u>	<u>Multiplier</u>
None	1.000
Light Clouds	0.325
Heavy Storm Clouds	0.018

In the great majority of cases, the presence of cloud cover renders any consideration of high-resolution photography of ground detail academic.

11.2 Target Reflectance

Target reflectance characteristics are determined by the surface texture, composition, and color of the target. Figure 2.11-7 shows the spectral reflectance (R_T) of three representative target types.

2.11-7

~~TOP SECRET~~ GHandle via BYEMAN
Control System Only

~~TOP SECRET~~ G

BIF-008- W-C-019839-RI-80

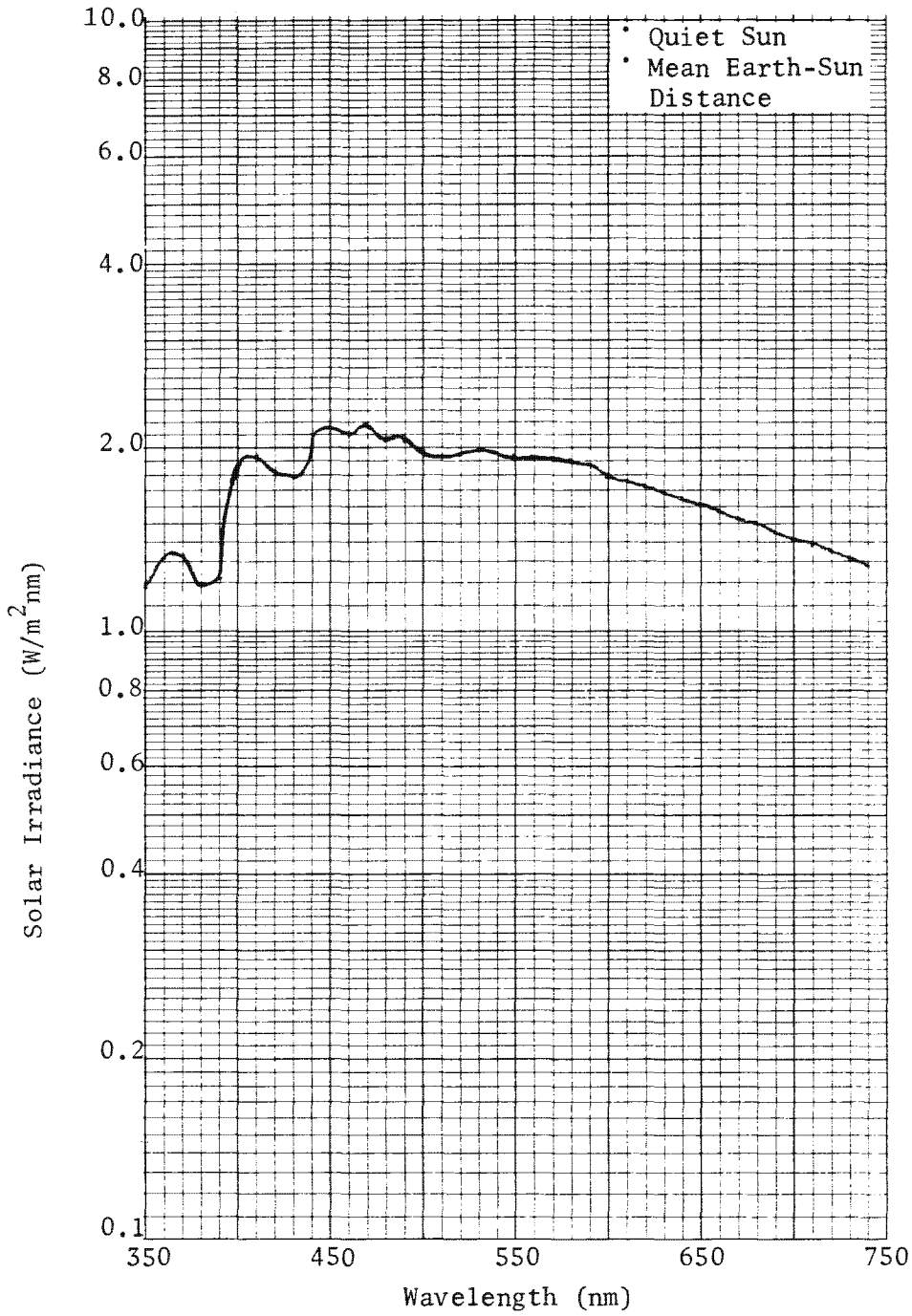


Figure 2.11-5. Solar Spectral Irradiance

2.11-8

~~TOP SECRET~~ G

Handle via BYEMAN
Control System Only

~~TOP SECRET~~ G

BIF-008- W-C-019839-RI-80

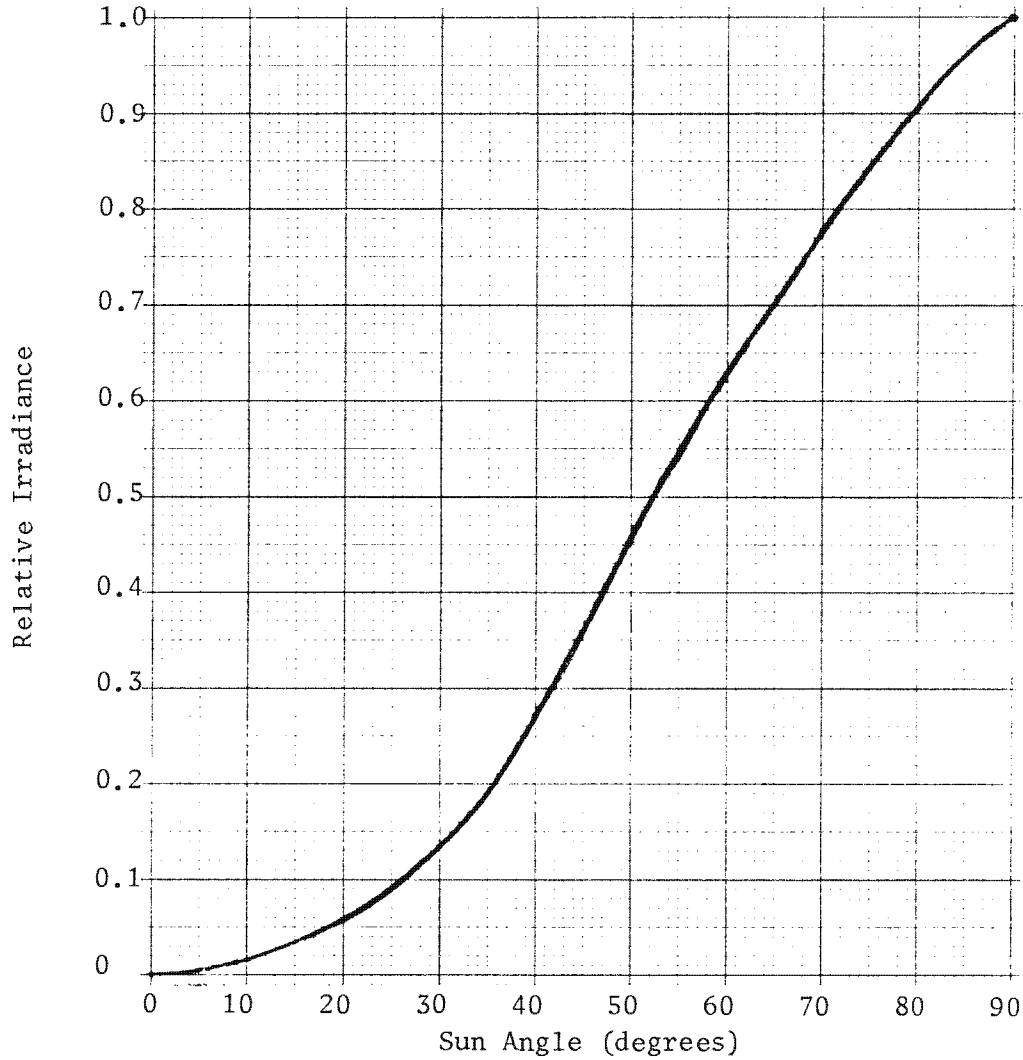


Figure 2.11-6. Relative Irradiance vs Sun Angle

2.11-9

~~TOP SECRET~~ G

Handle via **BYEMAN**
Control System Only

~~TOP SECRET~~ G

BIF-008- W-C-019839-RI-80

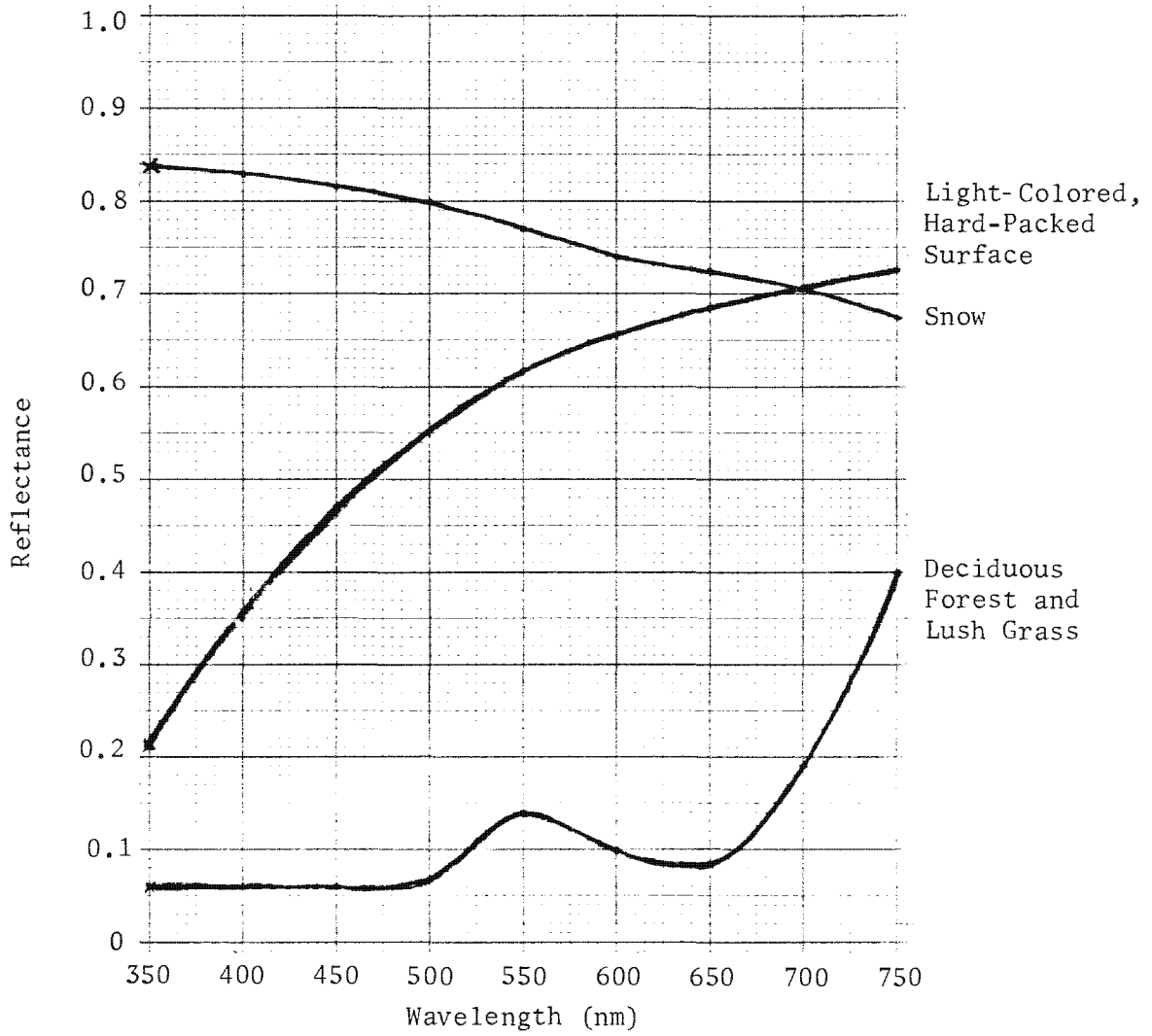


Figure 2.11-7. Spectral Reflectance of Ground Scenes

2.11-10

~~TOP SECRET~~ G

Handle via BYEMAN
Control System Only

~~TOP SECRET~~ GBIF-008- W-C-019839-RI-8011.3 Atmospheric Transmission

Atmospheric transmission (T_A) as discussed in this subsection includes only the optical properties of a clear atmosphere. Haze and clouds are treated elsewhere in this section. For energy from the target which enters the PPS/DP EAC optical system, the zenith angle is numerically equal to the vehicle obliquity angle (see Figure 2.11-8). Figure 2.11-9 shows the atmospheric transmission at zenith angles of 0 and 45 degrees.

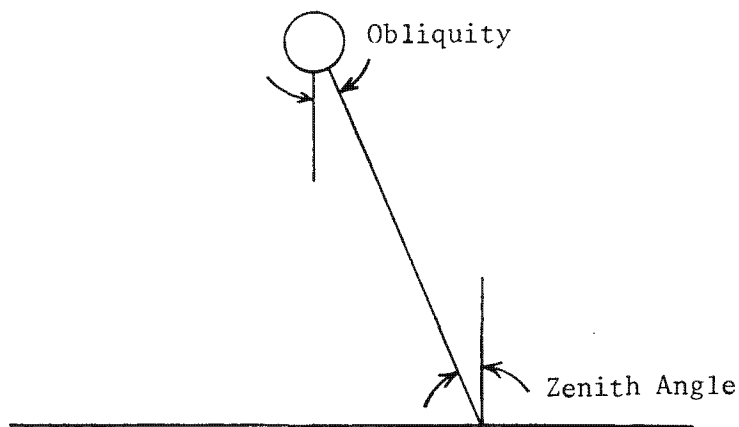


Figure 2.11-8. Zenith Angle and Obliquity

2.11-11

~~TOP SECRET~~ GHandle via BYEMAN
Control System Only

~~TOP SECRET~~ G

BIF-008- W-C-019839-RI-80

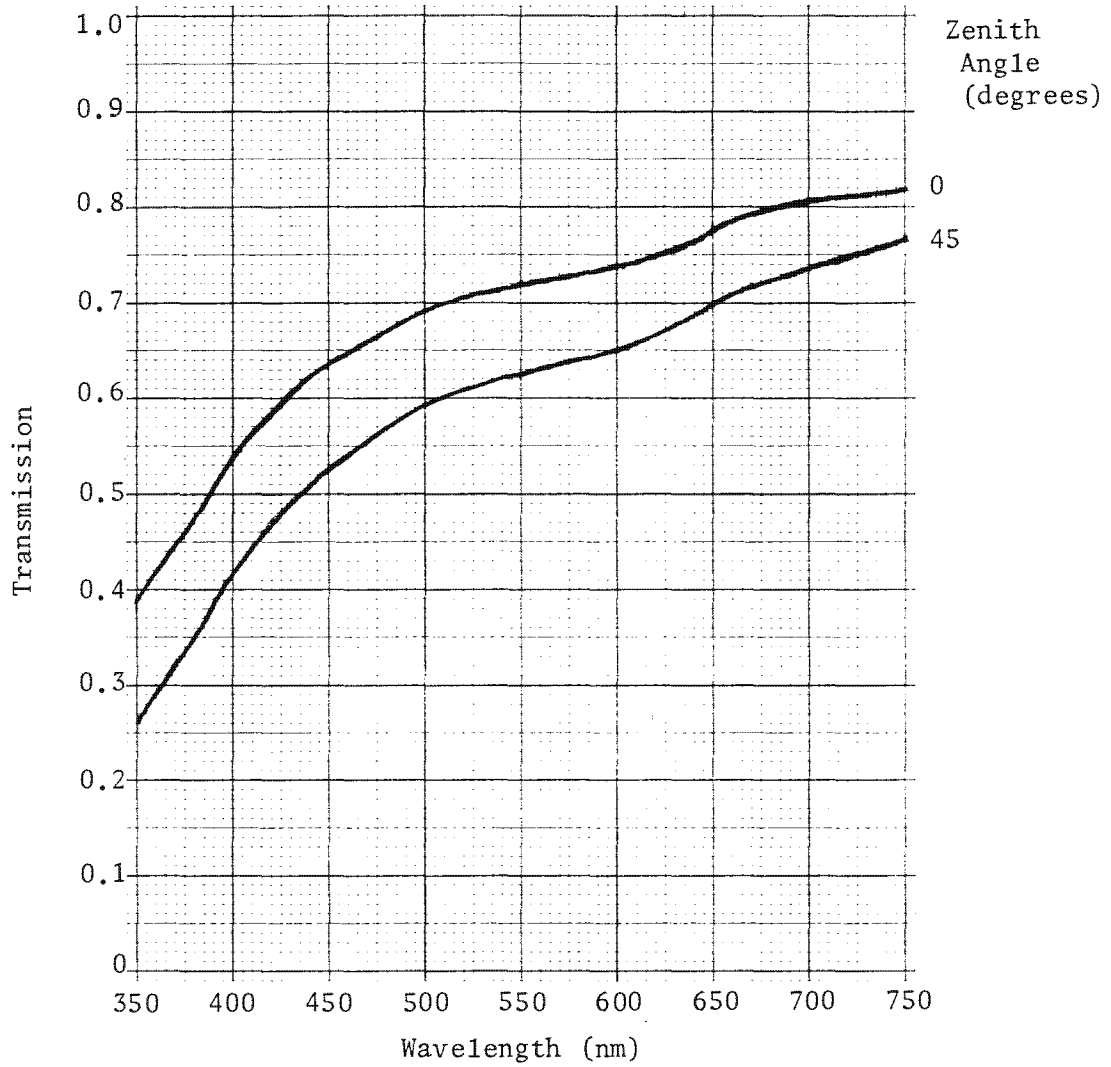


Figure 2.11-9. Atmospheric Transmission

2.11-12

~~TOP SECRET~~ G

Handle via **BYEMAN**
Control System Only

~~TOP SECRET~~ GBIF-008- W-C-019839-RI-8011.4 Haze

The atmospheric haze, consisting of a combination of aerosols, scatters sunlight and therefore contributes to the apparent scene radiance. Figure 2.11-10 shows the spectral radiance of this haze as viewed toward the nadir from an altitude of 90 nautical miles. The haze emits in a spatially diffuse manner and therefore causes a reduction in apparent scene contrast.

11.5 Radiation Effects

Operation of the Gambit vehicle in the EAC domain increases the probability of radiation effects arising from passage through the lower fringes of the Van Allen region.

Extensive studies have indicated substantial margin of safety for electronic components. Film, however, because of its sensitivity to ionizing radiation may exhibit an increase in base-plus-fog density. The degree of increase in base fog is dependent on the mission duration and altitude profile chosen.

A complex radiation model has been generated and is available to evaluate specific mission scenarios. A typical output from this model is shown in Figure 2.11-11

11.6 Summary

The integration shown in the beginning of this section has been approximated for several cases of haze, scene type, and sun angle. The integrated values for irradiance (H_I) on the entrance pupil of the PPS/DP EAC are shown in Table 2.11-2. This table also includes an approximation of the entrance pupil illumination using the definition that one watt of radiant energy at the wavelength of maximum visual sensitivity (555.0 nanometers) is equal to 680 lumens. Image plane illumination (or irradiance) may be found by introducing the appropriate transmission characteristics of the optical system.

2.11-13

~~TOP SECRET~~ GHandle via BYEMAN
Control System Only

~~TOP SECRET~~ G

BIF-008- W-C-019839-RI-80

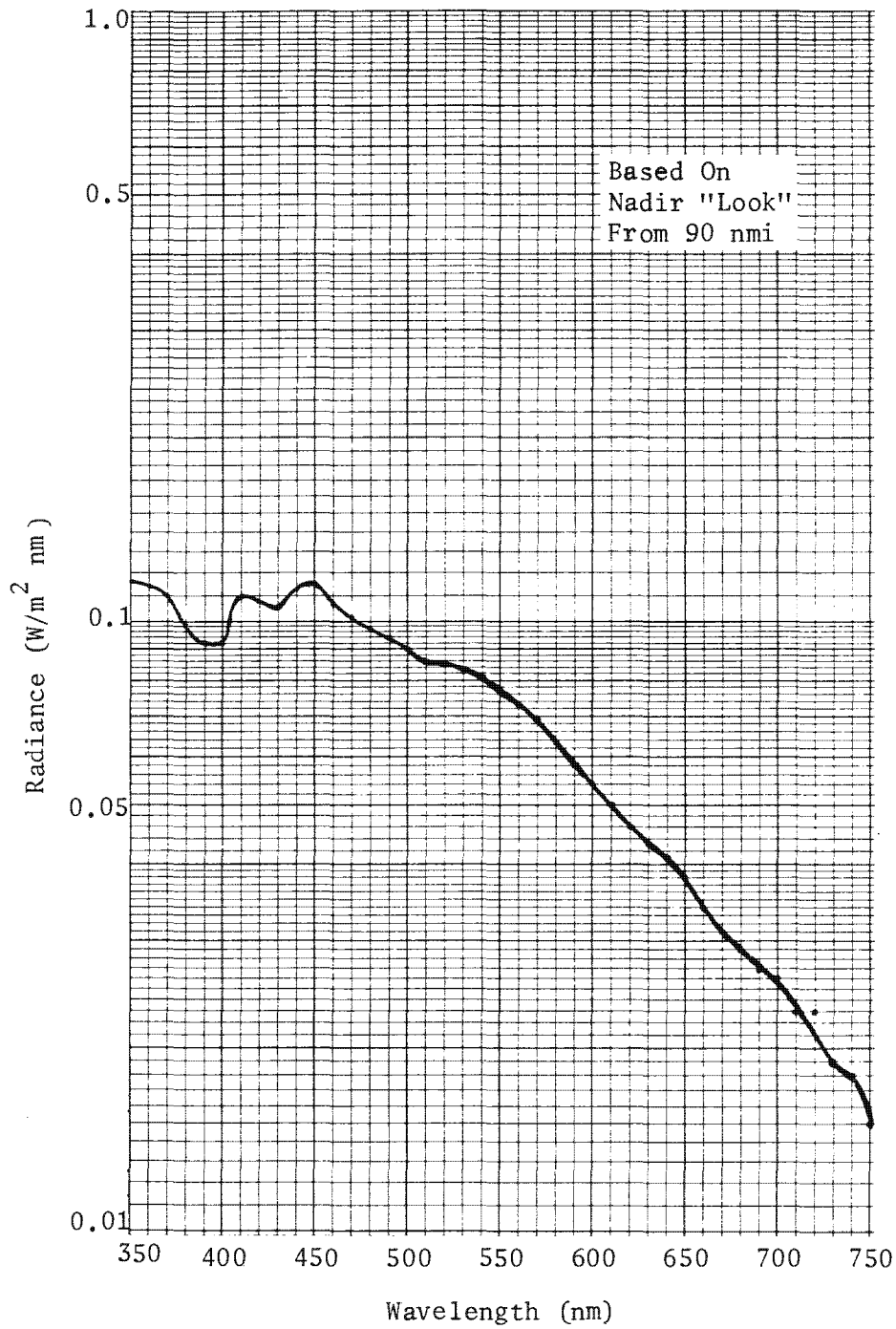


Figure 2.11-10. Haze Radiance

2.11-14

~~TOP SECRET~~ G

Handle via BYEMAN
Control System Only

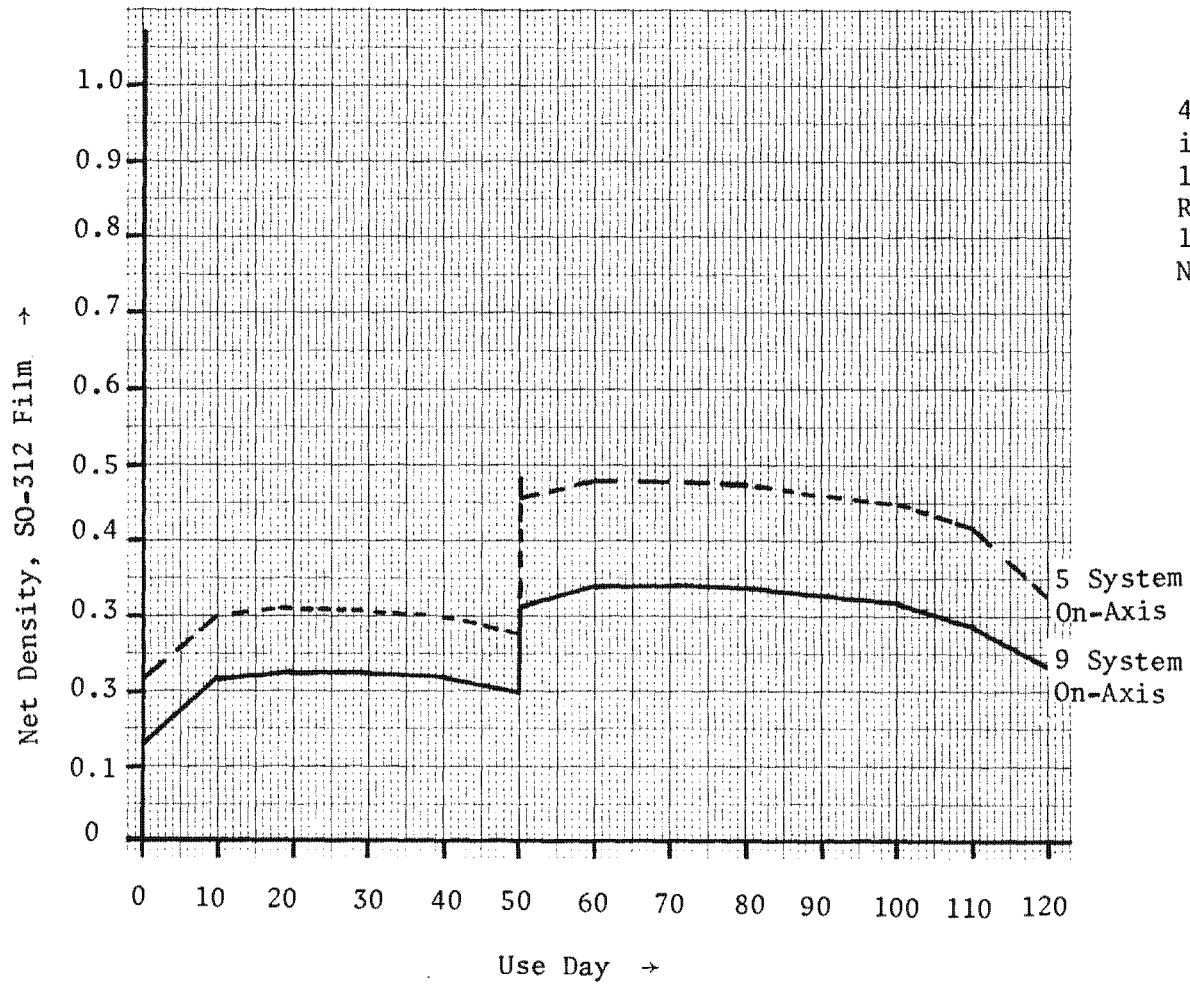


Figure 2.11-11. Radiation-Induced Fog

2.11-15

Approved for Release: 2017/02/14 C05097220

Approved for Release: 2017/02/14 C05097220

~~TOP SECRET~~ GBIF-008- W-C-019839-RI-80

TABLE 2.11-2

TOTAL INTEGRATED IRRADIANCE AND APPROXIMATE ILLUMINATION

<u>Haze</u>	<u>Scene</u>	<u>Sun Angle (degrees)</u>	<u>Irradiance (watts/m²)</u>	<u>Illumination (meter-candle)</u>
	Nominal	10	0.065	44.2
		40	0.33	224.4
		70	0.52	353.6
None	Snow	10	0.46	312.8
		40	2.32	1577.6
		70	3.6	2448.0
	Forest	10	0.074	50.3
		40	0.38	258.4
		70	0.58	394.4
	Nominal	10	0.12	81.6
		40	0.41	278.8
		70	0.59	401.2
Light	Snow	10	0.42	285.6
		40	1.93	1312.4
		70	2.94	1999.2
	Forest	10	0.13	88.4
		40	0.45	306.0
		70	0.64	435.2
	Nominal	10	0.137	93.2
		40	0.432	293.8
		70	0.61	414.8
Average	Snow	10	0.413	280.8
		40	1.84	1251.2
		70	2.79	1897.2
	Forest	10	0.143	97.2
		40	0.46	312.8
		70	0.66	448.8

2.11-16

~~TOP SECRET~~ GHandle via BYEMAN
Control System Only

~~TOP SECRET~~ GBIF-008- W-C-019839-RI-80

TABLE 2.11-2 (CONTINUED)

<u>Haze</u>	<u>Scene</u>	<u>Sun Angle (degrees)</u>	<u>Irradiance (watts/m²)</u>	<u>Illumination (meter-candle)</u>
	Nominal	10	0.16	108.8
		40	0.46	312.8
		70	0.64	435.2
Heavy	Snow	10	0.39	265.2
		40	1.61	1094.8
		70	2.41	1638.8
	Forest	10	0.17	115.6
		40	0.49	333.2
		70	0.68	462.4

2.11-17

~~TOP SECRET~~ GHandle via BYEMAN
Control System Only

~~TOP SECRET~~ G

BIF-008-W-C-019839-RI-80

This Page Intentionally Blank

2.11-18

~~TOP SECRET~~ G

Handle via BYEMAN
Control System Only

~~TOP SECRET~~ GBIF-008- W-C-019839-RI-80

12.0 OPTICAL ANALYSIS

Gambit system optical performance is examined through the techniques of modulation transfer function (MTF) and threshold modulation (TM) with the lens characteristics typical of the R-5 configuration. The analytic tools used in these techniques are discussed in this section, along with the concepts of MTF, TM, optical quality factor (OQF) and performance predictions based on these concepts.

12.1 Analytic Tools

The tools employed in the study of optical performance are based on the ability to describe, in analytic terms, the changes wrought in the energy distribution as the distribution passes through the optical system.

12.1.1 Spread Functions

If it were possible to start with an infinitesimally small spot of light and to image the spot with a lens, the image would not be infinitesimal. Diffraction and aberrations in the lens would spread the image out over a finite area. The intensity distribution of the energy over a cross-section of this image is called the point-spread function. A plot of the intensity generally would appear as shown in Figure 2.12-1.

2.12-1

~~TOP SECRET~~ GHandle via BYEMAN
Control System Only

~~TOP SECRET~~ G

BIF-008-W-C-019839-RI-80

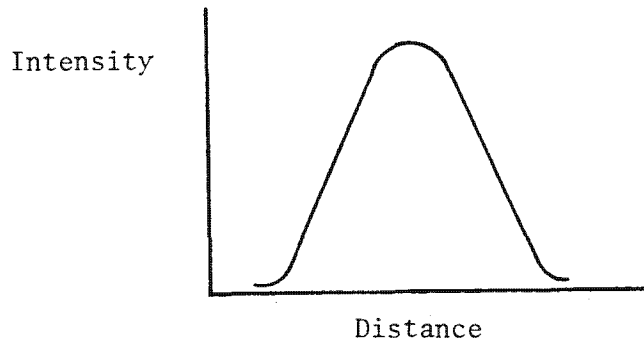


Figure 2.12-1. Point-Spread Function

Similarly, if it were possible to image an infinitesimal spot of light on a piece of film, the light distribution in the film would not be a narrow shaft through the thickness of the emulsion, but would spread out because of such effects as scattering by the emulsion, as illustrated in Figure 2.12-2.

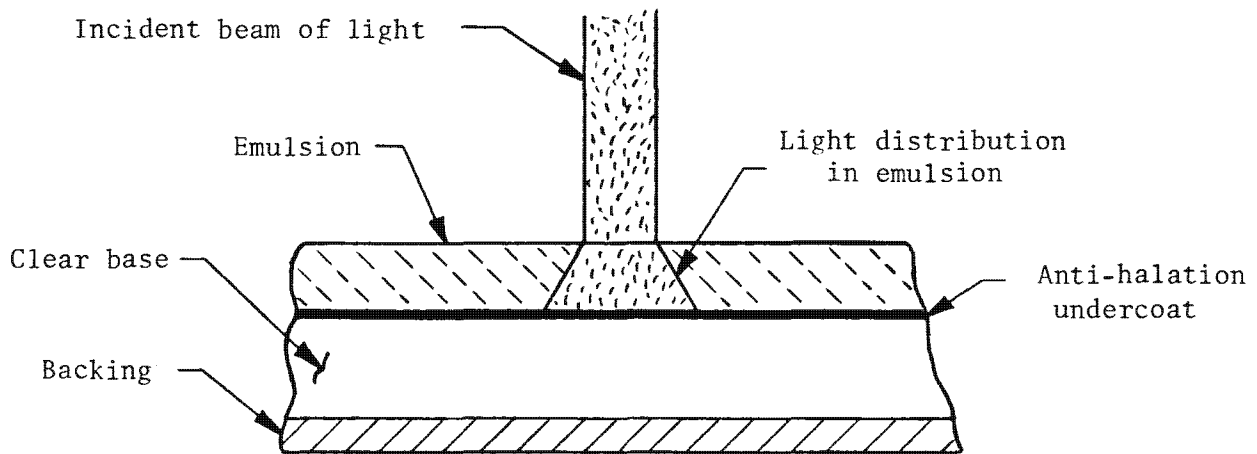


Figure 2.12-2. Light Scattering By The Emulsion

2.12-2

~~TOP SECRET~~ G

Handle via BYEMAN
Control System Only

~~TOP SECRET~~ G BIF-008- W-C-019839-RI-80

Now, consider a light source consisting of a small but finite spot, imaged on a piece of film by a lens. Each infinitesimal element of the source forms its own spread function and all of these combine to make the spot image. Similarly, each element of the image forms its own spread function in the emulsion. These elements combine to produce the light distribution in the emulsion which in turn determines the distribution of density in the developed film. This distribution of density is a fundamental index of the quality of the photographic image. However, it is difficult to measure the distribution in the image of a point source directly because the measuring sensor must be much smaller than the image. The sensor must have high sensitivity, and its position with respect to the image is critical. If a line source is used instead of a point source, the scanning aperture of the measuring device can be a slit and the energy available for measurement is greatly increased. A line source can be thought of as a series of point sources, and the image as a series of overlapping point-spread functions. The energy cross section of this image is called the line-spread function. The point-spread function and the line-spread function are not equal, but they are mathematically related. Therefore the line-spread function is also a valid measure of the quality of the image.

12.1.2 Test Objects

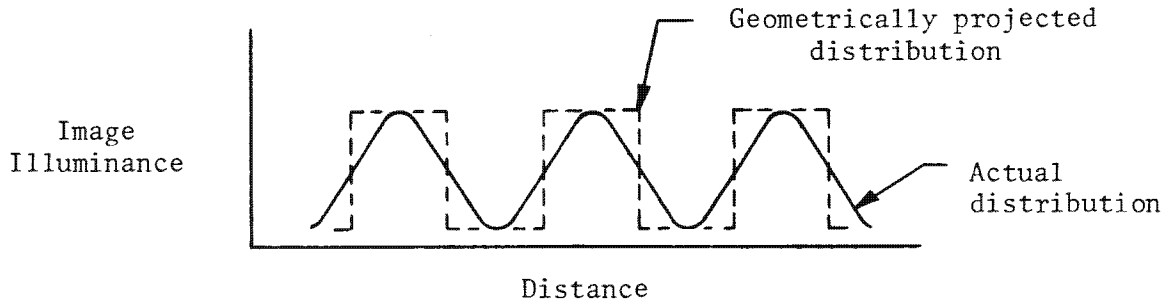
A common type of test object consists of a series of reflective bars and non-reflective spaces of equal width. The spacing (and therefore the width) of the bars determines the magnitude of the energy variation in the image. When bar spacing of the image is slightly larger than the image line-spread function, the energy distribution in the image, relative to a geometrically projected image, is as shown in Figure 2.12-3.

2.12-3

~~TOP SECRET~~ G Handle via BYEMAN
Control System Only

~~TOP SECRET~~ G

BIF-008-W-C-019839-RI-80



As the spacing and width of lines in the test object decrease, the light variation in the image decreases.

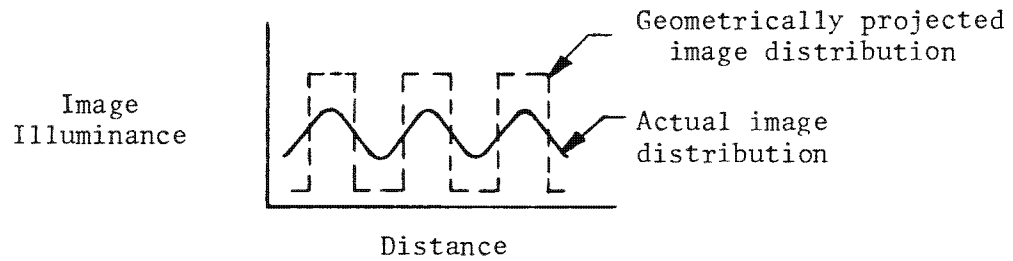


Figure 2.12-3. Actual and Geometric Image Distributions

2.12-4

~~TOP SECRET~~ G

Handle via BYEMAN
Control System Only

~~TOP SECRET~~ GBIF-008- W-C-019839-RI-80

The magnitude of the energy variations in the image is clearly related to the line-spread function, but establishing this relationship mathematically is tedious. Therefore square-wave test objects are used, primarily to determine the spatial frequency at which light variation in the image is no longer discernible to the eye. This is the well known resolving-power test. Because resolving power depends on the variation of light in the image which in turn is related to the spread function, there is, in general, good correlation between resolving power and the size of the spread function. The shape of the spread function, however, is not derivable from measurements of resolving power.

If the configuration of the object varies as a sine wave instead of as a square wave, the image produced is sinusoidal in character and is completely defined by measuring the maximum and minimum light values in the image. For a typical case, the actual image and the geometrically projected image of a sine-wave test object are as shown in Figure 2.12-4.

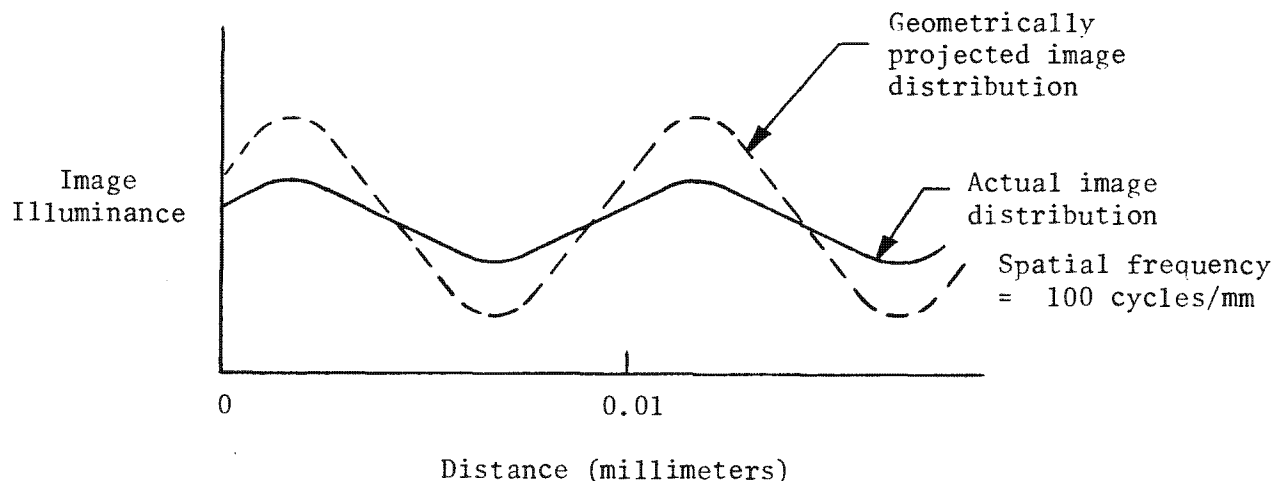


Figure 2.12-4. Image Distributions of Sinusoidal Object

2.12-5

~~TOP SECRET~~ GHandle via **BYEMAN**
Control System Only

~~TOP SECRET~~ GBIF-008- W-C-019839-RI-80

Although a sine-wave test object is very difficult to manufacture, an important advantage in its use is that it is relatively easy to show mathematically the relationship between the line-spread function and the light variations in the image measured over the spatial frequency spectrum.

12.1.3 Modulation

Assume that sine-wave test object transparencies are used, and the transmittance variation of the transparencies are measured as a function of the frequencies of the sine waves. When such a test object is placed in front of an extended source of known luminance, its modulation, M , at any spatial frequency, ν , can be expressed as:

$$M(\nu) = \frac{I_{\max}(\nu) - I_{\min}(\nu)}{I_{\max}(\nu) + I_{\min}(\nu)}$$

where: $I_{\max}(\nu)$ and $I_{\min}(\nu)$ are the maximum and minimum values of energy passing through the transparency at a location where the frequency of the sinusoid is ν .

The luminance distribution of the test object as a function of spatial frequency and position can be stated as:

$$f(\omega, x) = D(\omega) + A(\omega) \sin \omega x$$

where: $D(\omega) = \frac{I_{\max}(\nu) + I_{\min}(\nu)}{2}$,

the average luminance level of energy passing through the sinusoidal pattern,

$$A(\omega) = \frac{I_{\max}(\nu) - I_{\min}(\nu)}{2}$$

the amplitude of the luminance modulation,

2.12-6

~~TOP SECRET~~ GHandle via **BYEMAN**
Control System Only

~~TOP SECRET~~ GBIF-008-W-C-019839-RI-80

- $\omega = 2\pi\nu$, the spatial radian frequency of the object,
 $\nu =$ spatial frequency in lines per unit measure, and
 $x =$ distance

Rewriting the modulation equation in terms of the amplitude, $A(\omega)$, and the average luminance level, $D(\omega)$, the modulation is given by:

$$\begin{aligned}
 M(\nu) &= \frac{I_{\max}(\nu) - I_{\min}(\nu)}{I_{\max}(\nu) + I_{\min}(\nu)} \\
 &= \frac{A(\omega)}{D(\omega)}
 \end{aligned}$$

At low frequencies the minimum luminance from the test object can be made to approach zero, so that the modulation might appear as shown in Figure 2.12-5.

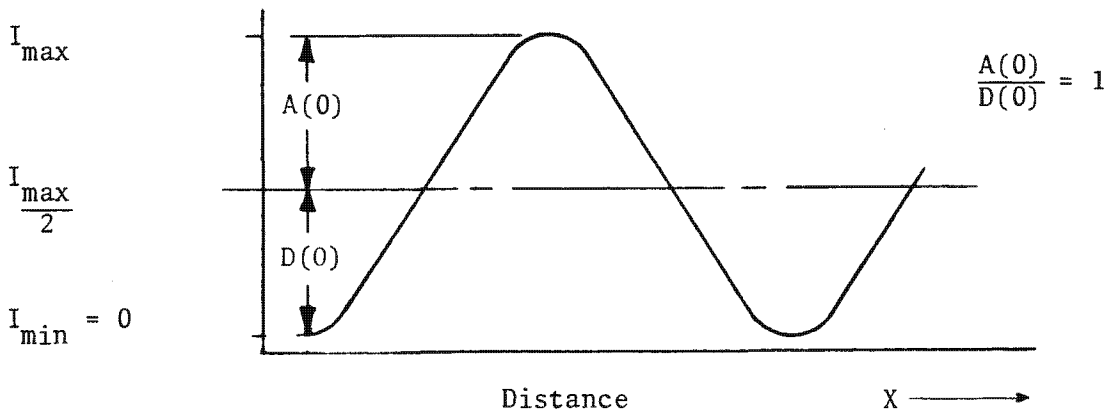


Figure 2.12-5. Low-Frequency Modulation

2.12-7

~~TOP SECRET~~ G

Handle via BYEMAN
Control System Only

~~TOP SECRET~~ G

BIF-008- W-C-019839-RI-80

In this case the modulation, $\frac{A(0)}{D(0)}$, is said to be 100 percent, or 1.0. Similarly, at some higher frequency the modulation of the test object might appear as shown in Figure 2.12-6.

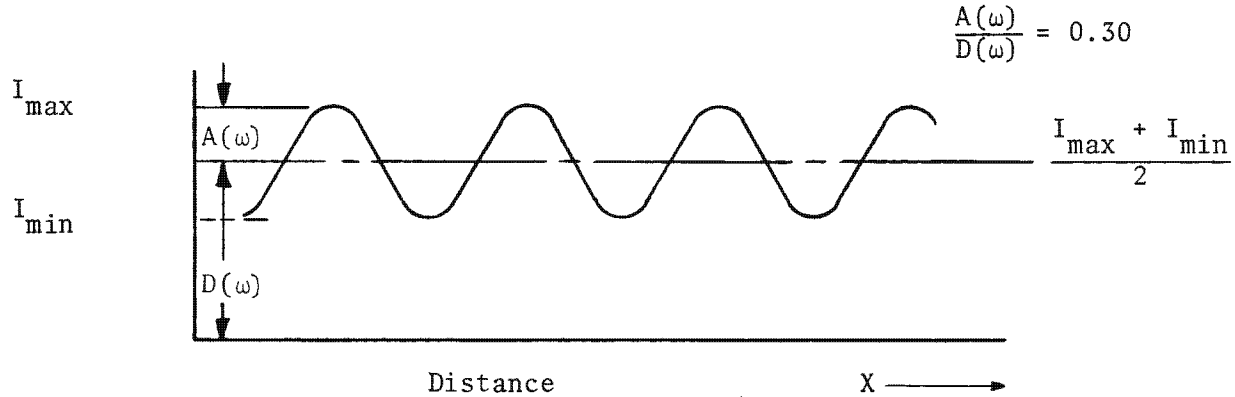


Figure 2.12-6. High-Frequency Modulation

The modulation, $\frac{A(\omega)}{D(\omega)}$, is 0.30 or 30 percent in this case.

12.2 Modulation Transfer Function (MTF)

The modulation transfer function characterizes the relationship between system input (object) and output (image) as a function of spatial frequency. Figure 2.12-7 illustrates this relationship.

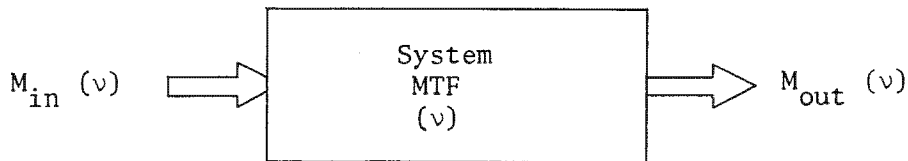


Figure 2.12-7. MTF Concept

2.12-8

~~TOP SECRET~~ G

Handle via BYEMAN
Control System Only

~~TOP SECRET~~ GBIF-008-W-C-019839-RI-80

12.2.1 Linear System

Suppose a sinusoidal test object is imaged by a lens onto a fine slit with a photodetector behind it. The output of the photodetector is measured as the slit scans the image. The effect of the spread function of the lens is to reduce the amplitude of modulation in the image without altering its sinusoidal character. This property of the lens to transfer energy from a sine-wave test object (input in units of luminance) into a sine-wave image (output in units of illuminance) is fundamental to the sine-wave analysis of a system and systems exhibiting this property are said to be linear systems.

The steady-state transfer characteristics of a lens performing as a linear system are shown as a straight line in Figure 2.12-8.

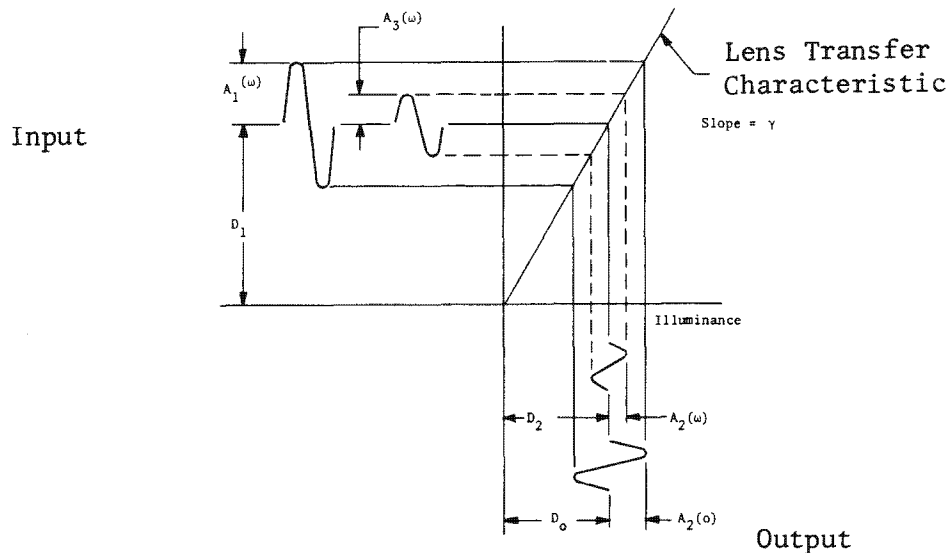


Figure 2.12-8. Transfer Characteristics of a Linear System

2.12-9

~~TOP SECRET~~ GHandle via BYEMAN
Control System Only

~~TOP SECRET~~ GBIF-008- W-C-019839-RI-80

12.2.1.1 Object Modulation. An ideal sine-wave test object has a constant amplitude for all spatial frequencies. The luminance distribution may be expressed as:

$$f(\omega, x) = D_1 + A_1 \sin \omega x$$

and the modulation as:

$$M_1 = \frac{A_1}{D_1}$$

12.2.1.2 Image Modulation. The illuminance variations in the image are given by:

$$g(\omega, x) = D_2 + A_2(\omega) \sin [\omega x + \phi(\omega)] ,$$

where $\phi(\omega)$ is the phase shift. Since a phase shift is associated with a non-symmetric spread function and lens system, and on-axis spread functions are generally symmetrical, the phase shift is considered to be zero. The expected modulation at all frequencies for a perfect system is equal to the modulation at very low frequency (limit as $\nu \rightarrow 0$):

$$M_0 = \frac{A_2(0)}{D_2(0)} .$$

The actual modulation at any spatial frequency is:

$$M_2 = \frac{A_2(\omega)}{D_2(\omega)} .$$

2.12-10

~~TOP SECRET~~ GHandle via BYEMAN
Control System Only

~~TOP SECRET~~ GBIF-008- W-C-019839-RI-80

The difference between these two equations represents the reduction in peak-to-peak amplitude of the signal and a possible shift in average level from $D_2(0)$ to $D_2(\omega)$ which would occur if the lens transfer characteristics varied with frequency.

12.2.1.3 System MTF. The ratio of the output modulation at some frequency to the modulation at zero frequency is, by definition, the MTF of the system at that frequency. Expressed in terms of equations previously shown:

$$\text{MTF}_L(\nu) = \frac{M_2}{M_0} = \frac{A_2(\omega)}{A_2(0)} \frac{D_2(0)}{D_2(\omega)}$$

or:
$$\text{MTF}_L(\nu) = \frac{A_2(\omega)}{A_2(0)}$$

because $D_2(0) = D_2(\omega)$ for a linear system.

12.2.2 Nonlinear System

An example of a nonlinear system is one in which the detection of energy is accomplished by photographic film. The nonlinearity arises in the transfer from exposure (product of illuminance and time) to density or transmittance. A nonlinear system using film is illustrated in block form in Figure 2.12-9 and schematically in Figure 2.12-10.

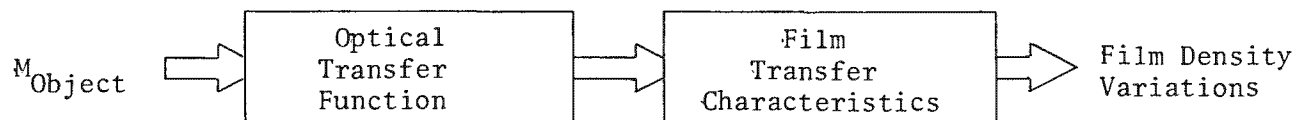


Figure 2.12-9. Nonlinear Transfer Concept

~~TOP SECRET~~ G

~~TOP SECRET~~ G

BIF-008- W-C-019839-RI-80

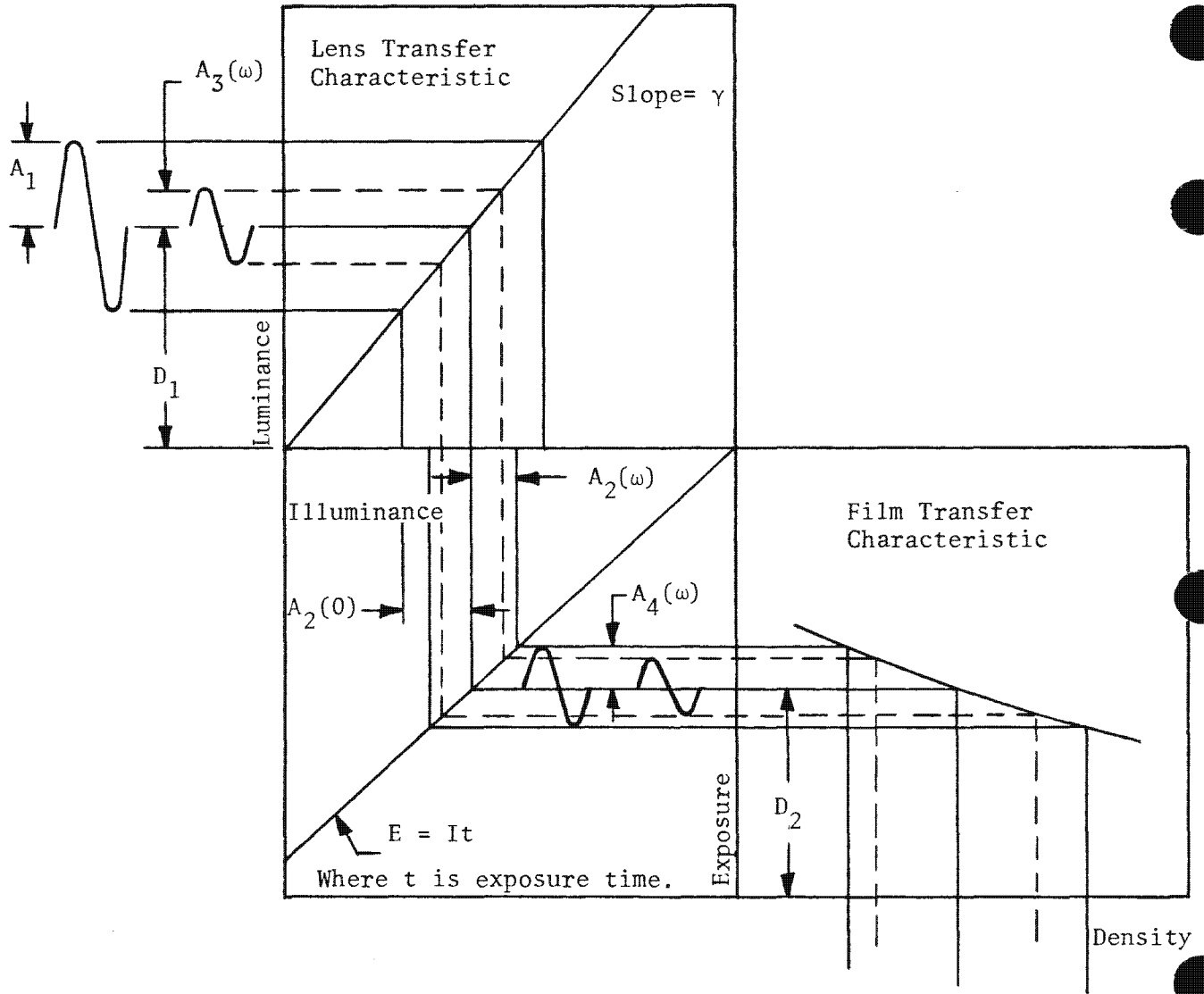


Figure 2.12-10. Transfer Characteristics of a Nonlinear System

2.12-12

~~TOP SECRET~~ G

Handle via **BYEMAN**
Control System Only

~~TOP SECRET~~ GBIF-008-W-C-019839-RI-80

12.2.2.1 Object Modulation. The modulation of an object is usually defined as the difference between its maximum and minimum reflectances divided by the sum of its reflectances. An alternate definition employs the energies reflected from the object. In either case, the spectral limits over which the measurement is to take place must be defined. Thus,

$$M_I = \frac{\int_{\lambda_1}^{\lambda_2} [R_1(\lambda)] [I(\lambda)] d\lambda - \int_{\lambda_1}^{\lambda_2} [R_2(\lambda)] [I(\lambda)] d\lambda}{\int_{\lambda_1}^{\lambda_2} [R_1(\lambda)] [I(\lambda)] d\lambda + \int_{\lambda_1}^{\lambda_2} [R_2(\lambda)] [I(\lambda)] d\lambda}$$

where: M_I = intrinsic object modulation (at 0 spatial frequency)

$R_1(\lambda), R_2(\lambda)$ = maximum and minimum spectral reflectances of the object

$I(\lambda)$ = spectral distribution of the target illuminant

λ_1 = short wavelength cut off

λ_2 = long wavelength cut off

Occasionally, the modulation of an object is defined as the modulation apparent to the eye, or perhaps the modulation apparent to a particular photocell with a given spectral response. In this case,

$$M_I = \frac{\int_{\lambda_1}^{\lambda_2} [R_1(\lambda)] [I(\lambda)] [E(\lambda)] d\lambda - \int_{\lambda_1}^{\lambda_2} [R_2(\lambda)] [I(\lambda)] [E(\lambda)] d\lambda}{\int_{\lambda_1}^{\lambda_2} [R_1(\lambda)] [I(\lambda)] [E(\lambda)] d\lambda + \int_{\lambda_1}^{\lambda_2} [R_2(\lambda)] [I(\lambda)] [E(\lambda)] d\lambda}$$

where: $E(\lambda)$ is the spectral response of the detector (e.g., the eye).

~~TOP SECRET~~ G

~~TOP SECRET~~ GBIF-008- W-C-019839-RI-80

With reference to Figure 2.12-10, the object modulation may be expressed as:

$$M_I = \frac{A_1}{D_1}$$

When square-wave (tribar) targets are used, the object modulation is:

$$M_I = \frac{C-1}{C+1}$$

where: C is the contrast, usually expressed as C:1.

12.2.2.2 Film MTF. The MTF of a film can be determined by using the film to photograph sine-wave test objects through a lens. The photographic images on the test film are developed along with a small gray scale which makes it possible to plot the transfer characteristics for the film. Because the photographic process is nonlinear, the photographic image of a sine-wave test object is not sinusoidal in transmittance or in density, and it becomes necessary to state the MTF of a film in terms of the effective exposure rather than in terms of transmittance.

Again with reference to Figure 2.12-10, the effective exposure modulation of the film, $\frac{A_4(\omega)}{D_2}$, can be determined by projection of the maximum and minimum density values back through the transfer characteristic of the film. The effective exposure modulation is then referred to the object space of the lens by projection through the transfer characteristics of the lens. The effective input modulation, $\frac{A_3(\omega)}{D_1}$, is then compared with the test object modulation, $\frac{A_1}{D_1}$, where the ratio $\frac{A_3(\omega)}{A_1}$ is the combined MTF of the lens and film. It follows then that the MTF of the film alone, $MTF_F(\omega)$, is obtained by dividing the MTF of the lens-film combination, $MTF_{LF}(\omega)$, by the MTF of the lens, $MTF_L(\omega)$.

2.12-14

~~TOP SECRET~~ GHandle via BYEMAN
Control System Only

~~TOP SECRET~~ GBIF-008- W-C-019839-RI-80

$$MTF_{LF}(\omega) = \frac{A_3(\omega)}{A_1}$$

$$MTF_L(\omega) = \frac{A_2(\omega)}{A_2(0)} = \frac{A_2(\omega)\gamma}{A_1}$$

$$MTF_F(\omega) = \left(\frac{A_3(\omega)}{A_1} \right) \left(\frac{A_1}{A_2(\omega)\gamma} \right) = \frac{A_3(\omega)}{A_2(\omega)\gamma}$$

where: γ is the slope of the linear lens transfer function.

12.2.3 System MTF. The sine-wave test of a lens consists of measuring the MTF at selected frequencies from very low frequencies to frequencies at which the lens MTF approaches zero. A typical plot of MTF_L versus spatial frequency is shown in Figure 2.12-11.

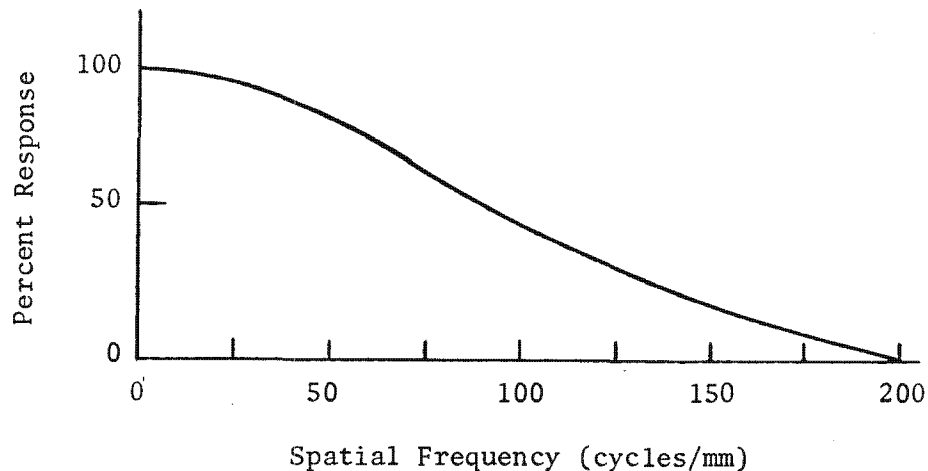


Figure 2.12-11. Typical Lens MTF

2.12-15

~~TOP SECRET~~ G

Handle via **BYEMAN**
Control System Only

~~TOP SECRET~~ GBIF-008- W-C-019839-RI-80

It may be seen from the previous discussion that if a sinusoidal test object is imaged through a lens system onto a film of known MTF, the lens MTF may be obtained. In like manner, if a test object is imaged through a lens of known MTF, the film MTF may be calculated. Within a given system, and for a stated spatial frequency, MTFs are multiplicative. Total system MTF is therefore the product of individual component MTFs in the order in which they act.

12.3 Threshold Modulation

Threshold modulation (TM) is defined as the modulation at spatial frequency, ν , which must be supplied to a given film in order that the resulting density variations (after processing) will be detectable. A typical curve showing TM as a function of spatial frequency is shown in Figure 2.12-12.

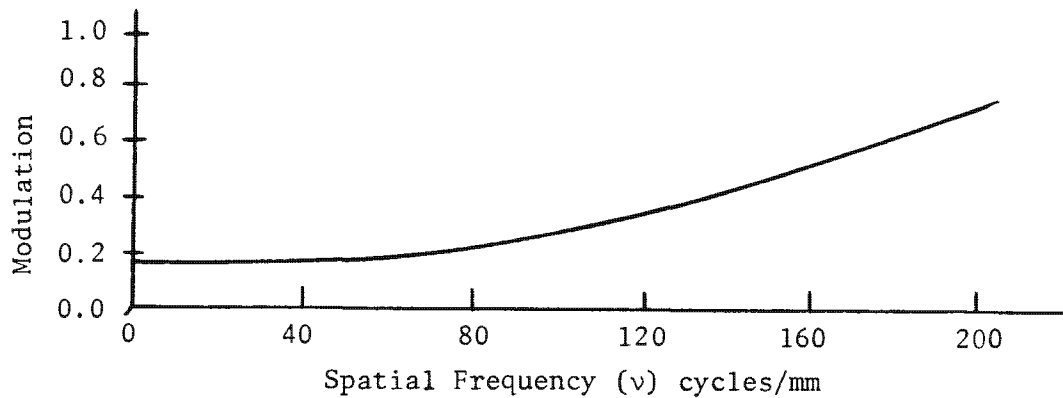


Figure 2.12-12. Typical TM Curve

2.12-16

~~TOP SECRET~~ G

Handle via **BYEMAN**
Control System Only

~~TOP SECRET~~ GBIF-008- W-C-019839-RI-80

12.3.1 Measurement

A resolving-power test target of known contrast is photographed in an exposure series by a lens of known MTF onto a photographic film. This film is given a specific development and is examined visually to obtain a numerical value for the limiting resolution at optimum exposure. The modulation of the aerial image (AIM) is calculated by the product of the modulation (M) of the target and the MTF of the image-forming lens for the target spatial frequency. Since this product describes the image modulation present at the resolution threshold, it is called threshold modulation.

Other TM values are obtained by changing the lens aperture and/or target contrast to obtain different modulations. These TM values are plotted vs limiting resolution; the line fitted to the points is called the TM curve for the particular film and process. The data generally can be fitted satisfactorily to a second-degree polynomial of the form:

$$TM(v) = a + bv + cv^2$$

where: v is spatial frequency
 a, b and c are constants determined by
 the fitting process. (Certain films are
 best fitted to a straight line in which
 case c = 0.)

12.3.1.1 Exposure. An exposure series is employed so that all reported values for TM may be stated for optimum exposure. Furthermore, it is often desirable to know the TM for various degrees of underexposure or overexposure. (See Part 2, Section 7 for TM equations applicable to the films currently used on the Gambit program.)

2.12-17

~~TOP SECRET~~ GHandle via BYEMAN
Control System Only

~~TOP SECRET~~ GBIF-008- W-C-019839-RI-80

12.3.1.2 Processing. TM values are stated for a specific film/process combination. When performance or image quality degradation predictions are made using TM techniques, care must be exercised to insure that the processing used in TM generation and that to be used in the case of interest are identical.

12.3.2 Assumptions

Certain assumptions are implicit in the preparation and use of a TM curve. These assumptions include the following.

- (1) There is a constant ratio between the tribar response and the sine-wave response of a lens.
- (2) The scattering characteristics of the emulsion do not vary with the cone angle of the lens forming the image, thereby varying the film MTF.
- (3) Readers are influenced only by the modulation of a tribar image and not by the waveform.
- (4) The target quality (frequency content) is essentially the same for making and using the TM curve.
- (5) The image characteristics of the tribar are determined by the lens MTF in one direction only, i.e., there are essentially no symmetry requirements. This assumption does not preclude differences between horizontal and vertical MTFs as is the case for image smear and for many aberrated lenses, but requires the appropriate MTF curve for the target orientation.

2.12-18

~~TOP SECRET~~ GHandle via **BYEMAN**
Control System Only

~~TOP SECRET~~ GBIF-008-W-C-019839-RI-8012.4 Optical Quality Factor (QQF)

Optical quality factor is a figure of merit which represents how well the optical formula is executed. QQF may be defined as the ratio of the MTF of the lens as manufactured to the MTF of the perfectly executed lens formula. Since MTF is dependent on spatial frequency, integration over spatial frequency is required. Mathematically:

$$QQF = \frac{\int_{\nu_1}^{\nu_2} MTF_E(\nu) d\nu}{\int_{\nu_1}^{\nu_2} MTF_P(\nu) d\nu}$$

where:

ν_1 and ν_2 define the range of spatial frequencies for which QQF is specified.

(For the R-5 lens, $\nu_1 = \square$ lpmm and $\nu_2 = \square$ lpmm.) $MTF_E(\nu)$ is the MTF of the lens as executed, and $MTF_P(\nu)$ is the MTF of a perfectly executed lens.

25X1

12.4.1 Calculation

The QQF rationale is satisfactory for performance estimation in the \square to \square lpmm range for highly corrected optics having an f -number between 3.0 and 5.0. Within these constraints, the QQF may be calculated by:

$$QQF = e^{-4\pi^2(\sigma)^2}$$

where: σ = root-mean squared random wavefront error in wavelengths.

The above equation is plotted for RMS errors up to 0.30λ in Figure 2.12-13.

2.12-19

~~TOP SECRET~~ GHandle via BYEMAN
Control System Only

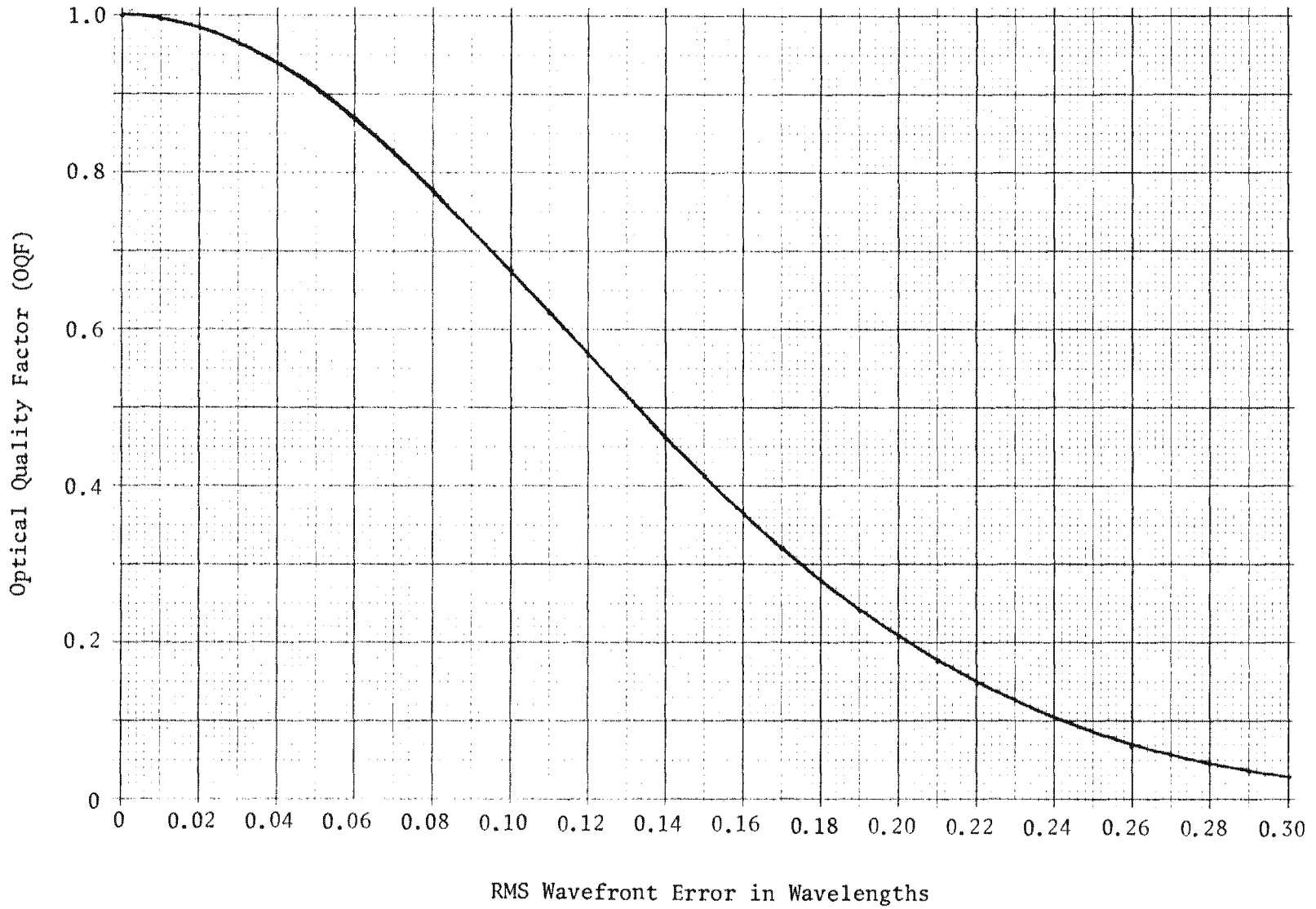


Figure 2.12-13. OQF vs RMS Wavefront Error

Handle via BYEMAN
Control System Only

Approved for Release: 2017/02/14 C05097220

2.12-20

Approved for Release: 2017/02/14 C05097220

~~TOP SECRET~~ GBIF-008- W-C-019839-RI-80

12.4.2 Contributors To OQF Reduction

Various tolerances associated with the manufacture and assembly of the lens elements contribute to a random wavefront error. The contributors are described below and summarized in Table 2.12-1 for the Gambit system.

TABLE 2.12-1
ROSS LENS SURFACE CONTRIBUTIONS TO WAVEFRONT ERROR

<u>Lens No.</u>	<u>RMS Surface Error (λ)*</u>	<u>Conversion Factor (n-1)</u>	<u>RMS Wavefront Error (λ)</u>
1	0.015	0.603	0.00905
	0.015	0.603	0.00905
2	0.015	0.603	0.00905
	0.015	0.603	0.00905
3	0.015	0.697	0.01050
	0.015	0.697	0.01050
4	0.005	0.697	0.00350
	0.005	0.697	0.00350
5	0.005	0.603	0.00300
	0.005	0.603	0.00300

Total Wavefront Error (RSS) = 0.0243

OQF = 0.976

*Applies over the axial beam diameter.

2.12-21

~~TOP SECRET~~ G

Handle via **BYEMAN**
Control System Only

~~TOP SECRET~~ GBIF-008- W-C-019839-RI-80

12.4.2.1 Surface Irregularity. In order to calculate the OQF of an element it is necessary to convert from RMS surface error to RMS wavefront error. For a refractive element in vacuum (index of refraction = 1.00000) this conversion is accomplished by multiplication of the RMS surface error by $n-1$, where n is the index of refraction of the element material. For reflective elements the conversion depends on the angle of incidence. At normal incidence (as for the primary mirror) the wavefront error is twice the surface error. At 45-degree incidence (representative of the stereo), the factor is $\sqrt{2}$.

Ross lens polishing produces lenses 1, 2, and 3 to within 0.015λ RMS surface error and lenses 4 and 5 to 0.005λ RMS surface error. Table 2.12-1 summarizes the contributions of the Ross elements' surface irregularity.

The tolerance for the surface irregularity of a mounted primary mirror is 0.016λ (RMS). Because the equivalent wavefront error is twice the surface irregularity for normal incidence, this surface irregularity becomes 0.032λ (RMS) wavefront error. The resultant OQF is 0.960.

The tolerance for the surface irregularity of a mounted stereo mirror is 0.032λ (RMS). At 45 degrees incidence, the equivalent wavefront error is $\sqrt{2}$ (0.032λ) = 0.045λ (RMS), which results in an OQF of 0.922.

These irregularity values for the primary and stereo mirrors reflect current capabilities in the areas of polishing and mounting.

12.4.2.2 Material and Assembly Contributors. Factors associated with material characteristics and assembly tolerances also influence the lens system OQF.

12.4.2.2.1 Thickness, Spacing, Radii, Tilt, and Decentering. A comparison between the assigned tolerances for thickness, spacing, radii, tilt, and de-

~~TOP SECRET~~ G

~~TOP SECRET~~ GBIF-008- W-C-019839-RI-80

centering and the actual distributions achieved is shown in Table 2.12-2. The effect on lens performance was predicted by a computer program which simulated manufactured lens assemblies using the actual tolerance distributions from Table 2.12-2. The program calculated the OQF at 80, 100, 120, 140, 160, and 180 lpmm for thirty simulated lens assemblies. The resultant OQF (2σ limit) was 0.979.

12.4.2.2.2 Inhomogeneity. The inhomogeneity values listed in Table 2.12-3 apply over the entire lens blank. Each average inhomogeneity value results from vendor (Schott) measurements on twenty blanks. BIF-008 experience with lens blanks of this size supplied by Schott indicates that the majority of inhomogeneity is radially symmetric. Since inhomogeneity is not truly random, it is appropriate to scale linearly the average inhomogeneity down to axial beam diameters and average axial lens thickness. This scaling and subsequent conversion to wavefront error and resultant OQF is presented in Table 2.12-3.

12.4.2.2.3 Primary and Secondary Color. To maintain R-5 off-axis performance the Abbe V-number is rigidly controlled by specifying the tightest tolerance to which the vendor will work. Even this control will allow an unacceptable percentage of the Ross lens sets to produce poor off-axis performance. Therefore, extra Number 2 lenses were procured to allow proper matching of lens blanks within a set to provide the necessary off-axis control of color.

The result of this off-axis control is exceptionally good color correction on-axis. Seventeen sets of Ross lenses, matched using this procedure, yielded an average OQF on-axis of 0.991. The 2σ limit was 0.980. Actual indices at seven wavelengths were used to calculate these values.

2.12-23

~~TOP SECRET~~ GHandle via BYEMAN
Control System Only

TABLE 2.12-2
SUMMARY OF TOLERANCES AND DISTRIBUTIONS

Element	Surface	Thickness/Spacing (In.)		Radii (In.)		Tilt Tol (Sec)*
		Tol	Dist	Tol	Dist	
Stereo	1	-	-	-	-	-
Primary	2	± 0.070	Normal; $2\sigma = 0.006$	± 0.070	Uniform, ± 0.070	± 8
	3	± 0.006	Normal; $2\sigma = 0.006$	± 0.051	Uniform, ± 0.051	± 10
Lens 1	4	± 0.003	Uniform; $+0.0035, -0.0005$	± 0.0062	Uniform, ± 0.0062	± 10
	5	± 0.002	Normal; $2\sigma = 0.002$	± 0.0004	Uniform, ± 0.0004	± 10
Lens 2	6	± 0.002	Uniform; ± 0.002	± 0.065	Uniform, ± 0.065	± 6
	7	± 0.0004	Normal; $2\sigma = 0.0004$	± 0.038	Uniform, ± 0.038	± 4
Lens 3	8	± 0.003	Uniform; $+0.0035, -0.0005$	± 0.0003	Uniform, ± 0.0003	± 10
	9	± 0.004	Normal; $2\sigma = 0.002$	± 0.0024	Uniform, ± 0.0016	± 10
Lens 4	10	± 0.003	Uniform; $+0.0035, -0.0005$	± 0.067	Uniform, ± 0.020	± 10
	11	± 0.004	Normal; $2\sigma = 0.002$	± 0.016	Uniform, ± 0.004	± 10
Lens 5	12	± 0.003	Uniform; $+0.0035, -0.0005$	± 0.002	Uniform, ± 0.002	± 10

*Distribution assumed to be zero (except for primary where uniform distribution, ± 3.6 sec, applies) since the alignment optimization (Ross match) of the Ross to the primary effectively nulls out any misalignment within the Ross for the on-axis case.

Note: Decentering tolerance included in tilt tolerance except for primary where tolerance is ± 0.018 inch, with uniform distribution of ± 0.008 inch.

2.12-24

Approved for Release: 2017/02/14 C05097220

Approved for Release: 2017/02/14 C05097220

TABLE 2.12-3

LENS INHOMOGENEITY OQF CONTRIBUTION

$$\text{Wavefront Error } (\lambda \text{ RMS}) = \left(\frac{\text{Axial Beam Dia}}{\text{Blank Dia}} \right) \left(\frac{\text{Lens Thickness}}{\text{Blank Thickness}} \right) \left(\frac{1}{5} \right) \left(\frac{1}{23.1 \times 10^{-6}} \right) \left(\text{Average Inhomogeneity} \right)$$

- Assuming: (1) One wavelength equals 23.1 microinches.
 (2) RMS wavefront error is 1/5 the peak to valley error.

2.12-25

<u>Lens</u>	<u>Blank Diameter (Inches)</u>	<u>Axial Beam Diameter (Inches)</u>	<u>Blank Thickness (Inches)</u>	<u>Average Lens Thickness (Inches)</u>	<u>Inhomogeneity Tolerance x 10⁻⁶</u>	<u>Average Inhomogeneity x 10⁻⁶</u>	<u>Wavefront Error (λ RMS)</u>
1	15.87	6.7	1.50	0.98	4	4.0	0.00955
2	15.65	6.4	2.28	1.82	4	4.0	0.01130
3	14.87	5.8	2.69	0.48	20	10.4	0.00314
4	12.03	1.8	1.85	0.43	20	10.4	0.00157
5	12.15	1.6	1.72	1.39	10	7.2	0.00332

Total Wavefront Error (RSS) = 0.0155 λ

OQF = 0.991

~~TOP SECRET~~ GBIF-008- W-C-019839-RI-80

12.4.2.2.4 Preferential Orientation. The primary and stereo mirrors can be oriented to each other six ways within the COA. The single-pass, wavefront OQF value for the six possible orientations is calculated using the mounted primary and stereo mirror surface irregularity data as determined from testing. The results of these calculations on improved optical systems indicate an average OQF gain of 0.018 if the best orientation is selected over the average of the six.

12.4.2.3 Summary. Because of the relationship between the RMS random wavefront errors and OQF, it is valid to multiply the individual OQF values to generate an estimate for total system OQF. Table 2.12-4 summarizes the OQF values arising from estimated wavefront errors. The predicted total system OQF is 0.839. The required value of 0.850 is within the error margin of the predicted OQF. Furthermore, experience with manufacture and assembly of the R-5 lens has shown that an OQF of 0.85 is readily obtainable in practice.

12.5 Lens Performance

Two approaches are available for lens performance assessment. One involves the comparison of the lens as-manufactured MTF to the MTF of a perfectly executed lens (OQF). The other uses an estimation of the limiting resolution of the system when imaging a tribar target of known contrast on a baseline film of known threshold modulation. Both techniques are illustrated for the R-5 system in the following discussion.

12.5.1 Lens MTF and OQF

Lens performance is best defined in terms of the MTF associated with either the design of the lens or the expected quality of the manufactured lens. However, a quality assessment can be made only by comparing these transfer

2.12-26

~~TOP SECRET~~ GHandle via BYEMAN
Control System Only

TABLE 2.12-4

OQF SUMMARY

<u>Contributor</u>	<u>Wavefront Error (In Wavelengths)</u>	<u>OQF</u>
Ross Corrector Lens Surface Irregularity	0.0243	0.976
Primary Mirror Surface Irregularity	0.0320	0.960
Stereo Mirror Surface Irregularity	0.0450	0.922
Ross Corrector Lens Inhomogeneity	0.0150	0.991
Ross Corrector Lens Primary and Secondary Color	0.0226	0.980
Thickness, Spacing, Radii, Tilt, Decentering	0.0232	0.979
Total Before Assembly		<hr/> 0.821
Add for Preferential Assembly		+ 0.018
Total		<hr/> 0.839

2.12-27

Approved for Release: 2017/02/14 C05097220

Approved for Release: 2017/02/14 C05097220

~~TOP SECRET~~ GBIF-008- W-C-019839-RI-80

functions with some baseline transfer function representing the ultimate performance level (i.e., the perfect design or the perfectly executed lens). Figure 2.12-14 presents the geometric mean (GM) heterochromatic MTF curves for the R-5 formula (OQF = 1.0) and for the lens as manufactured (OQF = 0.85). The heavy circles on Figure 2.12-14 are those six values of the formula MTF to which measured MTF is compared. The arithmetic mean of the ratio between measured values and these values at the six spatial frequencies shown is reported as the lens OQF.

12.5.2 Resolution Predictions

When the as-manufactured lens MTF is plotted together with a film TM, their intersection point occurs at a spatial frequency corresponding to the limiting resolution of the lens-film system.

12.5.2.1 Aerial Image Modulation (AIM). Aerial image modulation is that modulation present in an image at the film plane over the spatial frequency domain. AIM may be expressed mathematically as:

$$\text{AIM}(\nu) = M_T [\text{MTF}_L(\nu)]$$

Where: M_T is the target modulation, and $\text{MTF}_L(\nu)$ is the lens MTF.

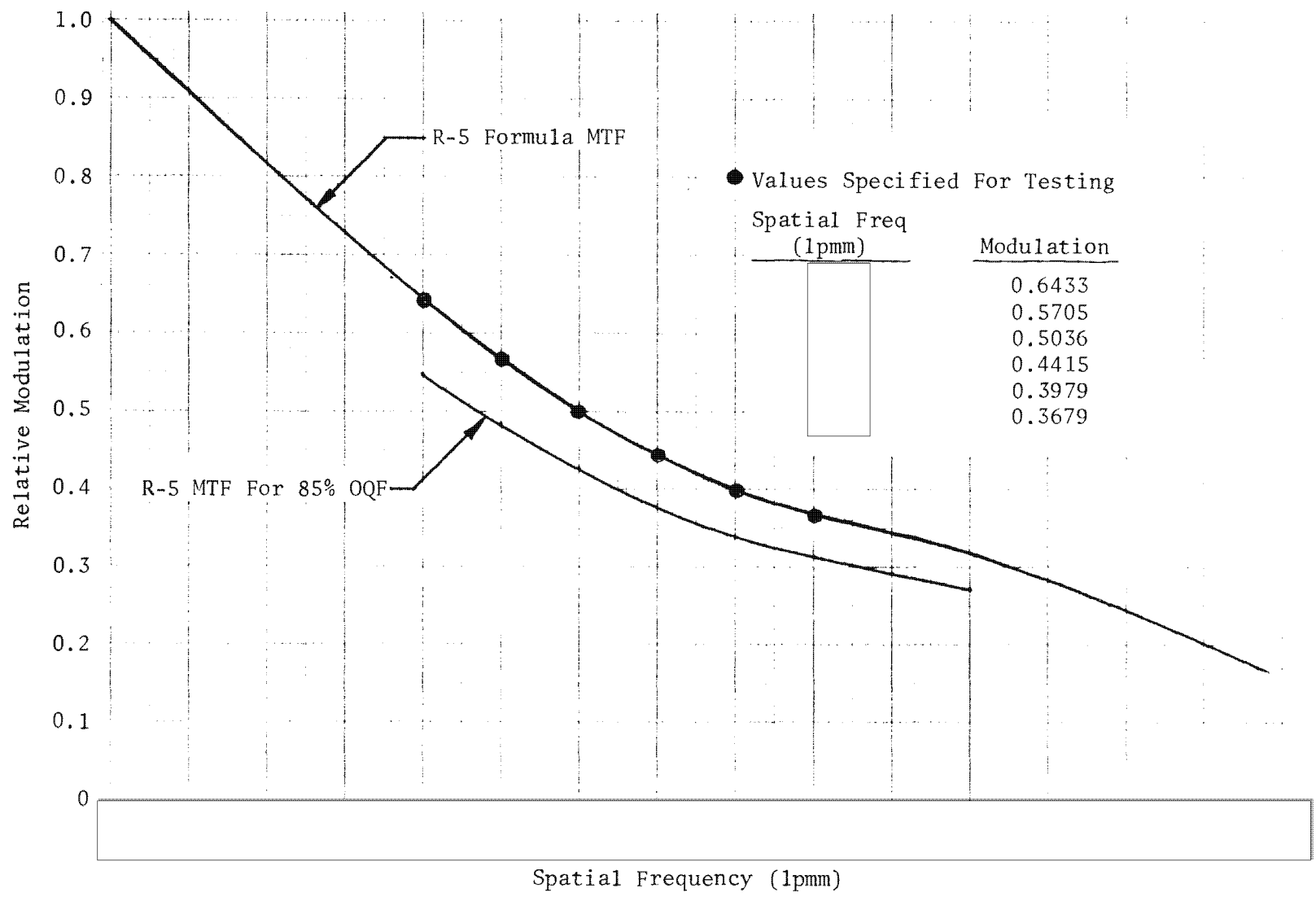
Target modulation may be inferred from target contrast, C, by the relationship:

$$M_T = \frac{C-1}{C+1}$$

Figure 2.12-15 shows the resulting AIM(ν) curve if a series of 4:1 contrast targets of different spatial frequencies are imaged by an optical system. Note that the system AIM is equivalent to the lens MTF for an infinite contrast target.

2.12-28

~~TOP SECRET~~ GHandle via BYEMAN
Control System Only



2.12-29

Figure 2.12-14. R-5 Lens MTF

Handle via **BYEMAN**
Control System Only

Approved for Release: 2017/02/14 C05097220

Approved for Release: 2017/02/14 C05097220

~~TOP SECRET~~ G

BIF-008- W-C-019839-RI-80

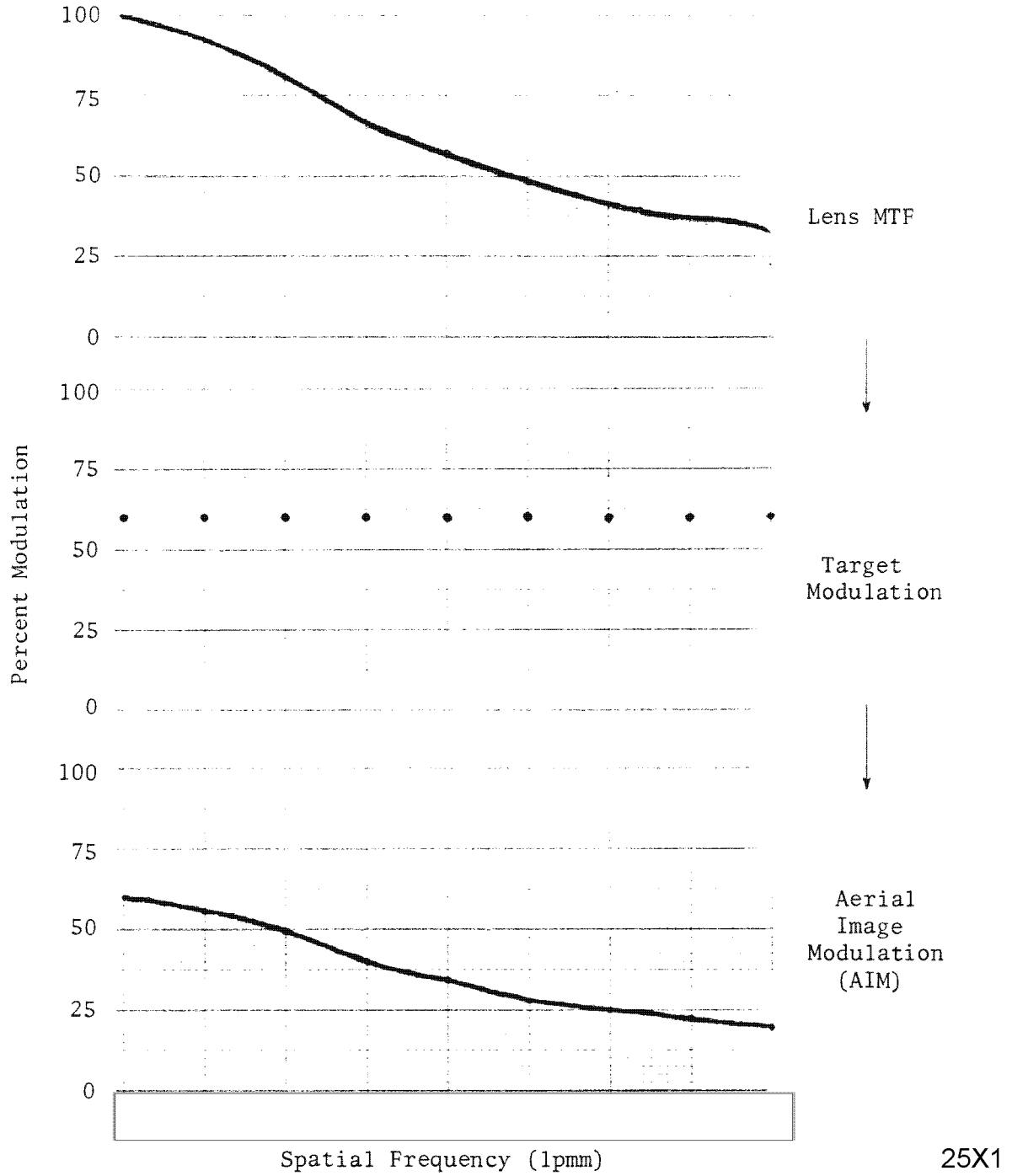


Figure 2.12-15. AIM Illustration

2.12-30

~~TOP SECRET~~ G

Handle via BYEMAN
Control System Only

~~TOP SECRET~~ GBIF-008- W-C-019839-RI-80

12.5.2.2 Adjustment for Contrast. Threshold modulation curves are published for the infinity contrast case (bars have 100-percent reflectance, spaces have 0-percent reflectance). This case represents the minimum TM (highest resolution). For any real case the threshold value at a given spatial frequency will be greater (lower resolution). TM may be adjusted for contrast by dividing each TM value by the contrast ratio, $\frac{(C-1)}{(C+1)}$.

Target contrast may be used to calculate AIM, or target contrast may be used to calculate an adjusted TM. The currently preferred method is to adjust TM to account for target contrast.

12.5.2.3 Representative Predictions. Figure 2.12-16 illustrates the resolution prediction techniques described. All curves shown are based on standard processing, and are adjusted to represent a 2:1 contrast.

12.6 Through-Focus Characteristics

An examination of the through-focus characteristics of the R-5 lens at various field positions provides information on the amount of field curvature present. Similarly, an examination of the monochromatic, through-focus curves yields information relative to the color correction achieved in the R-5 design.

12.6.1 Heterochromatic, Off-Axis, Through-Focus Characteristics

Figure 2.12-17 shows the heterochromatic, geometric-mean, through-focus resolution characteristics of the R-5 lens, based on the 1414 film TM curve at 2:1 contrast. Curves are shown for the 1.05-degree field position, and on-axis for comparison.

2.12-31

~~TOP SECRET~~ GHandle via BYEMAN
Control System Only

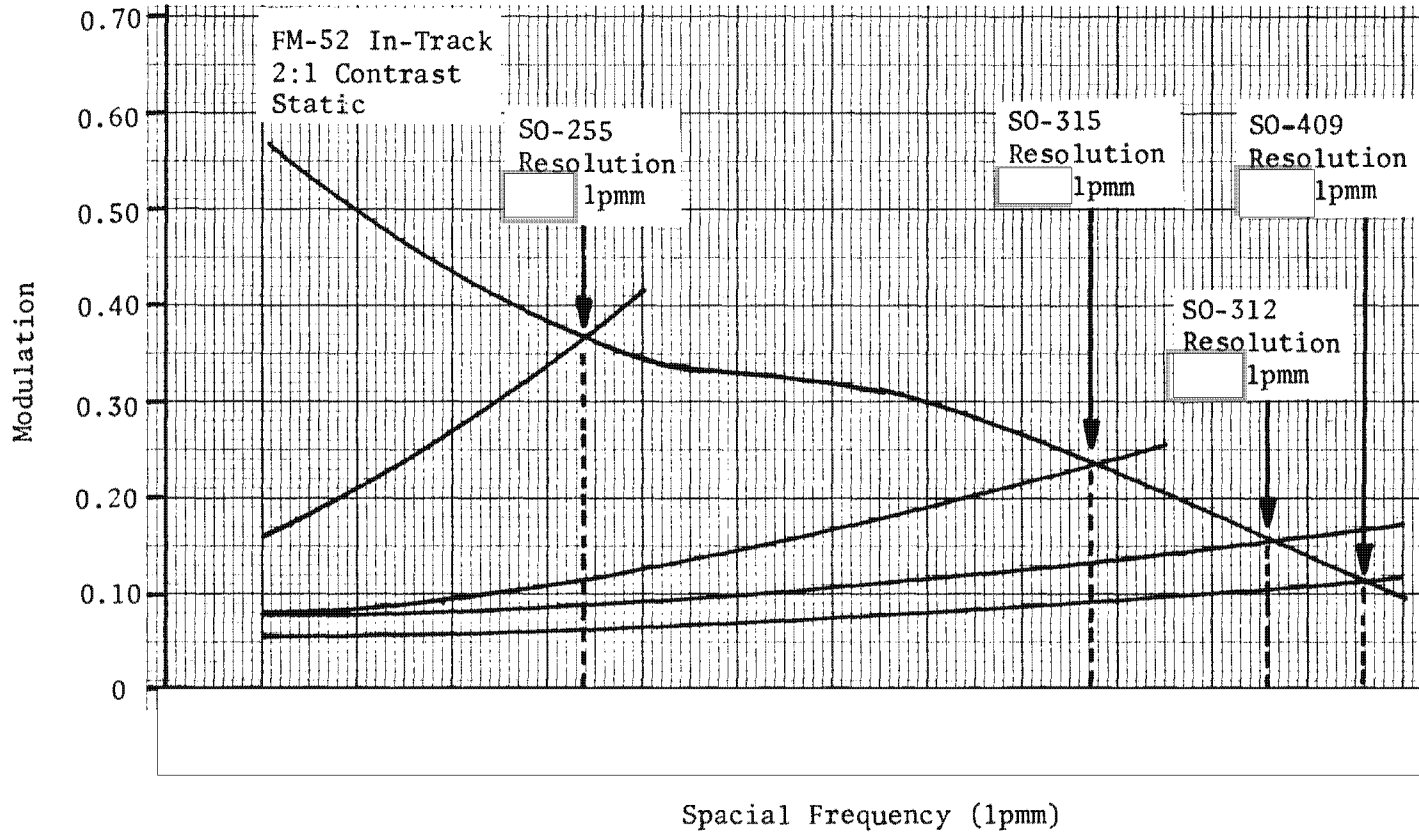


Figure 2.12-16. Limiting Resloution

Approved for Release: 2017/02/14 C05097220

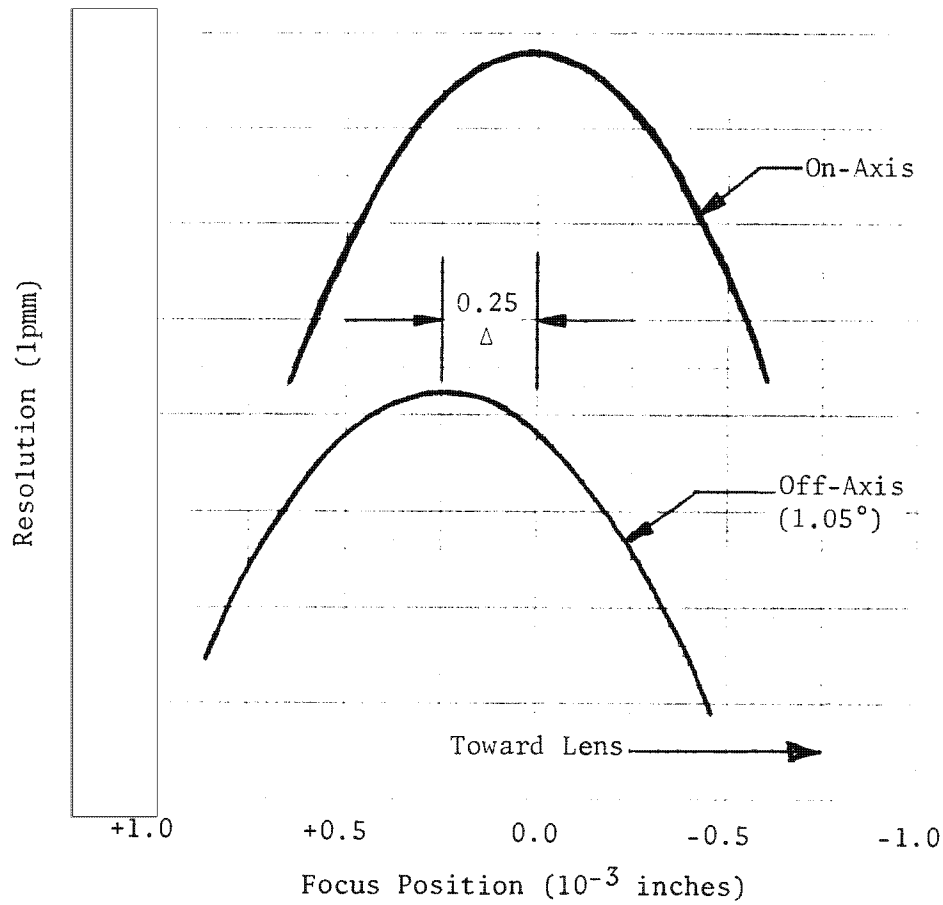
2.12-32

Approved for Release: 2017/02/14 C05097220

~~TOP SECRET~~ G

BIF-008-W-C-019839-RI-80

25X1



Conditions:

85% OQF
 R-5 Formula
 Type 1414 Film
 2:1 Contrast

Δ = Difference between best
 focus on-axis and at
 1.05° field.

Figure 2.12-17. Heterochromatic Off-Axis Through-Focus Curve

2.12-33

~~TOP SECRET~~ G

Handle via BYEMAN
Control System Only

~~TOP SECRET~~ GBIF-008- W-C-019839-RI-80

12.6.2 Monochromatic, Through-Focus Characteristics

Figure 2.12-18 presents monochromatic through-focus curves for four wavelengths between 0.4861 and 0.6869 micrometers. These curves are based on the 1414 TM, on-axis at 2:1 contrast, and illustrate the excellent color correction achieved in the R-5 lens. (Wavelengths not shown are within the stated focus band.)

12.7 Thermally Induced Focus Changes

12.7.1 Isothermal Analysis

The allowance made in the focus budget for isothermal effects of the COA is zero. This assumes that the focus sensor will back out the COA isothermal focus error contributors to within the accuracy/precision indicated by the error budget.

However, should the focus sensor be inoperative, the measured isothermal sensitivity of the optical assembly (average is 20×10^{-5} inches per degree Fahrenheit) could be used to compensate for isothermal changes. If temperature monitoring to 1F is assumed, the expected focus bias is 10×10^{-5} inches.

It should be noted that the static thermal analysis, based on the thermal expansion coefficient of materials used in the lens assembly, is reasonably exact but close correlation with experimental results has not been achieved to date. This occurs because of the variability in the thermal expansion coefficient of optical components. This source of thermal focus sensitivity can be controlled but not passively compensated. Therefore, the thermal sensitivity is measured for each COA and should be recognized for each mission.

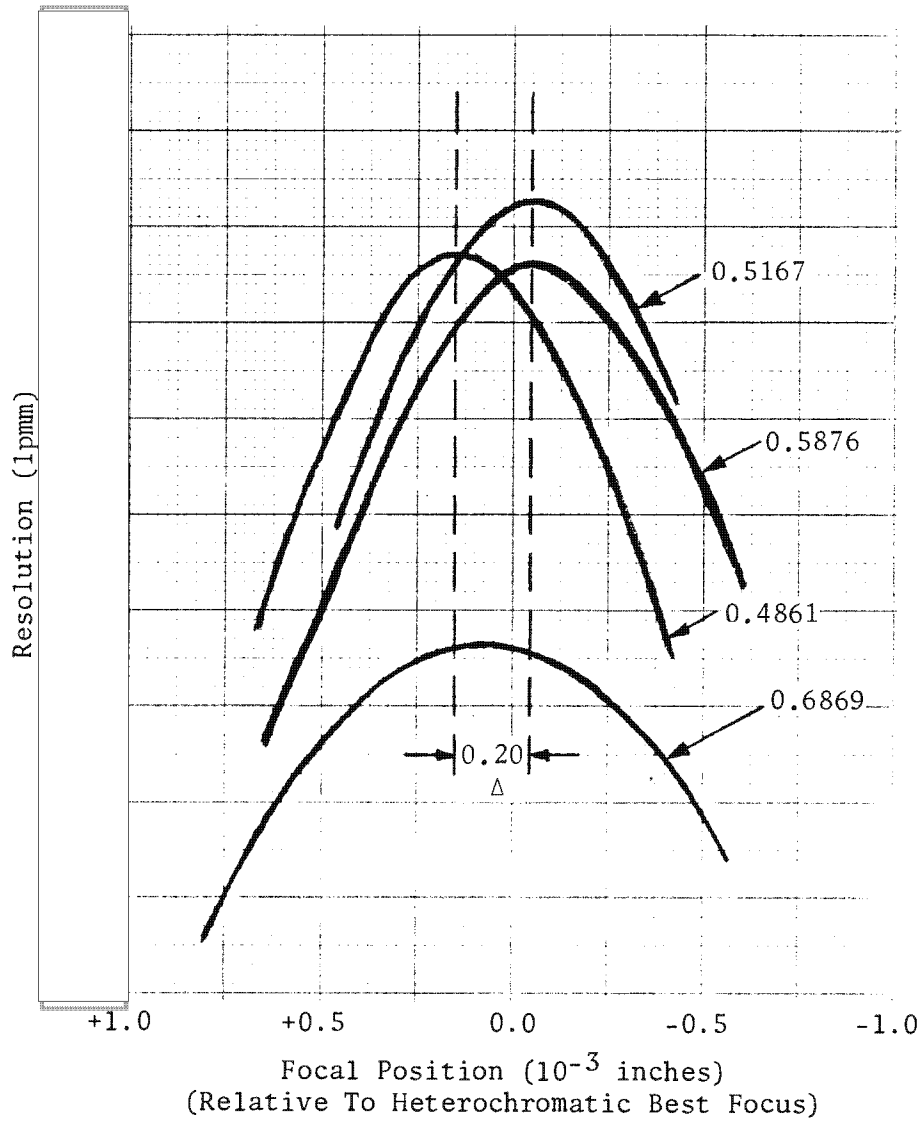
2.12-34

~~TOP SECRET~~ GHandle via BYEMAN
Control System Only

~~TOP SECRET~~ G

BIF-008-W-C-019839-RI-80

25X1



Conditions:

85% OQF
 R-5 Formula
 Type 1414 Film
 2:1 Contrast

Δ = Range of monochromatic best focus for wavelengths between 0.4861 and 0.6869 micrometers

Figure 2.12-18. Monochromatic Through-Focus Curves

2.12-35

~~TOP SECRET~~ G

Handle via BYEMAN
 Control System Only

~~TOP SECRET~~ GBIF-008-W-C-019839-RI-80

In the following analysis, a negative focus shift denotes a shift in a direction away from the Ross corrector. An optical analysis of the thermally induced changes in the figures of the Ross elements and the asphere and element spacings indicates that the residual focus shift is $+12.17 \times 10^{-5}$ inch per degree Fahrenheit. This is based on a primary mirror made from ultra-low expansion (ULE) material ($\alpha = 0.0 \times 10^{-6}$ inch per inch per degree Fahrenheit) and a Ross corrector housing and lens barrel made from Invar ($\alpha = 0.8 \times 10^{-6}$ inch per inch per degree Fahrenheit). A shift of the platen away from the Ross corrector of 2.69×10^{-5} inch per degree Fahrenheit is attainable in the design for the camera. Thus, for an isothermal environment within the allowed temperature range, the design provides focus compensation for the COA to within a residual of $+14.86 \times 10^{-5}$ inch per degree Fahrenheit.

Figure 2.12-19 summarizes the compensation for thermally induced focus shifts of the COA. As noted, the thermal expansion coefficient of Invar in the Ross corrector housing and the lens barrel tend to provide the positive focus-shift contributions to offset the negative contribution of the Ross corrector. The camera and Ross-corrector housing are both positive focus-shift contributors. These contributors move the focus in a direction away from the Ross corrector and require negative focus-shift contributors to account for their expansion.

12.7.2 Transient Thermal Analysis

The ULE substrate material [$\alpha = 0.00 (\pm 0.016) \times 10^{-6}$ inch per inch per degree Fahrenheit] for the stereo mirror has essentially eliminated any time varying focus shifts (approximately 0.00004 inch) produced by the small differential temperatures through the stereo mirror.

Theoretical analysis of the thermal gradients in the Ross corrector and field lens assembly (RCFLA) indicates the resulting focus shift is insignificant.

2.12-36

~~TOP SECRET~~ GHandle via BYEMAN
Control System Only

~~TOP SECRET~~ G

BIF-008- W-C-019839-RI-80

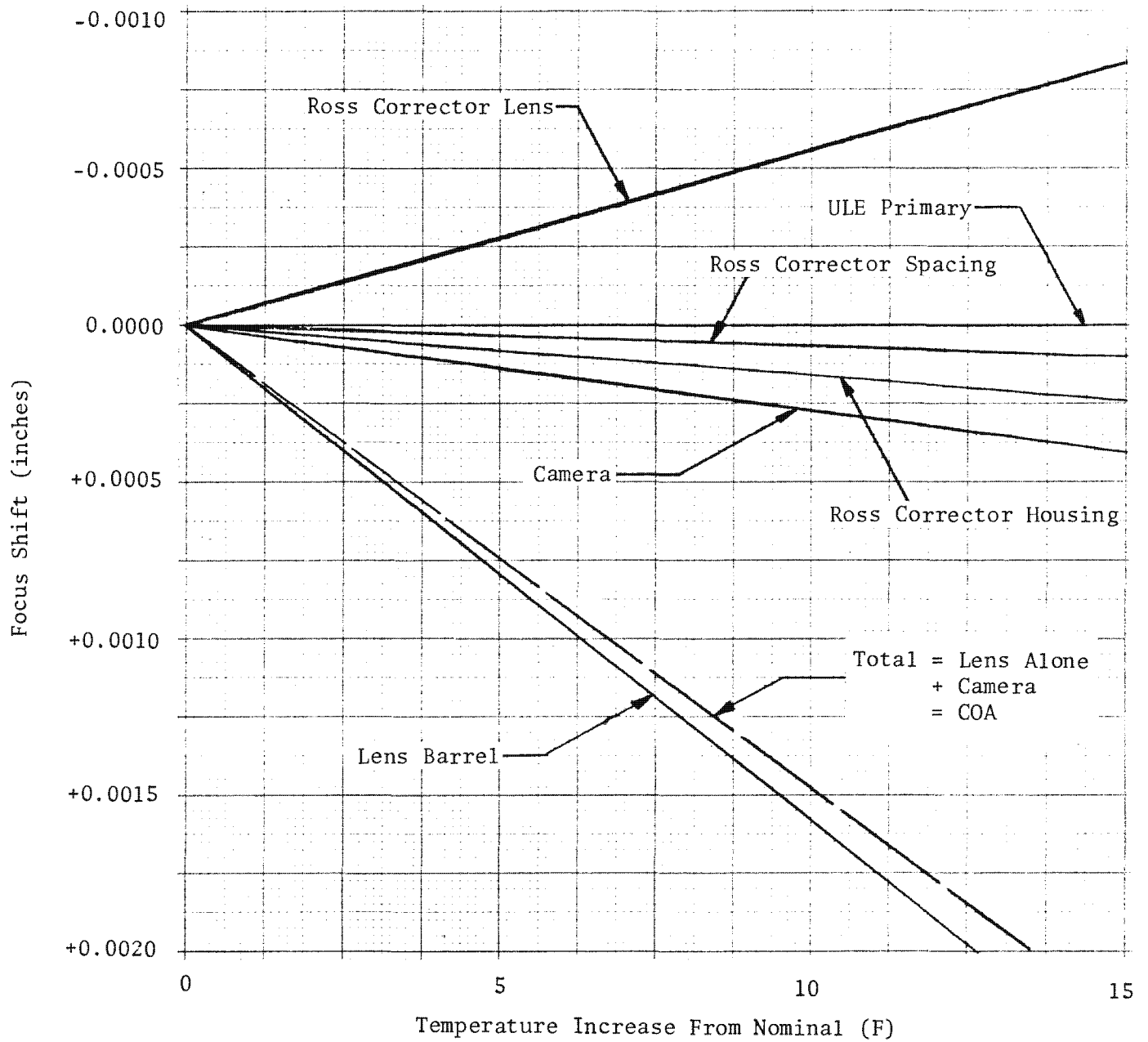


Figure 2.12-19. Thermal Focus Shift

2.12-37

~~TOP SECRET~~ G

Handle via BYEMAN
Control System Only

~~TOP SECRET~~ G

BIF-008-W-C-019839-RI-80

This page intentionally blank

2.12-38

~~TOP SECRET~~ G

Handle via **BYEMAN**
Control System Only

~~TOP SECRET~~ GBIF-008- W-C-019839-RI-80

13.0 VENTING ANALYSIS

During the lifetime of the PPS/DP EAC, it is exposed to ambient pressures from atmospheric to the near-vacuum of space. While being prepared for launch, conditioned air is supplied to a vehicle fitting to maintain temperature and humidity at acceptable levels. Air flow under various conditions has been examined analytically to identify any potential problem areas. Pressure differentials were found to be within the structural capability of the compartments.

13.1 Shipment

The PPS/DP EAC is shipped from the factory to the launch site by cargo aircraft with aircraft pressurization maintained at 8,000 to 10,000 feet. When the aircraft lands at the launch site and the pressure increases to atmospheric, provision must be made to allow air to enter the film supply enclosure (FSE), or an excessively high differential pressure will be developed across the walls of the enclosure.

Two filtered relief valves operate during aircraft descent to allow pressure to equalize while providing for the maintenance of cleanliness within the supply enclosure.

13.2 Venting Model

The requirement for correct ground-conditioning air flow together with adequate ascent venting provisions means that an iterative design analysis

2.13-1

~~TOP SECRET~~ GHandle via BYEMAN
Control System Only

~~TOP SECRET~~ GBIF-008- W-C-019839-RI-80

had to be used. Leakage areas, as determined from leakage tests of representative structures, were used in the analysis. To a large extent, the leakage controls the required vent areas.

Lockheed Missiles and Space Company (LMSC) performed the analysis of the entire PPS/DP EAC-SCS-Titan venting configuration. BIF-008 conducted an independent venting study to establish the PPS/DP EAC venting areas for the LMSC combined venting model. The compartment volumes, vent areas, and diaphragms (bulkheads) are illustrated in Figure 2.13-1 and defined in Table 2.13-1.

The ascent venting analysis was performed using a computer program which has the capability of analyzing interrelated, multivolume configurations. The basic fluid mechanical and thermodynamic considerations programmed into the internal logic include the following:

- (1) Perfect gas fluid
- (2) Nonviscous fluid
- (3) Orifice flow is isentropic/adiabatic
- (4) Chamber conditions assume instantaneous mixing and utilize the energy conservations principal
- (5) All orifices circular and sharp-edged

13.3 Ascent Venting

Provisions have been made to permit all sections of the PPS/DP EAC to vent air during ascent without damage to components, bulkheads, or the structure itself. Electronic boxes (except mirror positioning servos) are not sealed units and therefore vent by natural leakage. The entire PPS/DP EAC vents into the SCS through the Station 285 bulkhead (D₈)

2.13-2

~~TOP SECRET~~ GHandle via BYEMAN
Control System Only

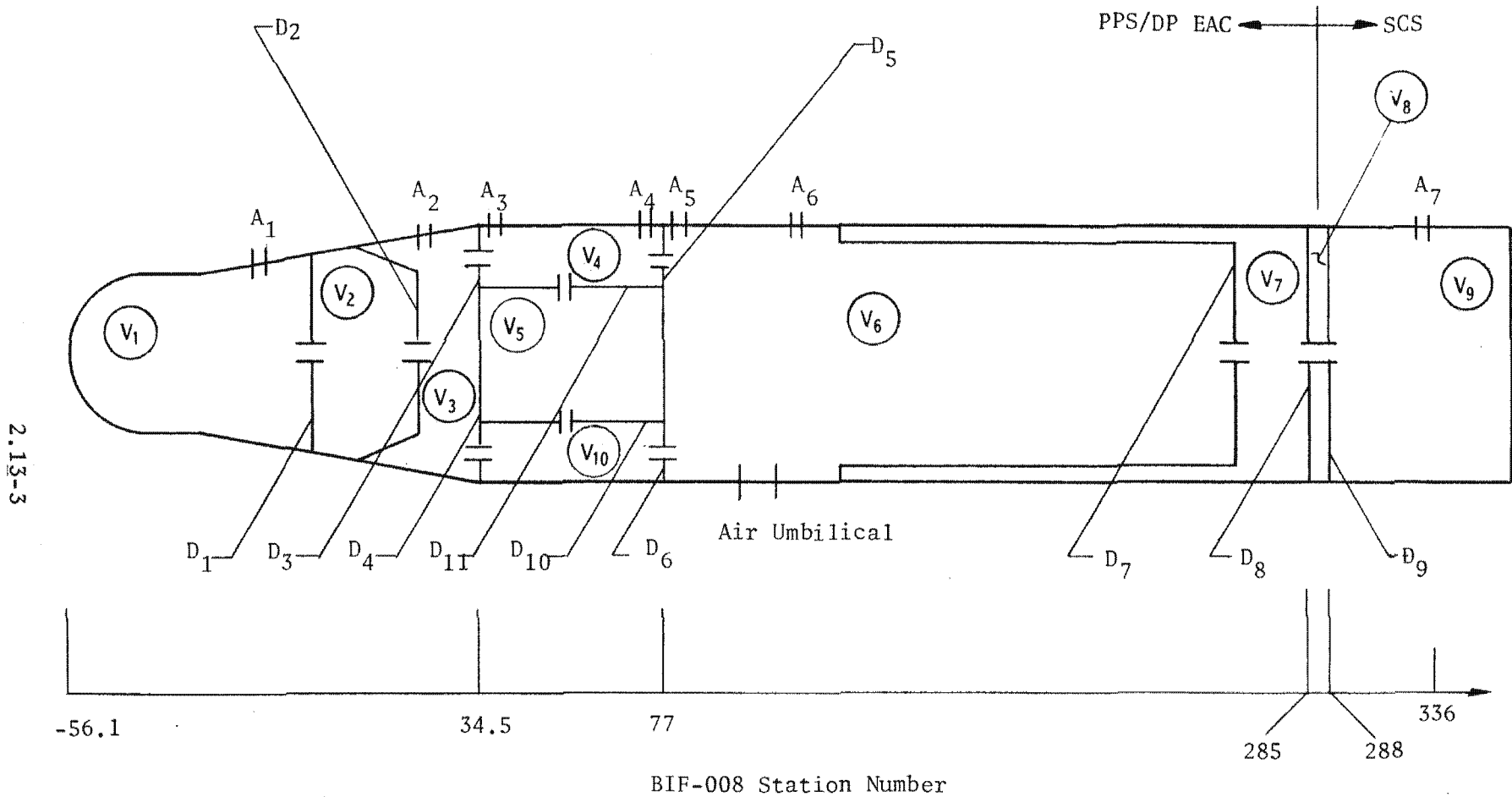


Figure 2.13-1. Venting Model Illustration

Handle via BYEMAN
Control System Only

Approved for Release: 2017/02/14 C05097220

Approved for Release: 2017/02/14 C05097220

2.13-3

TABLE 2.13-1
VENTING MODEL PARAMETERS

Diaphragm No. (D)	BIF-008 Station (In.)	Vent Area (In. ²)	Design Limit (psid)	Vol No. (V)	BIF-008 Station (In.)	Volume (Ft ³)	Vent No. (A)	BIF-008 Station (In.)	Vent Area(In. ²)		
									Min	Nom	Max
D ₁	-6.6	28.0 ± 5%	±0.3	V ₁	-28.25 to -6.6	15.5	A ₁	-16.2	0.0	3.0	6.0
D ₂	4.3/20.85	123.8 ± 5%	±0.5	V ₂	-6.6 to 4.3/20.85	24.0	A ₂	20.8	0.0	3.0	6.0
D ₃	34.5	76.2 ± 5%	±0.2	V ₃	4.3/20.85 to 34.5	29.0	A ₃	34.5	0.0	2.5	5.0
D ₄	34.5	1.57 ± 5%	±0.2	V ₄	34.5 to 77.0	32.0 Max	A ₄	75.8	0.0	2.5	5.0
D ₅	77.0	100.0 ± 10%	±0.2	V ₅	34.5 to 77.0	28.0 Max	A ₅	81.8	0.0	4.0	8.0
D ₆	77.0	10.0 ± 10%	±0.2	V ₆	77 to 149/272	286.8	A ₆	134.8	0.0	2.0	4.0
D ₇	272.0	104.0 to 192.0*	±0.2	V ₇	149/272 to 285	42.0	A ₇	336.0	45.0	47.5	50.0
D ₈	285.0	100.87 ± 2.0	±0.2	V ₈	285 to 288	4.9					
D ₉	288.0	65 - 85	±0.3	V ₉	288 to 354	70.0					
D ₁₀	--	1.6	±0.5	V ₁₀	34.5 to 77	1.2					
D ₁₁	--	2.4 to 3.2	±0.5								

* Aft Flow 138 to 192
Fwd Flow 104 to 151

2.13-4

Approved for Release: 2017/02/14 C05097220

Approved for Release: 2017/02/14 C05097220

Handle via **BYEMAN**
Control System Only

~~TOP SECRET~~ GBIF-008- W-C-019839-RI-80

The film path enclosure (volume V_5 , Figure 2.13-1) is a sealed system which is vented by six poppet valves (cracking pressure 0.29 psid). Analyses were performed for the case of one valve not operating as well as with all valves operating. The results of these analyses are presented in Table 2.13-2.

Air which is contained among the layers of the multilayer aluminized Mylar insulation must be vented rapidly enough during ascent to prevent excessive ballooning of the blanket and possible reduction of its usefulness. Additionally, interlayer pressures must be close to ambient during orbit to prevent gaseous conduction from reducing the insulating value of the blanket. Holes, 0.050-inch diameter, spaced on 3-inch centers, are used to allow trapped air to escape in a controlled manner from the space between the layers of the insulation blanket.

13.4 Conditioned Air Flow

During the time the PPS/DP EAC is in the launch configuration, it is enclosed in a clean room area that is maintained at a slight positive pressure with respect to ambient. Conditioned air is supplied to the vehicle through the air umbilical (see Figure 2.13-1) at a rate sufficient to meet the flow requirements from the PPS/DP EAC to the SCS through the 285 bulkhead. Conditioned air should exhaust from the vehicle into the clean room when access panels are removed. Under some combinations of clean room pressure and conditioned air delivery rate, air may be forced from the clean room into the vehicle. Figure 2.13-2 shows the combinations necessary to avoid flow of air from the clean room into the vehicle. The figure is based on an analysis of clean room pressurization and flow of conditioned air into the vehicle which

2.13-5

~~TOP SECRET~~ GHandle via BYEMAN
Control System Only

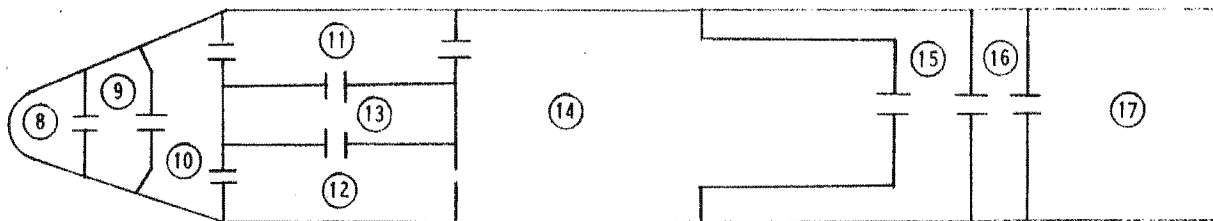
TABLE 2.13-2

MAXIMUM DIFFERENTIAL PRESSURES

Diaphragm	$P_9 - P_8$ (D ₁)	$P_{10} - P_9$ (D ₂)	$P_{11} - P_{10}$ (D ₃)	$P_{12} - P_{10}$ —	$P_{13} - P_{10}$ (D ₄)	$P_{13} - P_{11}$ (D ₁₁)	$P_{13} - P_{12}$ (D ₁₀)	$P_{14} - P_{11}$ (D ₅)	$P_{14} - P_{12}$ (D ₆)	$P_{14} - P_{13}$ —	$P_{15} - P_{14}$ (D ₇)	$P_{16} - P_{15}$ (D ₈)	$P_{17} - P_{16}$ (D ₉)
Allowable (psid)	±0.3	±0.5	±0.2	±0.2	±0.5	±0.5	±0.5	±0.2	±0.2	±0.5	±0.2	±0.2	±0.3
Maximum Calculated (psid)	-0.116	-0.019	-0.026	-0.035	0.458* 0.469**	0.454* 0.465**	0.452* 0.463**	0.027	-0.017	-0.467* -0.478**	-0.033	-0.035	-0.065

*All Valves Operating ** One Valve Inoperative

Circled Numbers Designate Volumes Between Which Differential Pressures Are Calculated



Handle via BYEMAN
Control System Only

Approved for Release: 2017/02/14 C05097220

2.13-6

Approved for Release: 2017/02/14 C05097220

~~TOP SECRET~~ G

BIF-008- W-C-019839-RI-80

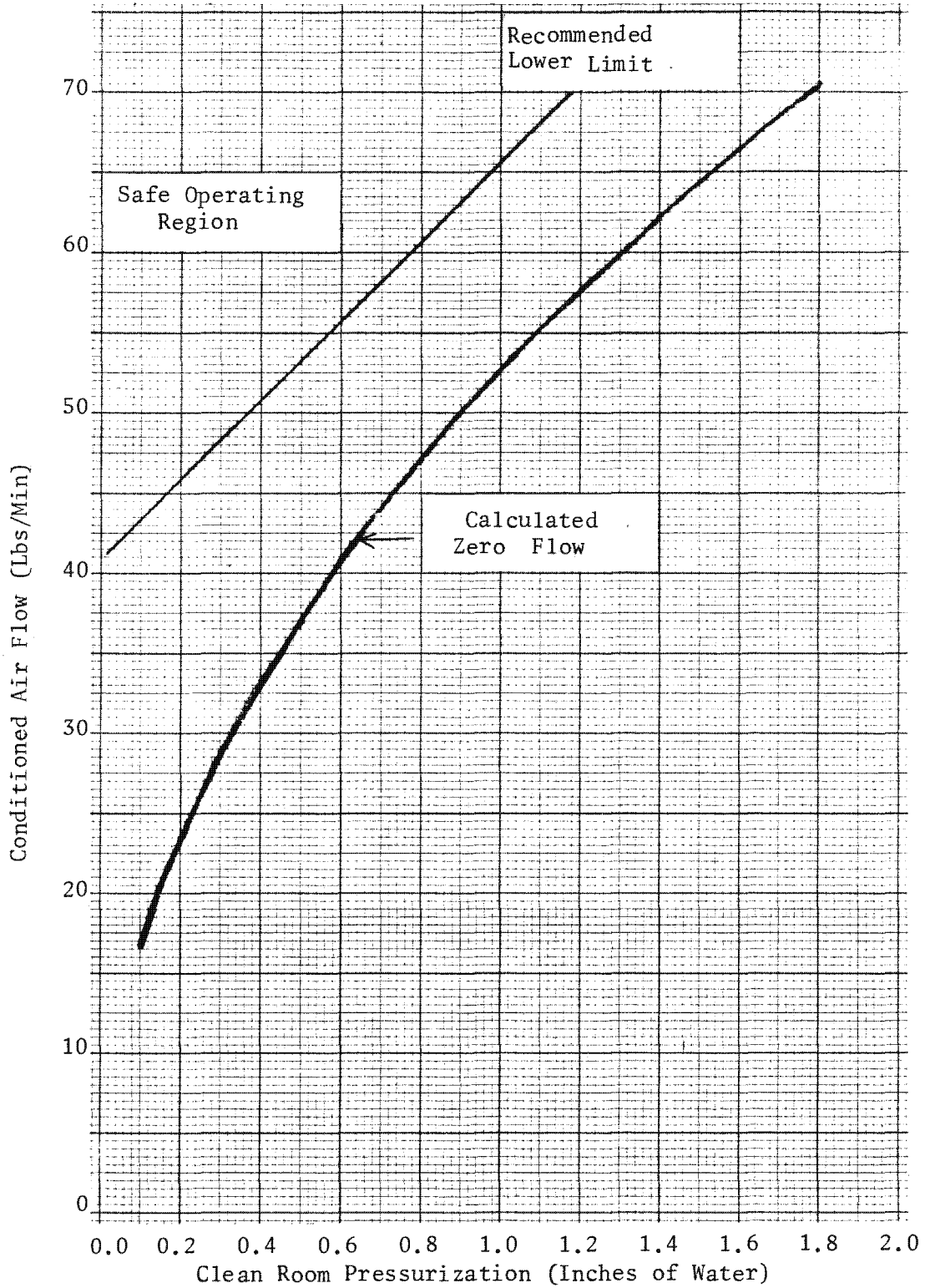


Figure 2.13-2. Recommended Operating Limits for Clean Room

2.13-7

~~TOP SECRET~~ G

Handle via BYEMAN
Control System Only

~~TOP SECRET~~ G

BIF-008-W-C-019839-RI-80

would insure an outward flow of air from the vehicle into the clean room. The baseline chosen was zero exchange of air between vehicle and clean room, with a discharge area large enough so as not to be a limiting factor.

The recommended lower limit is based on maintaining the same margin established between test results for zero flow on an early B² vehicle and the limit established for that series of vehicles.

2.13-8

~~TOP SECRET~~ G

Handle via BYEMAN
Control System Only

~~TOP SECRET~~ GBIF-008- W-C-019839-RI-80

14.0 THERMAL ANALYSIS

Continuous control of the PPS/DP EAC internal environment is essential from initial fabrication through recovery of the exposed flight film. Precise optical surfaces, close-tolerance moving parts, and film all must be protected from the degrading effects of out-of-tolerance levels of temperature and humidity, and excessive amounts of particulate contamination.

In general, achievement of optimum PPS/DP EAC performance requires temperature conditioning of the optical system to 65 to 75F prior to launch, and maintenance within this temperature range on orbit. It is a system requirement that thermal control be accomplished by passive means where practical. In addition, film temperatures and temperatures of electronic boxes must be maintained within prescribed ranges.

A discussion of the results of thermal analyses of the various phases of PPS/DP EAC operation follows. A description of the hardware associated with PPS/DP EAC thermal control is contained in Part 3, Section 8.

14.1 Prelaunch

The thermal analysis of FO-7 prelaunch conditions considers ambient temperature extremes of 24F and 98F, the launch site three-sigma temperature limits.

2.14-1

~~TOP SECRET~~ GHandle via **BYEMAN**
Control System Only

~~TOP SECRET~~ GBIF-008- W-C-019839-RI-80

14.1.1 Cold Environment

A thermostatically controlled ground heater tape system is provided on the film supply enclosure (FSE) and dual recovery module (DRM) film path components to provide protection against high relative humidity and condensation for the cold launch site environment.

The heaters maintain the enclosed film path above 60F, permitting exposure to a cold ambient environment for the required six hours. As a result of the heating of the film enclosure, all supply electronics module (SEM) electronic components are maintained above their lower 30F limits.

An analysis was conducted, using a model of a portion of the SEM-FSE area, to determine the cool-down characteristics of the FSE enclosure under conditions of ground heater failure. The FSE panel having the fewest stiffeners and, therefore, the fastest response was selected for analysis. While the FSE heaters were considered to be OFF, the camera optics module (COM) heaters were assumed to be ON, maintaining the COM at 65F.

The response shown in Figure 2.14-1 is that predicted for a 65F isothermal SEM exposed to a 24F environment at time zero. The response demonstrates that FSE ground heaters are required to allow exposure to the cold environment for extended periods.

2.14-2

~~TOP SECRET~~ GHandle via BYEMAN
Control System Only

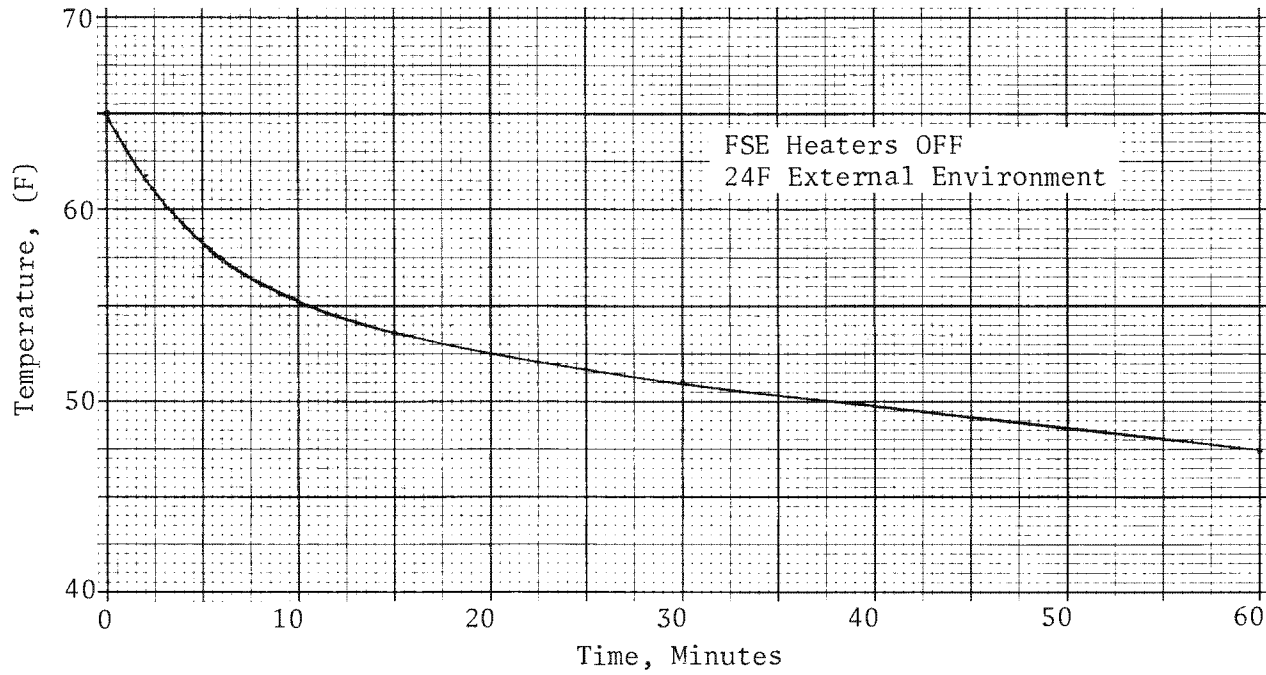


Figure 2.14-1. Time vs Temperature, +Z FSE Panel

~~TOP SECRET~~ GBIF-008- W-C-019839-RI-80

The following equation may be used to predict cool-down curves for other conditions of initial SEM temperature and environment temperature.

$$T_{FSE} = a_1 e^{-A_1 \theta} + a_2 e^{-A_2 \theta} + T_{\infty}$$

where: $a_1 = \frac{[T_0 - T_{\infty}]}{[1 + b]}$

$$a_2 = a_1 \times b$$

and: $A_1 = \text{constant} = 10.8$

$$A_2 = \text{constant} = 0.28$$

$$b = \text{constant} = 3.1$$

$$T_0 = \text{initial SEM temperature, degrees Fahrenheit}$$

$$T_{\infty} = \text{environmental temperature, degrees Fahrenheit}$$

$$T_{FSE} = \text{FSE panel temperature at time } \theta, \text{ degrees Fahrenheit}$$

$$\theta = \text{exposure time, hours}$$

14.1.2 Hot Environment

The 98F hot launch site environment is considered in conjunction with the operation of all internal components. All components are calculated not to exceed 100F following a six-hour exposure to the environment, with the exception of the 5-inch travel viewer box in the ejectable adapter (EA), its temperature being 130F. The analysis is considered to be conservative in that the solar vector is maintained directly on the minus Z-axis for the entire six-hour period.

2.14-4

~~TOP SECRET~~ GHandle via **BYEMAN**
Control System Only

~~TOP SECRET~~ G

BIF-008-W-C-019839-RI-80

Since film in the travel viewer box cannot be used for photography, only physical sticking of film to the roller must be considered. The predicted 130F roller temperature is not considered a problem since the film used does not exhibit undesirable effects at that temperature.*

In PPS/DP EAC prelaunch analysis, results are similar to the results of the FO-7 analysis except for the temperatures predicted for the 5-inch supply and looper assembly. The PPS/DP EAC analysis included the power dissipated by the 5-inch brake which was not included in the FO-7 analysis. The analysis results indicated that the 5-inch supply and looper assembly would exceed its temperature limits in less than one hour. Subsequent review of the PPS/DP EAC model showed that insufficient mass was included in the area of the 5-inch supply and the indicated heating response is not realistic. Actual operational response also supports this assessment.

14.2 Ascent

The ascent environment is established by the selected trajectory. As the duration of the ascent heat pulse is not long, the thermal capacity of the skins, substructure, and internal components, together with internal conduction and radiation isolation, provide acceptable temperatures.

14.2.1 Design Requirements

The following design requirements apply to the ascent phase:

- (1) Skin temperatures must be limited to 500F maximum due to a restriction imposed by the aluminum foil tape used as an external finish. PPS/DP EAC operation requires a maximum skin temperature limit of 400F due to titanium foil restrictions.

*Reference BIF-008-W-C-003842-KH-74, Temperature Monitoring of 5-Inch Take-Up Travel Viewer Box.

~~TOP SECRET~~ G

~~TOP SECRET~~ GBIF-008- W-C-019839-RI-80

- (2) Pinpuller temperatures must be maintained below qualification limits.
- (3) Temperatures of internal components must be maintained within requirements as shown in the Environmental Design Criteria Specification (BIF-008 document 1402-320) and appropriate component specifications.

14.2.2 Design Predictions

The maximum predicted skin temperatures for the ascent phase are presented as a function of station number in Figures 2.14-2 and 2.14-3. Both the highest and lowest values of peak skin temperatures (function of body angle) occurring at each station are shown on the figure. Ample skin temperature margin is demonstrated.

The predicted ascent pinpuller temperatures for the windward side pinpullers (SRV 1/EA and EA/FA separation joints) are shown in Figure 2.14-4. A maximum predicted temperature of 169F, exceeding the 160F qualification temperature, is shown for the EA/FA pinpuller. This condition is judged to be acceptable based on the results of a confidence test during which several squibs were successfully fired following exposure to a 300F environment. Predicted PPS/DP EAC configuration pinpuller temperatures meet their qualification requirements.

Analysis of the forward barrel main hatch pinpullers shows that they, like the SRV 1/EA pinpullers, are greatly isolated from the external skin and do not approach the qualification temperature.

SEM component temperatures have been calculated not to exceed operating temperatures for lift-off temperatures of 80F or less. For lift-off temperatures greater than 80F, and ascent in a worst-case trajectory, non-operating component temperature limits are not exceeded; however, operating temperatures of all components may not be achieved until the end of the first revolution.

2.14-6

~~TOP SECRET~~ GHandle via BYEMAN
Control System Only

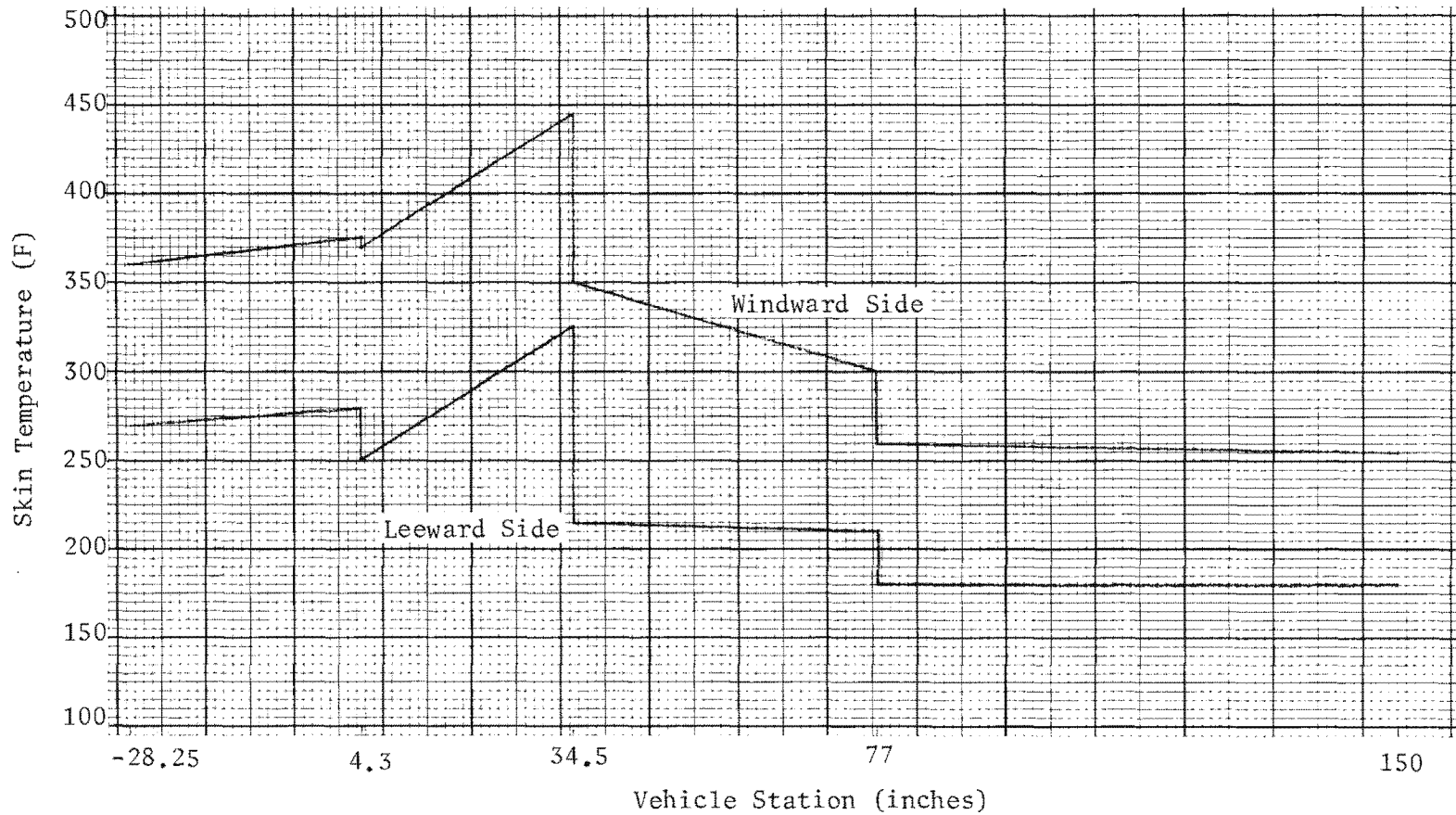


Figure 2.14-2. Ascent Maximum Longitudinal Skin Temperature Distribution

Handle via **BYEMAN**
Control System Only

Approved for Release: 2017/02/14 C05097220

2.14-7

Approved for Release: 2017/02/14 C05097220

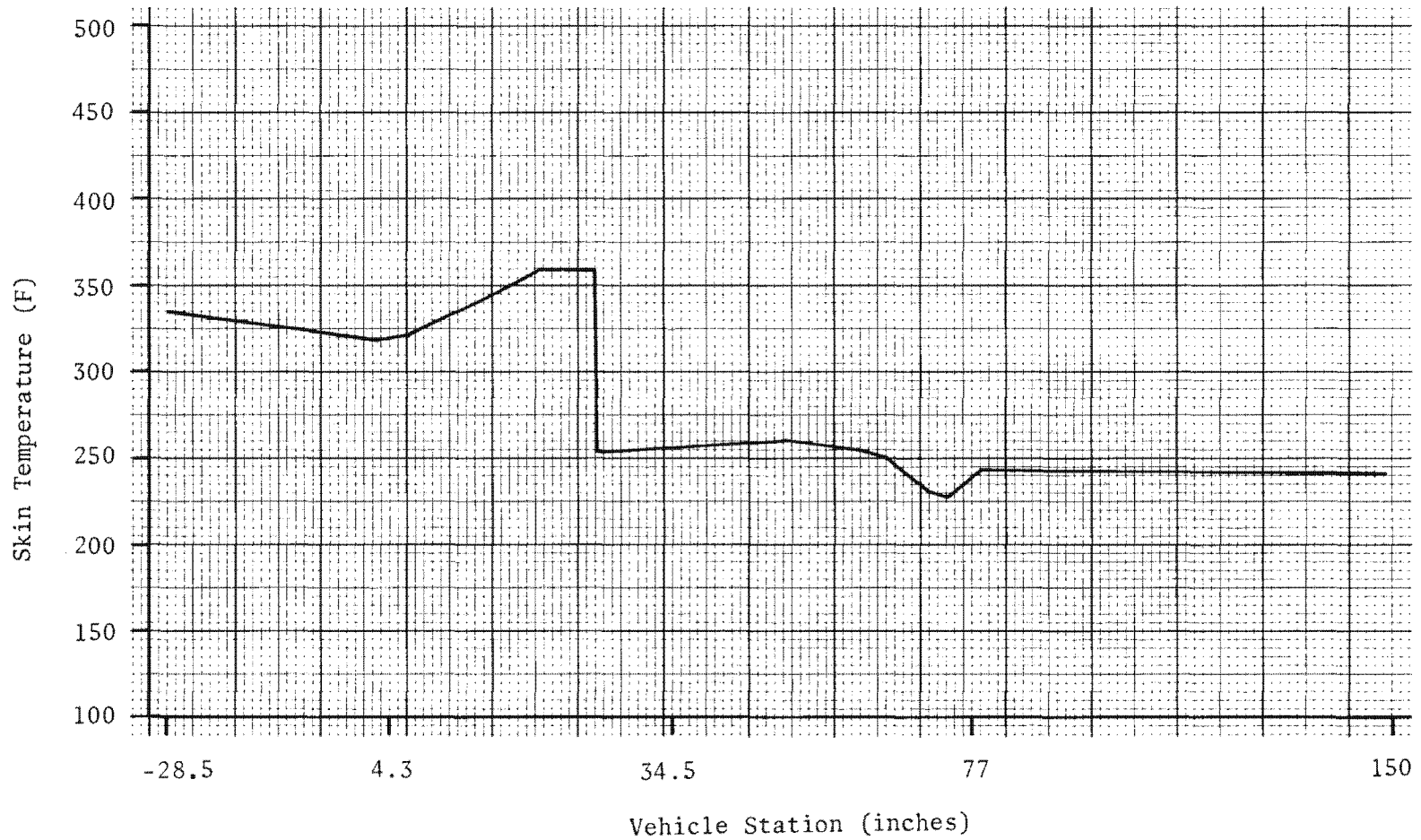


Figure 2.14-3. Ascent Maximum Longitudinal Skin Temperature Distribution
EAC Finish Patterns

Handle via BYEMAN
Control System Only

Approved for Release: 2017/02/14 C05097220

2.14-8

Approved for Release: 2017/02/14 C05097220

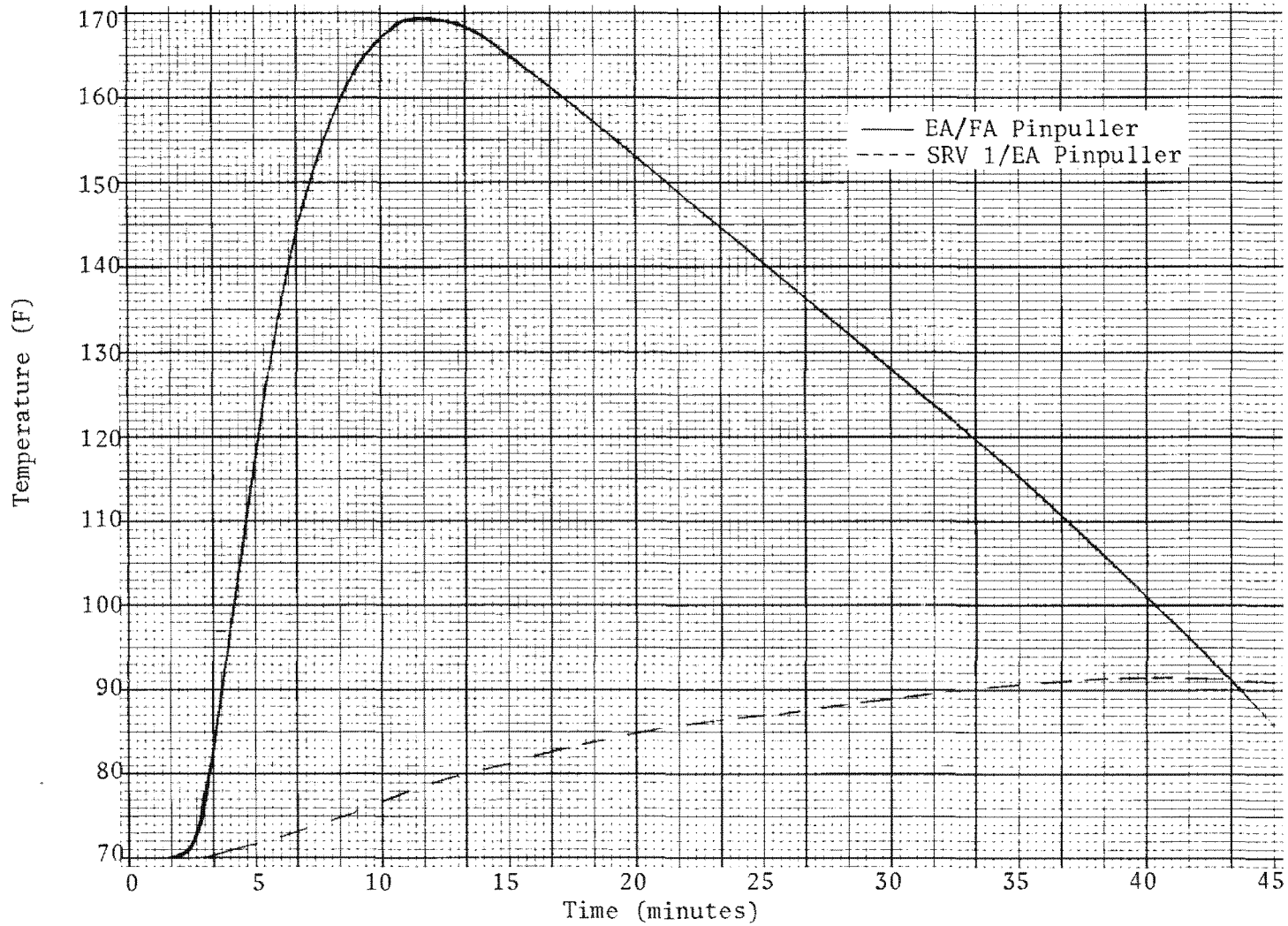


Figure 2.14-4. Ascent Pinpuller Temperatures

Handle via BYEMAN
Control System Only

Approved for Release: 2017/02/14 C05097220

2.14-9

Approved for Release: 2017/02/14 C05097220

~~TOP SECRET~~ GBIF-008- W-C-019839-RI-8014.3 Orbital

14.3.1 Design Parameters

Thermal design for orbital conditions is based on the following design parameter cases:

Case A

- (1) Beta angle, defined as the angle between the earth-sun line and its projection on the orbit plane, may vary from plus sixty to minus sixty degrees. Optimization for the plus sixteen to minus four-degree (sun-synchronous) range of beta angles is also required.
- (2) Minimum altitudes may range from 65 to 85 nautical miles.
- (3) Apogee altitudes may range from 175 to 300 nautical miles.

Case B

- (1) Beta angle may vary from plus forty to minus forty degrees with COM optimization available for zero to plus forty or zero to minus forty degrees.
- (2) Altitude ranges include low-mode elliptical orbits with minimum altitudes of 68 to 85 nmi with apogees of 175 to 270 nmi, respectively and high-mode circular orbits having altitudes from 300 to 500 nmi.

In addition, it is assumed that the vehicle is returned to the 0-degree roll position for the inactive portion of a revolution and that telemetry usage is restricted to PPS/DP EAC operations and station contacts.

A solar constant of 130 watts/sq ft nominal is used unless otherwise noted. Aerodynamic heating is calculated using data from U. S. STANDARD ATMOSPHERE 1962 and a 0.9 accommodation coefficient, unless otherwise noted.

14.3.2 Design Requirements

Three groups of PPS/DP EAC components require temperature control: the optics, the films, and the electronics. Of these, the most critical is the optics.

2.14-10

~~TOP SECRET~~ GHandle via **BYEMAN**
Control System Only

~~TOP SECRET~~ GBIF-008- W-C-019839-RI-80

Allowable optics temperatures establish the width of the temperature control range; photographic film properties establish the upper level of the range on the temperature scale. The electronics are designed to fit within the resulting environment.

Thermal control is to be achieved with the use of a minimum of electrical heater power.

14.3.2.1 Optics. Evaluation of the thermal limitations depends on analytical techniques, together with experience. The thermal model test program established the adequacy of the temperature control of the mirrors with the viewport door closed. Analytical techniques, in conjunction with flight data, were used during the Gambit-Cubed (G^3) program to determine mirror response to heat flux through the viewport doors.

The use of low coefficient of expansion (ULE) mirrors has served to reduce the transient thermal effects associated with door-open time. Current flight experience cannot identify any photographic degradation as resulting from extended door-open times, although a defocusing condition does occur. The amount of defocus is a function of the door-open time, has an easily observed effect on best electrical focus (BEF) provided by the focus detection subsystem, and is believed to affect photographic focus in a similar way.

Extremely long door-open times, which would result in a net energy loss, are restricted by operational considerations.

14.3.2.2 Films. Applicable films begin to deteriorate at temperatures above 90F, with an absolute tolerable temperature of 125F. The time-temperature limits for keeping high-resolution aerial negative films in a spooled condition are shown in Figure 2.14-5. This figure shows the keeping limits versus

2.14-11

~~TOP SECRET~~ GHandle via BYEMAN
Control System Only

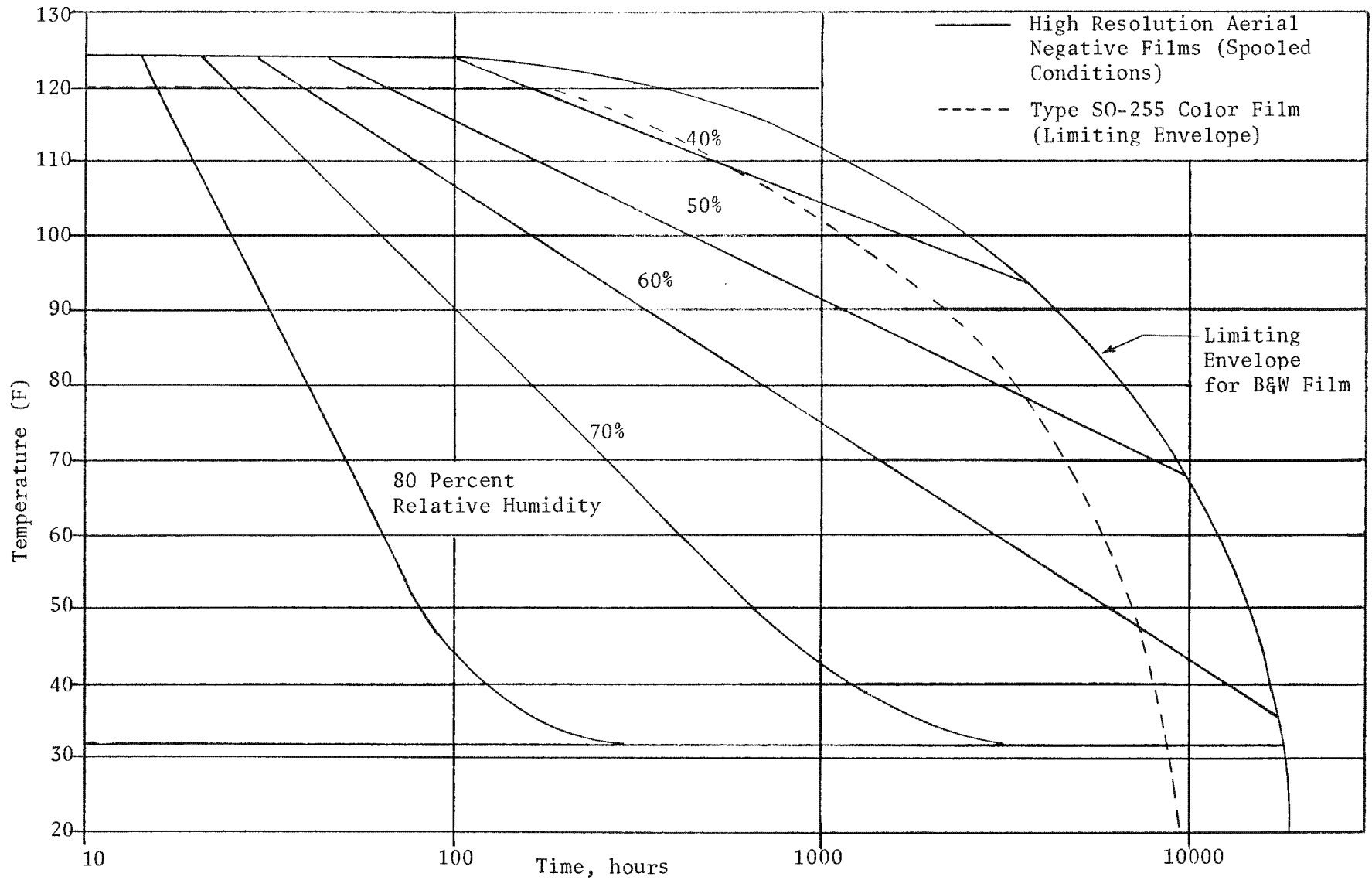


Figure 2.14-5. Film Temperature vs Time Limits

Handle via BYEMAN
Control System Only

Approved for Release: 2017/02/14 C05097220

2.14-12

Approved for Release: 2017/02/14 C05097220

~~TOP SECRET~~ GBIF-008- W-C-019839-RI-80

relative humidity. Also shown are the limiting envelopes which are independent of relative humidity. The 50 percent RH curve is recommended and is used for PPS/DP EAC environmental control purposes. The keeping limits for Type SO-255 Aerial Color Film are less well known than those for black and white aerial films. The dotted line shown in Figure 2.14-5 represents the best estimate of the limiting envelope for Type SO-255. Again, adherence to the 50 percent RH curve for PPS/DP EAC design assures that no degradation due to high temperatures will occur.

The film tolerance for low temperatures is based on the need to avoid condensation of moisture and to maintain mechanical properties. To avoid brittleness, a low temperature limit of 30F was established.

Pressures in the film-handling subsystem are reduced to approximately 0.1mm Hg after ascent, with slow leakage of the residual air permissible. Film-entrapped moisture evaporates as the film is transferred from the supply to the take-up reels. During film transfer, the pressure within the film supply enclosure momentarily increases to approximately 0.25mm Hg. Photographic performance is not degraded because of this effect; however, for a mission containing Type 1414 High Definition Aerial Film, approximately 3.2 pounds of moisture could be lost. A fixed orifice in one wall of the film supply enclosure controls the venting of water vapor from the film transport enclosure.

14.3.2.3 Electronic Boxes. The design of a stable electronics system is vastly simplified if component temperatures are limited to narrow ranges. The design parameters were, therefore, established over the range prescribed by the extremes of the optics and film limits. The sink temperatures for 9 x 5 configuration electronics were consequently established at 30F minimum

2.14-13
~~TOP SECRET~~ GHandle via BYEMAN
Control System Only

~~TOP SECRET~~ GBIF-008- W-C-019839-RI-80

and 110F maximum for most boxes. The maximum sink temperature of several boxes was limited to 100F in order to maintain the 30F minimum and limit the calibration range to 70F. The exception to these temperature ranges is the digital telemetry unit which operates between -20F and +140F.

14.3.3 Orbital Design

Temperatures occurring during orbital flight are a result of the balance between the energy radiated from the PPS/DP EAC and the energy absorbed by the PPS/DP EAC from the various sources of incident energy; i.e., solar radiation, both direct and reflected from the earth, earth emission, and aerodynamic heating. Internal power dissipation, while affecting internal temperatures, does not have any appreciable effect on the skin temperatures which enter into the heat balance. This is due to the low magnitude of the internal power dissipation compared to the magnitudes of the incident and radiated fluxes.

On-orbit temperature control is made as passive as possible through the selection of exterior surface coatings and the use of efficient internal insulation. Coating specifications depend on trade-offs among the constraints of available heater power, orbit beta angle, altitude, and equipment temperature requirements.

14.3.3.1 Dual Recovery Module (DRM) Design. The DRM is temperature-controlled by passive means with the exception of the satellite reentry vehicles (SRVs). Although heater circuits are provided in both SRV 1* and SRV 2, passive control is such as to preclude the use of the SRV 2 heaters during orbital flight.

*SRV 1 internal temperatures and heater power requirements are primarily established by the SRV associate contractor's thermal design.

~~TOP SECRET~~ G

~~TOP SECRET~~ GBIF-008-W-C-019839-RI-80

The DRM skin temperatures depend strongly on altitude [because of the angles of attack (FA = 9 degrees; EA = 15 degrees)] as well as on beta angle. In order to accommodate the full ranges of minimum altitudes and beta angles, three DRM external patterns are required.

Two patterns were developed for Case A use. The first, (Pattern 1A) is designed for the full range of beta angles ($\beta = \pm 60$ degrees) for minimum altitudes of 67 to 85 nautical miles. By restricting beta angle to the plus 16 to minus 4-degree sun synchronous range, this pattern may be used throughout the entire 65 to 85 nautical mile range of minimum altitudes. A second DRM pattern (Pattern 2A) is available to be used over the full range of beta angles ($\beta = \pm 60$ degrees) for minimum altitudes of 65 to 73 nautical miles.

The third pattern (PPS/DP EAC pattern) is designed for use at minimum altitudes of 68 to 85 nmi for elliptical orbits and for 300 to 500 nmi circular orbits. It also accommodates the full range of beta angles from plus forty to minus forty degrees.

All DRM paint patterns are symmetrical about the Z-axis and feature large areas of high-emittance black paint to reject the aerodynamic heating. The PPS/DP EAC pattern also utilizes areas of titanium foil for greater heat retention at increased altitudes.

FA skin temperature predictions shown in Figures 2.14-6, 2.14-7, and 2.14-8 illustrate the effects of minimum altitude and beta angle. The figures show FA skin temperatures at various body angles as a function of orbit position angle; orbit position angle being measured from the subsolar point of the satellite orbit, positive in the direction of satellite motion.

The improved blast shield (IBS), located in the EA, consists of an aluminized fabric shield with a Kapton Multi-Layer Insulation (MLI) blanket affixed to the forward surface. The IBS protects the PPS/DP EAC from contamination by the exhaust gases of SRV 1 at the time of SRV 1 retrofit and also provides protection from the thermal inputs experienced during the second portion of the flight.

2.14-15

~~TOP SECRET~~ GHandle via **BYEMAN**
Control System Only

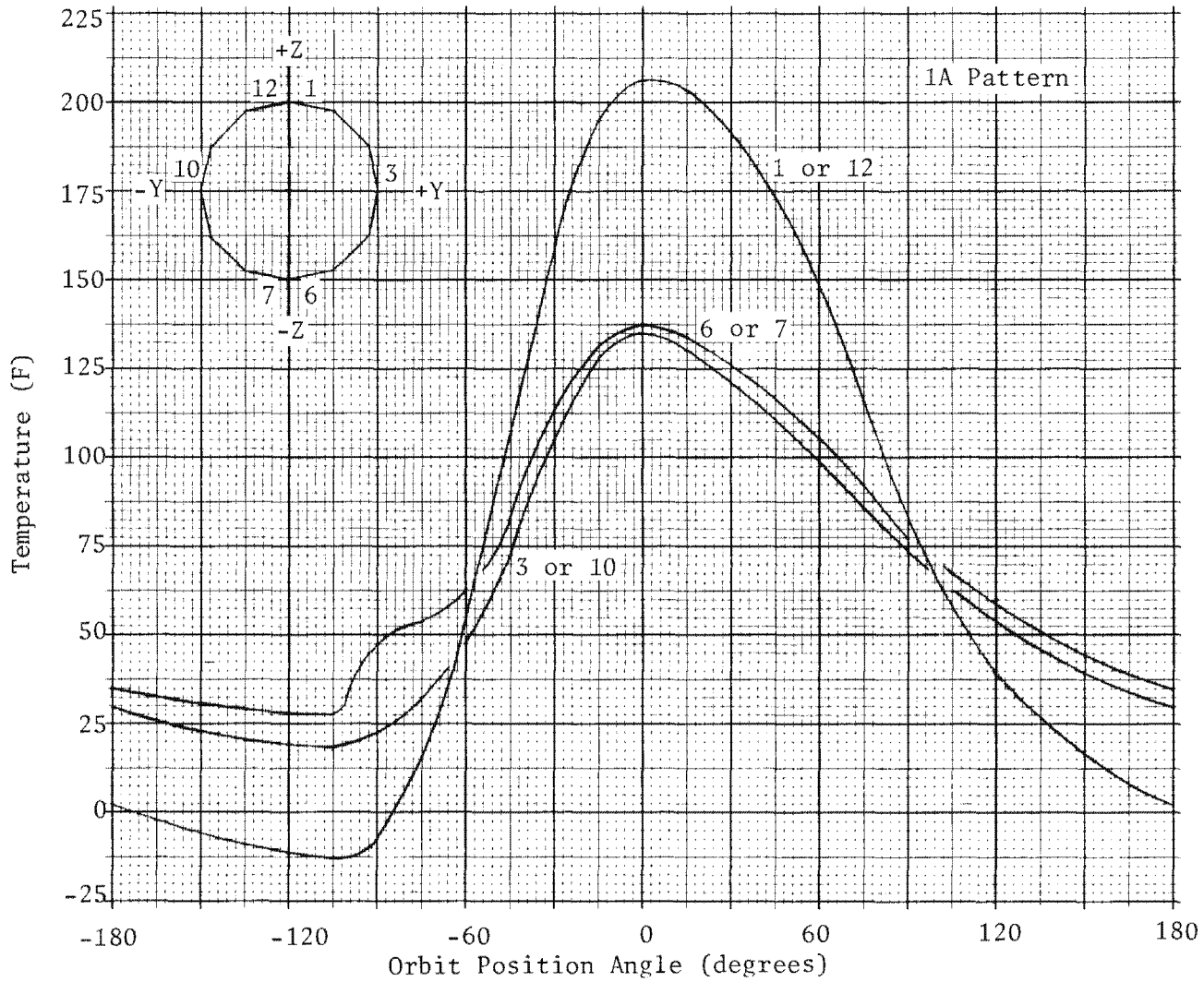


Figure 2.14-6. Fixed Adapter Skin Temperature
Minimum Altitude: 67 nmi; Beta Angle: 0 degree

Handle via BYEMAN
Control System Only



Approved for Release: 2017/02/14 C05097220

2.14-16

Approved for Release: 2017/02/14 C05097220

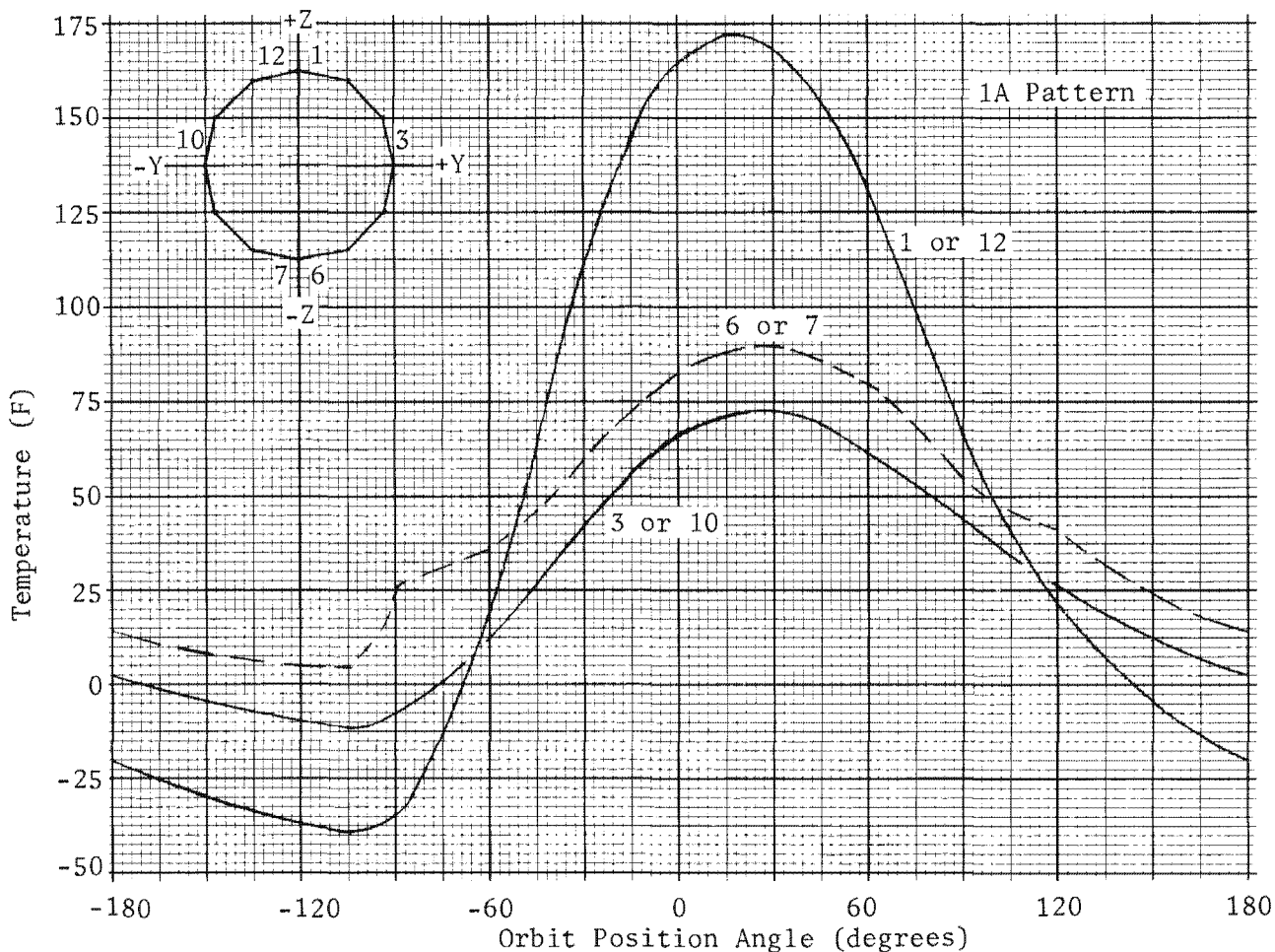


Figure 2.14-7. Fixed Adapter Skin Temperature
Minimum Altitude: 85 nmi; Beta Angle: 0 degree

2.14-17

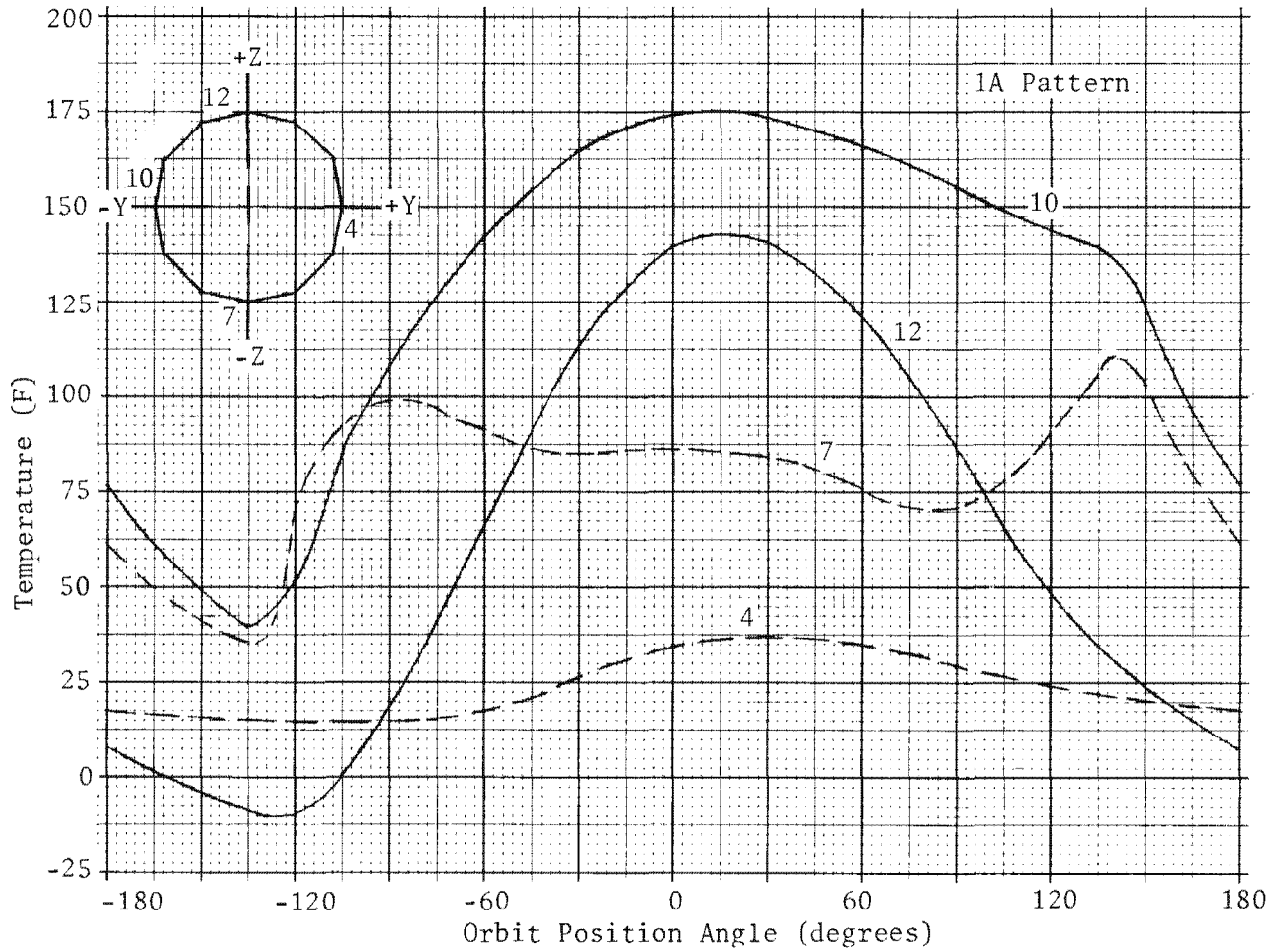


Figure 2.14-8. Fixed Adapter Skin Temperature
Minimum Altitude: 85 nmi; Beta Angle: 60 degrees

Handle via BYEMAN
Control System Only

Approved for Release: 2017/02/14 C05097220

2.14-18

Approved for Release: 2017/02/14 C05097220

~~TOP SECRET~~ GBIF-008- W-C-19839-RI-80

The effectiveness of the IBS in isolating the PPS/DP EAC from the extreme external environment encountered in a 65-nautical mile minimum altitude orbit is illustrated by the predictions shown in Figure 2.14-9. Predicted temperatures of the forward surface of the MLI blanket and the aft (internal) surface of the aluminized fabric are shown in the figure as a function of orbit position.

Passive control techniques employed in the DRM include minimizing the conduction paths between the skins and the interior, providing a low emittance finish on the interior of the EA skin forward of the blast shield to reduce the radiation exchange between the skin and SRV 1 thrust cone and retro-rocket, and the use of MLI blankets on film chutes and film path components. These blankets serve to decouple the chutes from the skins, forcing them to react to an average environment, with some coupling through the interior of the chutes to the film supply enclosure.

14.3.3.2 Supply Electronics Module (SEM) Design. SEM temperatures are controlled entirely by passive means.

Three Case A external finish patterns are provided for the SEM, each encompassing the entire range of minimum altitudes (65 to 85 nautical miles). The basic SEM pattern is designed for the entire range of beta angles, (± 60 degrees). A second pattern, a modification of the basic pattern, is provided for beta angles of ± 48 degrees. A sun-synchronous SEM pattern is optimized for the plus 16-degree to minus 4-degree range of beta angles.

A single PPS/DP EAC pattern was designed for the complete orbital boundaries as defined by PPS/DP EAC Case B parameters.

The basic SEM pattern is symmetrical about the Z-axis. Low absorptivity/low emittance materials are used on the vehicle sides to attenuate temperature extremes caused by high-energy impingement on the sunlit vehicle side, and to prevent excessively low temperatures on the shaded side in orbits with high beta angles. The orbit average incident heat fluxes for a cylindrical section

~~TOP SECRET~~ G

~~TOP SECRET~~ G

BIF-008- W-C-019839-RI-80

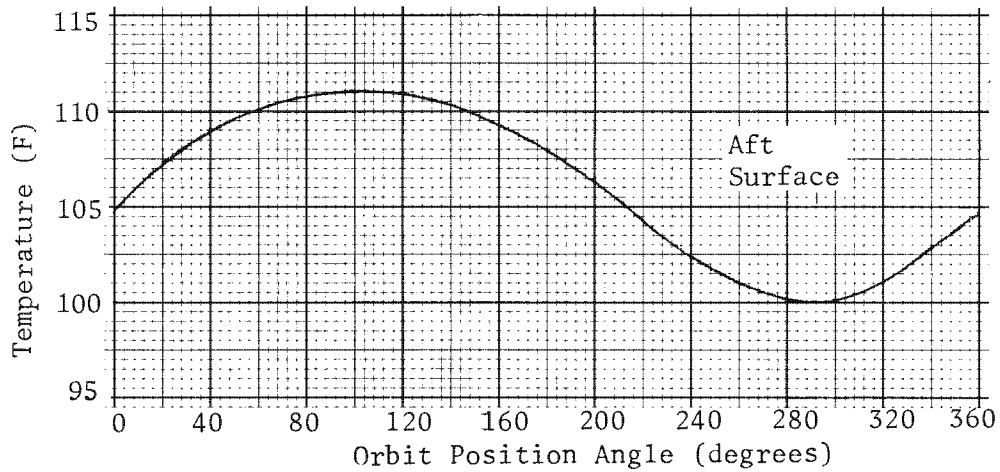
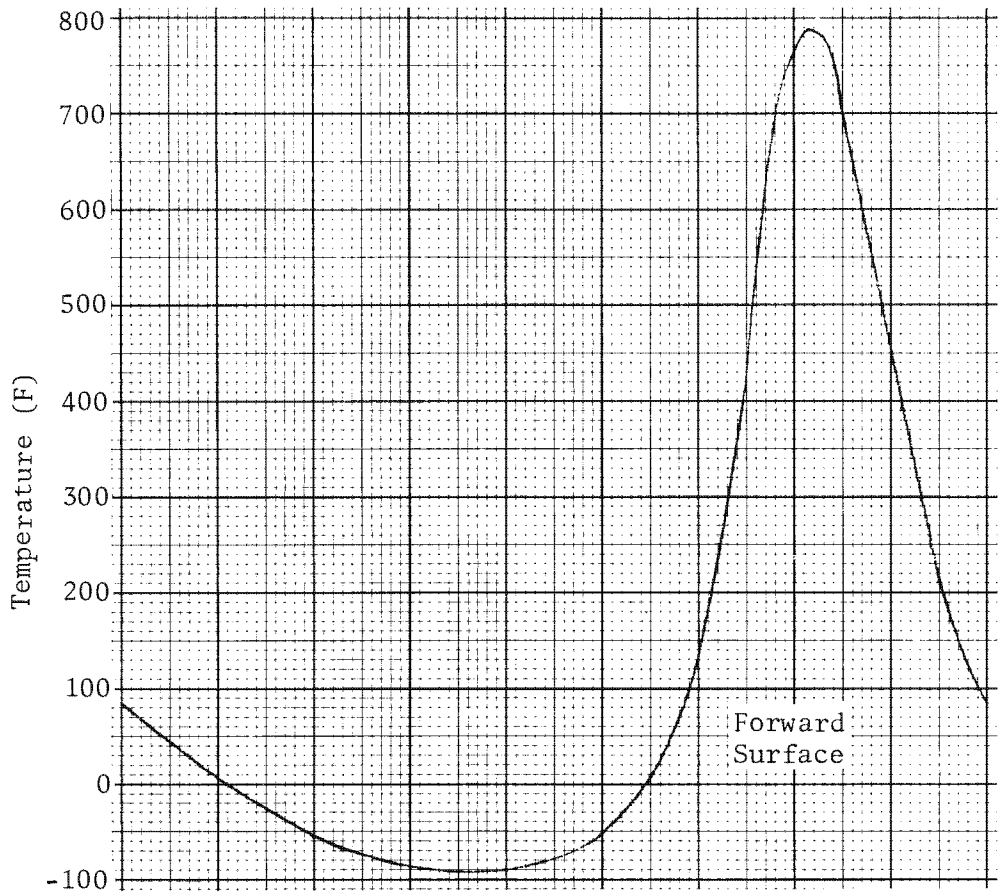


Figure 2.14-9. IBS Blanket Temperature
Minimum Altitude 65 nmi

2.14-20

~~TOP SECRET~~ G

Handle via BYEMAN
Control System Only

~~TOP SECRET~~ G BIF-008-W-C-019839-RI-80

are illustrated as functions of vehicle body angle in Figure 2.14-10 for beta angles of 0 degree and plus 60 degrees. Predicted SEM orbit average skin temperatures for the basic SEM pattern at beta angles of 0 degree and plus 60 degrees are shown in Figure 2.14-11.

To force internal components to react to their local average environmental temperature (time and space average) rather than to the rapid changes of skin temperature (function of time), components are thermally decoupled from the skins. The film supply is centrally located in the SEM and forced to react to the average (time-space average) SEM skin temperature. A low emittance bulkhead is provided between the SEM and DRM to isolate the SEM from the variations of DRM temperatures which occur as a result of aerodynamic heating.

The SEM is isolated from the camera optics module (COM) by MLI blankets which are part of the COM. To avoid a net heat transfer from the SEM to the COM through the skins and film tunnel, the SEM average temperature at hot orbital conditions is maintained below 65F, the COM heater set-point. Should the SEM temperature exceed the COM temperature, undesirable longitudinal temperature gradients would be established in the COM. To prevent excessive heat losses from the COM to the SEM, the SEM temperature is maintained as close to the 65F upper limit as possible.

14.3.3.3 Camera Optics Module (COM) Design. The design approach for selecting the COM external finish included the following:

- (1) dividing the vehicle into twelve 30-degree facets parallel to the vehicle X-axis.
- (2) computation of total incident heat flux on each facet for the worst-case combinations of orbital parameters.
- (3) selection of an external finish which, when exposed to the previously computed fluxes, would produce average skin temperatures and circumferential temperatures

2.14-21

~~TOP SECRET~~ G Handle via BYEMAN
Control System Only

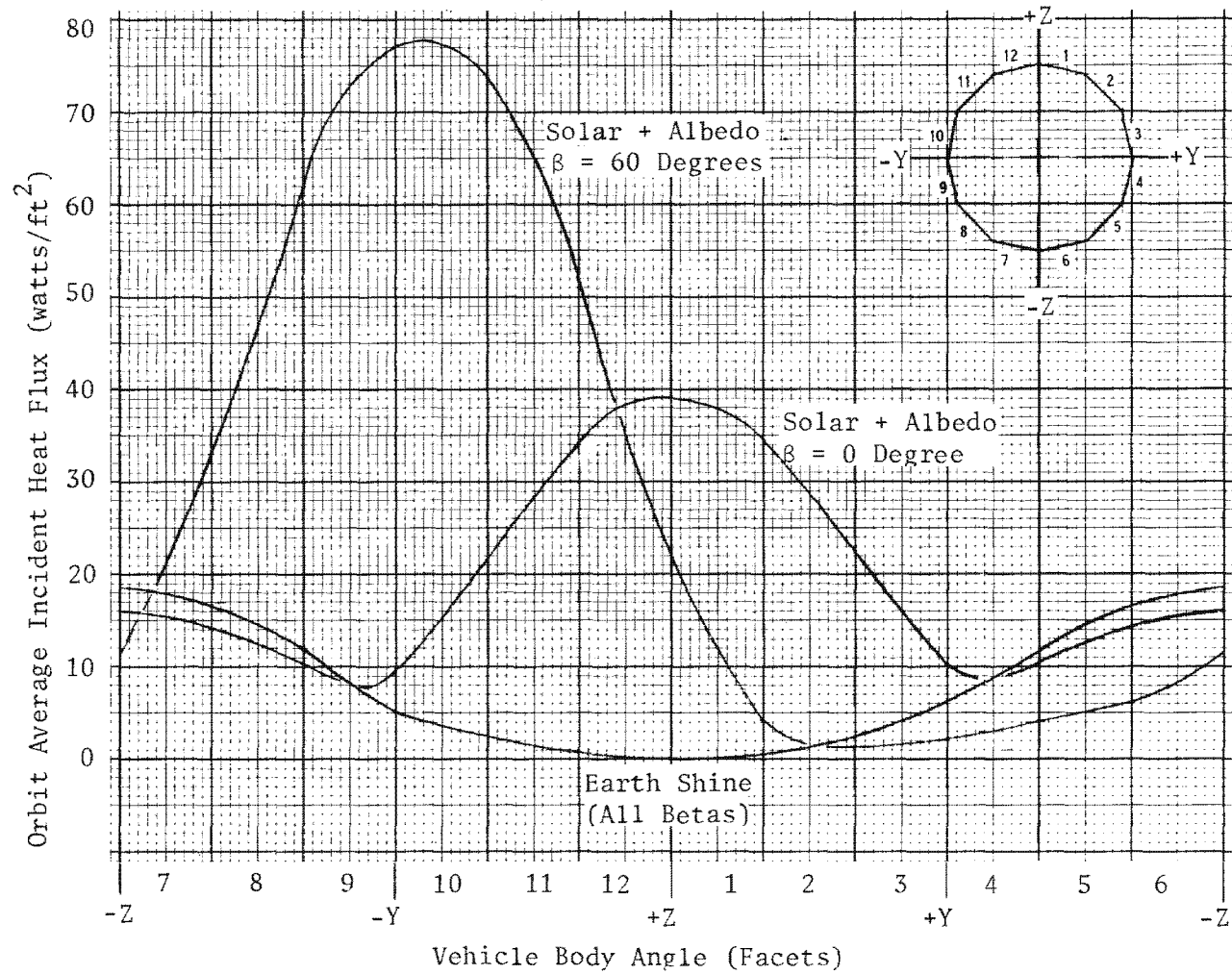


Figure 2.14-10. Orbit Average Heat Fluxes, Cylindrical Section

Handle via BYEMAN
Control System Only

2.14-22

Approved for Release: 2017/02/14 C05097220

Approved for Release: 2017/02/14 C05097220

~~TOP SECRET~~ G

BIF-008-W-C-019839-RI-80

Conditions:

Minimum Altitude = 85 nmi

Low Equipment Power

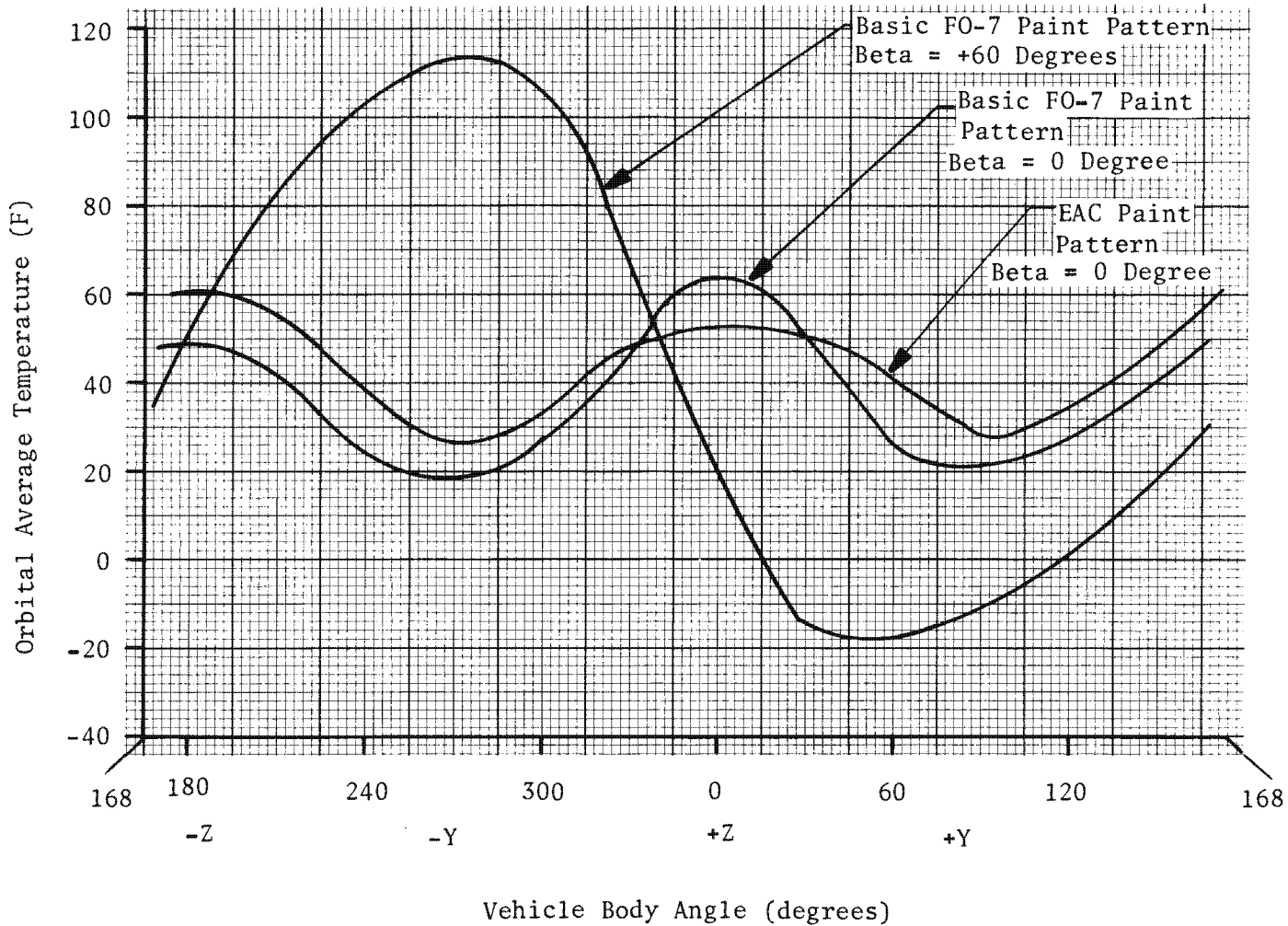


Figure 2.14-11. SEM Orbital Average Skin Temperature Distributions

2.14-23

~~TOP SECRET~~ G

Handle via **BYEMAN**
Control System Only

~~TOP SECRET~~ GBIF-008- W-C-019839-RI-80

compatible with internal temperature requirements, hotdogging (vehicle bending) restrictions, and available heater power.

An orbital heat balance computer program (OHBCP) was developed to aid in this design. It is capable of calculating on-orbit skin temperatures and of optimizing surface finishes for narrow launch windows.

The operational requirement for beta angles between plus 60 and minus 60 degrees, or between plus 40 and minus 40 degrees, means that any finish can be optimal for only one set of orbital parameters. For this reason, the design objectives of passive thermal control to satisfy internal temperature requirements and minimal hotdogging require some degree of compromise.

Limits imposed on environmental energy consumption necessitated the use of nonuniform patterns on the COM. Six patterns were designed. Four patterns for Case A use: one suitable for beta angles between minus 30 and plus 30 degrees, the second suitable for beta angles between minus 48 and plus 48 degrees, the third suitable for beta angles between minus 60 and plus 60 degrees, and the fourth for the sun-synchronous plus 16 to minus 4-degree beta angle range. Case B required three patterns: one for beta angles from minus 40 to plus 40 degrees, the second for use between 0 to plus 40 degrees, and a third pattern suitable from 0 to minus 40 degrees.

A high-absorptance, high-emittance, black finish was selected for the bottom (-Z) quadrant to take advantage of the relatively high and constant (with respect to beta angle) flux inputs that occur at that section of the COM. The same black finish was also selected for the top (+Z) quadrant to absorb the high solar energy available in that section. The high-altitude Case B designs required the inclusion of titanium foil on the bottom (-Z) quadrant to permit greater heat inputs to the COM. As was done with the SEM pattern, a low-absorptance/low-emittance finish was chosen for the side (+Y and -Y) quadrants to attenuate the temperature extremes between orbits due to the large variation of incident flux as a function of beta angle, and to prevent a large energy loss from occurring during cold conditions. Some high-emittance white paint is added to the sides to reject energy at high

2.14-24

~~TOP SECRET~~ GHandle via BYEMAN
Control System Only

~~TOP SECRET~~ GBIF-008- W-C-019839-RI-80

beta angles and to establish the hot temperature limit. A plot of predicted COM skin temperatures for a beta = 0-degree orbit is shown in Figure 2.14-12 as a function of orbital position.

Each COM finish pattern is designed to achieve near-passive temperature control in the orbit with the maximum incident flux, that is, the maximum time in direct exposure to the sun. The orbital heaters in the COM are capable of providing sufficient energy to offset losses under the minimum heating condition (beta = 0-degree). Conduction isolation and efficient radiation insulation blankets are used to minimize these losses and thereby conserve battery power. The operating temperature range of each of the seven COM finish patterns is illustrated in Figure 2.14-13. The expected temperature range indicated in the illustration is derived using finish tolerances (absorptance, emittance, and tape width) of nominal ± 50 percent of the combined tolerance. The total range indicated in the illustration is realized only with worst-case tolerances. The predicted COM Case A heater power consumptions for the expected cold temperatures of Figure 2.14-12 are 605, 575, 505, and 410 watt-hours per day for the ± 60 , ± 48 , ± 30 , and sun-synchronous patterns respectively. The COM Case B pattern heater power consumptions for the expected cold temperature are 565 and 535 watt-hours/day for the symmetric (± 40) and asymmetric (-40 to 0 or 0 to $+40$) patterns respectively. The operating temperature ranges shown in the illustrations are obtained from the Preliminary Results of Thermal Studies (CCN No. 3), BIF-008-K-062549-OH-69 and from the Sun-Synchronous Operation Thermal Studies Final Report, BIF-008-W-N-008457-RH-73.

The PPS/DP EAC total heater power requirement consists of the energy required by the COM heaters plus the SRV 1 heater power requirement. Figures 2.14-14 through 2.14-19 present the COM heater power requirements for each of the six COM paint patterns for varying conditions of beta angle, minimum altitude, and time of year. The maximum, expected, and minimum energy requirements, as determined by the surface finish tolerances, are included.

2.14-25
~~TOP SECRET~~ GHandle via BYEMAN
Control System Only

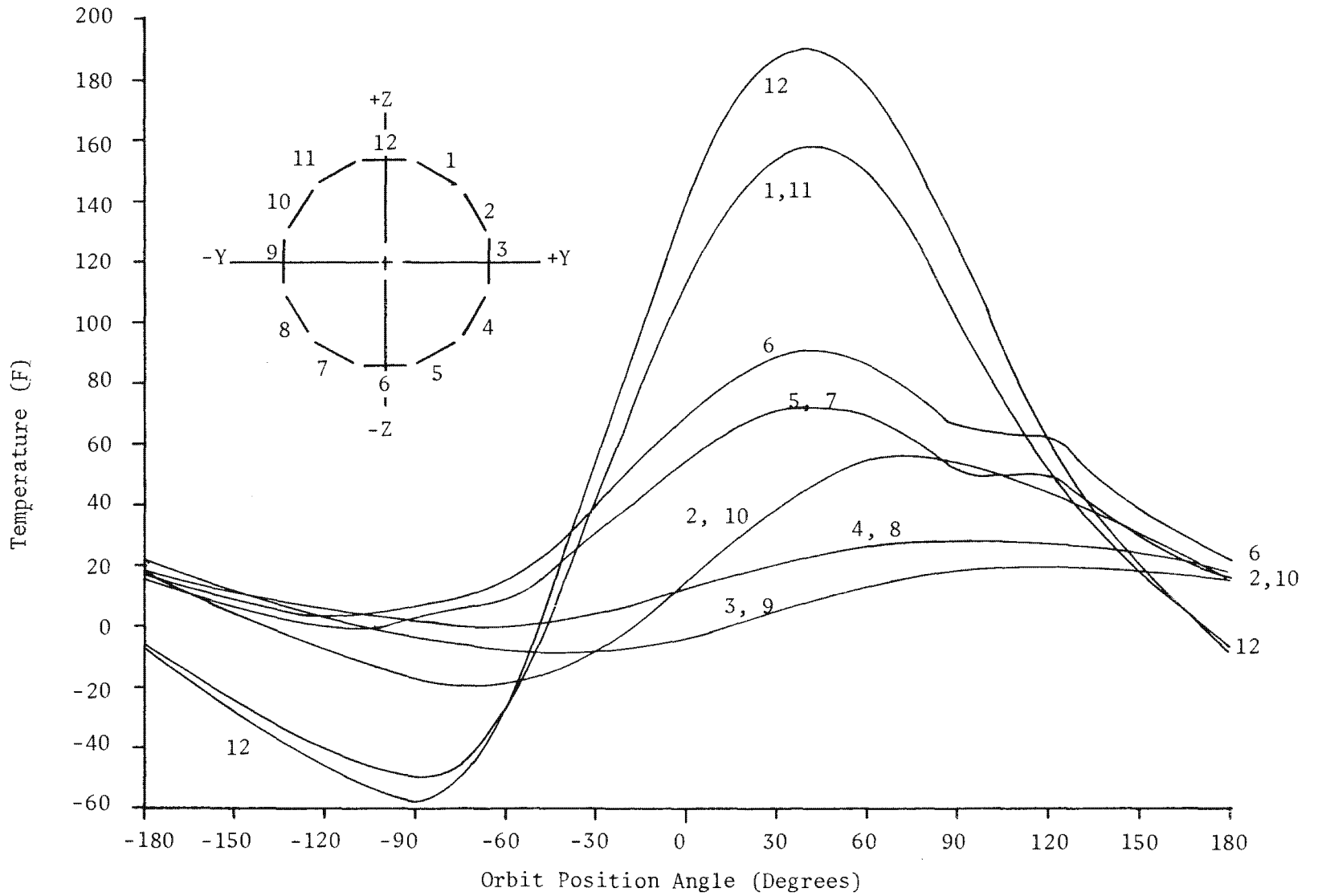


Figure 2.4-12. COM Skin Temperature vs Orbit Position Angle ($\beta=0^\circ$, Roll= 0°)
For Pattern $-60^\circ \leq \beta \leq 60^\circ$

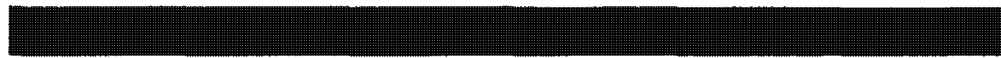
Handle via BYEMAN
Control System Only

Approved for Release: 2017/02/14 C05097220

2.14-26

Approved for Release: 2017/02/14 C05097220

ΔT Expected = 40.1F



EAC Asymmetric Pattern
0 to +40 Degrees or
0 to -40 Degrees

ΔT Expected = 44.1F



EAC Symmetric Pattern
±40-Degree

ΔT Expected = 43.7F



±60-Degree Pattern

ΔT Expected = 40.6F



±48-Degree Pattern

ΔT = 36.8F



±30-Degree Pattern

ΔT = 32.4F



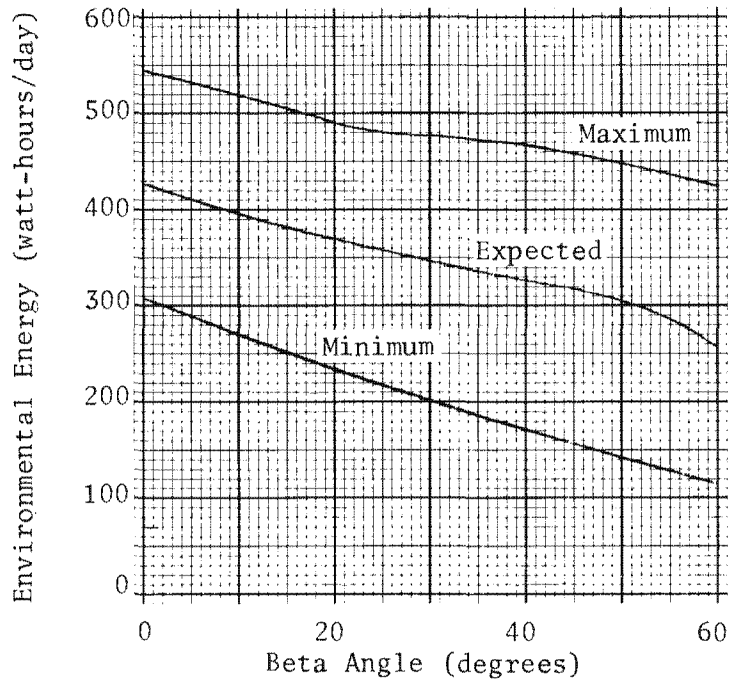
Sun-Synchronous Pattern



COM Average Temperature (F)

2.14-27

Figure 2.14-13. COM Paint Pattern Temperature Range



2.14-28

1. Curves shown are for min h = 70 nmi.
2. For minimum h other than 70 nmi add quantity shown in Table 1 below to values from the curves.

Table 1

Beta	Minimum h				
	65	70	75	80	85
0	-105	0	+30	+45	+60
30	-65	0	+22	+39	+50
60	-25	0	+15	0	-10

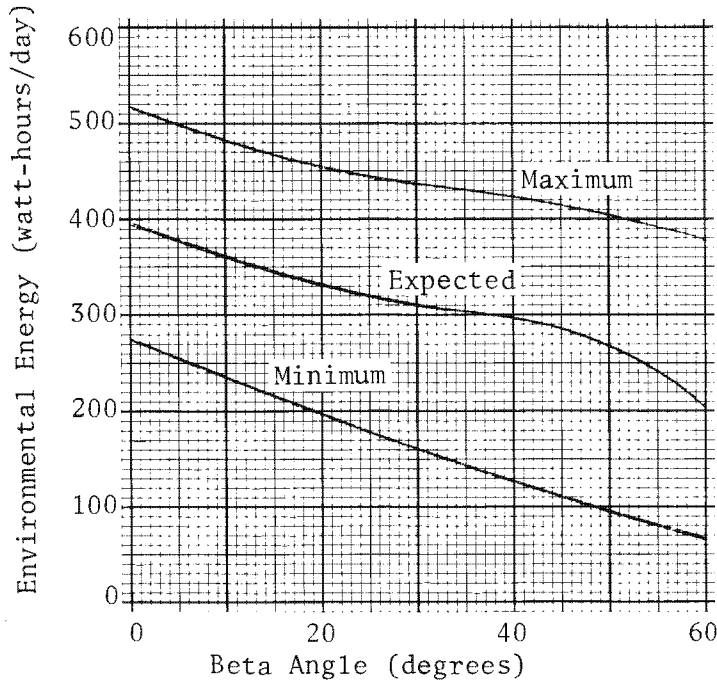
3. For desired date, make appropriate corrections by adding quantity from Table 2 below to result of Step 2 above.

Table 2

Date	Max	Exp	Min
1/1	-50	-25	0
2/1, 12/1	-37	-22	13
3/1, 11/1	-25	-12	25
4/1, 10/1	-15	0	35
5/1, 9/1	-7	12	43
6/1, 8/1	-2	22	48
7/1	0	25	50

Figure 2.14-14. COM Environmental Energy Requirements, 60-Degree Pattern

Handle via **BYEMAN**
Control System Only



2.14-29

*Note: Pattern for 48° may be used for Beta greater than 48° only if minimum h is greater than 70 nmi.

1. Curves shown are for min h of 70 nmi.
2. For minimum h other than 70 nmi add quantity shown in Table 1 to value from curves.

Table 1

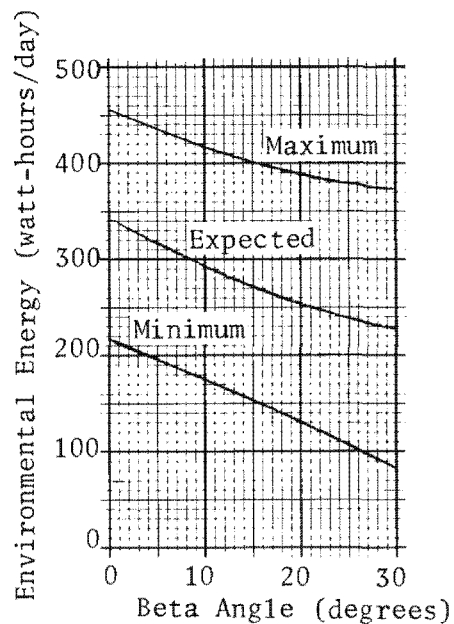
Beta	Minimum h				
	65	70	75	80	85
0	-105	0	+30	+40	+60
24	-90	0	+32	+50	+75
48	-100	0	+35	+50	+75
60	*	0	+40	+50	+70

3. For desired date, make appropriate corrections by adding quantity from Table 2 to result of Step 2.

Table 2

Date	Max	Exp	Min
1/1	-50	-25	0
2/1, 12/1	-37	-22	13
3/1, 11/1	-25	-12	25
4/1, 10/1	-15	0	35
5/1, 9/1	-7	12	43
6/1, 8/1	-2	22	48
7/1	0	25	50

Figure 2.14-15. COM Environmental Energy Requirement, 48 - Degree Pattern



2.14-30

1. Curves shown are for min h of 70 nmi.
2. For minimum h other than 70 nmi add quantity shown in Table 1 to value from curve.

Beta	Minimum h				
	65	70	75	80	85
0	-110	0	+20	+35	+50
15	-110	0	+30	+50	+70
30	-95	0	+45	+65	+85

3. For desired date, make appropriate corrections by adding quantity from Table 2 to result of Step 2.

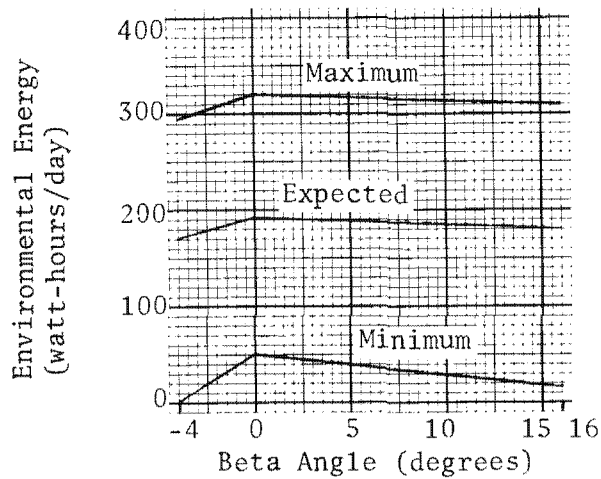
Date	Max	Exp	Min
1/1	-50	-25	0
2/1, 12/1	-37	-22	13
3/1, 11/1	-25	-12	25
4/1, 10/1	-15	0	35
5/1, 9/1	-7	12	43
6/1, 8/1	-2	22	48
7/1	0	25	50

Figure 2.14-16. COM Environmental Energy Requirement, 30-Degree Pattern

Handle via BYEMAN
Control System Only

Approved for Release: 2017/02/14 C05097220

Approved for Release: 2017/02/14 C05097220



2.14-31

1. Curves shown are for min h of 70 nmi.
2. For minimum h other than 70 nmi add quantity shown in Table 1 to value from curves.

Table 1

Beta	Minimum h				
	65	70	75	80	85
-4	-110	0	+25	+45	+65
0	-70	0	+40	+70	+90
+16	-75	0	+40	+65	+80

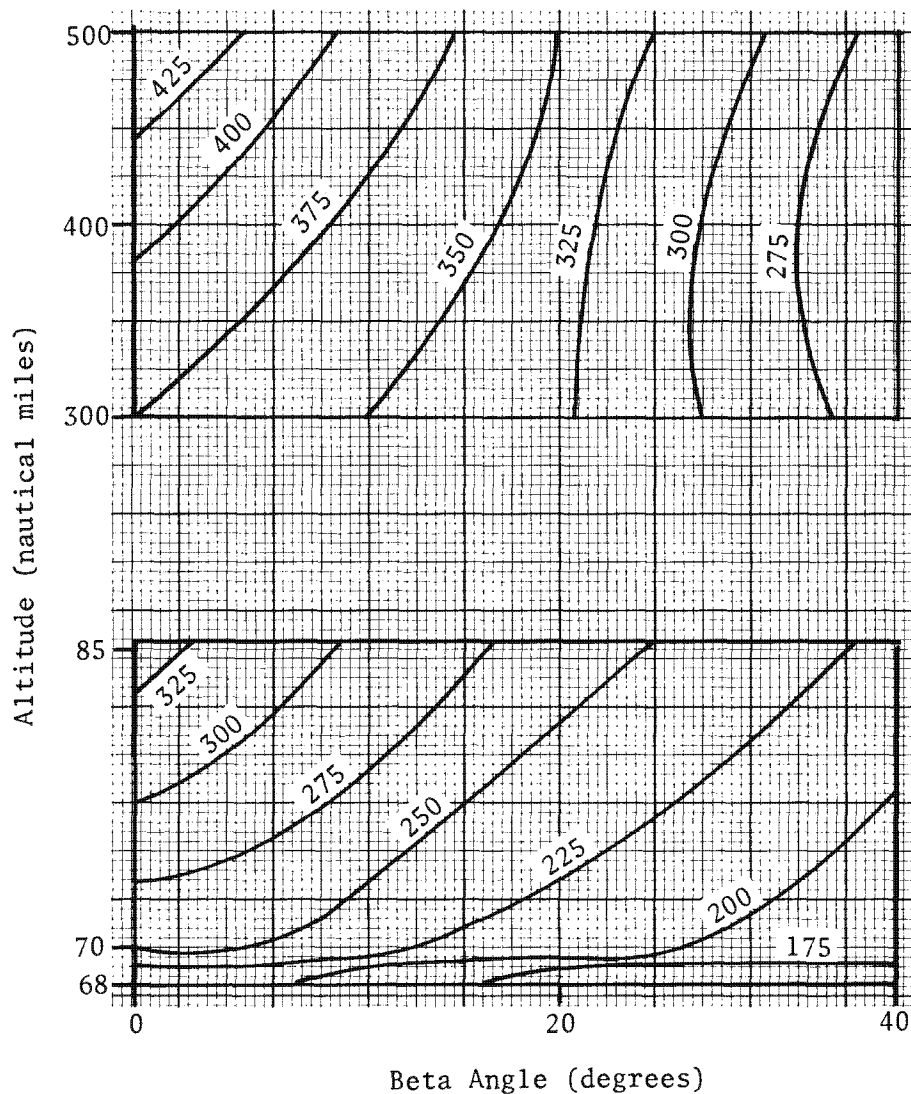
3. For desired date, make appropriate corrections by adding quantity from Table 2 to result of Step 2.

Table 2

Date	Max	Exp	Min
1/1	-50	-25	0
2/1, 12/1	-37	-22	13
3/1, 11/1	-25	-12	25
4/1, 10/1	-15	0	35
5/1, 9/1	-7	12	43
6/1, 8/1	-2	22	48
7/1	0	25	50

Figure 2.14-17. COM Environmental Energy Requirement, Sun-synchronous Pattern

Handle via **BYEMAN**
Control System Only

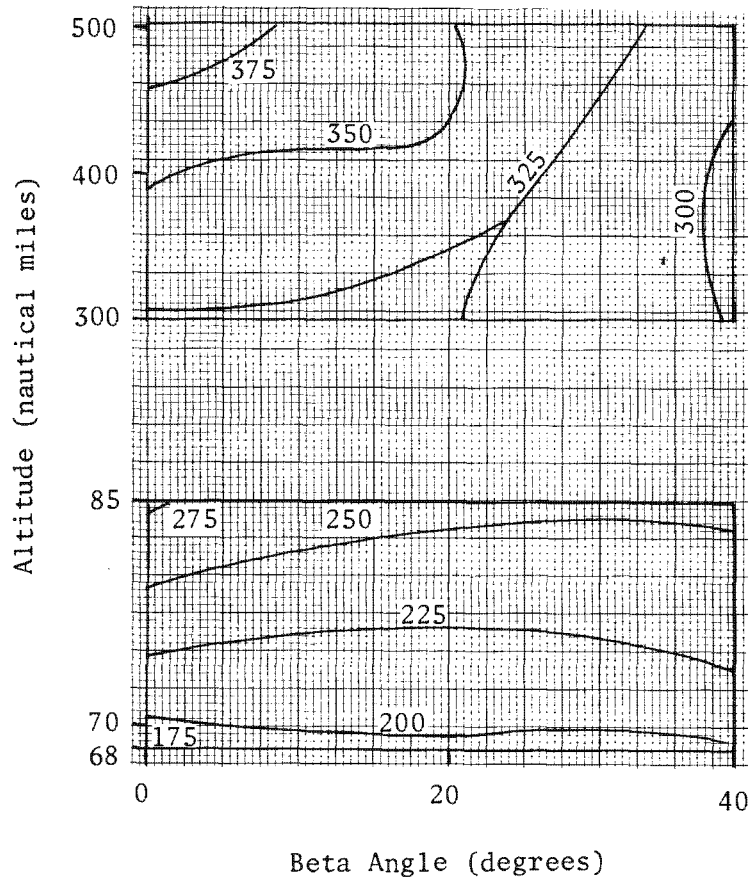


1. Curves shown are for the expected environmental energy requirements. To determine the maximum requirement, add 50 to the value from the curves. To determine the minimal requirement, subtract 50 from the curve value.
2. For desired date, make appropriate corrections by adding the quantity from the proceeding table to the result of step 1.

<u>Date</u>	<u>Max.</u>	<u>Exp.</u>	<u>Min.</u>
1/1	-50	-25	0
2/1, 12/1	-37	-22	13
3/1, 11/1	-25	-12	25
4/1, 10/1	-15	0	35
5/1, 9/1	- 7	12	43
6/1, 8/1	- 2	22	48
7/1	0	25	50

Figure 2.14-18. COM Environmental Energy Requirements (Watt-Hours/Day)
EAC Symmetric Pattern

Handle via **BYEMAN**
Control System Only



1. Curves shown are for the expected environmental energy requirements. To determine the maximum requirement, add 50 to the value from the curves. To determine the minimal requirement, subtract 50 from the curve value.
2. For desired date, make appropriate corrections by adding the quantity from the proceeding table to the result of step 1.

<u>Date</u>	<u>Max.</u>	<u>Exp.</u>	<u>Min.</u>
1/1	-50	-25	0
2/1, 12/1	-37	-22	13
3/1, 11/1	-25	-12	25
4/1, 10/1	-15	0	35
5/1, 9/1	-7	12	43
6/1, 8/1	-2	22	48
7/1	0	25	50

Figure 2.14-19. COM Environmental Energy Requirements (Watt-hours/Day)
 EAC Asymmetric Pattern (0 to +40, or, 0 to -40 degrees)

Handle via **BYEMAN**
 Control System Only

Approved for Release: 2017/02/14 C05097220

2.14-33

Approved for Release: 2017/02/14 C05097220

~~TOP SECRET~~ GBIF-008-W-C-019839-RI-80

Temperature variations within the camera optics assembly (COA) are minimized by the use of many small heater zones with close-set point (heater ON) tolerances and low hysteresis. In addition, with the exception of the three points of contact between the COA and the external structure (high-conduction resistance provided), temperatures are smoothed by the high radiation resistance of the insulation blankets together with a high radiation exchange within the COA.

The finish of the mirrors is such that the thermal resistance between any part of the mirrors and its surrounding environment is relatively high (compared to the thermal resistance between any other components). Consequently, the mirrors respond to the average temperature within the COA rather than any locally high or low temperature. Power dissipating components within the COA (servo mechanisms and primary camera) are finished with low-emittance surfaces to further decouple them from the optical components.

14.3.3.4 Temperature Induced Curvature (Hotdogging). In addition to providing temperature control, the COM paint patterns also determine the amount of hotdogging (bending of the external structure induced by a nonuniform temperature distribution) which will occur.

The method used to calculate curvature from a given temperature distribution is contained in Section 14.7.2, with a derivation of the structural model used to compute deflections.

As hotdogging results in both displacements and rotations of the COA with respect to the external structure, it is necessary to limit the amount of hotdogging during operation to avoid film tracking problems. (Pointing errors associated with hotdogging may be accounted for in the pointing software.)

2.14-34

~~TOP SECRET~~ GHandle via BYEMAN
Control System Only

~~TOP SECRET~~ GBIF-008-W-C-019839-RI-80

Maximum allowable curvatures for the operating condition have been established as R_Z (pitch curvature) = $\pm 25,000$ inches and R_Y (yaw curvature) = $\pm 17,000$ inches. Displacements associated with these radii are included in the film tracking misalignment budget.

Predicted curvatures for orbits having beta angles of 0 degree and 60 degrees are shown in Figures 2.14-20 and 2.14-21 for the COM ± 60 -degree paint pattern. As shown in the figures, yaw curvature is maximized at high beta angles, reducing to near zero at beta = 0, while pitch curvature reaches its maximum value at beta = 0. The predictions consider the PPS/DP EAC to be rolled 23 degrees throughout the period of photographic operations (between orbit position angles minus 75 degrees and plus 30 degrees). The roll is considered as representing a worst-case operation roll sequence: only positive roll angles ranging from 0 degree to 45 degrees during the period of photography. While a zero-degree roll position throughout the orbit would increase the pitch curvature, conservative factors within the analyses (selected values of finish properties) would tend to negate such increases. Special instrumentation on several flights has confirmed the analytical model used to predict PPS/DP EAC hotdogging.

High-altitude activity has introduced a strip shot requirement where the PPS/DP EAC may be rolled at ± 45 degrees for the entire photographic period. Figure 2.14-22 illustrates the effect of this maneuver on the COM curvature profile.

Also of concern during operation is the angular displacement of the COA optical axis from the normal to the PPS/DP EAC-SCS (Satellite Control Section) interface which, if not compensated, will result in aiming errors. These angular displacements are shown in Figure 2.14-23 as a function of radius of curvature.

2.14-35

~~TOP SECRET~~ GHandle via BYEMAN
Control System Only

Conditions:
 $\beta = 0$
60° Pattern

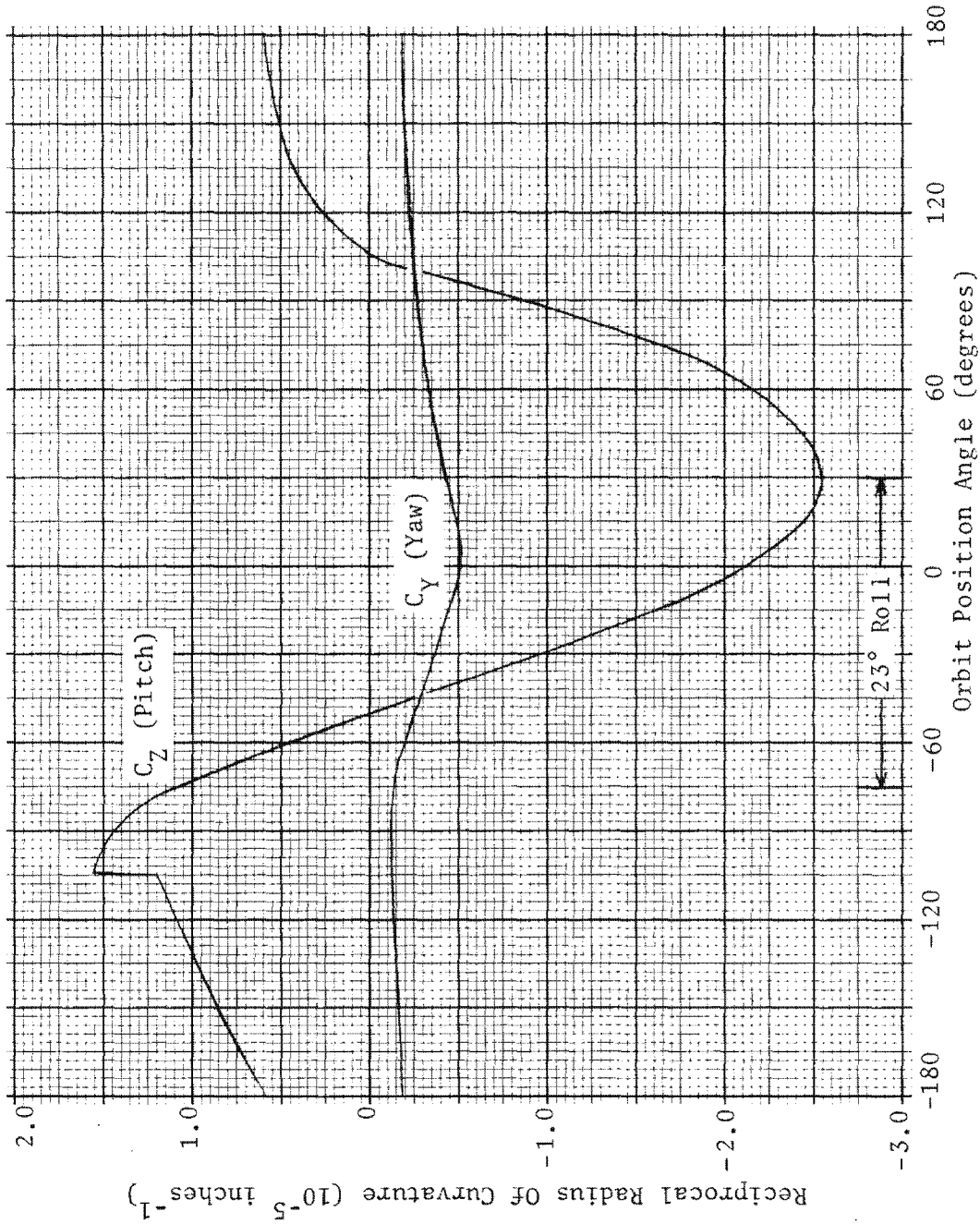
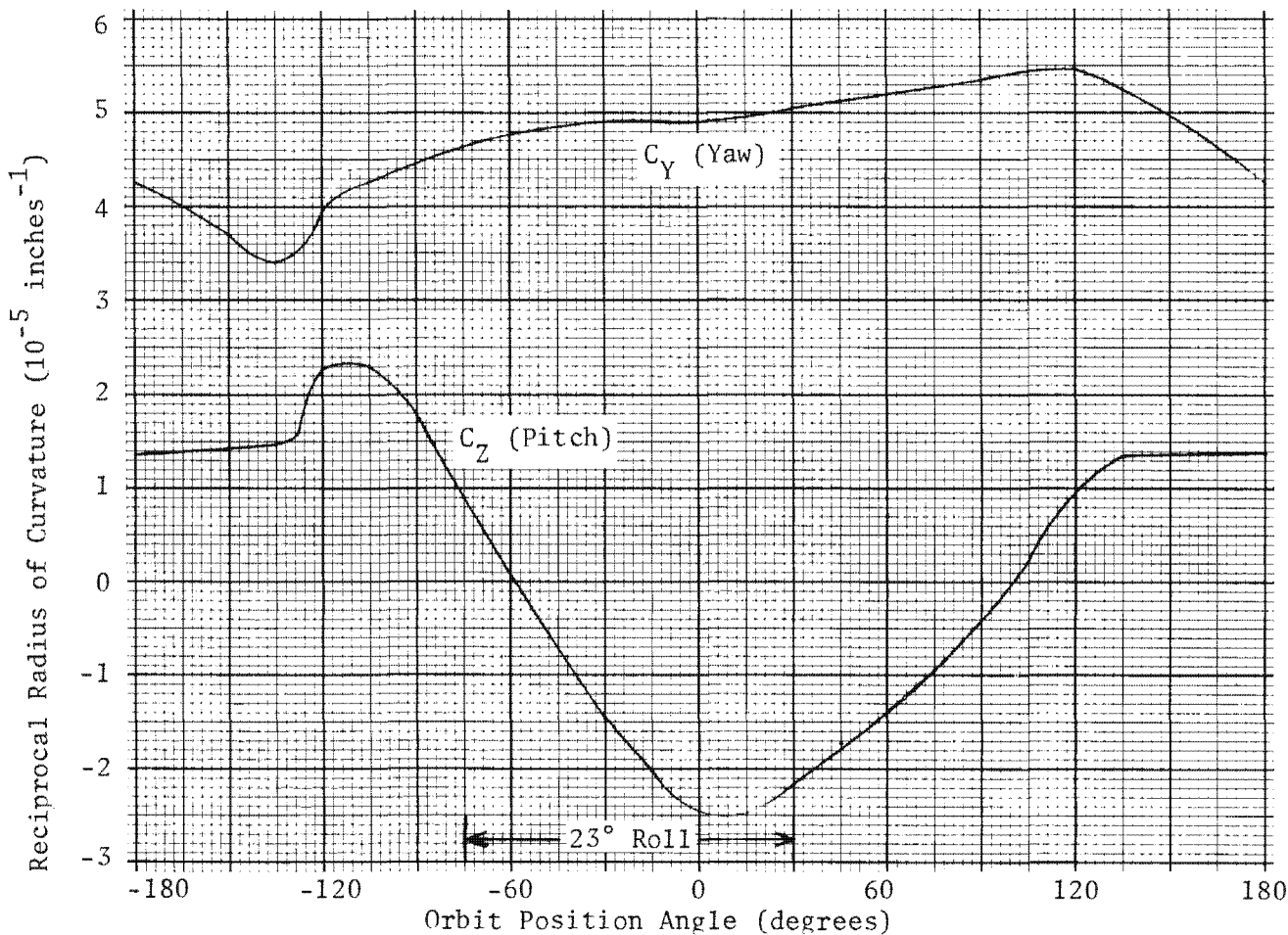


Figure 2.14-20. Predicted COM Curvature



Conditions:
 $\beta = 60^\circ$
60° Pattern

Figure 2.14-21. Predicted COM Curvature

2.14-37

Approved for Release: 2017/02/14 C05097220

Approved for Release: 2017/02/14 C05097220

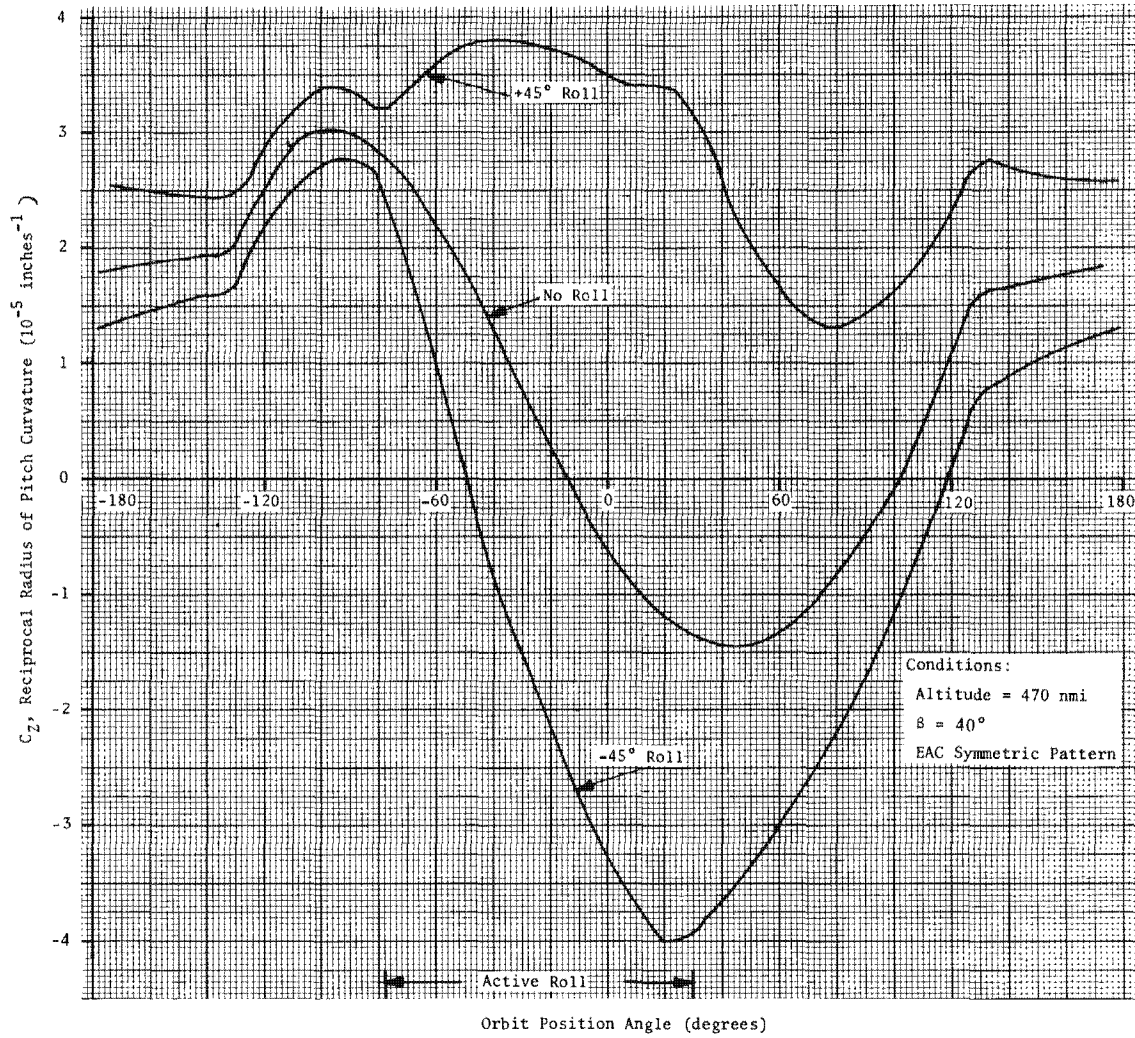


Figure 2.14-22. Predicted COM Curvature

Handle via **8YEMAN**
Control System Only

Approved for Release: 2017/02/14 C05097220

2.14-38

Approved for Release: 2017/02/14 C05097220

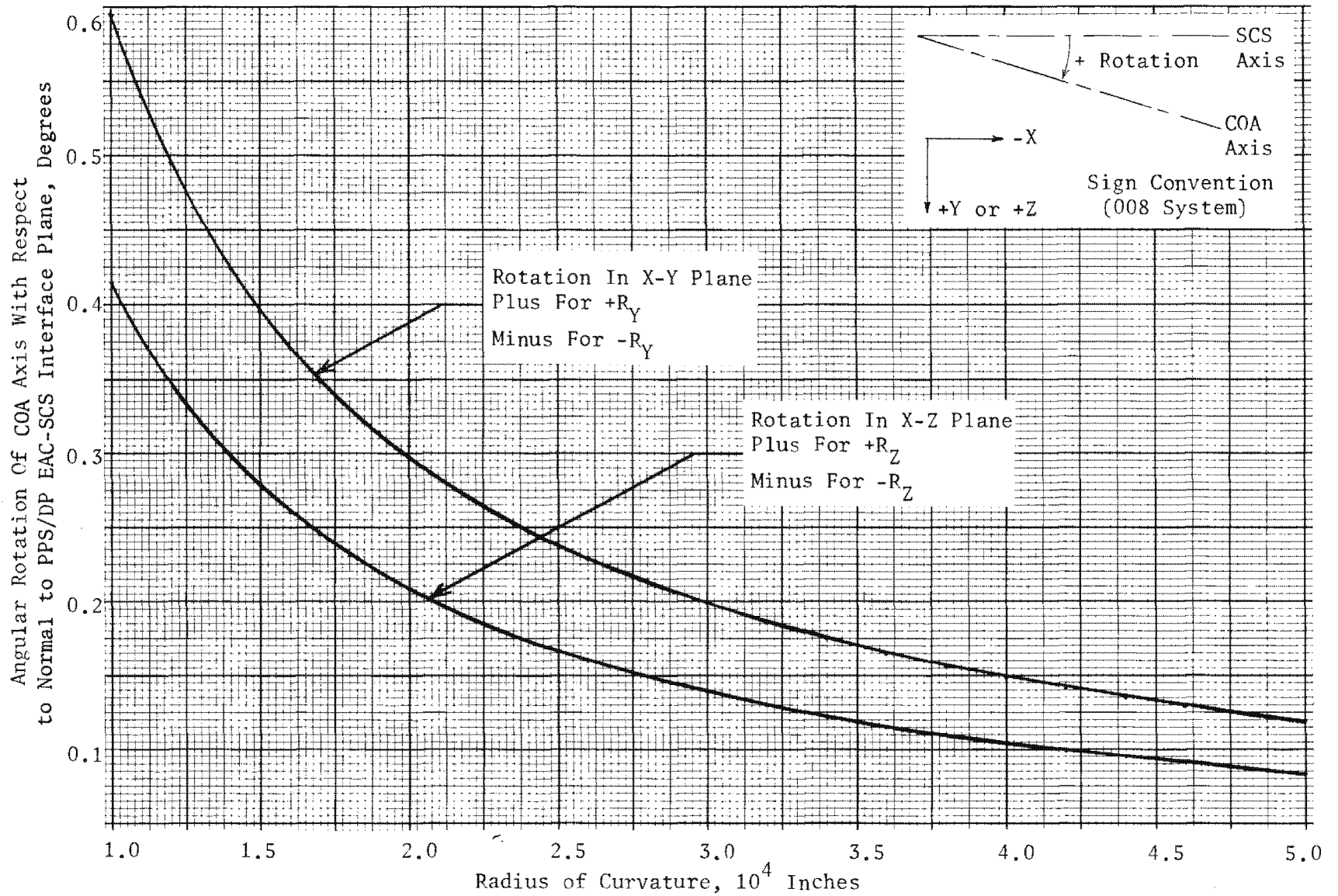


Figure 2.14-23. Rotation of COA Optical Axis

Handle via BYEMAN
Control System Only

Approved for Release: 2017/02/14 C05097220

2.14-39

Approved for Release: 2017/02/14 C05097220

~~TOP SECRET~~ GBIF-008- W-C-019839-RI-80

To make aiming corrections, it is necessary to determine the COM skin temperature distribution, calculate the curvature, and determine the angular displacement. To simplify the curvature determination, the following approach has been used:

- (1) Using the OHBCP, compute COM curvatures as a function of orbit position for various beta angles and COM paint patterns. (Various values of minimum altitude were initially considered but determined to be of secondary importance due to the uniform variation of aerodynamic heating with respect to vehicle body angle.)
- (2) Fit the resulting data to an equation which predicts curvature as a function of orbit position and beta angle. Determine an equation for each COM paint pattern. (To improve the resulting fit, the data included was restricted to the sunlit portion of the revolution.)
- (3) The fitted equation for a particular COM paint pattern is solved for a beta angle and orbit position of interest to determine curvature. (Orbit position is expressed as time from umbral exit in the fitted equation, since this parameter is more conveniently used.)

The resulting equations for determining COM curvature during the sunlit portion of a revolution are presented in Table 2.14-1.

Subjecting the COM to curvatures more severe than the operating range curvatures may result in interference between the COA and the external structure, and/or binding of the viewport doors. The curvature limits to which the PPS/DP EAC may be subjected in a nonoperating state are discussed in Section 14.7.2 and in the PPS/DR Radius of Curvature Study, BIF-008-W-N-014194-OH-75.

2.14-40

~~TOP SECRET~~ GHandle via BYEMAN
Control System Only

~~TOP SECRET~~ G

BIF-008-W-C-019839-RI-80

TABLE 2.14-1
COM CURVATURE EQUATIONS

Equation Form: C_Y or $C_Z = C_1 \beta + C_2 \beta^2 + C_3 \beta^3 + C_4 \beta T^2 + C_5 T + C_6 T^3 + C_7 T^4 + C_8$

Where: C_Y and C_Z are curvature components (inverse inches)
 β is the beta angle (degrees)
 T is the time from umbral exit (seconds)
 C_1 through C_8 are constants

Paint Pattern	C_1 (10^{-7})	C_2 (10^{-9})	C_3 (10^{-12})	C_4 (10^{-14})	C_5 (10^{-8})	C_6 (10^{-15})	C_7 (10^{-19})	C_8 (10^{-5})
<u>Case A</u>								
C_Y Sun Sync	8.9506	0.0000	-27.3300	2.65720	0.049874	0.0000	0.0000	-1.2952
	± 30	8.5906	0.0000	-39.8120	3.11640	0.000000	0.0000	-2.925×10^{-7}
	± 48	7.9526	0.0000	-9.3893	2.62610	0.000000	0.0000	-1.1159×10^{-2}
	± 60	7.7365	0.0000	-8.8717	2.51130	0.000000	0.0000	-1.5940×10^{-6}
C_Z Sun Sync	0.0000	4.0053	0.0000	1.07520	-2.8741	1.3968	4.9886	1.5116
	± 30	0.0000	4.7671	0.0000	0.00000	-2.9658	1.5058	5.0692
	± 48	0.0000	4.2067	0.0000	0.71428	-2.4146	0.0000	8.2458
	± 60	0.0000	4.6394	0.0000	0.00000	-2.4189	0.0000	8.4575
<u>Case B</u>								
C_Y Symmetric Finish								
	Low**	0.79744	0.0000	0.30246	0.24357	0.0000	0.0000	0.13153×10^{-5}
	High**	0.87288	0.0000	0.22188	0.19261	0.0000	0.0000	0.1926×10^{-5}
	Asymmetric Finish							
Low**	0.74198	0.099703	0.0000	0.6222	0.05216	0.0000	0.3251	-2.0803
	High**	0.86901	0.09484	0.0000	0.36877	0.04510	0.0000	-2.1408
C_Z Symmetric Finish								
	Low**	0.0000	0.53770	0.0000	0.0000	-0.3250	0.78799	0.42901
	High**	0.0000	0.65193	0.0000	0.0000	-0.2380	-2.56570	0.97154
	Asymmetric Finish							
Low**	0.0000	0.59333	-0.44688	0.32941	-0.12517	-11.31	4.3878	2.32
	High**	0.08854	0.76460	0.0000	0.2092	-0.13307	-7.0691	2.1355

*Multiply table entry by multiplier in parenthesis to obtain appropriate constant.
 ** For perigees of 68 to 85 nmi use "low" constants.
 For circular orbits 300 to 500 nmi use "high" constants.

2.14-41
~~TOP SECRET~~ G

Handle via BYEMAN
Control System Only

~~TOP SECRET~~ GBIF-008- W-C-019839-RI-80

14.4 PPS/DP EAC Overrange Analysis

An extended operating range for the two PPS/DP EAC paint patterns has been established and is illustrated in Figures 2.14-24 and 2.14-25. These ranges are subjected to the following:

1. Operation within the defined ranges is to be in accordance with the limitations, constraints, and considerations defined in the OHSS.
2. Flight with SRV 1 in place is subject to constraints defined by the SRV contractor. This constraint is not addressed in the following discussion.
3. Flight at minimum altitudes of less than 66.5 nautical miles shall be by a "fly-by-wire" technique, appropriate temperature being monitored with the option to increase the minimum altitude of the orbit if required.

As illustrated by the figures, a liberal operating range is provided by each of the PPS/DP EAC finish patterns. Referring to Figure 2.14-24 symmetric pattern, it is shown that operation at minimum altitudes of less than 66 nmi is possible at beta angles less than 25 degrees during the second half of a mission; the limitation being SRV 2 internal temperatures. To account for the uncertainties of the analysis, it is required that a "fly-by-wire" technique be employed at minimum altitudes less than 67 nmi, the time constant of the SRV 2 interior being sufficiently large to allow this mode of operation to be feasible. During the first half of a slight when SRV 1 is in place, a somewhat more restrictive constraint is placed upon low altitude operation by the temperatures of the TSRTs and the forward film chutes leading to SRV 1. As shown in Figure 2.14-24, these temperatures form the constraint at 68 nmi; beta = 40, the point at which the design was fixed, and relax at lower beta angles to allow first half operation at minimum altitudes of 67 nmi. The COM temperature serves to limit the beta angle range which can be achieved to approximately 45 degrees. It is noted that the beta angles range reduces to 40 degrees at 68 nmi, the point at which the design was fixed, and becomes somewhat more restrictive at lower altitudes.

2.14-42

~~TOP SECRET~~ GHandle via **BYEMAN**
Control System Only

~~TOP SECRET~~ G

BIF-008-W-C-019839-RI-80

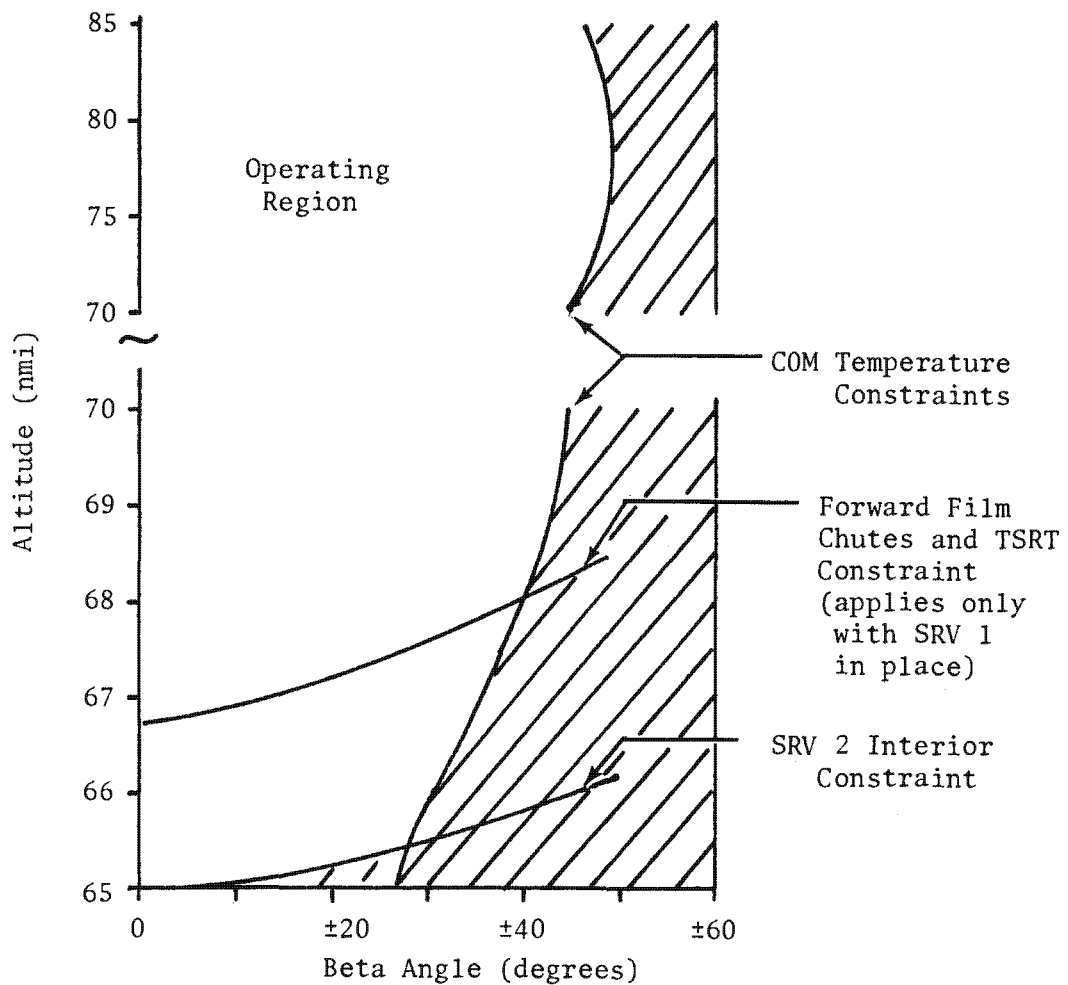
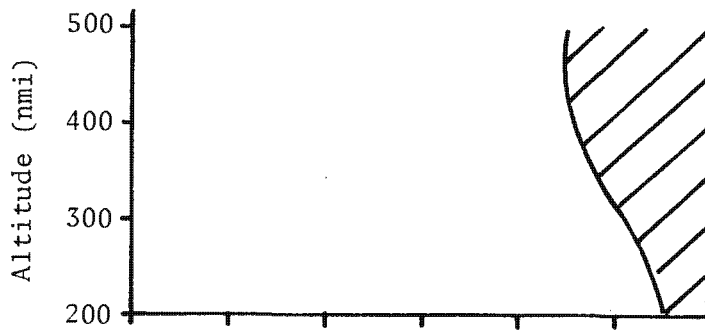


Figure 2.14-24. Operating Constraint EAC Symmetric Finish Pattern

2.14-43

~~TOP SECRET~~ G

Handle via BYEMAN Control System Only

~~TOP SECRET~~ G

BIF-008- W-C-019839-RI-80

The operating range provided by the asymmetric pattern as shown in Figure 2.14-25 shows the constraint as it would be defined for a finish applied for positive beta angles. For application of the finish in the opposite sense to allow operation at negative beta angles, the sign of beta shown would reverse. As the same SEM/DRM finish is used with both symmetric and asymmetric finishes, only the COM portion of the constraint is different from Figure 2.14-24. As might be expected, a more restricted operating range is defined, the difference being the power savings realized by the use of this pattern.

14.5



Thermal Analysis

25X1



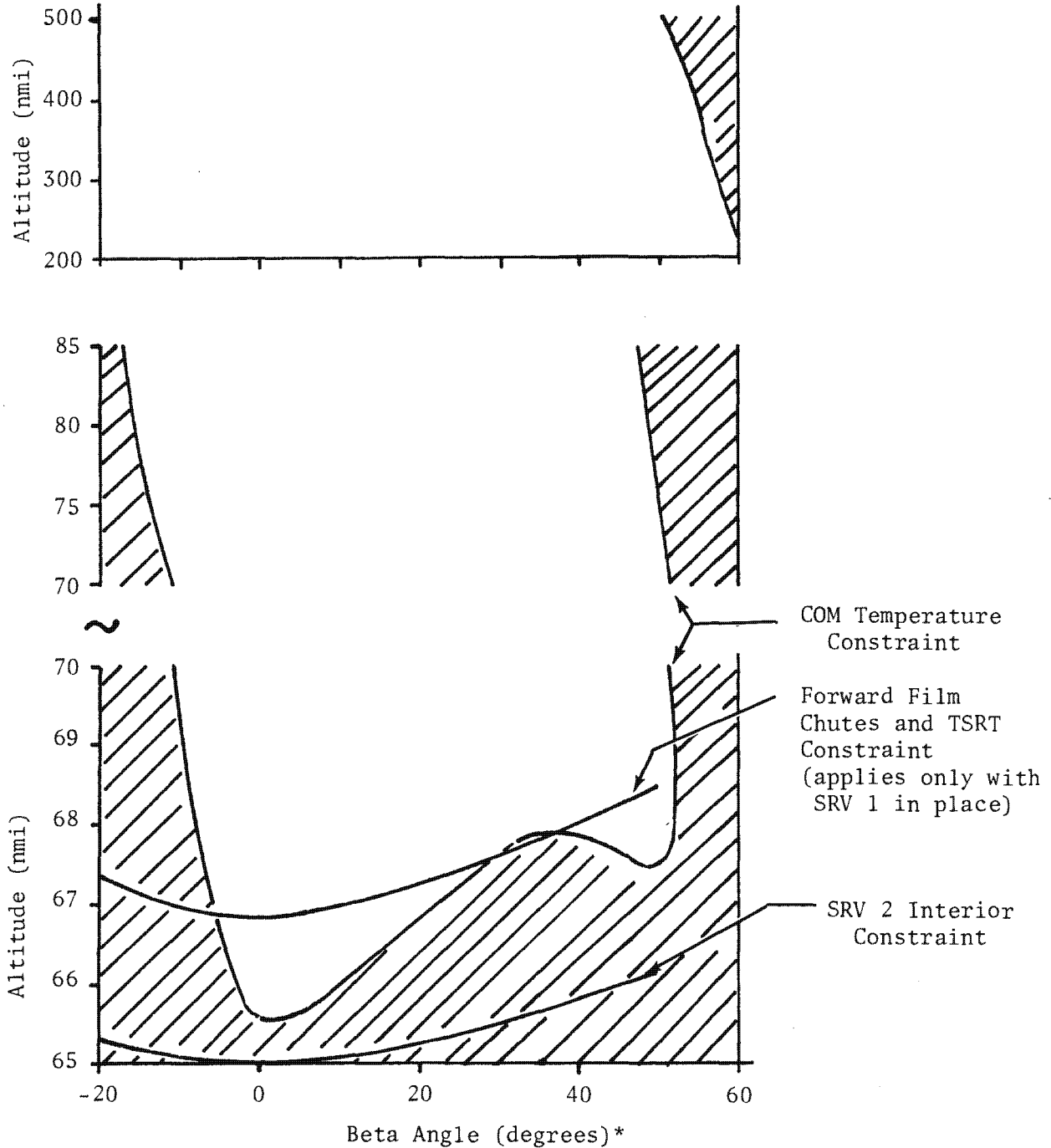
2.14-44

~~TOP SECRET~~ G

Handle via **BYEMAN**
Control System Only

~~TOP SECRET~~ G

BIF-008-W-C-019839-RI-80



*Scale shown for finish as applied for
+Beta reverse sign for finish as applied to -Beta

Figure 2.14-25. Operating Constraint EAC
Asymmetric Finish Pattern

2.14-45

~~TOP SECRET~~ G

Handle via **BYEMAN**
Control System Only

~~TOP SECRET~~ G

BIF-008-W-C-19839-RI-80

25X1



14.6 Recovery

The recovery sequence includes nose aft flight for up to three revolutions followed by a pitch maneuver, either inertial or powered, to orient the PPD/DP EAC in the pitched down recovery attitude.

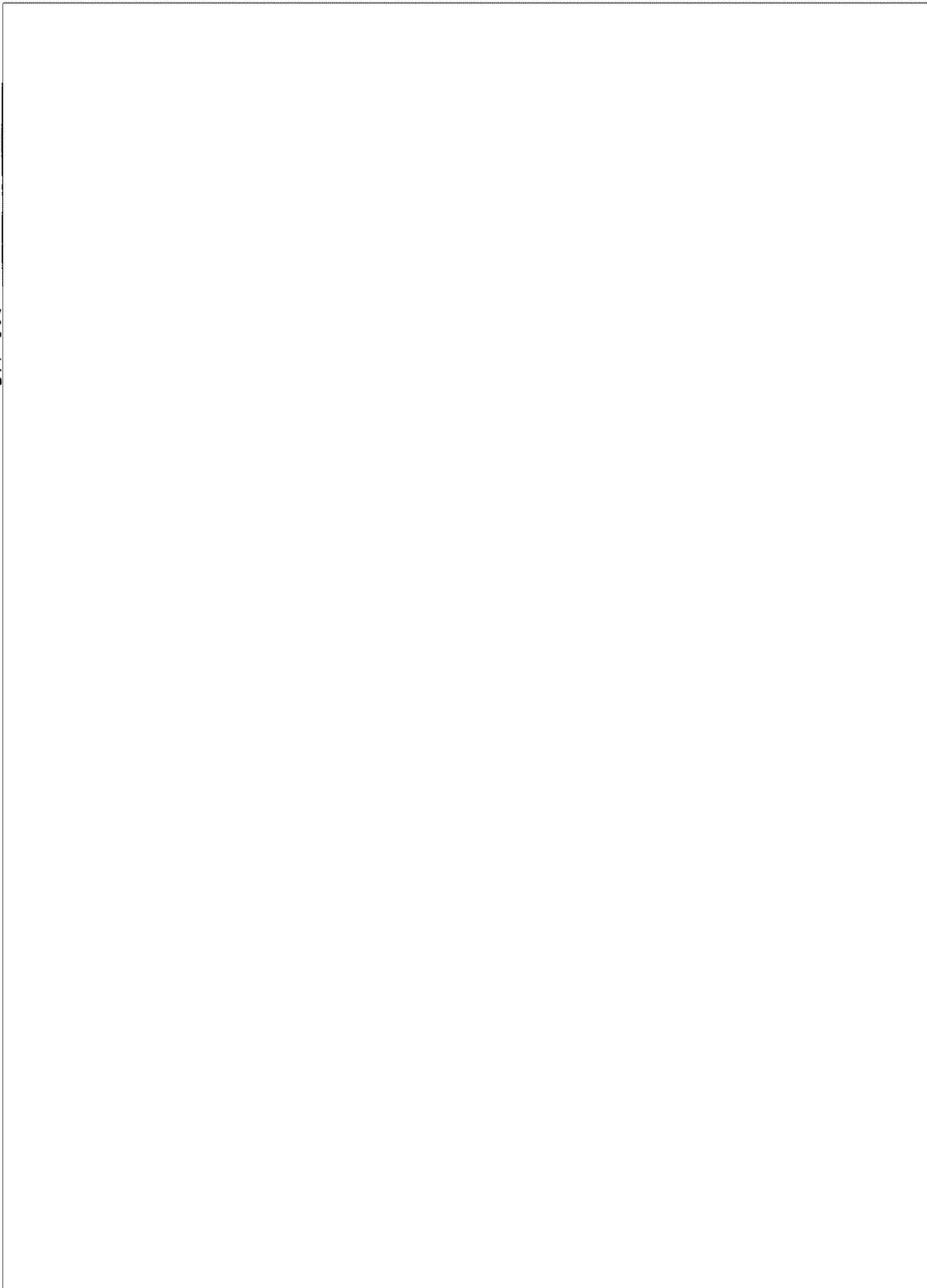
2.14-46

~~TOP SECRET~~ G

Handle via **BYEMAN**
Control System Only

BIF-008- W-C-019839-RI-80

~~TOP SECRET~~ G



2.14-47

Figure 2.14-26. Lens Tube Constraints On Viewport Door Open Time

Handle via **BYEMAN**
Control System Only

~~TOP SECRET~~ G

25X1

~~TOP SECRET~~ G BIF-008 - W-C-019839-RI-80



2.14-48

Figure 2.14-27. Ross Corrector Constraints On Viewport Door Open Time

Handle via BYEMAN Control System Only

~~TOP SECRET~~ G



~~TOP SECRET~~ GBIF-008- W-C-019839-RI-80

14.6.1 Nose-Aft Flight

Nose-aft flight results in elimination of all aerodynamic heating from the DRM, producing temperatures comparable to those predicted for high altitude normal flight. An analysis of the nonsymmetrical, sun-synchronous SEM pattern shows that the components neither overheat nor cool excessively when the SEM is used in the yawed aft orientation. Nose-aft operation of the sun-synchronous COM was considered for orbital parameters throughout its design range. In all cases, the radii of curvature remained within operating limits and the average increase of internal temperature was predicted not to exceed 8F in the steady state. Due to the long COA time constant (approximately 140 hours), the expected COA temperature increase in three revolutions will be much less.

14.6.2 Pitchdown

Analysis of recovery sequences is accomplished utilizing a version of the BIF-008 orbital heat balance computer program modified to compute heat rates and skin temperatures for a vehicle maneuvered about three axes. Models of the substructure in the vicinity of the EA/FA and SRV 1/EA pinpullers are used to compute pinpuller temperatures.

Of concern during a recovery sequence are skin temperatures, COM curvature, and pinpuller temperatures. As a result of the recovery analysis, a need for operational constraints to prevent excessive curvatures and EA/FA pinpuller temperatures from occurring was established.

The use of powered pitch maneuvers into and/or out of the recovery attitude, and the use of a roll of the PPS/DP EAC during the recovery revolution to position the EA/FA pinpullers away from the direction of flight were determined to be effective in achieving satisfactory curvatures and pinpuller temperatures.

2.14-49

~~TOP SECRET~~ GHandle via BYEMAN
Control System Only

~~TOP SECRET~~ GBIF-008- W-C-019839-RI-80

Predicted COM skin temperatures, curvature, and pinpuller temperatures for an inertial recovery from an orbit having a 68-nautical mile minimum altitude are presented in Figure 2.14-28. The PPS/DP EAC is assumed to be rolled throughout the revolution. At 70 orbital degrees prior to minimum altitude (minimum altitude at orbit position angle minus 83 degrees), the PPS/DP EAC is fixed in an inertial attitude which is maintained throughout the revolution. The maneuver results in a pitchdown angle of 70 degrees at minimum altitude.

Predicted temperatures and curvatures for a recovery from an orbit having a 65-nautical mile minimum altitude are presented in Figure 2.4-29. The PPS/DP EAC is assumed to be rolled throughout the revolution. At orbit position angle -91.39 degrees, a powered pitch maneuver at 60.1-degree pitch-per-minute is initiated and continued to achieve a 66-degree pitchdown at orbit position angle -87 degrees, one minute before minimum altitude. An inertial pitch is then assumed for two minutes resulting in a 70-degree pitchdown at minimum altitude. A second power maneuver is then used to return the PPS/DP EAC to level nose-aft flight.

Both of these pitchdown cases consider a beta angle of 0 degree, maximum solar flux input, and the COM to have the sun-synchronous paint pattern with nominal finish properties. The location of minimum altitude was selected such that maximum solar heating would coincide with maximum aerodynamic heating for the pitched-down PPS/DP EAC.

Additional results of recovery analyses are contained in Summary Pinpuller Thermal Analysis, BIF-008-W-C-003745-OH-74 and Thermal Analysis of Recovery and Tumbling, BIF-008-W-C-003034-OH-74.

14.6.3 PPS/DP EAC Recovery

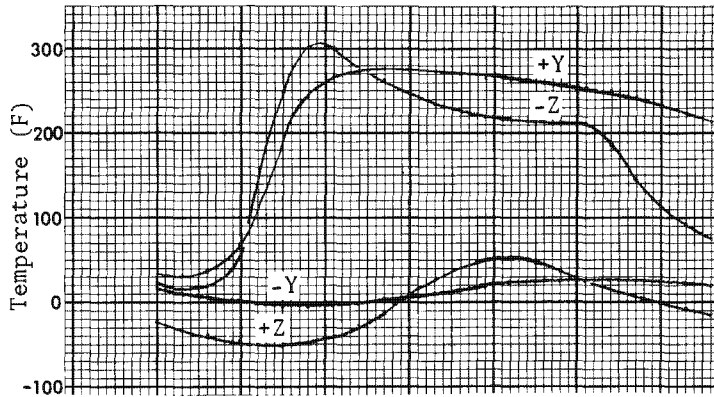
Recovery from PPS/DP EAC operation requires no constraints differing from those evident in FO-7.

2.14-50

~~TOP SECRET~~ GHandle via BYEMAN
Control System Only

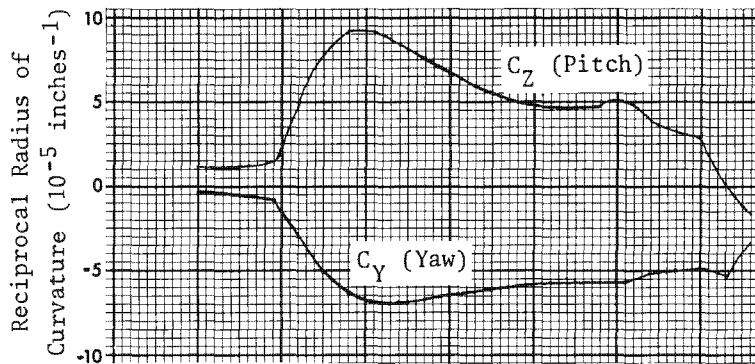
~~TOP SECRET~~ G

BIF-008-W-C-019839-RI-80



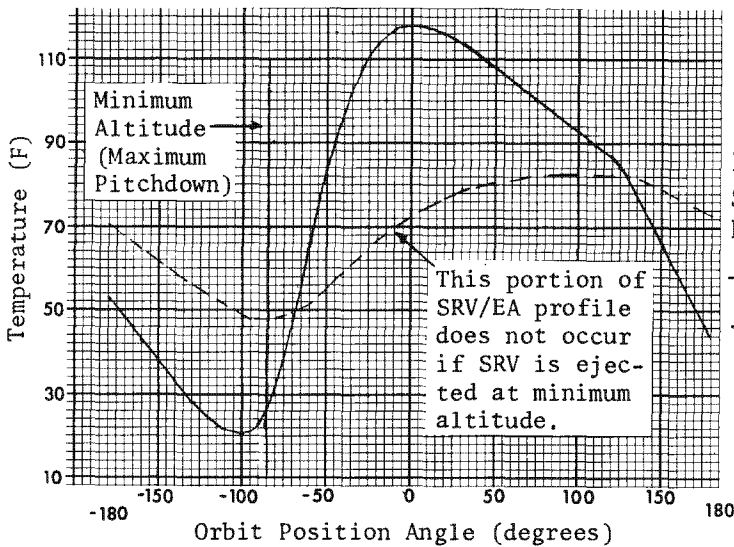
Predicted COM Skin Temperatures

Inertial Recovery at 68 nmi
PPS/DP EAC Rolled 36.5 Deg
Sun-synchronous Paint
Pattern



Predicted COM Curvature

Inertial Recovery at 68 nmi
PPS/DP EAC Rolled 36.5 Deg
Sun-synchronous Paint
Pattern



Predicted Pinpuller Temperatures

Inertial Recovery at 68 nmi
PPS/DP EAC Rolled 36.5 Deg
Sun-synchronous Paint
Pattern

— EA/FA Pinpuller
- - - SRV 1/EA Pinpuller

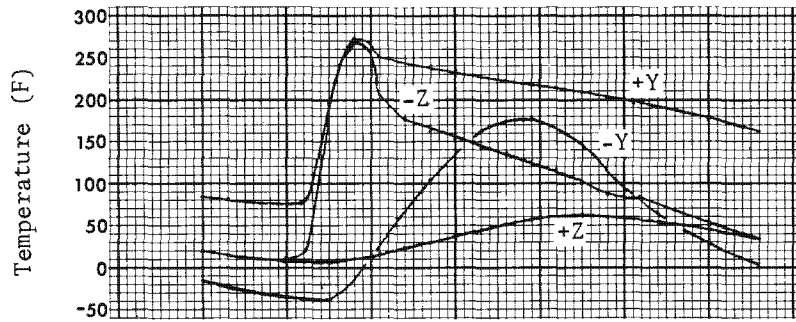
Figure 2.14-28. COM Predictions for 68 nmi Recovery

~~TOP SECRET~~ G

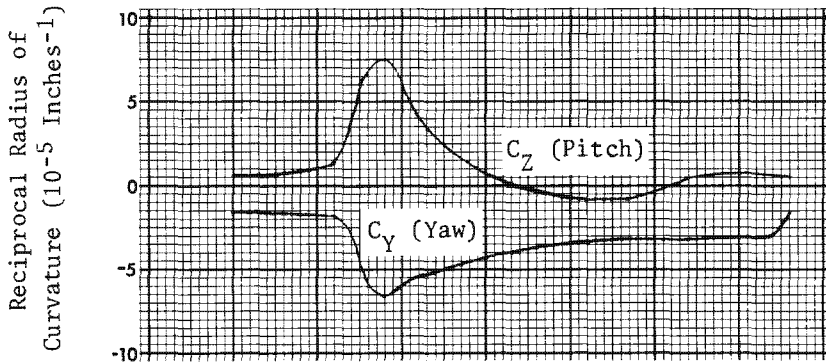
Handle via **BYEMAN**
Control System Only

~~TOP SECRET~~ G

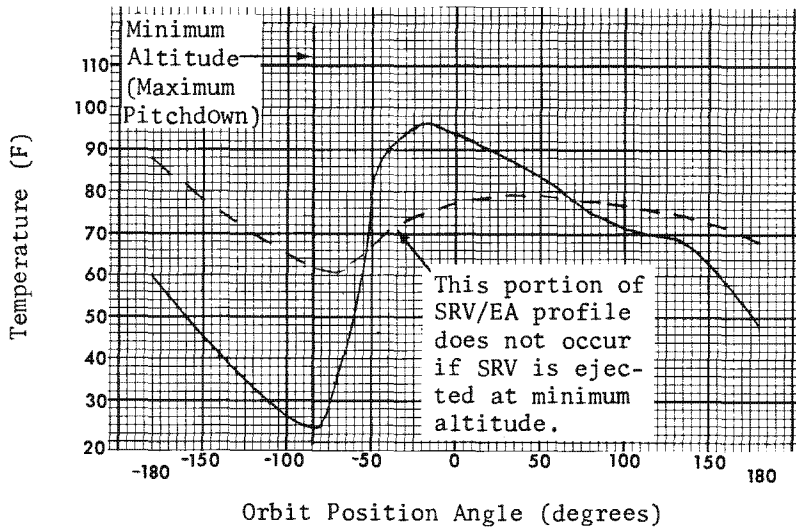
81F-008-W-C-019839-RI-80



Predicted COM Skin Temperatures
 Powered Recovery at 65 nmi
 PPS/DP EAC Rolled 36.5 Deg
 Sun-synchronous Paint
 Pattern



Predicted COM Curvature
 Powered Recovery at 65 nmi
 PPS/DP EAC Rolled 36.5 Deg
 Sun-synchronous Paint
 Pattern



Predicted Pinpuller Temperatures
 Powered Recovery at 65 nmi
 PPS/DP EAC Rolled 36.5 Deg
 Sun-synchronous Paint
 Pattern
 — EA/FA Pinpuller
 - - - SRV 1/EA Pinpuller

Figure 2.14-29. COM Predictions for 65 nmi Recovery

~~TOP SECRET~~ G

Handle via **BYEMAN**
 Control System Only

~~TOP SECRET~~ ^GBIF-008- W-C-019839-RI-80

Recovery analysis is contained in Final Report for SEM/DRM Dual Mode Thermal Study and Design, BIF-008W-C-018714-IH-79 and EAC Thermal Study Final Report, BIF-008W-C-019583-OH-80.

14.7 Additional Considerations

14.7.1 Tumbling

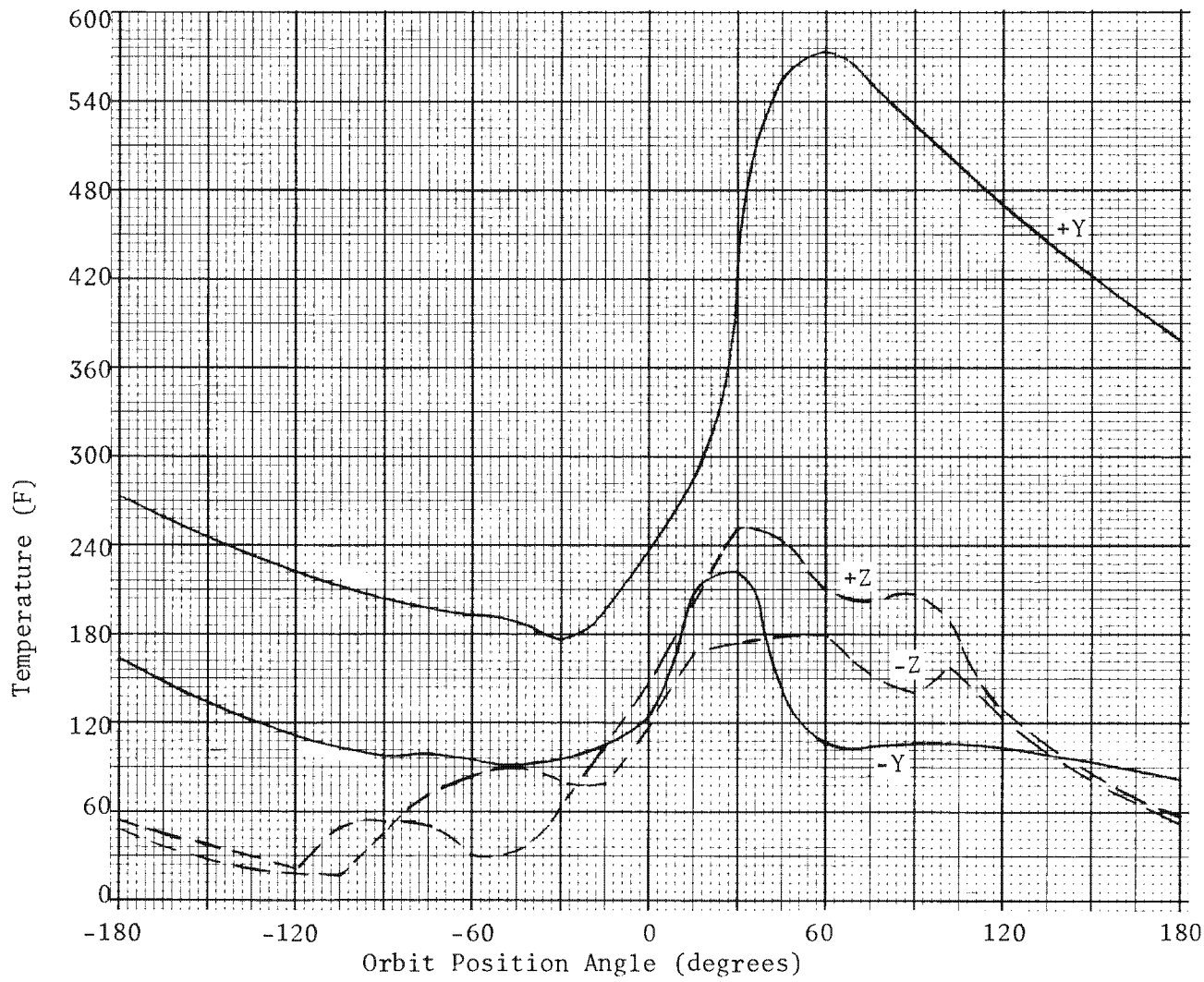
The tumbling analysis is accomplished utilizing a version of the BIF-008 orbital heat balance computer program modified to compute heat rates and skin temperatures for a vehicle maneuvered about three axes. Models of the sub-structure in the vicinity of the EA/FA and SRV 1 EA pinpullers are used to compute pinpuller temperatures.

The tumbling case analyzed consisted of three revolutions at 65 nmi minimum altitude, with tumbling rates and initial vehicle orientation defined by a Lockheed Mission and Space Company (LMSC) model. The resulting predicted COM skin temperatures and curvatures were more severe than those encountered during recovery. Predicted COM skin temperatures and curvatures occurring during the third tumbling revolution are presented in Figures 2.14-30 and 2.14-31, respectively. It is noted that the yaw and pitch curvature values shown in Figure 2.14-31 are interchangeable, or nearly so, depending on the initial roll position of the PPS/DP EAC.

Since the PPS/DP EAC could be in an operating state (responding to stored commands) during the period of tumbling, it is possible that subsequent PPS/DP EAC operability could be impaired.

2.14-53

~~TOP SECRET~~ ^GHandle via **BYEMAN**
Control System Only



Conditions:
Min Altitude
= 65 nmi
Synchronous Pattern

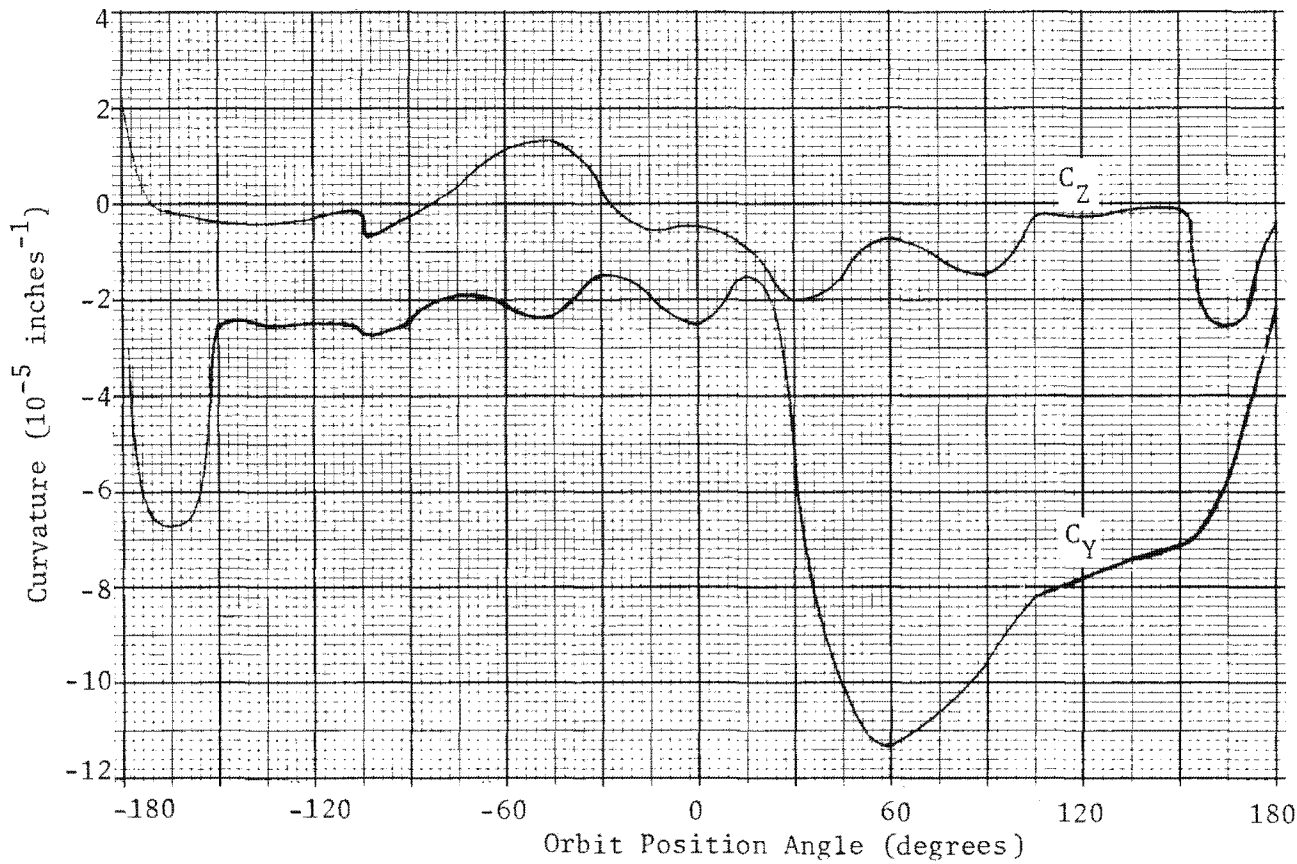
2.14-54

Figure 2.14-30. COM Skin Temperatures, Tumbling Rev 3

Handle via BYEMAN
Control System Only

Approved for Release: 2017/02/14 C05097220

Approved for Release: 2017/02/14 C05097220



Conditions:
Min Altitude
= 65 nmi
Synchronous Pattern

2.14-55

Figure 2.14-31. COM Curvature, Tumbling Rev 3

Handle via **BYEMAN**
Control System Only

~~TOP SECRET~~ G

BIF-008-W-C-019839-RI-80

The maximum incident flux profiles encountered by the EA and FA during the three-rev tumbling case were used to compute pinpuller temperatures. The predicted pinpuller temperatures are shown in Figure 2.14-32. Since the SRV 1/EA pinpullers are located at a different body angle than the EA/FA pinpullers, the temperatures shown in the figure cannot occur simultaneously. However, depending on the initial roll position of the PPS/DP EAC at the outset of the tumbling case, either profile could occur. Temperatures in excess of the 160F pinpuller qualification limit are predicted.

Results of the tumbling analysis are included in the Thermal Analysis of Recovery and Tumbling, BIF-008-W-C-003034-OH-74.

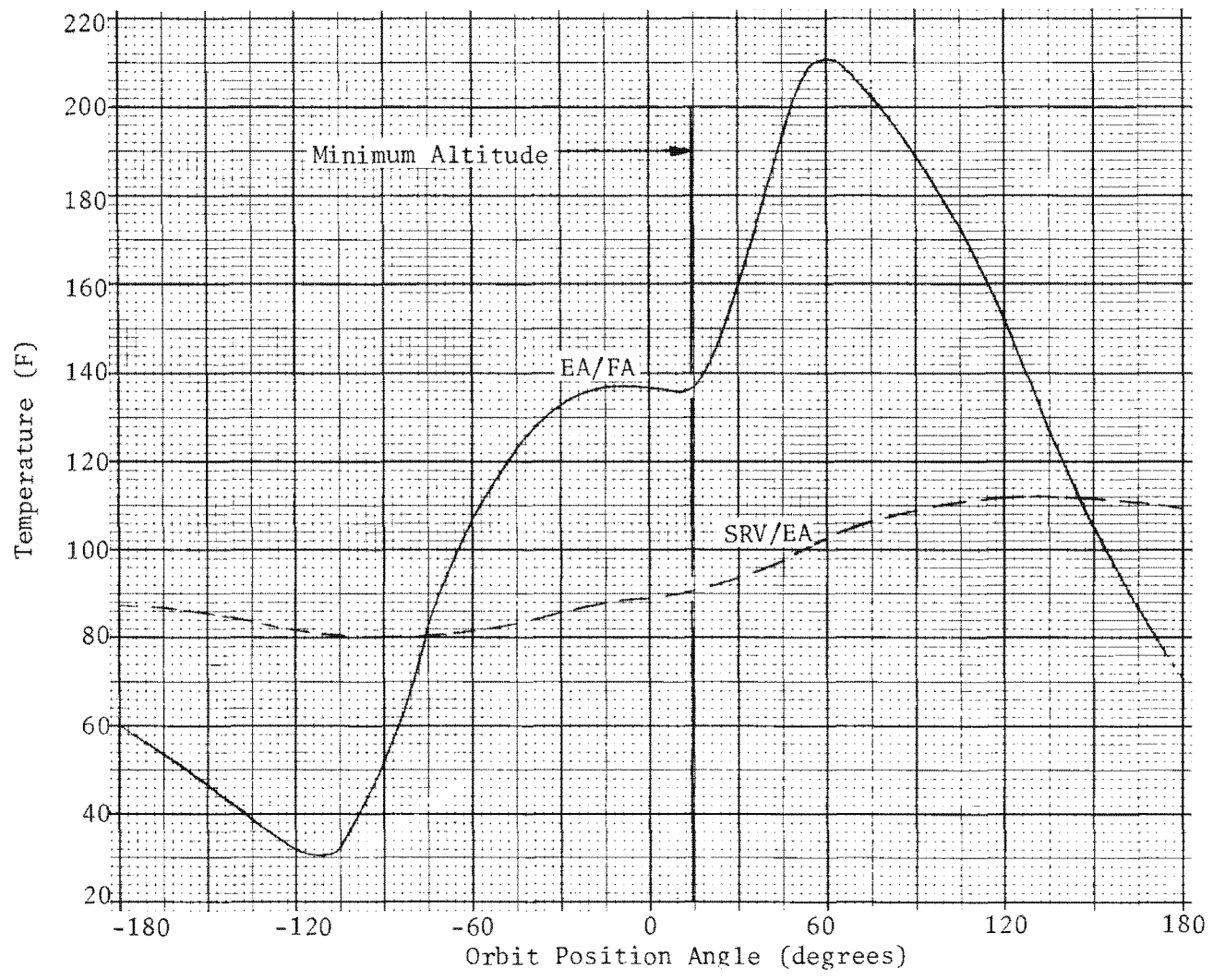
14.7.2 Hotdogging

Bending of the external structure resulting from nonuniform circumferential temperature distributions results in deflections of the COA with respect to the external structure. Calculation of these deflections is necessary to determine aiming error corrections and structural clearances at high curvatures.

Derivation of COM curvature from a given temperature distribution is accomplished with reference to Figure 2.14-33.

2.14-56

~~TOP SECRET~~ GHandle via BYEMAN
Control System Only



Conditions:
Min Altitude
= 65 nmi

Note:
Profiles Shown Do
Not Occur On The
Same Revolution.

Figure 2.14-32. Pinpuller Temperature, Tumbling Rev

Handle via **BYEMAN**
Control System Only

Approved for Release: 2017/02/14 C05097220

2.14-57

Approved for Release: 2017/02/14 C05097220

~~TOP SECRET~~ G

BIF-008- W-C-019839-RI-80

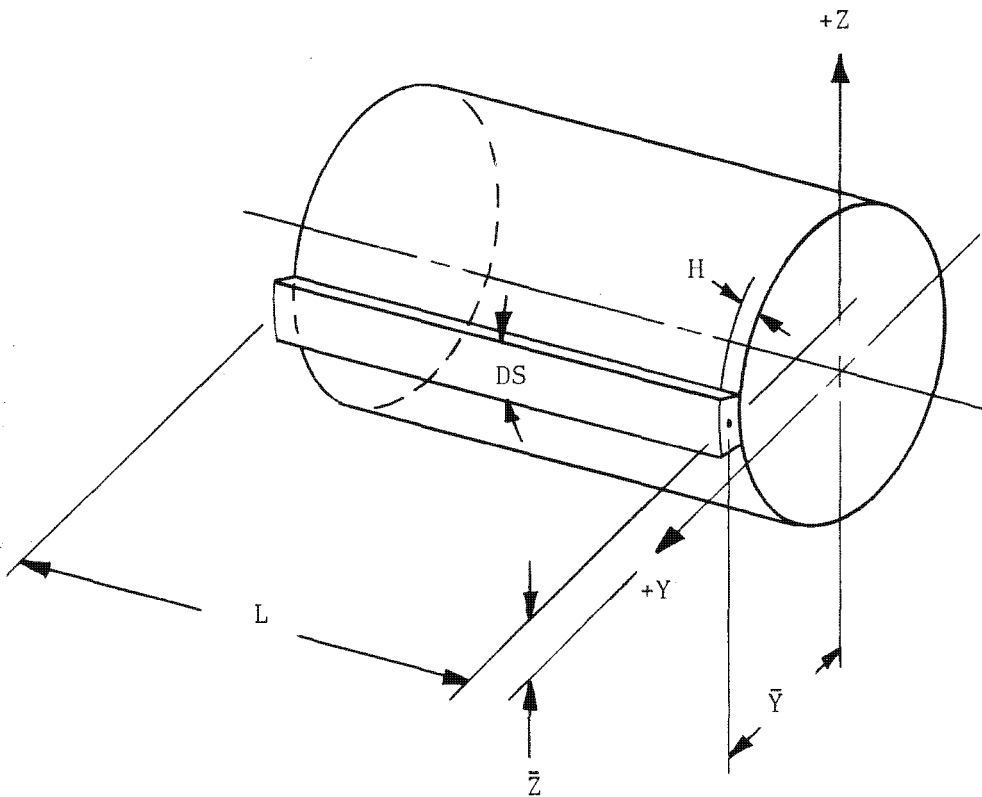


Figure 2.14-33. COM Curvature Derivation

2.14-58

~~TOP SECRET~~ G

Handle via **BYEMAN**
Control System Only

~~TOP SECRET~~ GBIF-008- W-C-019839-RI-80

Considering the expansion of an element of a cylinder:

Element length	L
Element width	DS
Element thickness	H
Coefficient of thermal expansion	α
Modulus of elasticity	E

Expansion of an element: $\Delta L = \alpha L \Delta T$

Strain of an element: $\epsilon = \frac{\Delta L}{L} = \alpha \Delta T$

Stress of an element: $\sigma = E\epsilon = E\alpha \Delta T$

Force acting on an element: $F = \sigma A = E\alpha \Delta T (H) (DS)$

Bending moments acting on cylinder: $M_{YY} = \sum F(\bar{Z})$ and $M_{ZZ} = \sum F(\bar{Y})$

Curvature components of the cylinder:

$$C_Z = \frac{-M_{YY}}{E I_{YY}} \quad \text{and} \quad C_Y = \frac{-M_{ZZ}}{E I_{ZZ}}$$

or

$$C_Z = \frac{-\sum E \alpha \Delta T (H) (DS) (\bar{Z})}{E I_{YY}} \quad \text{and} \quad C_Y = \frac{-\sum E \alpha \Delta T (H) (DS) (\bar{Y})}{E I_{ZZ}}$$

Removing material properties from the summations and assuming equal width elements:

$$C_Z = \frac{-\alpha (DS)}{I_{YY}} \sum \Delta T (H) (\bar{Z}) \quad \text{and} \quad C_Y = \frac{-\alpha (DS)}{I_{ZZ}} \sum \Delta T (H) (\bar{Y})$$

The above equations are evaluated for a given temperature distribution to determine the curvature components. The equations may be used in the area of the

~~TOP SECRET~~ GHandle via **BYEMAN**
Control System Only

~~TOP SECRET~~ GBIF-008- W-C-019839-RI-80

viewport door cutout and the cylindrical sections by including the proper number of elements in the summation, using the appropriate effective element thicknesses (H), centroid coordinates (\bar{Y} , \bar{Z}), and cross sectional moments of inertia (I_{YY} , I_{ZZ}).

The geometry of the COA suspension system is depicted in Figure 2.14-34. The suspension was chosen to minimize displacement in the X-Y plane of the film with respect to the camera at BIF-008 Station 77. A flexible bellows connects the internal structure-mounted camera to the external structure-mounted film supply.

The diagram of the COA suspension system from which the mathematical model is formulated is shown in Figure 2.14-35. The model assumes that the effective centerline length of both the internal and external structures remains constant.

Referring to Figure 2.14-36; X-Y view:

$$S = R_Y \theta \text{ or } \theta = \frac{S}{R_Y} \quad (1)$$

- where:
- S is the distance from the spherical bearing to the Sta 147.11 reference (S = 137.88 inches).
 - R_Y is the radius of curvature of a cylindrical section of the external structure in the X-Y plane (inches).
 - θ is the angle shown in the figure (radians).

2.14-60

~~TOP SECRET~~ GHandle via **BYEMAN**
Control System Only

~~TOP SECRET~~ G

BIF-008-W-C-019839-RI-80

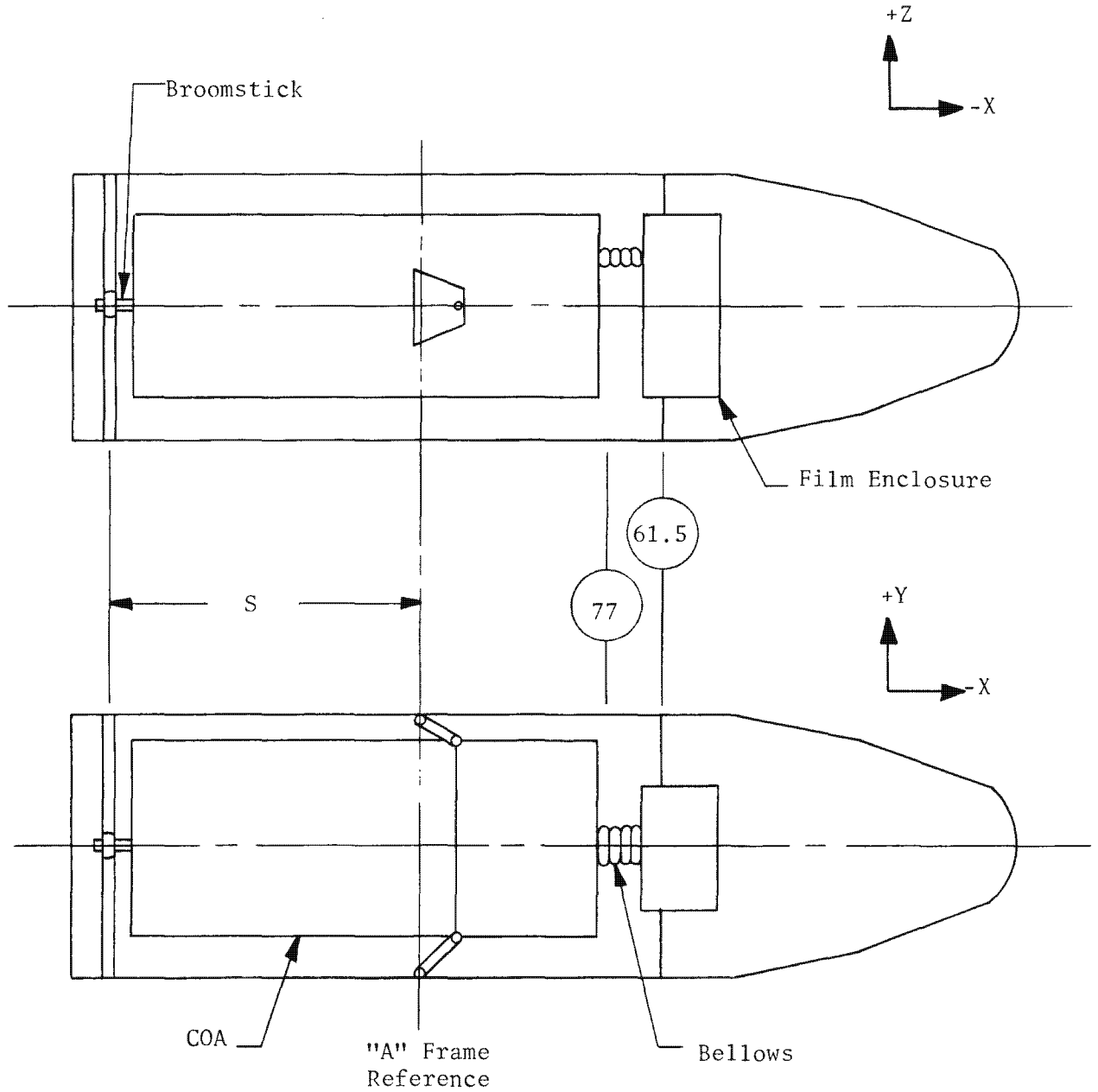


Figure 2.14-34. COA Suspension System Geometry

2.14-61

~~TOP SECRET~~ G

Handle via BYEMAN
Control System Only

~~TOP SECRET~~ G

BIF-008- W-C-019839-RI-80

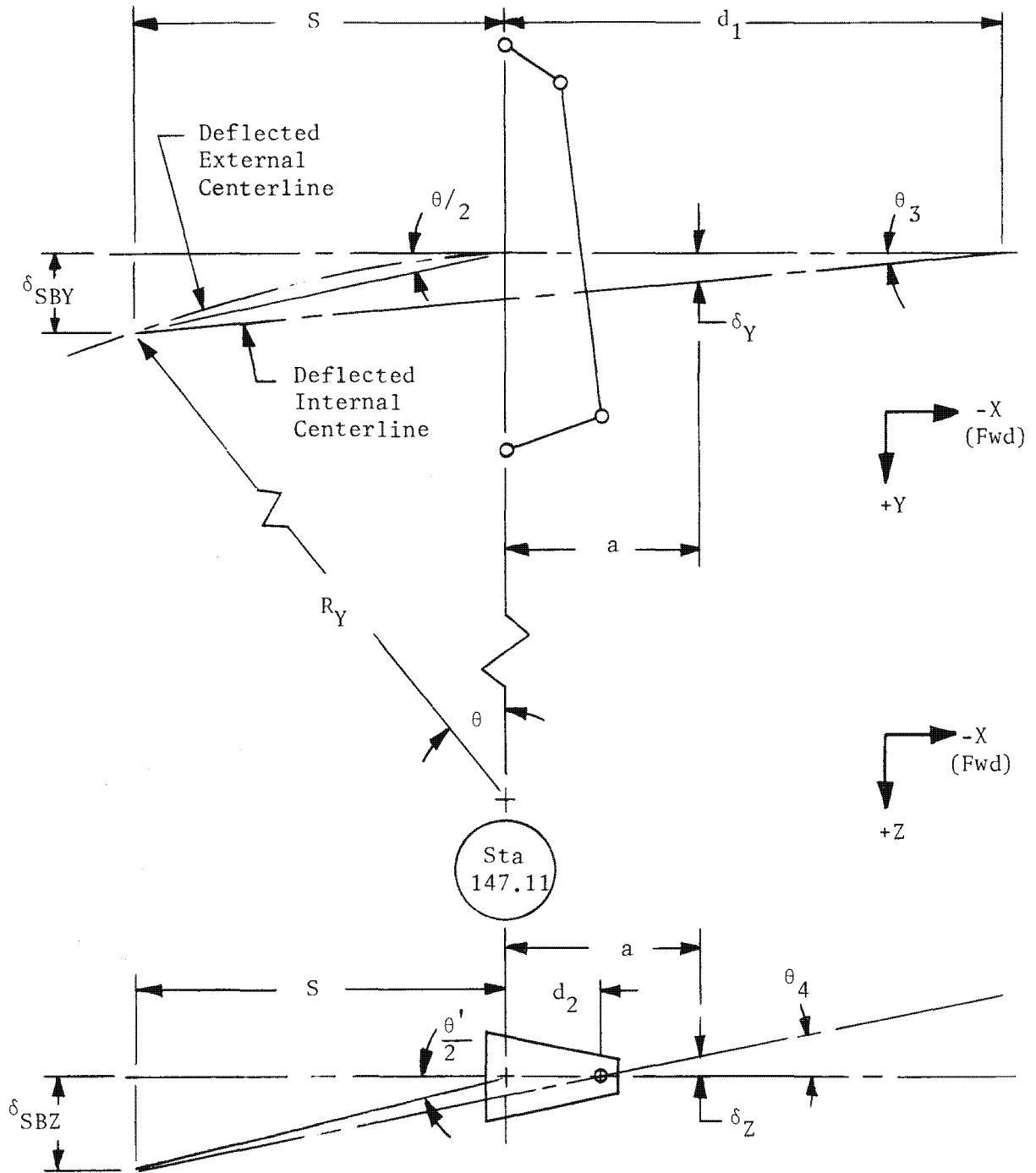


Figure 2.14-35. COA Suspension System Model

2.14-62

~~TOP SECRET~~ G

Handle via **BYEMAN**
Control System Only

~~TOP SECRET~~ G

BIF-008-W-C-019839-RI-80

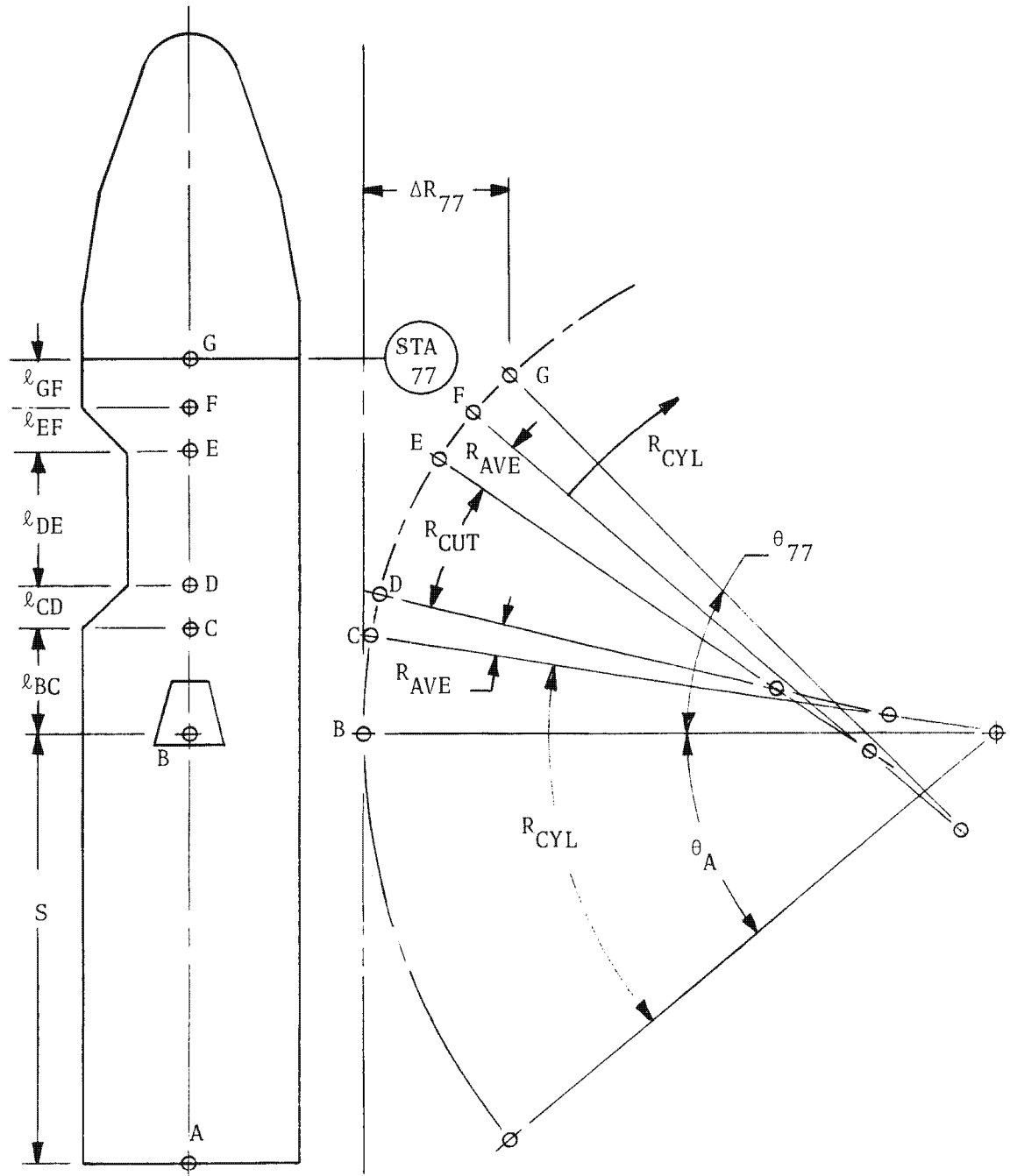


Figure 2.14-36. External Structure Centerline Deflection Model

2.14-63

~~TOP SECRET~~ G

Handle via BYEMAN
Control System Only

~~TOP SECRET~~ GBIF-008- W-C-019839-RI-80

$$\delta_{\text{SBY}} = S \left[\frac{\theta}{2} \right] \quad (2)$$

where: δ_{SBY} is the deflection of the spherical bearing in the Y direction with respect to the external structure centerline at Sta 147.11 (inches).

$$\theta_3 = \frac{\delta_{\text{SBY}}}{d_1 + S} \quad (3)$$

where: θ_3 is the angle of rotation in the X-Y plane of the internal structure centerline with respect to the external structure centerline at Sta 147.11 (radians).

d_1 is the distance from the Sta 147.11 reference to the location of the instantaneous center of rotation of the internal structure with respect to the external structure ($d_1 = 139.81$ inches for radii of curvature of interest).

$$\delta_Y = \theta_3 [d_1 - a] \quad (4)$$

where: a is the longitudinal location with respect to Sta 147.11 at which deflections are to be computed ($a = 147.11$ minus Sta number, inches).

δ_Y is the deflection of the internal structure in the Y direction at location a with respect to the external structure centerline at Sta 147.11 (inches).

2.14-64

~~TOP SECRET~~ GHandle via BYEMAN
Control System Only

~~TOP SECRET~~ GBIF-008- W-C-019839-RI-80

combining equations (1), (2), and (3):

$$\theta_3 = \frac{1}{R_Y} \left[\frac{S^2}{2(d_1 + S)} \right] = \frac{34.23}{R_Y} \text{ (radians)} = \frac{1961}{R_Y} \text{ (degrees)} \quad (5)$$

combining equations (4) and (5):

$$\delta_Y = \left[\frac{34.23}{R_Y} \right] [d_1 - a] = \left[\frac{34.23}{R_Y} \right] [\text{Sta No. } -7.3] \quad (6)$$

evaluated at Sta 77.0

$$\delta_Y = \frac{2386}{R_Y} \quad (6a)$$

Referring to Figure 2.14-35; X-Z view:

$$\theta' = \frac{S}{R_Z} \quad (\text{similar to equation (1)}) \quad (7)$$

Although not shown on the illustration due to space limitations, the location of R_Z may be inferred from the location of R_Y .

$$\delta_{SBZ} = S \left[\frac{\theta'}{2} \right] \quad (\text{similar to equation (2)}) \quad (8)$$

$$\theta_4 = \frac{\delta_{SBZ}}{d_2 + S} \quad (\text{similar to equation (3)}) \quad (9)$$

where: θ_4 is the angle of rotation in the X-Z plane of the internal structure centerline with respect to the external structure centerline at Sta 147.11 (radians).

d_2 is the distance from the Sta 147.11 reference to the A-frame pivot ($d_2 = 7.853$ inches).

$$\delta_Z = -\theta_4 (a - d_2) = \theta_4 [d_2 - a] \quad (10)$$

(similar to equation (4))

2.14-65

~~TOP SECRET~~ GHandle via BYEMAN
Control System Only

~~TOP SECRET~~ GBIF-008- W-C-019839-RI-80

combining equations (7), (8), and (9):

$$\theta_4 = \frac{1}{R_Z} \left[\frac{S^2}{2(d_2 + S)} \right] = \frac{65.22}{R_Z} \text{ (radians)} = \frac{3737}{R_Z} \text{ (degrees)} \quad (11)$$

combining equations (10) and (11):

$$\delta_Z = \left[\frac{65.22}{R_Z} \right] [d_2 - a] = \left[\frac{65.22}{R_Z} \right] [\text{Sta No. } -139.26] \quad (12)$$

evaluated at Sta 77.0:

$$\delta_Z = \frac{-4061}{R_Z} \quad (12a)$$

The model of the external structure used to determine centerline deflections is shown in Figure 2.14-36, the effect of the viewport door opening being included. A given curvature is applied to the cylindrical portion of the structure and a second curvature to the area of the cutout. An average of the two curvatures is applied to the transition sections. The following relationships between curvatures in the cylindrical and cutout sections have been determined by comparing curvatures calculated at various typical temperature distributions.*

Pitch Curvature (bending in X-Z plane):

$$C_{\text{CUT-Z}} = 2.15 C_{\text{CYL-Z}} - 5.7 \times 10^{-5} \quad (13)$$

Yaw Curvature (bending in X-Y plane):

$$C_{\text{CUT-Y}} = 1.34 C_{\text{CYL-Y}} \quad (14)$$

where: subscript CUT refers to viewport door cutout area,
 and subscript CYL refers to a cylindrical section.

*Reference PPS/DR Radius of Curvature Study, BIF-008-W-N-014194-OH-75.

~~TOP SECRET~~ G

~~TOP SECRET~~ G

BIF-008-W-C-019839-RI-80

Referring to Figure 2.14-36:

$$\theta_A = \frac{S}{R_{CYL}} = \frac{137.88}{R_{CYL}} \text{ (radians)} = \frac{7900}{R_{CYL}} \text{ (degrees)} \quad (15)$$

where: θ_A is the angle of rotation of the normal to the PPS/DP EAC-SCS interface with respect to the external structure centerline at Sta 147.11.

R_{CYL} is the radius of curvature of a cylindrical section, either Y or Z.

$$\theta_{77} = \theta_{BC} + \theta_{CD} + \theta_{DE} + \theta_{EF} + \theta_{FG} \quad (16)$$

where: θ_{77} is the angle between the external structure centerline at Sta 77.0 and the external structure centerline at Sta 147.11.

and $\theta_{BC} = l_{BC} / R_{CYL} = l_{BC} C_{CYL} = 11.308 C_{CYL}$

$$\theta_{CD} = l_{CD} / R_{AVG} = l_{CD} C_{AVG} = 11.170 C_{AVG}$$

$$\theta_{DE} = l_{DE} / R_{CUT} = l_{DE} C_{CUT} = 33.175 C_{CUT}$$

$$\theta_{EF} = l_{EF} / R_{AVG} = l_{EF} C_{AVG} = 11.170 C_{AVG}$$

$$\theta_{FG} = l_{FG} / R_{CYL} = l_{FG} C_{CYL} = 3.287 C_{CYL}$$

2.14-67

~~TOP SECRET~~ GHandle via BYEMAN
Control System Only

~~TOP SECRET~~ GBIF-008- W-C-019839-RI-80

Substituting the above definitions into equation (16) and combining with equations (13) and (14) yields the following:

$$\theta_{77-Z} \text{ (radians)} = \left[\frac{1}{R_{\text{CYL-Z}}} \right] \left[121.11 \right] - 252.77 \times 10^{-5} \quad (17a)$$

$$\theta_{77-Y} \text{ (radians)} = \left[\frac{1}{R_{\text{CYL-Y}}} \right] \left[85.187 \right] \quad (17b)$$

Equations (17a) and (17b) may be written for any point forward of the viewport door cutout at which the cylindrical curvature can be assumed to apply as follows:

$$\theta_Z \text{ (radians)} = \left[\frac{121.11}{R_{\text{CYL-Z}}} \right] - \left[252.77 \times 10^{-5} \right] + \left[\frac{77.00\text{-Sta No.}}{R_{\text{CYL-Z}}} \right] \quad (18a)$$

$$\theta_Y \text{ (radians)} = \left[\frac{85.187}{R_{\text{CYL-Y}}} \right] + \left[\frac{77.00\text{-Sta No.}}{R_{\text{CYL-Y}}} \right] \quad (18b)$$

Referring to Figure 2.14-36:

$$\Delta R_{77} = \Delta R_{\text{BC}} + \Delta R_{\text{CD}} + \Delta R_{\text{DE}} + \Delta R_{\text{EF}} + \Delta R_{\text{FG}} \quad (19)$$

where: ΔR_{77} is the radial deflection of the external structure centerline at Sta 77.0 with respect to the external structure centerline at Sta 147.11.

2.14-68

~~TOP SECRET~~ GHandle via BYEMAN
Control System Only

~~TOP SECRET~~ GBIF-008-W-C-019839-RI-80

and

$$\begin{aligned} \Delta R_{BC} &= R_{CYL} \left[1 - \cos \theta_{BC} \right] \\ \Delta R_{CD} &= R_{AVG} \left[\cos \theta_{BC} - \cos \theta_{BD} \right] \\ \Delta R_{DE} &= R_{CUT} \left[\cos \theta_{BD} - \cos \theta_{BE} \right] \\ \Delta R_{EF} &= R_{AVG} \left[\cos \theta_{BE} - \cos \theta_{BF} \right] \\ \Delta R_{FG} &= R_{CYL} \left[\cos \theta_{BF} - \cos \theta_{BG} \right] \end{aligned}$$

Equation (19) may be modified for any point forward of the viewport door cutout at which cylindrical curvature can be assumed to apply as follows:

$$\Delta R = \Delta R_{77} + R_{CYL} \left\{ \cos \theta_{77} - \cos \left[\theta_{77} + \frac{(77.00 - \text{Sta No.})}{R_{CYL}} \right] \right\} \quad (20)$$

Calculation of rotation of COA optical axis with respect to SCS

Referring to Figure 2.14-37; X-Y view:

$$\phi_Y = \theta_A - \theta_3 \quad (21)$$

where:

ϕ_Y is the angular rotation in the X-Y plane of the internal structure (COA) axis with respect to the external structure axis at the SCS interface.

θ_A is the angular rotation of the external structure centerline at Sta 147.11 with respect to the external structure centerline at the SCS interface (equation (15)).

2.14-69

~~TOP SECRET~~ GHandle via BYEMAN
Control System Only

~~TOP SECRET~~ G

BIF-008- W-C-019839-RI-80

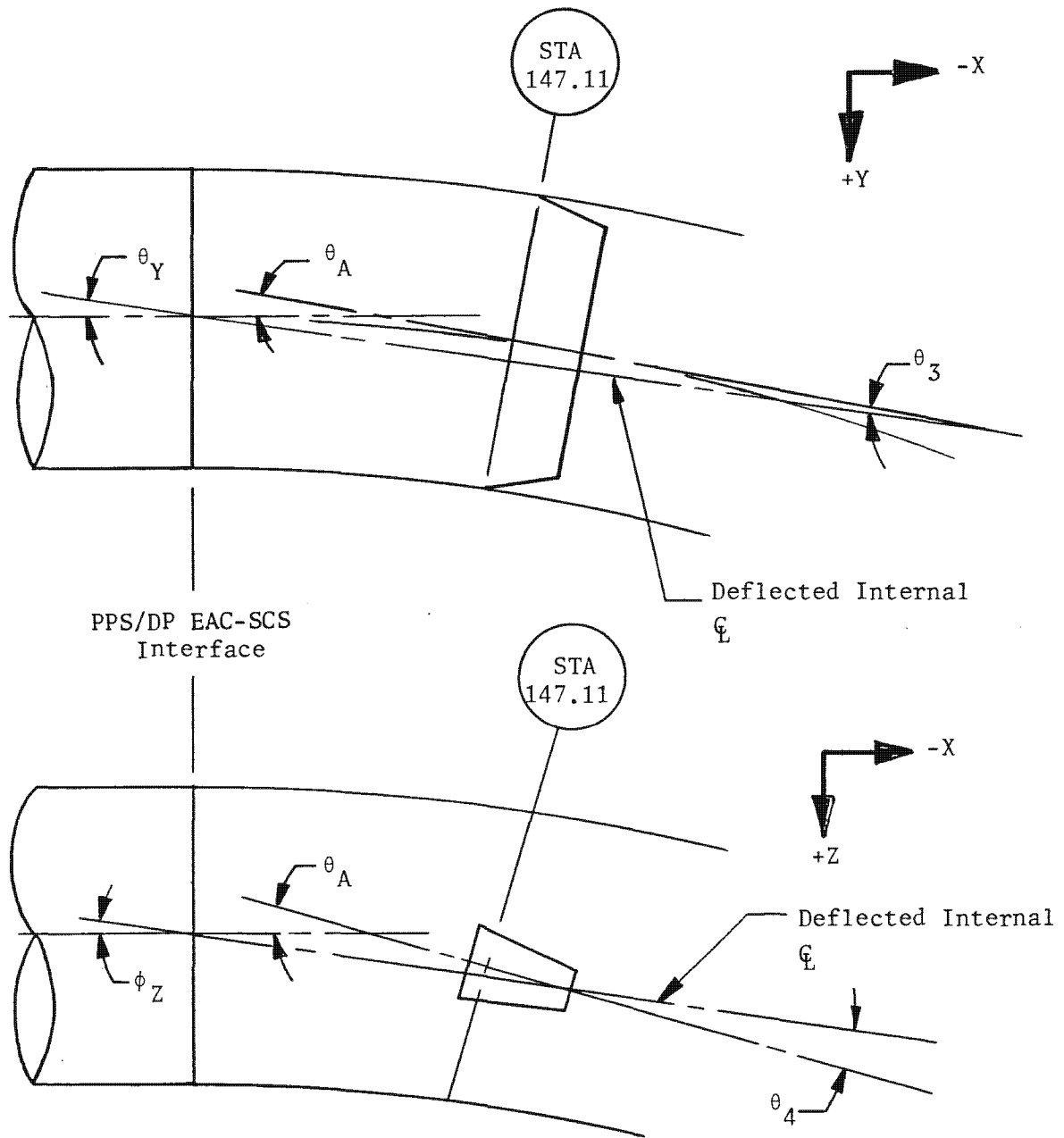


Figure 2.14-37. Angular Rotation Of COA Axis With Respect To SCS Axis

2.14-70

~~TOP SECRET~~ G

Handle via BYEMAN
Control System Only

~~TOP SECRET~~ GBIF-008- W-C-019839-RI-80

θ_3 is the angular rotation of the internal structure centerline with respect to the external structure centerline at Sta 147.11 (equation (5)).

Combining equations (21), (15), and (5):

$$\phi_Y \text{ (degrees)} = \frac{7900}{R_Y} - \frac{1961}{R_Y} = \frac{5939}{R_Y} \quad (22)$$

Referring to Figure 2.14-37; X-Z view:

$$\phi_Z = \theta_A - \theta_4 \quad (\text{similar to equation (21)}) \quad (23)$$

Combining equations (21), (15), and (11):

$$\phi_Z \text{ (degrees)} = \frac{7900}{R_Z} - \frac{3737}{R_Z} = \frac{4163}{R_Z} \quad (24)$$

Equations (22) and (24) have been solved at various radii to obtain the curves shown in Figure 2.14-23.

The suspension system model derivation is extended in the PPS/DR Radius of Curvature Study to include computation of both axial and radial deflections of off-axis points. The model is incorporated in a Fortran IV-G computer program which allows the displaced positions of points on either internal or external structures to be readily computed for any external structure curvature. A comparison of the displaced positions of internal and external structure points is made and interference conditions are flagged.

2.14-71

~~TOP SECRET~~ GHandle via BYEMAN
Control System Only

~~TOP SECRET~~ GBIF-008- W-C-019839-RI-80

A hardware review and analysis, reported in the PPS/DR Radius of Curvature Study, identified possible locations of structural interference and derived the appropriate curvature constraints. The curvature constraint for the PPS/DP EAC based on the results reported, is shown in Figure 2.14-38.

The operating curvature range of Figure 2.14-38 corresponds to radii of curvature of $R_Y = \pm 17,000$ inches and $R_Z = \pm 25,000$ inches. The deflections calculated at these radii have been included in the film tracking budget. The nonoperating curvature range represents those curvatures to which the PPS/DP EAC may be subjected in a nonoperating state. Structural interferences have been calculated for curvatures greater than the nonoperating range of Figure 2.14-38.

2.14-72

~~TOP SECRET~~ GHandle via BYEMAN
Control System Only

~~TOP SECRET~~ G

BIF-008- W-C-019839-RI-80

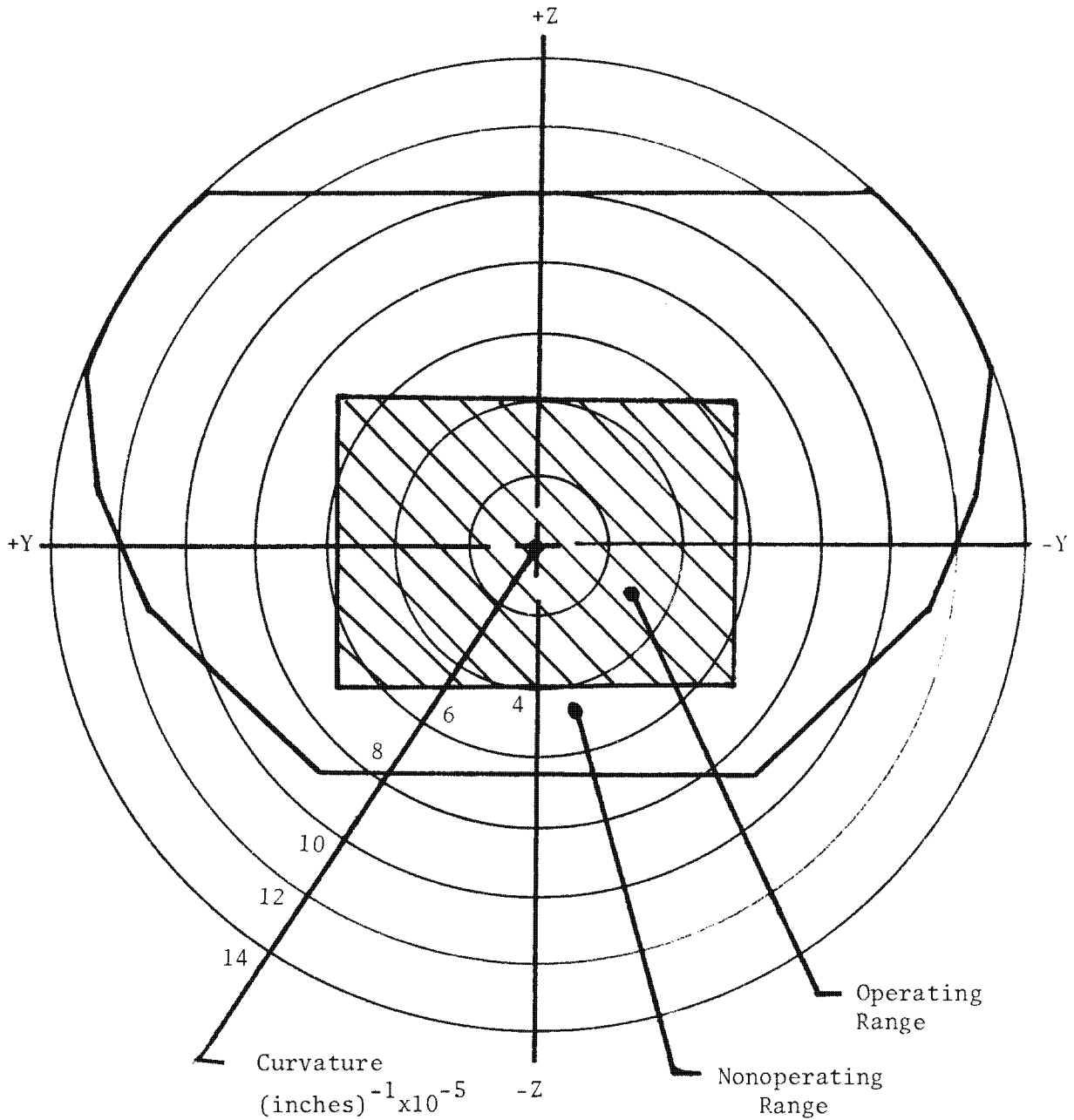


Figure 2.14-38. Operating and Nonoperating Curvature Constraints

2.14-73

~~TOP SECRET~~ G

Handle via BYEMAN
Control System Only

~~TOP SECRET~~ G

BIF-008- W-C-019839-RI-80

This page intentionally blank

2.14-74

~~TOP SECRET~~ G

Handle via BYEMAN
Control System Only

~~TOP SECRET~~ GBIF-008- W-C-019839-RI-80

15.0 EJECTION ANALYSIS

During the course of a Gambit mission, four items must be successfully ejected from the PPS/DP EAC. These four are:

- (1) main hatch
- (2) SRV 1
- (3) ejectable adapter
- (4) SRV 2

Each of these is discussed below with particular emphasis on those cases where the possibility of contact between an ejected component and the PPS/DP EAC could not be dismissed.

15.1 Main Hatch

The main hatch is ejected prior to insertion of the vehicle into orbit. Pyro operated pin-pullers are actuated to release the hatch which is then given a velocity increment ("pushed off") perpendicular to the PPS/DP EAC X-axis by leaf-type springs. Since the photographic satellite vehicle (PSV) is still in the ascent phase at this time, any reasonable incremental velocity will insure successful ejection.

15.2 Dual Recovery Module (DRM) Ejectable Components

Figure 2.15-1 shows the location of the ejectable and fixed components of the DRM. All ejectable components are released by pyro-actuated pin-pullers prior to actual ejection.

2.15-1

~~TOP SECRET~~ GHandle via BYEMAN
Control System Only

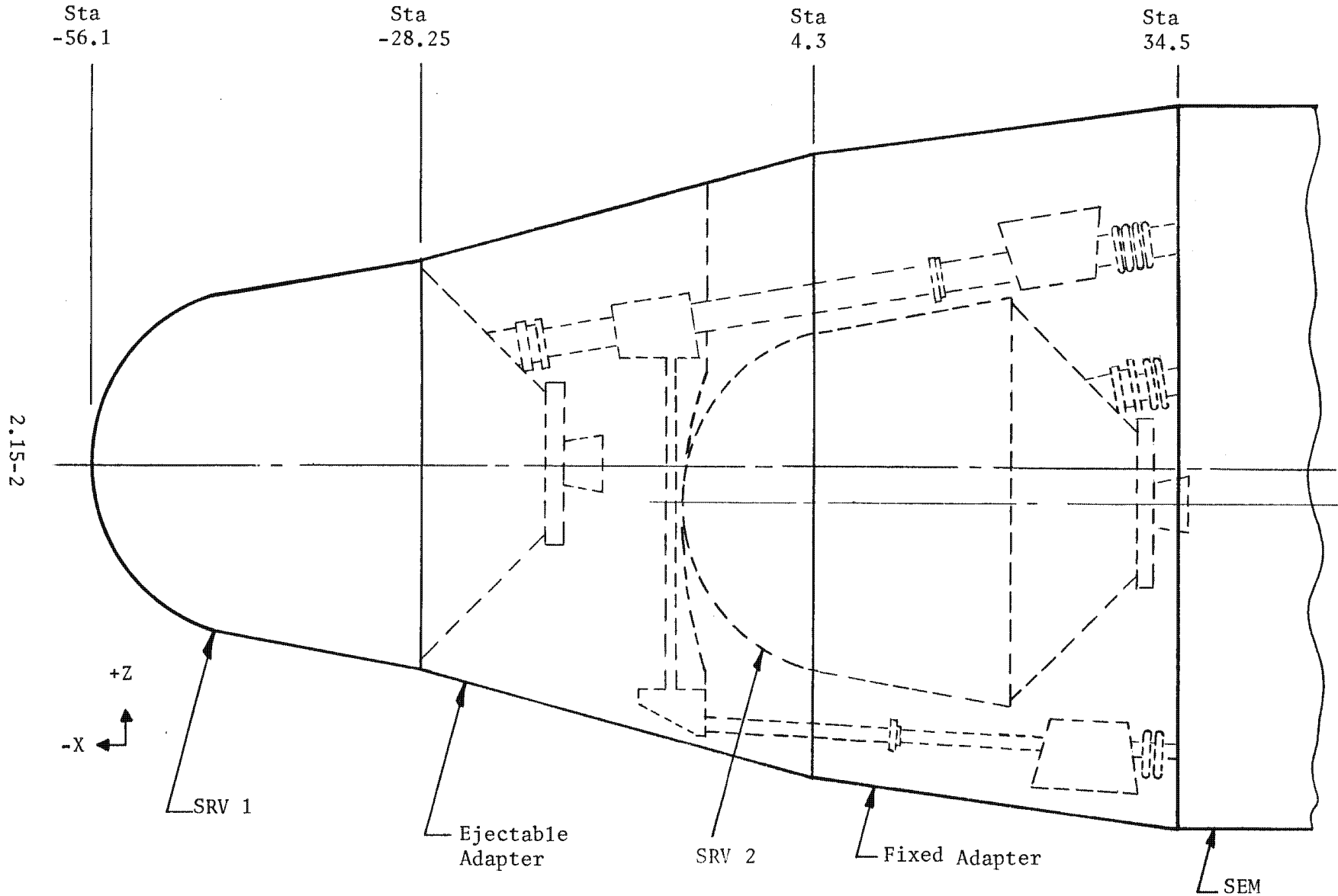


Figure 2.15-1. PPS/DP EAC Ejectable Components

Handle via BYEMAN
Control System Only

Approved for Release: 2017/02/14 C05097220

Approved for Release: 2017/02/14 C05097220

~~TOP SECRET~~ GBIF-008- W-C-019839-RI-80

15.2.1 SRV 1 and SRV 2

Both SRV 1 and SRV 2 are ejected by four spring ejectors powered by coil springs. An additional force is provided by the compression of the film tunnel gasket but successful ejection is in no way dependent on this force.

Because of the extreme forward location of SRV 1 and the lack of any potentially interfering hardware, a formal ejection analysis was not performed.

15.2.2 Ejectable Adapter (EA)

The ejectable adapter (EA) is ejected near the completion of the second mission segment. The EA must be successfully ejected in order for the SRV 2 ejection sequence to proceed. In the case of failure of SRV 1 to eject, the EA may be ejected with SRV 1 attached. Under these conditions, successful recovery of SRV 1 is highly unlikely. The case assuming failure of SRV 1 to eject was not investigated.

15.3 Ejection Model

During the ejection process, both the EA and the SRV may be treated as a rigid body under the influence of unbalanced and time-varying forces. The ejection model consists of the appropriate free-body equations describing motions in the X-Z plane, along with the distributions of the forces, misalignments, etc. needed to trace the ejection path.

2.15-3

~~TOP SECRET~~ GHandle via BYEMAN
Control System Only

~~TOP SECRET~~ GBIF-008- W-C-019839-RI-80

15.3.1 General Free-Body Equations

In the reference plane shown in Figure 2.15-2, the general free-body equations are:

$$\begin{aligned} \Sigma F_x &= m \ddot{X} \\ \Sigma F_z &= m \ddot{Z} \\ \Sigma M_{CG} &= I_{CG} \ddot{\theta} \end{aligned} \quad \text{OR} \quad \begin{Bmatrix} \Sigma F_x \\ \Sigma F_z \\ \Sigma M_{\theta} \end{Bmatrix} = \begin{bmatrix} m & 0 & 0 \\ 0 & m & 0 \\ 0 & 0 & I_{CG} \end{bmatrix} \begin{Bmatrix} \ddot{X} \\ \ddot{Z} \\ \ddot{\theta} \end{Bmatrix}$$

Where:

m = mass of ejected body

$\ddot{X}, \ddot{Z}, \ddot{\theta}$ = accelerations in the x-direction,
z-direction, and angular about a Y-axis through the
center of gravity, respectively.

ΣF_x = summation of forces in the x-direction

ΣF_z = summation of forces in the z-direction

ΣM_{CG} = summation of the moments about the center of gravity

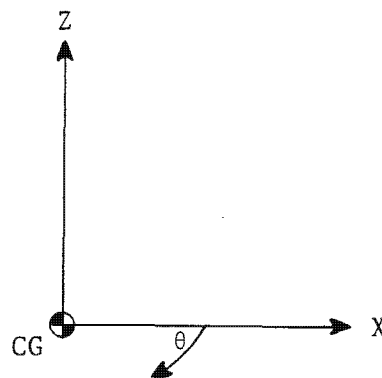


Figure 2.15-2. Free-Body Reference Plane

2.15-4

~~TOP SECRET~~ GHandle via BYEMAN
Control System Only

~~TOP SECRET~~ GBIF-008- W-C-019839-RI-80

15.3.2 Spring Ejectors

The forces acting on the SRVs are applied by 4 spring ejectors and a tunnel gasket. The EA is accelerated by 3 spring ejectors. Theoretically, the force-deflection curve for a push-off spring is as shown in Figure 2.15-3.

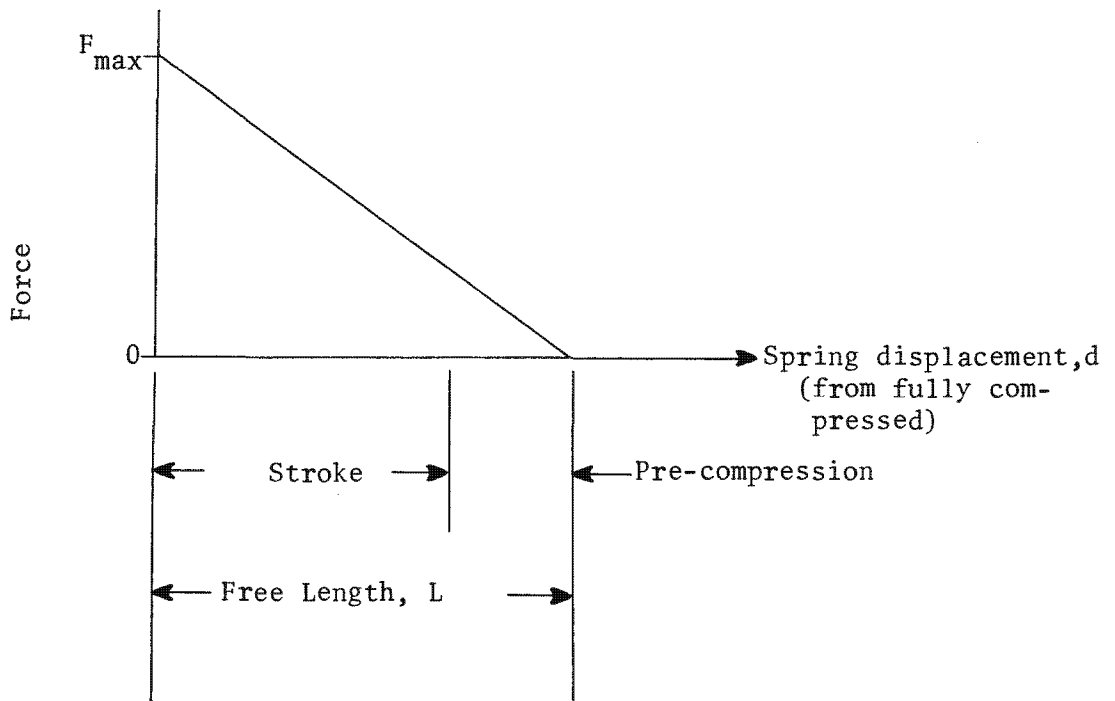


Figure 2.15-3. Theoretical Force-Displacement Curve

The equation describing force as a function of displacement from the fully compressed state is:

$$F = F_{max} \left(1 - \frac{d}{L}\right)$$

Where: F = force

F_{max} = force at maximum compression

d = displacement from maximum compression

L = free length

~~TOP SECRET~~ G

~~TOP SECRET~~ GBIF-008- W-C-019839-RI-80

15.3.2.1 Spring Force Adjustments. Theoretically, spring force is calculated simply by multiplying spring rate by spring deformation. However, because these springs are placed in a spring ejector assembly, it is expected that the spring force will be somewhat lower than theory predicts. Figure 2.15-4 depicts a spring ejector assembly. The expected reduction in force is a result of frictional forces, such as contact between spring coils and spring guide rod. A number of spring ejector assemblies were tested to determine force-deflection curves. Results of these tests are then used to modify the spring rates to account for assembly losses.

15.3.2.2 Spring Force Alignment. Ideally, the spring ejector pistons should be aligned perfectly with the X-axis; in reality this situation is very unlikely to occur. There are 2 ways in which the pistons can be misaligned: the shell with respect to the vehicle X-axis, and the piston with respect to the shell centerline. The first of these two misalignments is constant during the ejection; the second is dependent on the position of the piston within the shell, and thus varies during the ejection.

15.3.2.3 Piston Alignment. A tolerance study of the spring ejector assembly has shown that the maximum piston misalignments (ϕ) are:

extended position	ϕ_{em}	= + 5.15 deg
compressed position	ϕ_{cm}	= \pm 0.52 deg

It is assumed that piston alignment is linearly dependent on the position of the piston within the shell. Therefore, knowing the stroke, maximum compressed misalignment, ϕ_{cm} , and maximum extended misalignment, ϕ_{em} , it is possible to write an expression relating maximum piston misalignment to piston position within the shell.

2.15-6

~~TOP SECRET~~ GHandle via BYEMAN
Control System Only

2.15-7

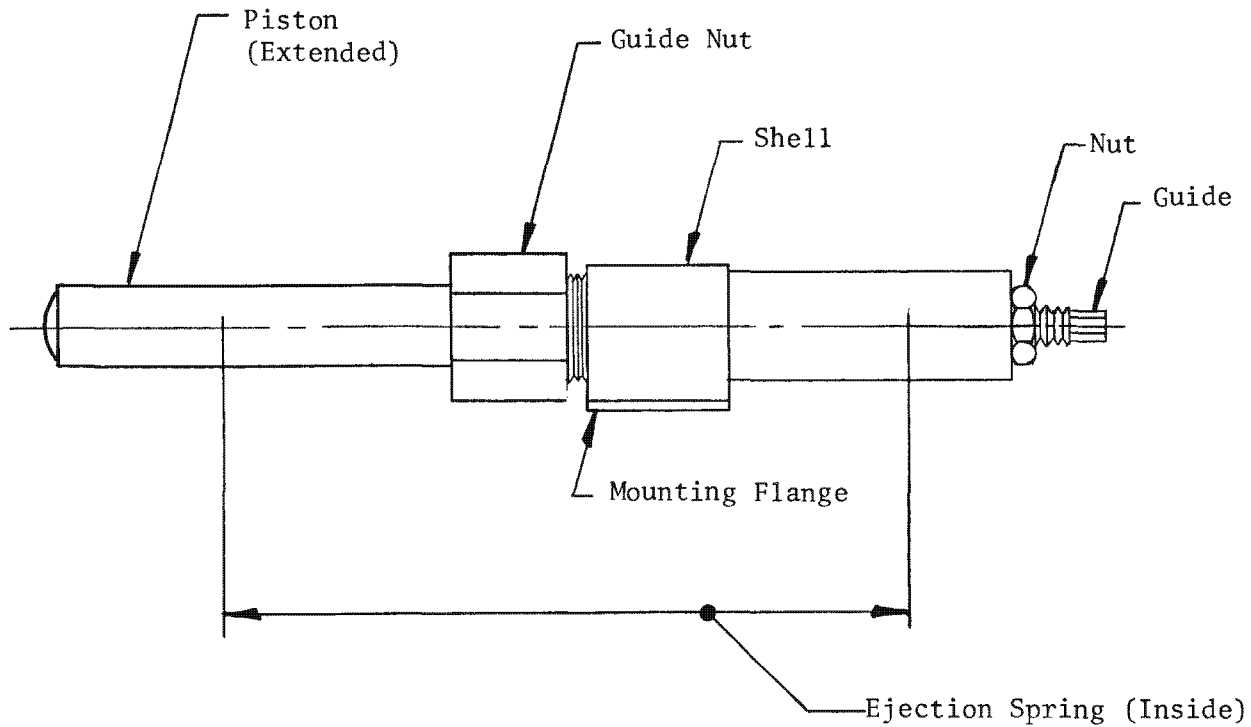


Figure 2.15-4. Spring Ejector Assembly

Approved for Release: 2017/02/14 C05097220

Approved for Release: 2017/02/14 C05097220

~~TOP SECRET~~ GBIF-008- W-C-019839-RI-80

It is further assumed that the piston will not slip on the pad provided. Thus, in order to determine the piston misalignment as a function of displacement, it is necessary to monitor the piston-pad contact points. As the component is pushed off, piston misalignment is updated by comparing maximum allowed misalignment with the misalignment calculated by monitoring the piston-pad contact point.

15.3.3 Mass Properties

15.3.3.1 Center of Gravity Offset. Values for center of gravity offset (\bar{Z}) for an SRV vary with the amount of film on each take-up spool. Additionally, the normal statistical variability about the mean offset value must be accounted for. Table 2.15-1 summarizes the parameters of the distributions used for the analysis.

TABLE 2.15-1
Center of Gravity Offsets (\bar{Z})

<u>SRV Configuration</u>	<u>\bar{Z}</u> <u>(inches)</u>	<u>3σ</u> <u>(inches)</u>
9-inch spool full; 5-inch spool full	0.04	0.02
9-inch spool empty; 5-inch spool full	0.04	0.02
9-inch spool full; 5-inch spool empty	0.15	0.02
9-inch spool empty; 5-inch spool empty	0.15	0.02
EA	-1.700	0.02

15.3.3.2 Other Mass Properties. The remaining mass properties (weight, location of center-of-gravity along the X-axis, and moment of inertia) are denoted W , \bar{X} and I_{YY} respectively. The assumed values for these properties are summarized in Table 2.15-2.

2.15-8

~~TOP SECRET~~ GHandle via BYEMAN
Control System Only

~~TOP SECRET~~ GBIF-008-1 W-C-019839-RI-80

The SRV mass properties represented the best available estimates for worst-case conditions.

TABLE 2.15-2
Mass Properties
(1/78 Estimate)

	Weight (pounds)	\bar{X} (inches)	I_{YY} (Slug/ft ²)
SRV			
9-inch spool full; 5-inch spool full	470.0	11.26	16.44
9-inch spool empty; 5-inch spool full	407.8	12.64	14.98
9-inch spool full; 5-inch spool empty	460.9	11.27	16.46
9-inch spool empty; 5-inch spool empty	399.0	12.67	14.90
EA	83.5	-9.70	4.70

Results based on mass properties are included in Section 15.5.

15.3.4 Monte Carlo Approach

A Monte Carlo approach to analysis requires an analytic expression which may be solved explicitly. The parameters required for solution are chosen randomly from known or assumed distributions, or are taken to be worst-case values.

For the present case, the free-body equations are numerically integrated to determine the X, Z, and θ (rotational) components of velocity and displacement of the center of gravity. Knowing the geometric relationship between the CG and potential interfering points on both ejectable and fixed bodies, miss-distances are then calculated. Over a number of trials, populations of miss-distance and ejection velocity are constructed. The resulting populations are examined by application of the Kolmogorov-Smirnov test to evaluate normality. In all cases, the distributions are acceptably normal.

2.15-9
~~TOP SECRET~~ G

Handle via BYEMAN
Control System Only

~~TOP SECRET~~ GBIF-008- W-C-019839-RI-80

15.3.4.1 Parameters. The parameters for the distributions used are summarized in Table 2.15-3.

TABLE 2.15-3
Distribution Parameters

Parameter	Symbol	Mean	3σ
Spring Housing Misalignment	-	0.00 degree	1.00 degree
Maximum Compressed Plunger Misalignment	ϕ_{cm}	0.00 degree	0.52 degree
CG Offset, SRV	\bar{z}		
9-inch full; 5-inch full		0.04 inch	0.02 inch
9-inch empty; 5-inch full		0.04 inch	0.02 inch
9-inch full; 5-inch empty		0.15 inch	0.02 inch
9-inch empty; 5-inch empty		0.15 inch	0.02 inch
CG Offset, EA	\bar{z}	-1.700 inches	0.02 inch

The maximum extended piston misalignment, ϕ_{em} , is calculated from the randomly chosen compressed piston misalignment, ϕ_{cm} . It is assumed that the ratio of maximum compressed misalignment to maximum extended misalignment is constant. Therefore, once the maximum compressed misalignment is selected, the maximum extended misalignment may be calculated.

15.4 Application of the Model

15.4.1 Ejectable Adapter Geometry

The ejection force geometry of the ejectable adapter and the applicable free-body diagram are shown in Figures 2.15-5 and 2.15-6 respectively. Figures 2.15-7 shows the SRV 2 space allocation and locates those areas where possible encroachment or collision is of concern for both EA and SRV 2 ejections.

~~TOP SECRET~~ G

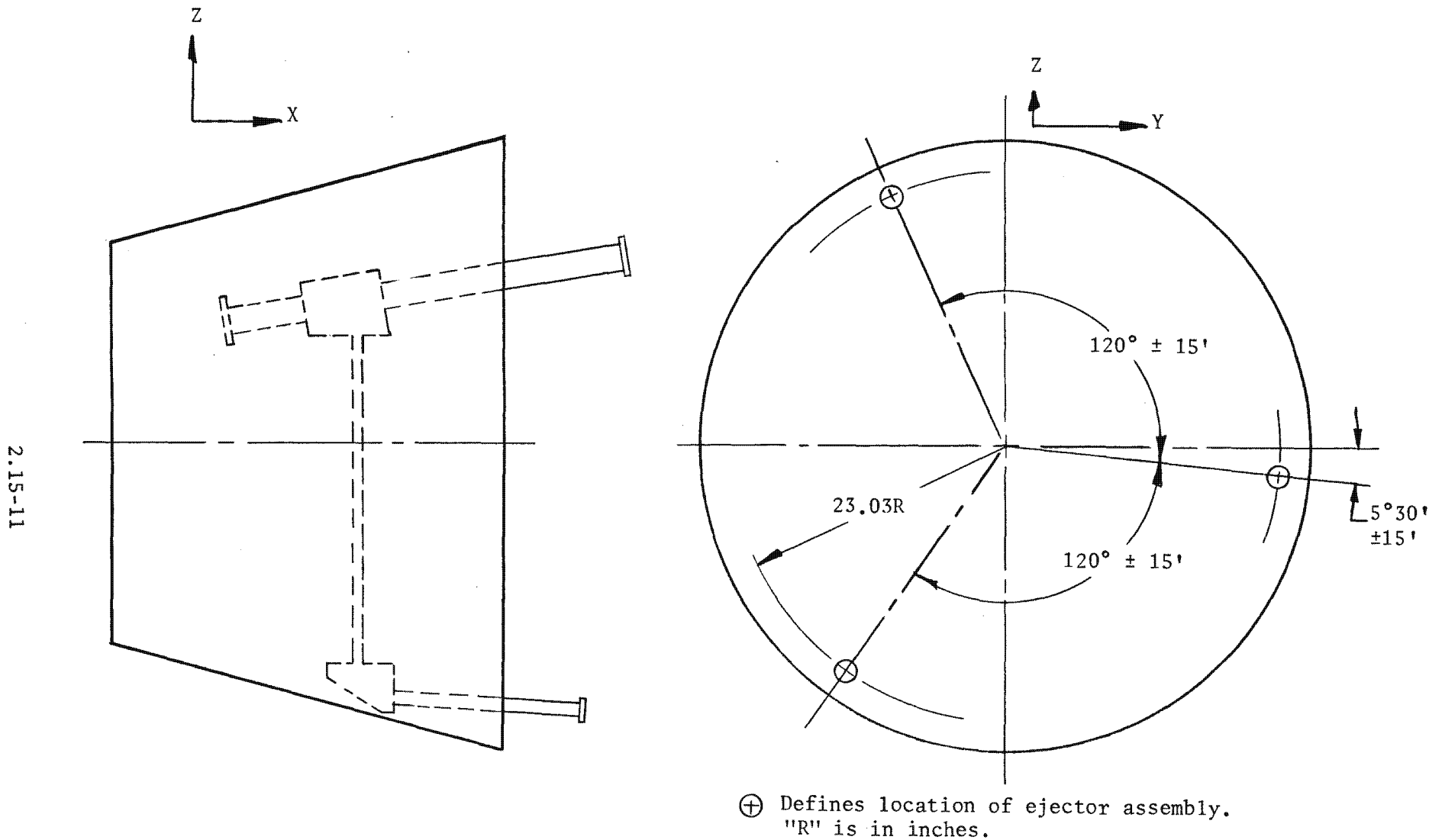


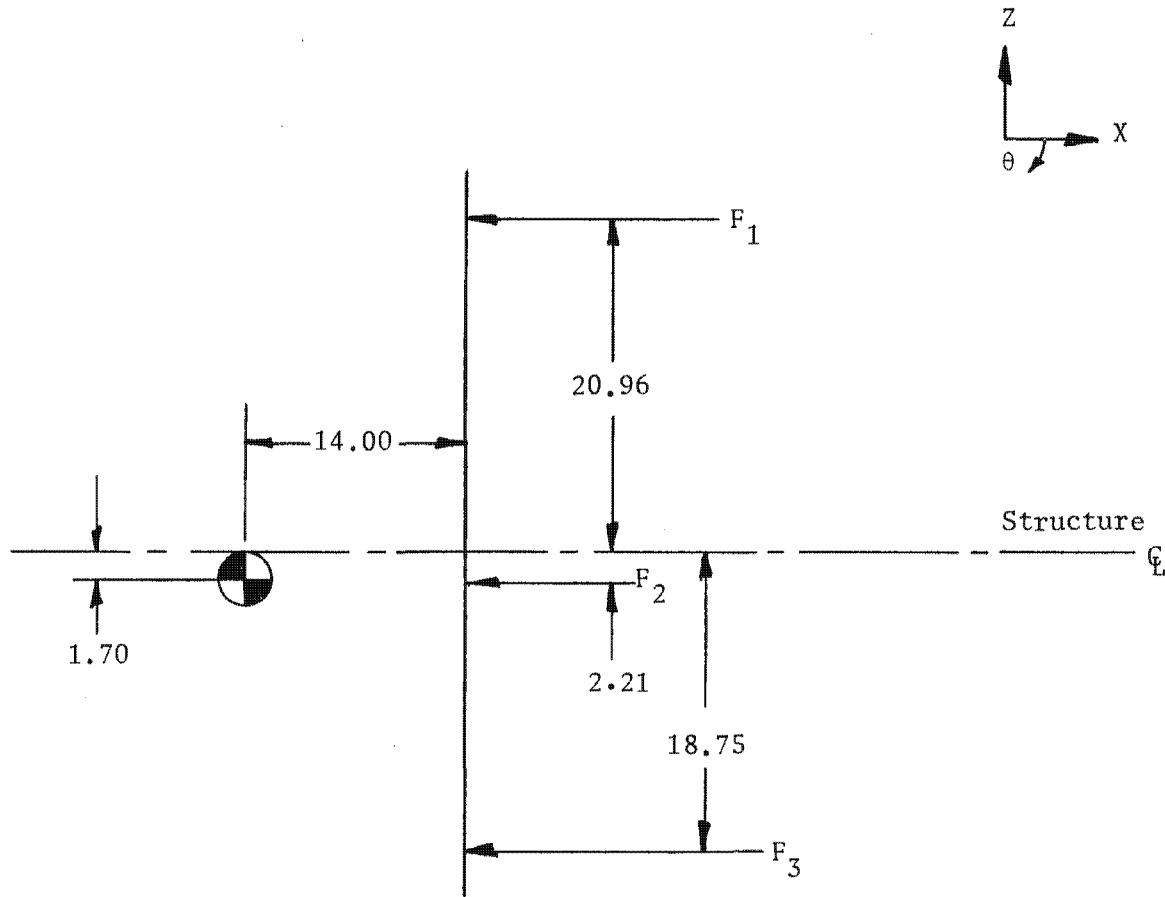
Figure 2.15-5. Ejection Force Geometry, Ejectable Adapter

Handle via BYEMAN
Control System Only

Approved for Release: 2017/02/14 C05097220

Approved for Release: 2017/02/14 C05097220

2.15-12



Dimensions in inches

Figure 2.15-6. Free-Body Diagram, Ejectable Adapter

Handle via BYEMAN
Control System Only

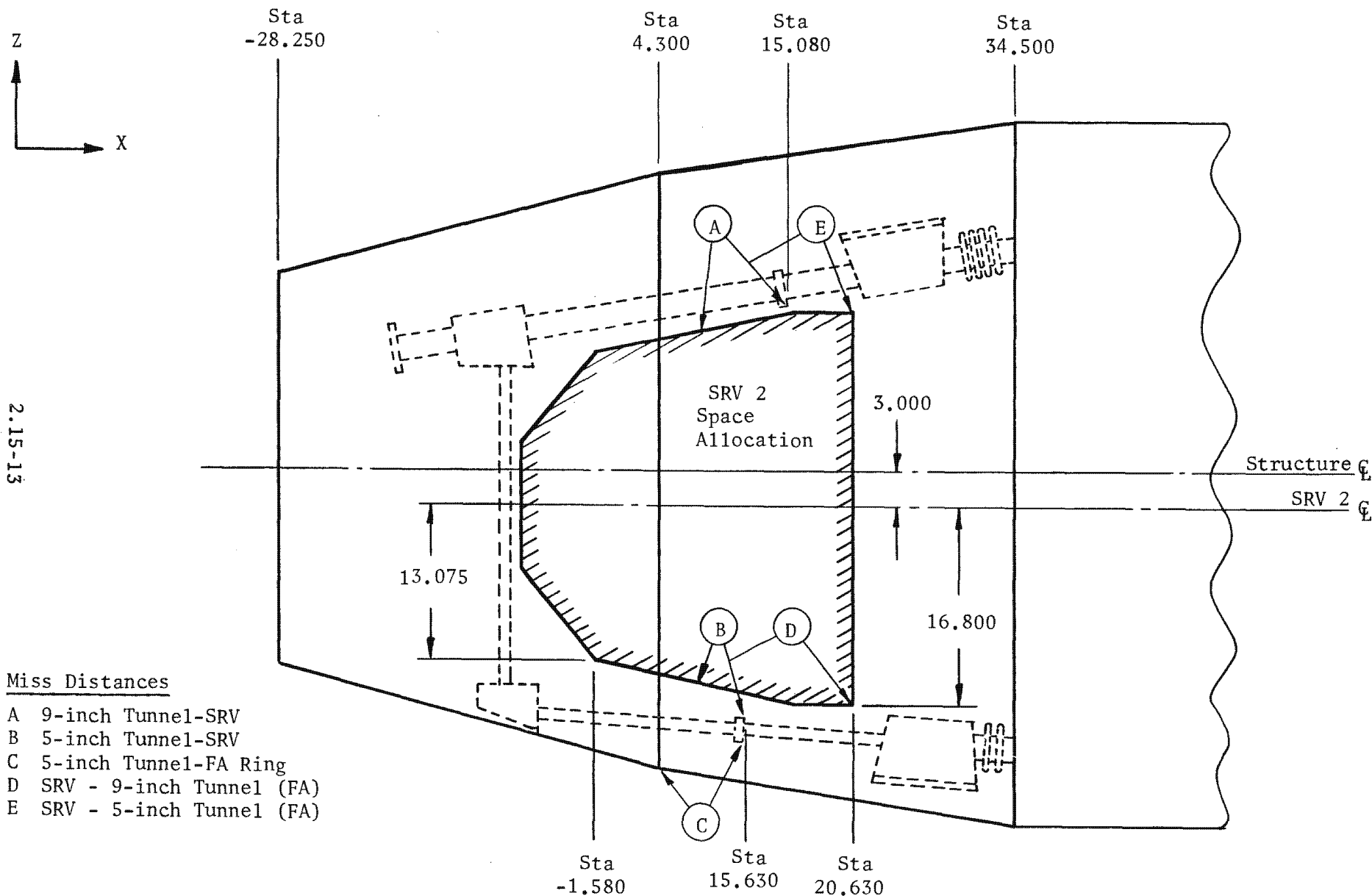


Figure 2.15-7. Ejectable Adapter Configuration

Handle via **BYEMAN**
Control System Only

Approved for Release: 2017/02/14 C05097220

2.15-13

Approved for Release: 2017/02/14 C05097220

~~TOP SECRET~~ GBIF-008- W-C-019839-RI-80

15.4.2 SRV 2 Geometry

The ejection force geometry of the SRV and the appropriate free-body diagram are shown in Figures 2.15-8 and 2.15-9 respectively.

15.5 Results

For the EA ejection case, the 9-inch tunnel moved (in all 150 trials) away from the SRV space allocation (miss-distance A in Figure 2.15-7), so that minimum miss-distance was prior to ejection. In all but 4 trials, the 5-inch tunnel moved away from the SRV space allocation (miss-distance B in Figure 2.15-7). The minimum miss-distance calculated was 1.622 inches. The critical miss-distance for EA ejection is, therefore, the 5-inch tunnel to fixed adapter ring miss-distance, shown as C on Figure 2.15-7. For the SRV ejection case, the minimum distances are D and E, both of which must be monitored.

The means and standard deviations of miss-distances and ejection velocities for the critical cases using the mass properties defined in Tables 2.15-1 and 2.15-2 are presented in Table 2.15-5.

A comparison of miss-distance ranges is shown in Table 2.15-4.

TABLE 2.15-4

Estimated Range of Miss-Distances*
(Mean $\pm 3.811\sigma$)

<u>SRV Configuration</u>	<u>Distance E</u> <u>(inches)</u>	<u>Distance D</u> <u>(inches)</u>
9-inch full; 5-inch full	0.039/0.653	0.380/1.656
9-inch full; 5-inch empty	0.073/0.691	0.340/1.560
9-inch empty; 5-inch full	0.117/0.623	0.456/1.498
9-inch empty; 5-inch empty	0.143/0.654	0.422/1.422

EA

Distance C = 1.446/1.712

*See Figure 2.15-7.

2.15-14

~~TOP SECRET~~ GHandle via BYEMAN
Control System Only

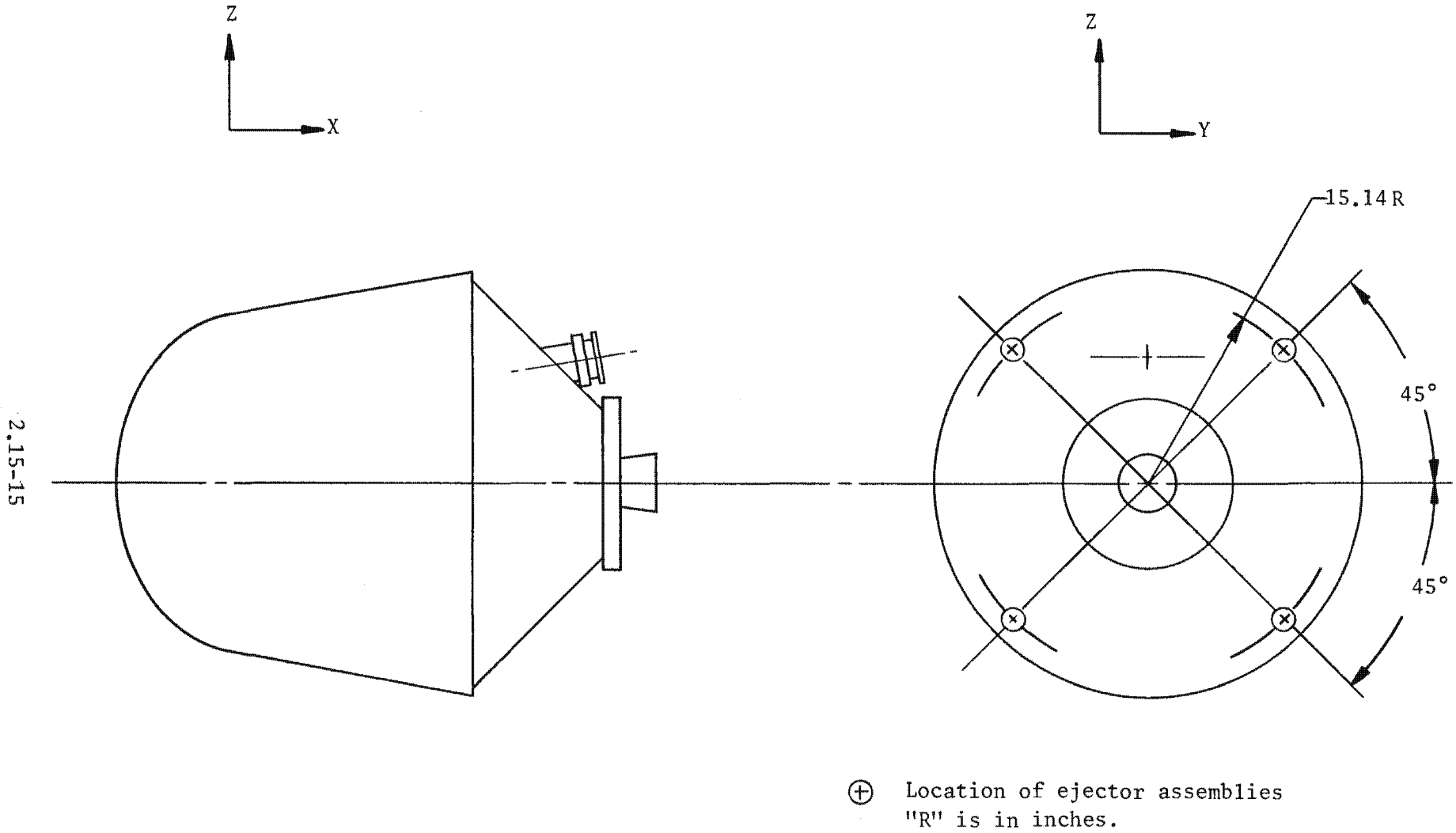


Figure 2.15-8. Ejection Force Geometry, SRV

Handle via **BYEMAN**
Control System Only

Approved for Release: 2017/02/14 C05097220

Approved for Release: 2017/02/14 C05097220

TABLE 2.15-5
Analysis Result for Mass Properties

<u>Configuration</u>	<u>Miss-Distance</u>		<u>Ejection Velocity</u>		<u>Ejection Velocity</u>		<u>Ejection Velocity</u>	
	Mean (inches)	Std Dev (inches)	\dot{X} (in/sec) Mean	Std Dev	\dot{Z} (in/sec) Mean	Std Dev	$\dot{\theta}$ (rad/sec) Mean	Std Dev
<u>EA Ejection</u>								
Distance C*	1.579	0.186	-30.696	0.630	0.466	0.135	-0.119	0.033
<u>SRV Ejection</u>								
Distance E*								
9-inch full; 5-inch full	0.346	0.081	-15.135	0.279	- 0.046	0.079	- 0.019	0.020
9-inch full; 5-inch empty	0.382	0.081	-15.286	0.281	- 0.072	0.080	- 0.011	0.020
9-inch empty; 5-inch full	0.370	0.066	-16.258	0.304	- 0.071	0.079	- 0.019	0.022
9-inch empty; 5-inch empty	0.399	0.067	-16.429	0.303	- 0.095	0.080	- 0.012	0.022
<u>SRV Ejection</u>								
Distance D*								
9-inch full; 5-inch full	1.018	0.167	-15.135	0.279	- 0.046	0.079	- 0.019	0.020
9-inch full; 5-inch empty	0.950	0.160	-15.286	0.281	- 0.072	0.080	- 0.011	0.020
9-inch empty; 5-inch full	0.977	0.137	-16.258	0.304	- 0.071	0.079	- 0.019	0.022
9-inch empty; 5-inch empty	0.922	0.131	-16.429	0.303	- 0.095	0.080	- 0.012	0.022

* Distance C, D, and E are defined on Figure 2.15-7.

2.15-17

~~TOP SECRET~~ G

BIF-008- W-C-019839-RI-80

15.6 Conclusions

15.6.1 SRV 1

Due to the lack of potentially interfering hardware the probability of interference of SRV 1 with any portion of the PPS/DP EAC is near zero.

15.6.2 Ejectable Adapter

At the 99% confidence level, the probability of the 5-inch tunnel approaching closer than 1.446-inches to the fixed adapter ring is 0.001.

15.6.3 SRV 2

It is concluded that the probability is 0.99 that at least 0.999 of the SRV ejections will not hit the FA.

2.15-18

~~TOP SECRET~~ G

Handle via BYEMAN
Control System Only

~~TOP SECRET~~ GBIF-008- W-C-019839-RI-80

16.0 CONSUMABLES MANAGEMENT

When a Gambit photographic reconnaissance vehicle is placed in orbit it carries with it various expendable items. These expendables are:

- (1) photographic film
- (2) electrical power (energy)
- (3) attitude control gas
- (4) orbit maintenance fuel

The limited quantity of these expendables must be utilized in such a fashion as to maximize the return of photographic intelligence information for a given mission. Some of the factors considered and techniques employed in this effort are discussed herein.

16.1 Photographic Film

Photographic film is the most crucial consumable; when the film supply has been exhausted, the photographic mission is terminated. The rate of usage of film is controlled so that, within a safety margin, the film and some other expendable are depleted at approximately the same time.

16.1.1 Film Usage Control

For Surveillance Missions, a list of targets, scaled by relative importance to the user community, is supplied. For Search Missions, the "targets" input to the mission software are centers of 1/2 WAC (World Aeronautical Chart) cells. Targeting software selects a path through the acquirable targets which is compatible with timing constraints and pointing limits. Film usage is controlled

2.16-1

~~TOP SECRET~~ GHandle via BYEMAN
Control System Only

~~TOP SECRET~~ G

BIF-008-W-C-019839-RI-80)

by adjusting the weather threshold (in a manner similar to that described in Part 2, Section 8.3) to require a greater or lesser probability of a cloud-free photograph, or by adjusting the pad multiplier (see Part 2, Section 2.3.2.1).

16.1.2 Film Usage Influences

If other intelligence sources indicate a specific need for surveillance of a particular area or target, the rate of film usage may be adjusted accordingly. Unusual events occurring during Gambit flight operations may result in a real-time reordering of priorities. (e.g.,: The 1973 mideast conflict significantly affected flight operations.) Such events may also influence when a major orbit change occurs in a Gambit mission.

16.2 Electrical Power

Electrical energy for the Gambit vehicle may be taken from two sources: on-board batteries and a solar panel array. The solar array does not satisfy the energy requirements; therefore the batteries have a net depletion rate approximately equal to the difference between that available from the solar array and that required by the satellite.

16.2.1 Power Usage Control

Power usage may be minimized by reducing the photographic activity, by reducing the amount of instrumentation recorded for subsequent transmission to the ground, or by shutting down selected heaters. Orbit parameters and vehicle paint pattern may be selected prior to the flight to minimize power usage.

16.2.2 Power Usage Influences

The major influences on PPS/DP EAC power usage are those related to the activation of in-flight heaters. Orbit inclination, beta angle, and height of perigee,

2.16-2

~~TOP SECRET~~ GHandle via BYEMAN
Control System Only

~~TOP SECRET~~ GBIF-008- W-C-019839-RI-80

in conjunction with the paint pattern chosen, influence the amount of solar and aerodynamic heating experienced by the vehicle, and therefore directly influence power usage. A major portion of vehicle power is used by the SCS and is not influenced appreciably by PPS/DP EAC parameters.

16.3 Attitude Control Gas

In order to maintain the vehicle line-of-sight (LOS) pointing at the surface of the earth, a continuous pitch-down rate is maintained by the dual attitude control system (DACS) in the SCS. Any vehicle roll rate arising from a PPS/DP EAC roll or crab maneuver, not compensated by the roll joint, is reduced to system deadband limits by the DACS.

16.3.1 Control Gas Usage Control

Much of the gas usage is controlled by a closed-loop system where a usage reduction can be achieved only by shutting down part of the system. During preparations for SRV ejection, the use of an inertial maneuver to achieve the proper attitude results in considerable savings in control gas in comparison to the powered maneuvers.

16.3.2 Control Gas Usage Influences

The degree of mismatch between roll-joint momentum compensation and the actual PPS/DP EAC roll moment influences the amount of control gas which must be expended to maintain a stable, properly oriented PPS/DP EAC. A technique known as adaptive bias, which decouples the roll thrusters until the completion of a PPS/DP EAC roll maneuver, reduces gas expenditures. Powered maneuvers to position the PSV for SRV ejection use relatively large amounts of control gas.

25X1

2.16-3

~~TOP SECRET~~ GHandle via BYEMAN
Control System Only

~~TOP SECRET~~ GBIF-008- W-C-019839-RI-80

25X1

16.4 Orbit Maintenance Fuel

Orbital energy lost to aerodynamic drag must be replaced periodically if desired orbital parameters are to be maintained. Orbital energy is replaced by operation ("burns") of the integrated secondary propulsion system (ISPS) located in the SCS. Because of the large amounts of fuel required to place the Gambit vehicle in Search orbits, available fuel versus flight duration must be monitored to ensure required deboost capability.

16.4.1 Orbit Maintenance Fuel Usage Control

Operation of the ISPS is accomplished at appropriate times by command. The amount of fuel (and oxidizer) used is dependent on the commanded duration of the burn, which is in turn dependent on the energy required to maintain the desired orbit.

16.4.2 Orbit Maintenance Fuel Usage Influences

The major influences on the usage of orbit maintenance fuel are the desired orbit parameters. The orbital energy lost per revolution is proportional to the drag force integrated over the orbital path. Since the drag force varies inversely with altitude, orbits having a lower average altitude will require a larger expenditure of orbit maintenance fuel. In special cases (such as those described in Part 2, Section 16.1.2), the desired parameters may be changed during a flight. Because of the greatly reduced aerodynamic drag which results from operation at Search altitudes ($h \geq 300$ nmi), orbit maintenance fuel expenditures are reduced.

2.16-4

~~TOP SECRET~~ GHandle via **BYEMAN**
Control System Only

~~TOP SECRET~~

G

BIF-008-W-C-019839-RI-80

PART 3 HARDWARE DESCRIPTION

1.0 PHOTOGRAPHIC PAYLOAD SECTION/DUAL PLATEN EXTENDED ALTITUDE CAPABILITY

The photographic payload section/dual platen extended altitude capability (PPS/DP EAC) comprises the deliverable hardware manufactured by BIF-008 under contract (Revision I dated 1 January 1979).

25X1

All references and figures in Part 3 use the BIF-008 vehicle coordinate system or PPS/DP EAC cylindrical coordinate system. For a description of these and other Gambit related coordinate systems, refer to Part 2, Section 1.

1.1 PPS/DP EAC General Description

The PPS/DP EAC is the forward portion of the Gambit photographic satellite vehicle, containing the 9 x 5 dual platen camera and imaging optics. The PPS/DP EAC has been designed and manufactured to meet or exceed all requirements set forth in the Gambit General System Specification. Part 3 of this document describes the major assembly modules and structure of the PPS/DP EAC (Section 1), and the basic operational subsystems located within the PPS/DP EAC (Sections 2 through 13).

1.1.1 PPS/DP EAC Assembly Modules

Three separate modules comprise the PPS/DP EAC:

- (1) the dual recovery module (DRM); front section
- (2) the supply and electronics module (SEM); center section
- (3) the camera optics module (COM); aft section

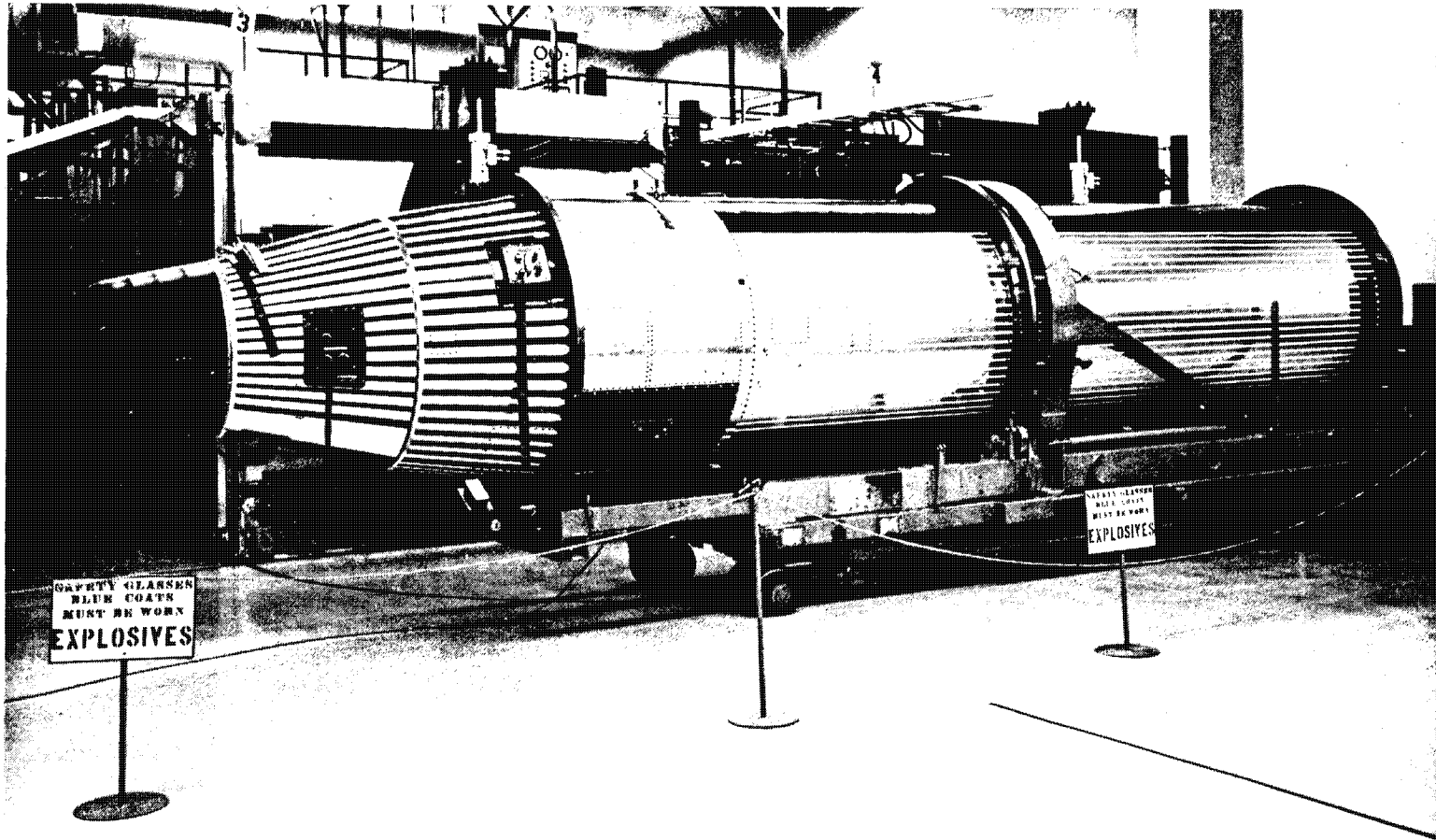
Figure 3.1-1, a photograph of a previous Gambit vehicle, is representative of the PPS/DP EAC. Figure 3.1-2 illustrates the internal layout of the PPS/DP EAC,

3.1-1

~~TOP SECRET~~

G

Handle via BYEMAN
Control System Only



3.1-2

Note: Hardware shown is representative of FM-47. FM-48 differs in that the aft diameter of SRV 1 is slightly greater than the forward diameter of the ejectable adapter.

Figure 3.1-1. PPS/DP EAC

Handle via **BYEMAN**
Control System Only

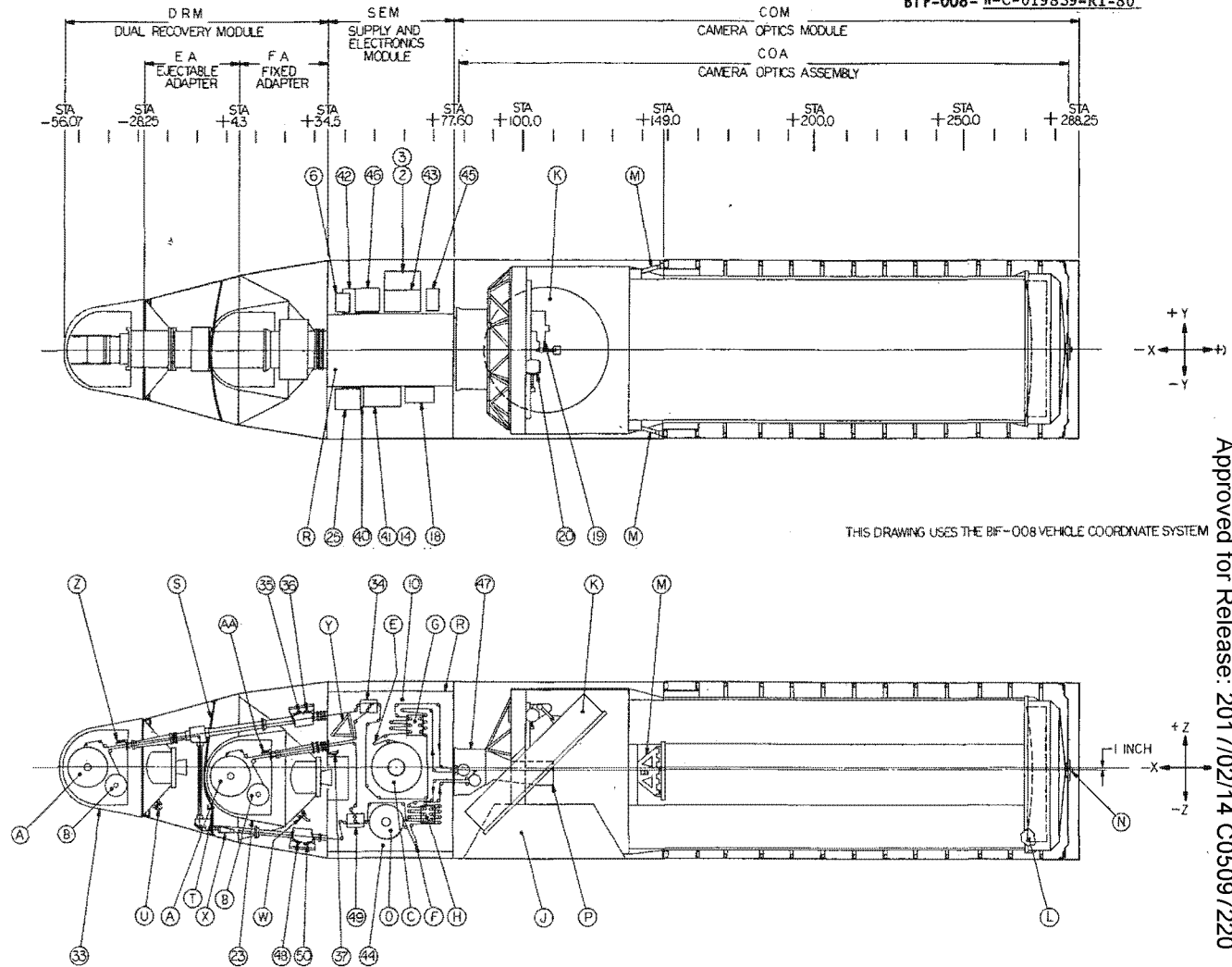
Approved for Release: 2017/02/14 C05097220

Approved for Release: 2017/02/14 C05097220

MAJOR COMPONENTS

- ITEM DESCRIPTION
- 2 COMMAND PROCESSOR
- 3 POWER MONITOR AND CONTROL UNIT
- 6 FILM CONTROL ELECTRONICS
- 10 9 SUPPLY ASSEMBLY
- 14 INSTRUMENTATION PROCESSOR
- 18 VIEWPORT DOOR ELECTRONICS
- 19 STEREO SERVO
- 20 GRAB SERVO
- 23 SATELLITE RE-ENTRY VEHICLE NO.2
- 25 DIGITAL TELEMETRY UNIT
- 33 SATELLITE RE-ENTRY VEHICLE NO.1
- 34 9 SPLICER MECHANISM
- 35 CUTTER/SEALER NO.3
- 36 9 TUNNEL SEAL AND RECORD TRAP
- 37 AFT BACKUP CUTTER
- 40 5 FREQUENCY PHASE LOCK LOOP ELECTRONICS
- 41 9 FREQUENCY PHASE LOCK LOOP ELECTRONICS
- 42 5 CAMERA ELECTRONICS ASSEMBLY
- 43 9 CAMERA ELECTRONICS ASSEMBLY
- 44 5 SUPPLY ASSEMBLY
- 45 FILM HANDLING ELECTRONICS
- 46 INITIATOR ELECTRONICS UNIT
- 47 9x5 DUAL PLATEN CAMERA
- 48 CUTTER/SEALER NO.4
- 49 5 SPLICER MECHANISM
- 50 5 TUNNEL SEAL AND RECORD TRAP

- A 9 TAKE-UP SPOOL
- B 5 TAKE-UP SPODL
- C 9 SUPPLY SPOOL
- D 5 SUPPLY SPOOL
- E 9 TENSION LOOPER
- F 5 TENSION LOOPER
- G 9 STORAGE LOOPER
- H 5 STORAGE LOOPER
- J VIEWPORT DOOR
- K STEREO MIRROR
- L PRIMARY MIRROR
- M A-FRAME ARM
- N BROOMSTICK
- P ROSS CORRECTOR
- R FILM SUPPLY ENCLOSURE
- S BLAST SHIELD
- T BLAST SHIELD VALVE
- U IN-FLIGHT DISCONNECT NO.1
- W IN-FLIGHT DISCONNECT NO.2
- X SPIN OFF DISCONNECTS 1&2 (ONE BEHIND THE OTHER)
- Y FILM SHIELD
- Z CUTTER/SEALER NO.1
- AA CUTTER/SEALER NO.2



THIS DRAWING USES THE BIF-008 VEHICLE COORDINATE SYSTEM

Figure 3.1-2. PPS/DP EAC Major Components

3.1-3/3.1-4

Handle via BYEMAN
Control System Only

~~TOP SECRET~~ GBIF-008- W-C-019839-RI-80

showing all major components residing in this portion of the photographic satellite vehicle (PSV).

1.1.1.1 DRM General Description.* The DRM is approximately 90 inches long and attaches to the forward end of the SEM. Major components of the DRM include two satellite reentry vehicles (SRV 1 and SRV 2), the ejectable and fixed adapters, the blast shield, and the film tunnels. The primary functions of the DRM are to provide a system wherein exposed film can be transported within a controlled environment and stored in the SRVs, and to eject the SRVs (and the EA when necessary) upon command for film recovery.

1.1.1.2 SEM General Description.* The SEM, which serves as the structural link between the DRM and the COM, is approximately 43 inches long. The primary functions of the SEM are to house, in a protected environment, the film supplies and film handling components, and to support most of the electronic units used in the PPS/DP EAC.

1.1.1.3 COM General Description.* The COM is the aft module of the PPS/DP EAC, attaching to the satellite control section (SCS) near station number 288. The COM consists of the external structure and the camera optics assembly (COA). The external structure supports the COA and contains the viewport doors through which light enters the optical system. The COA consists of the dual platen camera and the imaging optics, mounted within a rigid internal structure. The internal structure is supported in a strain-free manner at three points by the external structure. This arrangement allows the external structure to deflect without introducing stresses or deflections of the internal structure that could affect the optical characteristics.

* Mass properties for the vehicle and its modules can be found in Appendix F.

~~TOP SECRET~~ GHandle via BYEMAN
Control System Only

~~TOP SECRET~~ GBIF-008- W-C-019839-RI-80

1.1.2 PPS/DP EAC External Finish

Control of the PPS/DP EAC temperature to within a specified range is necessary to realize the full performance capabilities of the system. This control is achieved by passive means to the greatest extent possible, minimizing power consumption by the internal electrical heater tapes (reference Part 3, Section 8).

The exterior of the PPS/DP EAC is covered by a thermal finish (a combination of paint and foil tape) designed to limit skin temperature variations throughout the entire range of orbital parameters. Several patterns have been created for the three modules (three for the DRM, four for the SEM, and six for the COM) with the selection of a particular pattern to be used dictated by the orbit chosen. The forebody of SRV 1 is covered by a special ablative material and is painted, as necessary, by the associate contractor.

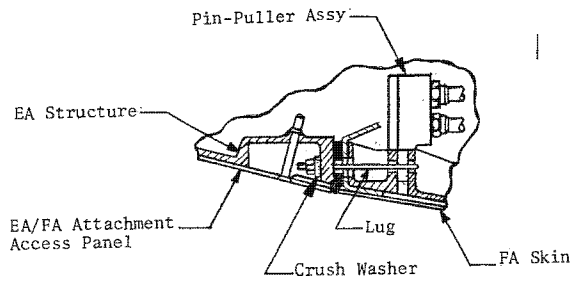
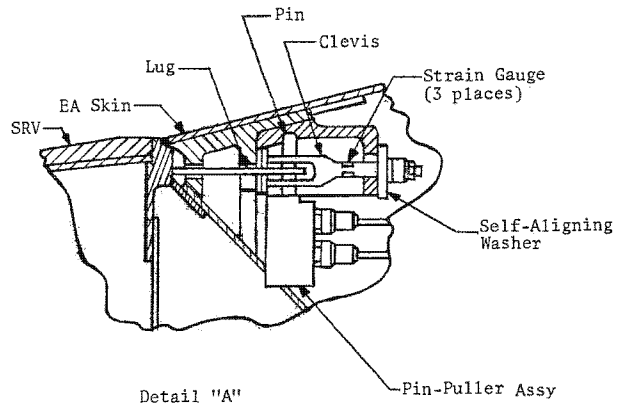
To implement the multiple pattern approach a master pattern is applied to the PPS/DP EAC, and the appropriate modifications, consisting only of tape removal or painting titanium foil, are performed upon identification of the flight parameters. Criteria for determining the proper patterns are discussed in Part 2, Section 14. The material characteristics and application patterns are described in Part 3, Section 8.

1.2 Dual Recovery Module

The dual recovery module (DRM) provides the structure to support the two SRVs and to support the auxiliary equipment used for film transfer and SRV separation (see Figures 3.1-3 and 3.1-4).

Externally the DRM is composed of SRV 1, the ejectable adapter (EA) and fixed adapter (FA). SRV 2 is mounted internally. Other major components within the DRM include the film passages, the blast shield and blast-shield valve, the upper and lower travel viewer (TV) boxes, the 5 and 9 tunnel seal and record trap (TSRT) assemblies, and the pyrotechnically actuated in-flight disconnects

3.1-6
~~TOP SECRET~~ GHandle via **BYEMAN**
Control System Only



EA/FA Attachment Detail, Typical 3 Places (Sta 4.3: 36°, 156°, 276°)

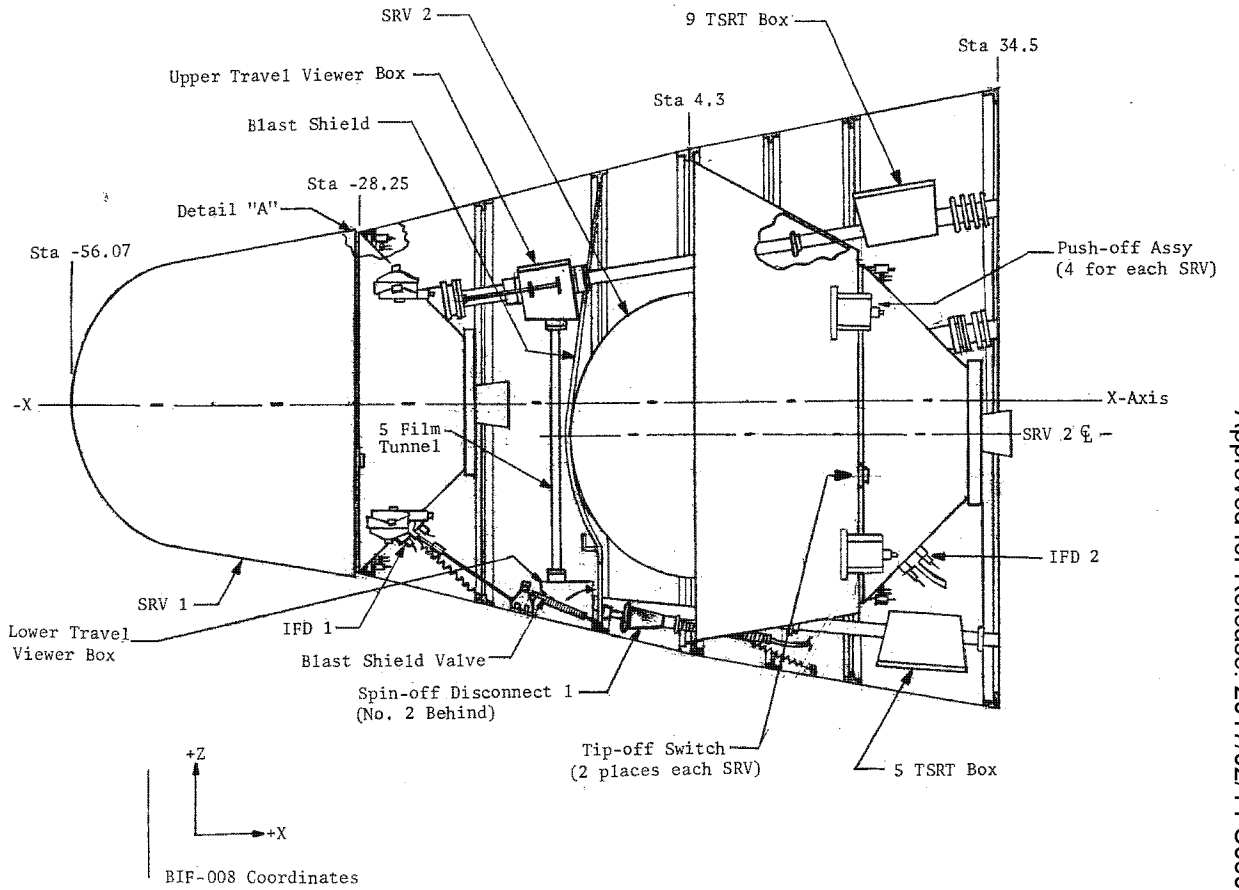


Figure 3.1-3. DRM Internal Components

3.1-7/3.1-8

Handle via BYEMAN
Control System Only

Approved for Release: 2017/02/14 C05097220

Approved for Release: 2017/02/14 C05097220

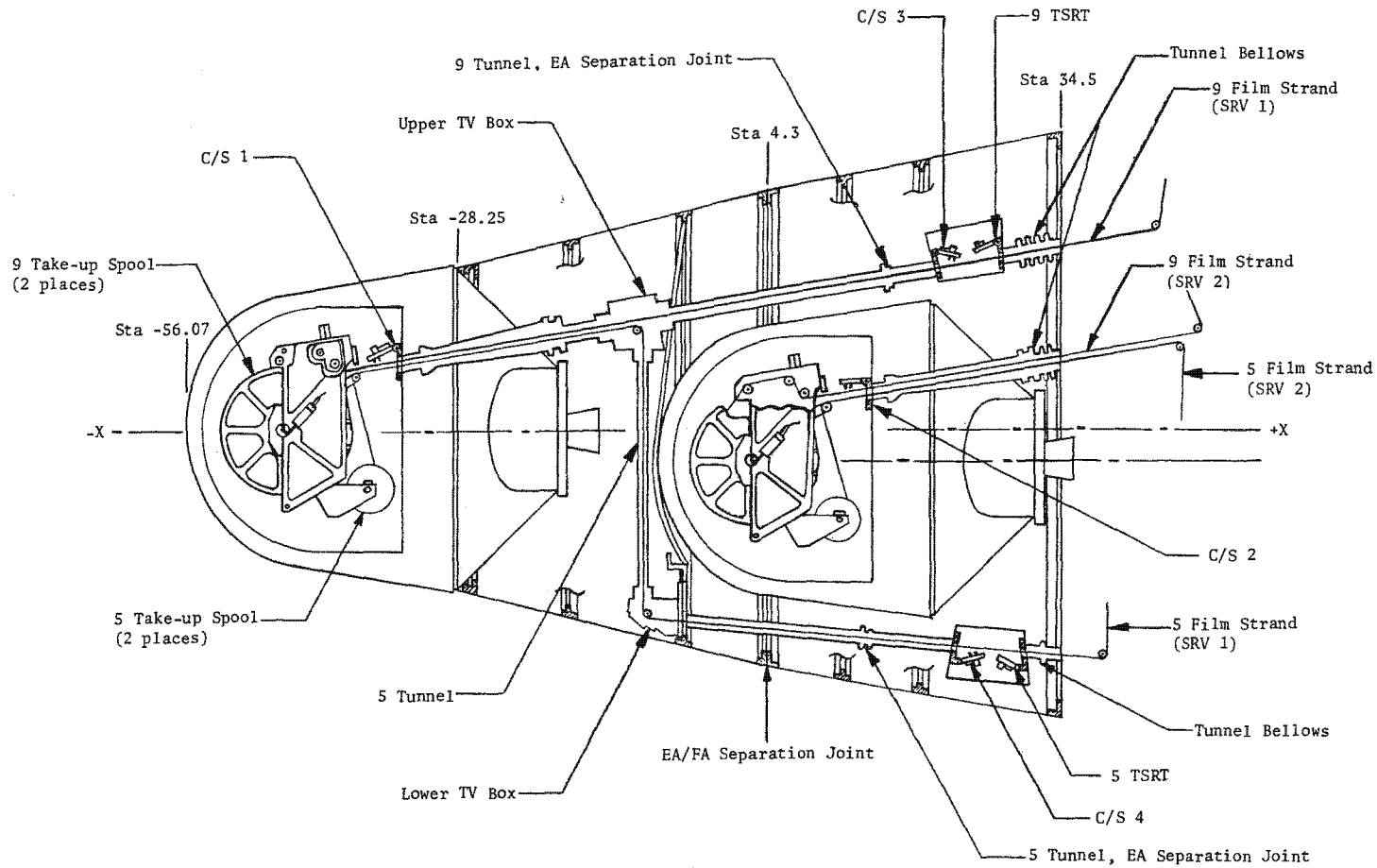


Figure 3.1-4. DRM Film Path Details (Internal SRV)

3.1-9/3.1-10

Handle via BYEMAN
Control System Only

Approved for Release: 2017/02/14 C05097220

Approved for Release: 2017/02/14 C05097220

~~TOP SECRET~~ GBIF-008- W-C-019839-RI-80

①

(IFDs) and separation pin-pullers. The 9 x 5 take-up assemblies and the SRV cutter/sealers (C/Ss) are contained within the recoverable capsule portion of the reentry vehicles.

1.2.1 DRM Access Panels

The surface of the DRM (Figure 3.1-5) has several removable structural panels to aid in assembly and testing of the vehicle. Table 3.1-1 is a listing of the DRM panels and major components accessible through their removal. When in place, these panels are flush with the DRM surface, and fit closely to exclude rain, snow, and dust. Where a particular panel must be removed several times prior to launch, two are provided with the vehicle: a shipping panel and a flight panel. Use of the shipping panels through assembly and testing precludes the possibility of damage to the prime flight panels. (Note: "socket-saver" panels, also categorized as shipping panels, are support equipment that allow mating of test equipment to socket-saver cables rather than prime connectors.)

1.2.2 DRM Structure and Internal Components

The following subsections describe in detail most of the major components as well as the overall structural aspects of the dual recovery module. The design and internal functioning of the SRVs, take-up mechanisms, and the cutter/sealer and tunnel seal and record trap (TSRT) assemblies are discussed in Part 3, Sections 2 and 12.

1.2.2.1 Ejectable Adapter (EA). The EA (Figures 3.1-6 and 3.1-7) is a truncated, conical, magnesium shell with major and minor diameters of 50.6 inches and 32.55 inches respectively. The EA attaches to the forward end of the fixed adapter and provides the support for SRV 1. The EA contains the release and ejection assemblies for SRV 1, as well as film tunnels, the blast shield, and electrical cabling. The EA normally remains in place after SRV 1 ejection to provide thermal protection for SRV 2, and is ejected just prior to SRV 2 ejection (refer to Part 3, Section 12).

"WARNING - THIS DOCUMENT SHALL NOT BE USED AS A SOURCE FOR DERIVATIVE CLASSIFICATION"

3.1-11
~~TOP SECRET~~ G

Handle via **BYEMAN**
Control System Only

~~TOP SECRET~~ G

BIF-008- W-C-019839-RI-80

This page intentionally left blank.

3.1-12
~~TOP SECRET~~ G

Handle via BYEMAN
Control System Only

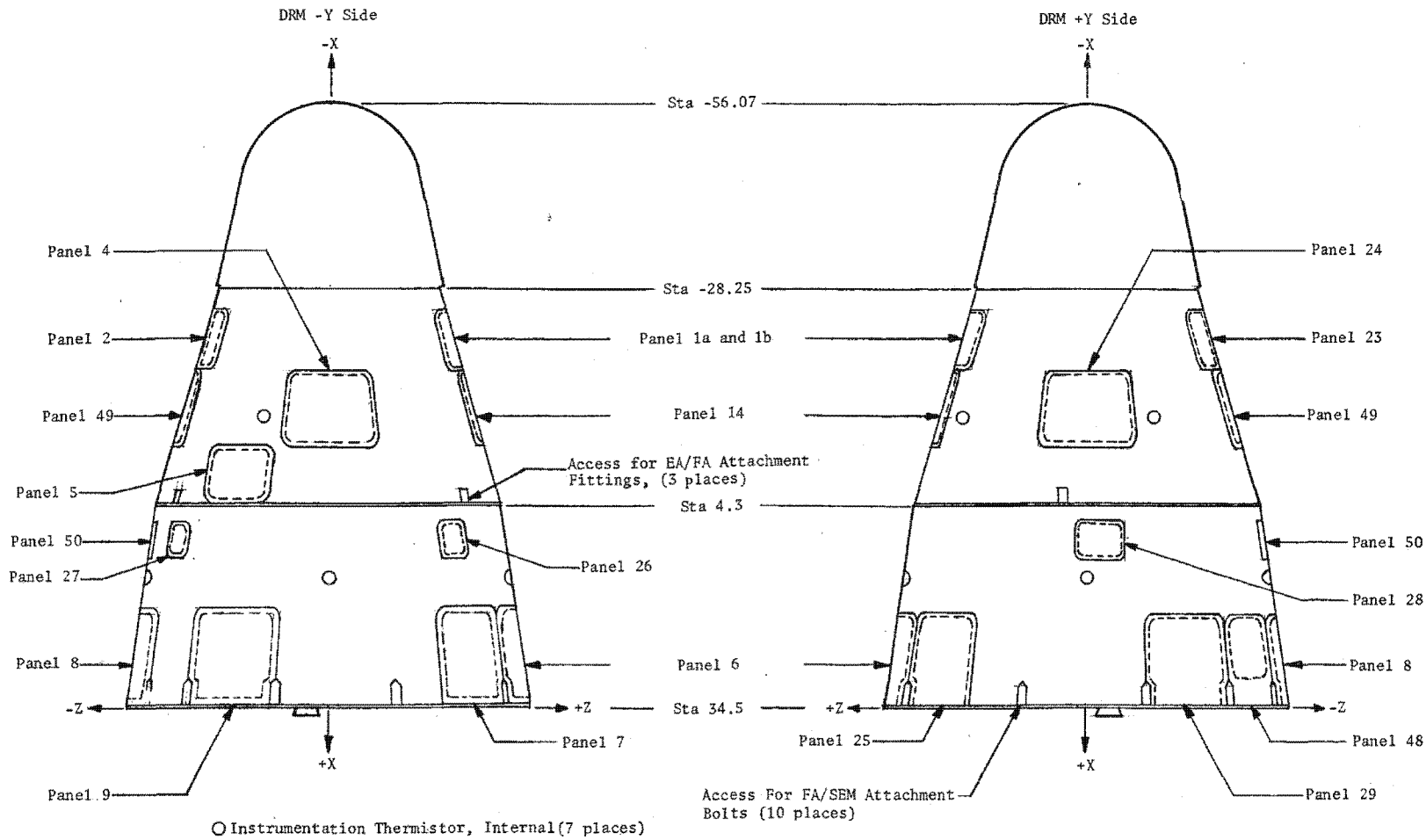


Figure 3.1-5. Dual Recovery Module Access Panels

Handle via BYEMAN Control System Only

3.1-13/3.1-14

Approved for Release: 2017/02/14 C05097220

Approved for Release: 2017/02/14 C05097220

TABLE 3.1-1
DRM ACCESS PANELS*

<u>Ejectable Adapter</u>		<u>Fixed Adapter</u>	
<u>Panel No.</u>	<u>Accessible Component(s)</u>	<u>Panel No.</u>	<u>Accessible Component(s)</u>
1 A	SRV 1 Tunnel Seal/SRV 1 Arming/ SRV 1 Pin-Puller	6	9 TSRT Enclosure
1 B	SRV 1 Tunnel Seal/SRV 1 Arming	7	9 TSRT Enclosure/SRV 2 Arming
2	Socket-Saver/IFD 1	8	5 TSRT Enclosure
4	5 Tunnel, Intermediate/SRV 1 Ignitor Installation/SRV 1 Gas Charging	9	Socket Saver/IFD 2/SRV 2 Gas Charging
5	Spin-Off Disconnect 1/ Spin-Off Disconnect 2	25	9 TSRT Enclosure/Arm Plugs
14	Upper TV Box/5 and 9 Tunnel Junction/5 Roller	26	EA/FA Pin-Puller
23	IFD 1/SRV 1 Pin-Puller	27	EA/FA Pin-Puller
24	Socket Saver/SRV 1 Ignitor Installation/ SRV 1 Gas Charging	28	EA/FA Pin-Puller
49	Lower TV Box/5 Roller	29	Socket Saver/SRV 2 Gas Charging
		48	SRV 2 Arming
		50	5 Tunnel Separation Seal

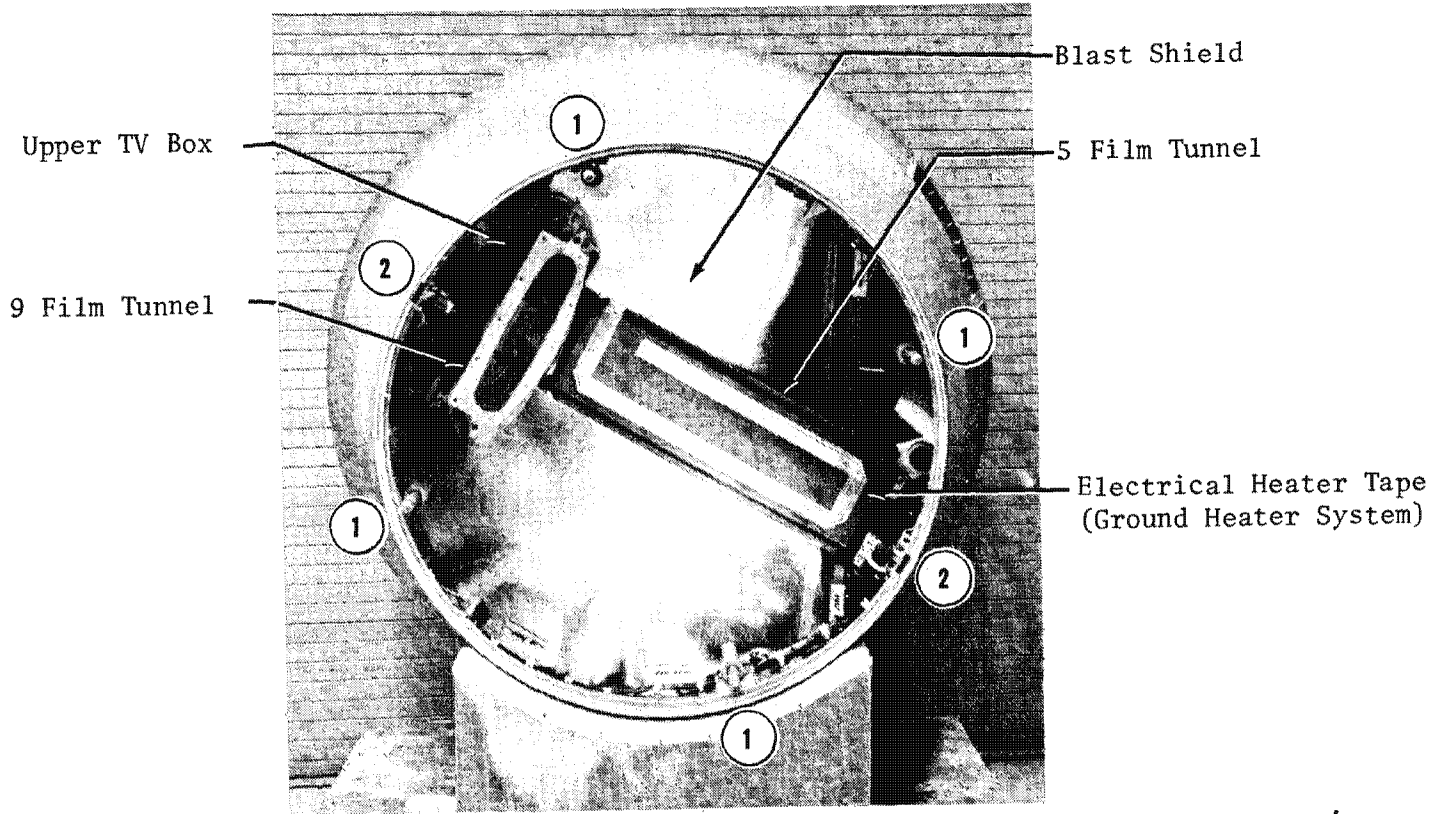
*Note: Excludes mating bolt panels (3 on the EA, 10 on the FA).

Handle via **BYEMAN**
Control System Only

Approved for Release: 2017/02/14 C05097220

3.1-15

Approved for Release: 2017/02/14 C05097220



- 1. SRV 1 Ejection Piston
- 2. SRV 1 Pin-puller

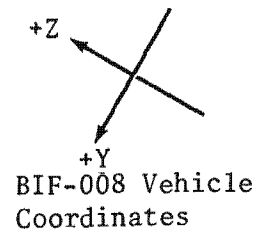


Figure 3.1-6. Ejectable Adapter (-X View)

Handle via **BYEMAN**
Control System Only

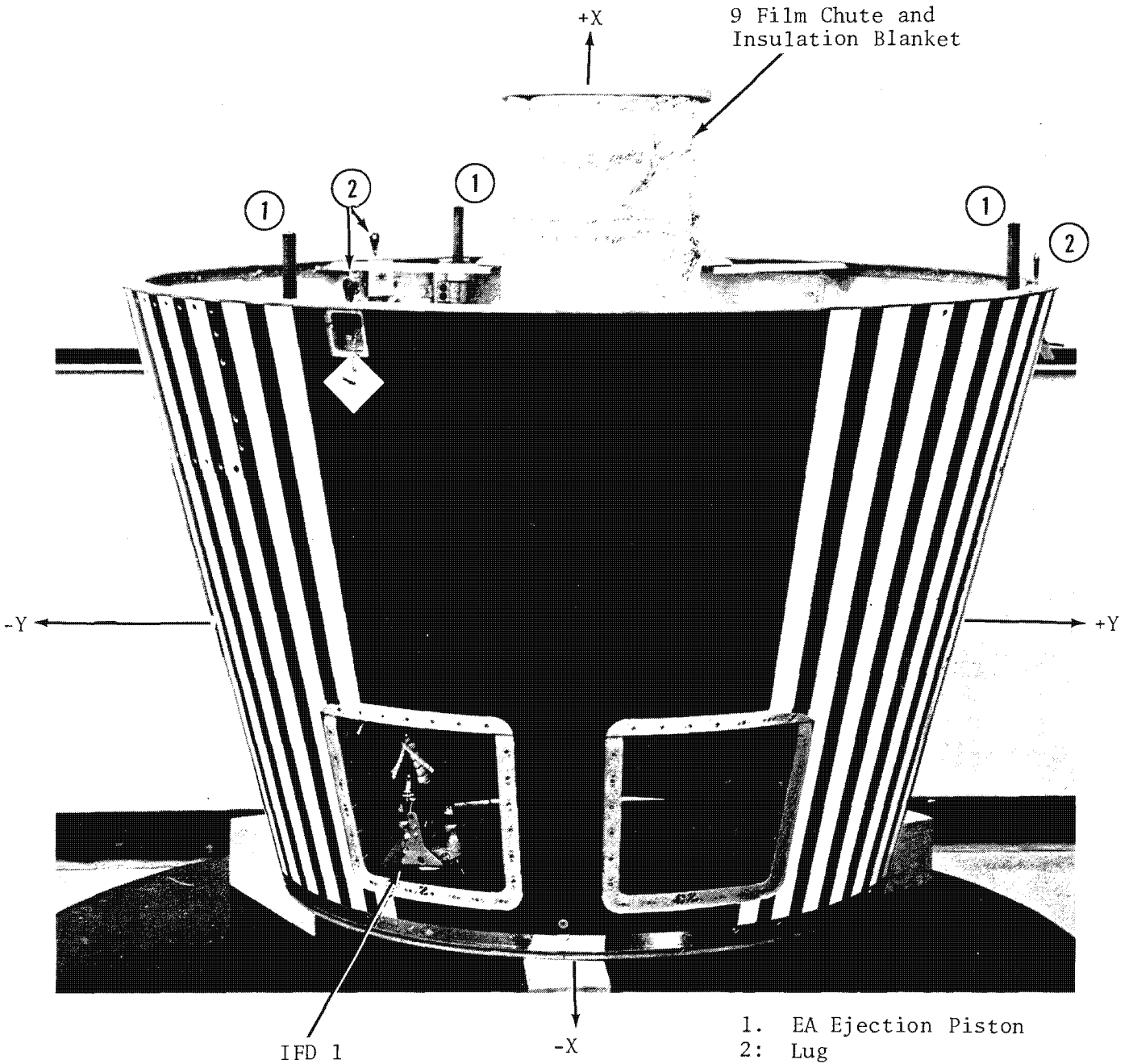
Approved for Release: 2017/02/14 C05097220

Approved for Release: 2017/02/14 C05097220

3.1-16

~~TOP SECRET~~ G

BIF-008- W-C-019839-RI-80



Note: The hardware shown is representative of FM-47.
The exterior of FM-52 is changed only in the location and number of access panels.

Figure 3.1-7. Ejectable Adapter (-Z View)

3.1-17

~~TOP SECRET~~ G

Handle via **BYEMAN**
Control System Only

~~TOP SECRET~~ GBIF-008- W-C-019839-RI-80

1.2.2.1.1 SRV 1 Mating. SRV 1 is attached to the EA by means of two clevis/pin-puller assemblies. The pin-pullers are secured to the EA with self-aligning washers and nuts. Three strain gauges, spaced symmetrically around each clevis, are used to indicate when the desired amount of preload is applied to each lug. Alignment registration of the SRV to the EA is accomplished with a pin/bushing arrangement. The mating ring on SRV 1 fits inside the forward ring of the EA to carry shear loads between the two sections, while tension loads are taken by the clevis bolts.

Two electrically initiated pyros are used in each pin-puller assembly for withdrawal of the release pin. Should one pyro fail to actuate, the redundant pyro is capable of generating sufficient force to retract the pin. After the release pins have been withdrawn, four matched ejection-spring assemblies provide the forward thrust which separates the SRV from the EA. Two microswitches mounted on the EA, diametrically opposed to each other, provide an indication of successful separation.

A 55-conductor in-flight disconnect (IFD 1) forms the electrical interface between SRV 1 and the remainder of the PPS/DP EAC. The IFD is operated by two electrically initiated, 0.9-second delay pyros which cause the mated connector to shear and disconnect. Following firing of the pyros, a spring-loaded retracting mechanism within the EA pulls the disconnected portion of the harness rearward and away from the SRV so that no mechanical interference will occur during separation. Simultaneously, a lanyard attached to the retractor releases a door (the blast-shield valve) which covers the vent opening in the blast shield.

1.2.2.1.2 Blast Shield. The blast shield is located in the EA forward of SRV 2 and prevents SRV 1 retro-rocket exhaust gases from entering the PPS/DP EAC. It also thermally protects SRV 2 following SRV 1 ejection. The shield is made of silicone-rubber coated aluminized fiberglass, capable of

3.1-18

~~TOP SECRET~~ GHandle via BYEMAN
Control System Only

~~TOP SECRET~~ GBIF-008- W-C-019839-RI-80

withstanding a differential pressure of 1.0 psi when the blast-shield valve is closed. A thermal insulation blanket covers the forward surface of the blast shield and provides protection against the aerodynamic heating associated with perigee conditions of orbital flight. The blanket consists of multiple layers of aluminized polyimide film sheets and open-weave cloth. An opening in the shield (covered by the blast-shield valve) provides venting of the EA and SRV 1 during ascent. The valve is a spring-loaded door which rotates 75 degrees from opened to closed and is located on the forward side of the blast shield such that, in the closed position, the retro-rocket gas pressure tends to seat the door and gasket. The valve is held closed with a force sufficient to preclude unseating when a back pressure of 0.1 psi is applied. During flight, the blast-shield valve remains open until separation of IFD 1. A potentiometer mounted on the hinge bracket monitors the valve position for purposes of instrumentation.

1.2.2.2 DRM Film Enclosures. The DRM film enclosures (reference Figure 3.1-4) consist of a series of boxes, aluminum tunnels, bellows, and seals which provide a lighttight and pressure-tight environment for the film path between the film supply enclosure (FSE) in the SEM and each SRV. The DRM enclosures are designed to withstand a differential burst pressure of 0.5 psi. Thermal control is maintained by insulation blankets wrapped around the tunnel sections. Heater tapes on the tunnel exteriors are a part of the ground heater system used prior to launch (reference Part 3, Section 8).

The 9.5-inch wide film* follows a direct path from the FSE to SRV 1. The 5-inch wide film requires two directional changes which are made by idler rollers mounted in the upper and lower travel viewer (TV) boxes. Both films follow a direct path from the FSE to SRV 2. The TV boxes allow insertion of a viewing mirror during assembly to verify that the film is tracking properly at the upper and lower TV boxes and at the input rollers on take-up 1.

* Components handling 9.5-inch wide film are referred to as 9 film subsystem components.

~~TOP SECRET~~ GHandle via BYEMAN
Control System Only

~~TOP SECRET~~ GBIF-008- W-C-019839-RI-80

The TSRT boxes each contain a cutter/sealer and a tunnel sealer (the TSRT mechanism) which provide redundant film strand cutting for the SRV 1 film path, and a redundant seal in the tunnels leading to the FSE.

Lighttightness and pressure tightness are maintained at the tunnel separation points between the EA/FA and SRV tunnel sections by means of flanged adapters and compression gaskets. Adjustment of the seal at SRV 1 is accomplished by extending the forward tunnel section. The seal on SRV 2 is adjusted by shimming the bellows assembly between the FSE and the aft tunnel of the SRV. The bellows in the tunnel sections connecting the FSE to the TSRT boxes and to SRV 2 allow for adjustment and path length changes as the PPS/DP EAC expands and contracts.

1.2.2.3 Fixed Adapter. The fixed adapter (Figures 3.1-8 and 3.1-9) is a truncated, conical, magnesium shell with forward and aft diameters of 50.6 inches and 60 inches respectively. The FA attaches to the forward end of the SEM and supports SRV 2. The FA provides the release and ejection functions for SRV 2 and the EA, and also houses film tunnels, the TSRT assemblies, electrical cabling, and the safe/arm plug connectors associated with the SRV pyrotechnic devices.

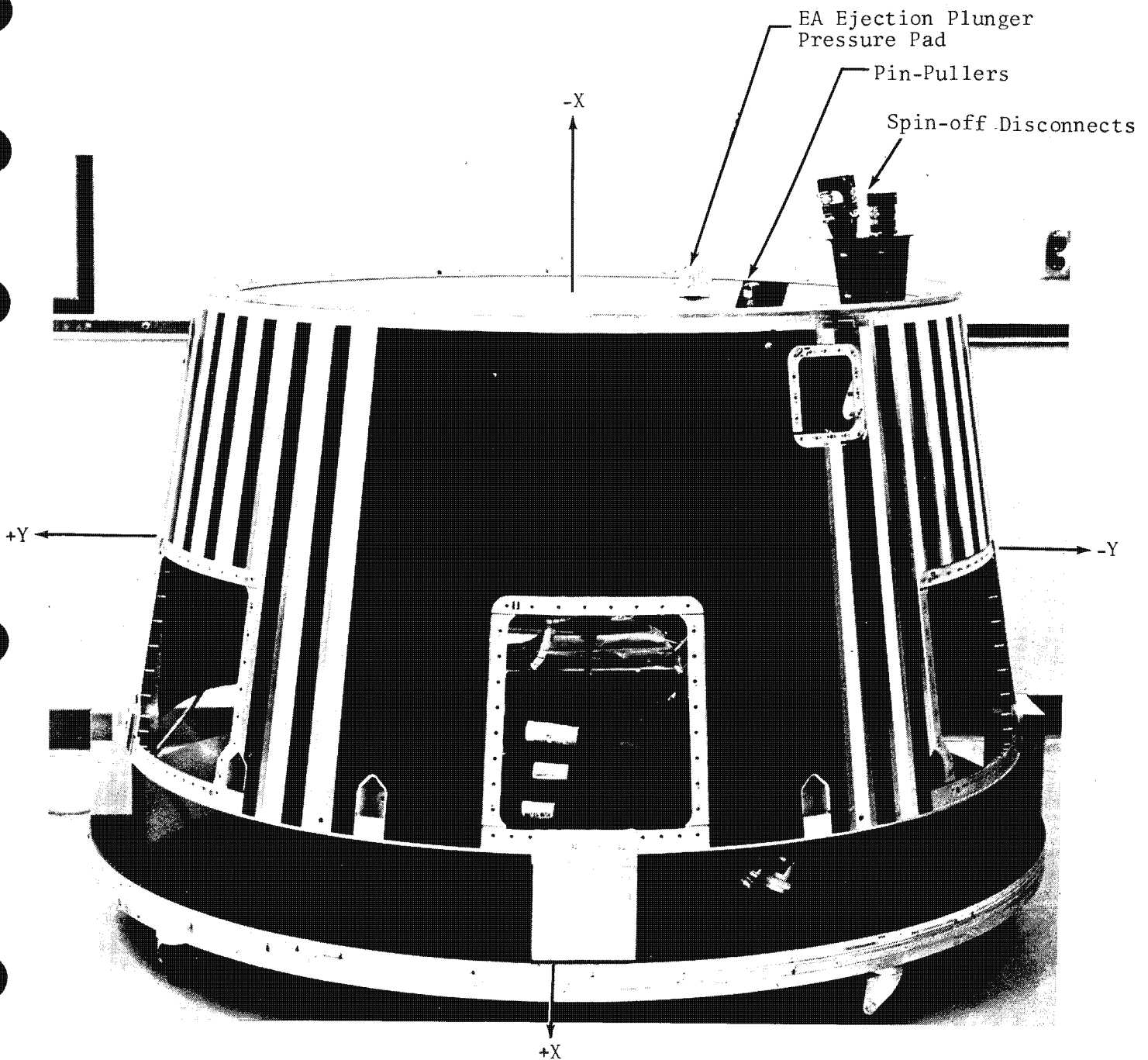
1.2.2.3.1 EA/FA Mating. The EA is mated to the FA electrically through two 61-conductor, pyro-actuated spin-off disconnects. Spin-off 1 carries the electrical signals for SRV 1 and the IFD 1 firing signals. Spin-off 2 carries signals for the SRV 1 pin-pullers and all ejectable adapter-mounted instrumentation points: the SRV 1 separation monitors, the blast-shield valve monitor, and the EA skin temperature sensors (see Figure 3.1-5 for thermistor locations). Separation of either of these connectors serves to isolate the signals that it carried from the remainder of the PPS/DP EAC. Spin-off 1 is actuated simultaneously with SRV 1 separation. Spin-off 2 is commanded separately, and is normally actuated just prior to EA separation.

3.1-20

~~TOP SECRET~~ GHandle via **BYEMAN**
Control System Only

~~TOP SECRET~~ G

BIF-008- W-C-019839-RI-80



Note: The hardware shown is representative of FM-47. The exterior of FM-52 is changed only in the location and number of access panels.

Figure 3.1-8. Fixed Adapter (-Z View)

3.1-21

~~TOP SECRET~~ G

Handle via BYEMAN
Control System Only

~~TOP SECRET~~ G

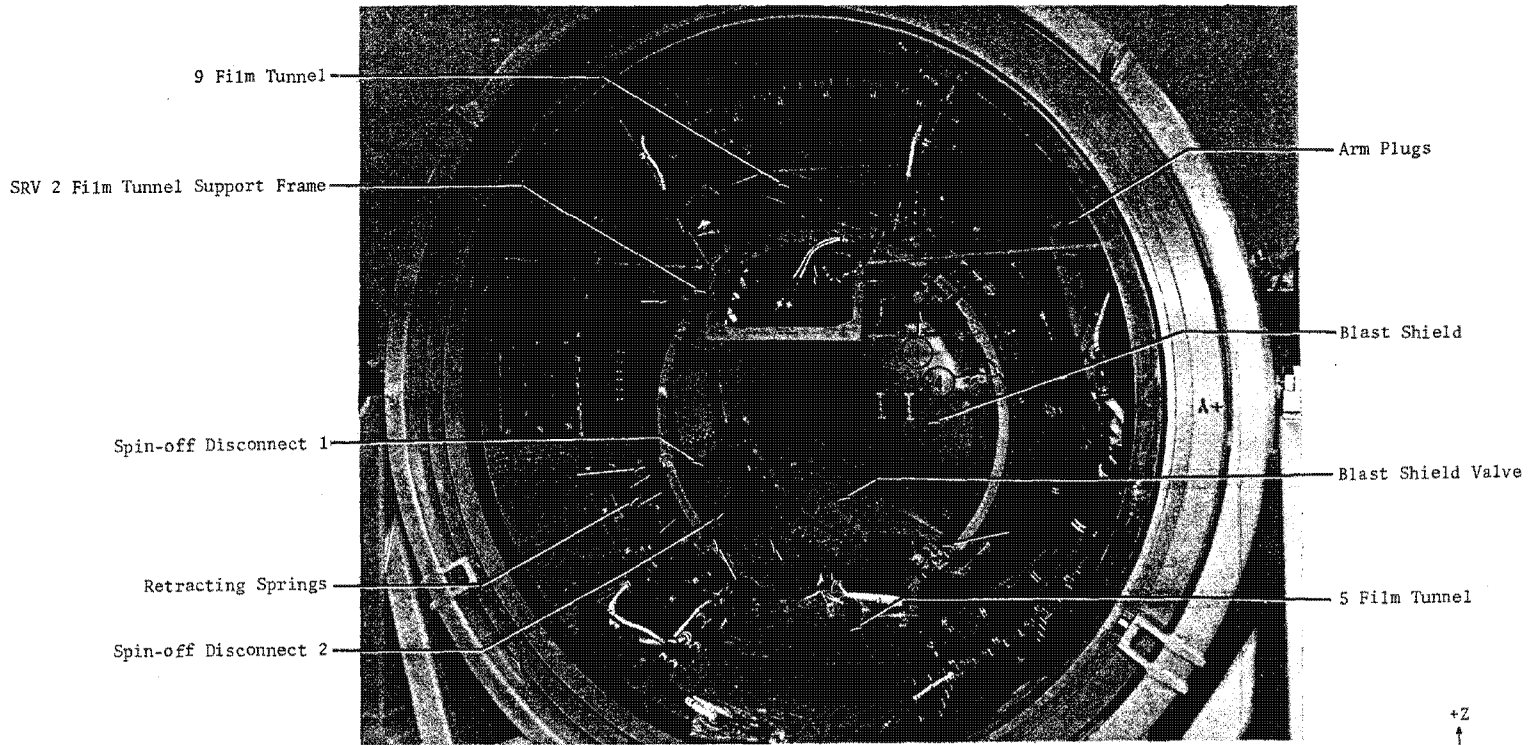
BIF-008- W-C-019839-RH-80

This page intentionally left blank.

3.1-22

~~TOP SECRET~~ G

Handle via **BYEMAN**
Control System Only



- 1. SRV 2 Ejection Piston
- 2. SRV 2 Pin-puller
- 3. EA Ejection Piston (3 total, 120 degrees apart)
- 4. Separation Monitor (Tip-off Switch)

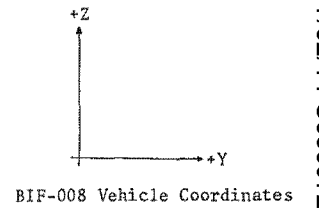


Figure 3,1-9. Fixed Adapter (+X View, EA Attached)

3.1-23/3.1-24

Handle via BYEMAN
Control System Only

Approved for Release: 2017/02/14 C05097220

Approved for Release: 2017/02/14 C05097220

~~TOP SECRET~~ GBIF-008- W-C-019839-RI-80

Upon release of the connectors, spring-loaded retractors attached to the fixed adapter pull each cable rearward to prevent interference with ejection of the EA and SRV 2. A single continuity loop through spin-off 1 and two parallel loops through spin-off 2 monitor the status of these connectors for telemetry.

The EA is secured to the FA mechanically at three points by a lug and pin-puller arrangement similar to that used on the SRV assembly. The lug is attached to the EA, and the pyrotechnic operated pin-puller portion is mounted on the fixed adapter section. Indicating washers are used to monitor the applied preload. The lug/pin-puller assemblies are reinforced by fittings which distribute the lug loads into the FA. Shear loads are carried by the cup/cone interface of the mating rings similar to the SRV 1/EA interface.

After pin-puller actuation, three matched ejection spring assemblies on the EA provide the thrust which separates the EA from the remainder of the vehicle. The normal separation velocity is 30 inches/second. Six switch assemblies, one on either side of each pin-puller, monitor the separation for telemetry.

1.2.2.3.2 SRV 2 Mating. SRV 2 is mounted within the FA, three inches below the X-axis. The support for SRV 2 is the frustum of a cone the large end of which attaches to the forward FA ring. SRV 2 is aligned and held in the same manner as SRV 1, using two clevis/pin-puller assemblies and a locating pin. The clevis bolts are backed by fittings which extend the length of the cone, distributing the load into the skin of the cone where it is transferred to the forward FA ring. The ejection force is provided by four matched spring pistons, and separation is monitored by two microswitch assemblies. The electrical interface between SRV 2 and the PPS/DP EAC consists of a 55-conductor in-flight disconnect,

3.1-25

~~TOP SECRET~~ GHandle via **BYEMAN**
Control System Only

~~TOP SECRET~~ GBIF-008- W-C-019839-RI-80

(IFD 2) which, like IFD 1, is separated by delayed action pyros. A spring retractor attached to the SEM forward bulkhead retracts and positions the harness upon release.

1.2.2.4 DRM/SEM Mating. The DRM is mated to the SEM by ten attachment bolts which provide continuity between longerons in the DRM and SEM. The longerons act to distribute any loads carried by the bolts. Two locating pins assure proper alignment of the mated DRM and SEM. Eight connectors on the SEM forward bulkhead constitute the electrical interface. Venting of the DRM during ascent is provided by approximately 78 square inches of effective open area through the forward SEM bulkhead.

1.3 Supply and Electronics Module

The supply and electronics module (SEM), shown in Figure 3.1-10, contains the 9 and 5 film supply assemblies and most of the PPS/DP EAC electronic control units, excluding the focus electronics module and the S-1/PRG* processing units. The structural portion of the SEM, referred to as the supply electronics structure (SES), is the load-carrying link between the DRM and the COM. The supply assemblies, mounted within the lighttight film supply enclosure of the SES, perform the major task of the supply and electronics module, the storage and precision handling of film.

1.3.1 Supply Electronics Structure

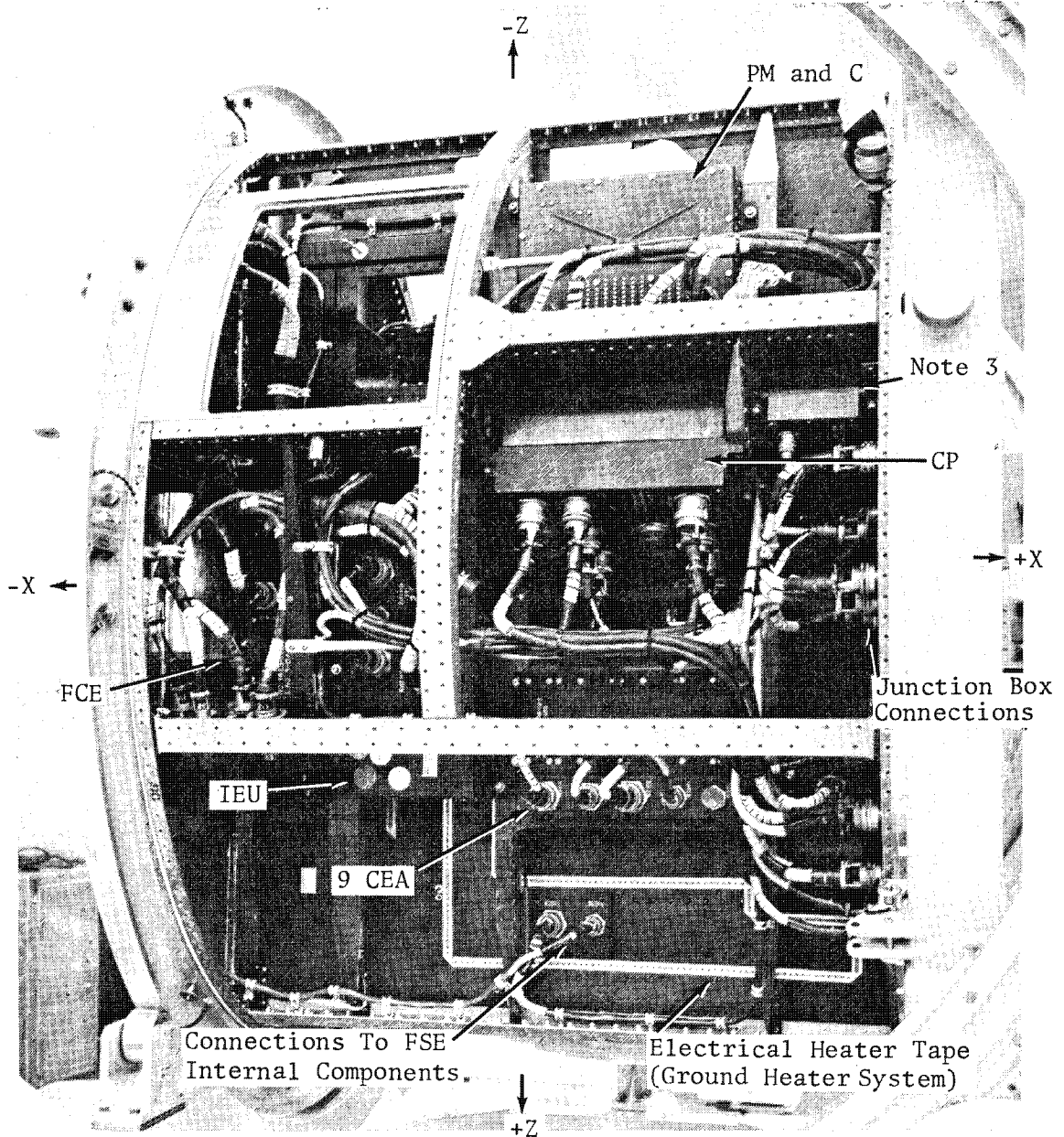
The SES is a ring- and longeron-stiffened, cylindrical, magnesium shell structure with bulkheads at both ends. Internally the SES consists of the film supply enclosure (FSE), the junction box, electrical cabling, and structural mounts for the film supply assemblies and electronic control units.

* PRG - Platen Reference Gauge

~~TOP SECRET~~ G

~~TOP SECRET~~ G

BIF-008- W-C-019839-RI-80



- Notes:
1. For placement of units see Figure 3.1-14.
 2. FHE and 5 CEA not shown.
 3. Test unit; not present on flight hardware.
 4. Illustration uses BIF-008 vehicle coordinates.

Figure 3.1-10. Supply Electronics Module (+Y Side)

3.1-27

~~TOP SECRET~~ G

Handle via BYEMAN
Control System Only

~~TOP SECRET~~ GBIF-008- W-C-019839-RI-80

1.3.1.1 SES Access Panels. The external skin of the SES consists entirely of removable access panels fastened to the rings and longerons with screws (see Figure 3.1-11). For assembly and testing, many of these panels are replaced by shipping panels (including one "socket-saver" panel) to prevent damage to flight panels during ground handling. Restrictions are placed on the number and combination of panels removed at any one time to maintain the structural integrity of the module.

1.3.1.2 SES Bulkheads. The forward bulkhead, shown in Figure 3.1-11, is attached to the forward SES ring. The middle section of the bulkhead is sheet magnesium and forms the forward end of the FSE. This portion contains openings into the FSE for film passage, and an opening into the SRV 2 retro-rocket nozzle access box. This opening was enlarged to accommodate the larger retro-rocket nozzle on the SRV for PPS/DP EAC use. Arming is performed through this access opening located aft of the bulkhead (reference Figure 3.1-17, SEM Electronic Unit Locations (+Y Side)). Additional openings in this area serve as vent holes. The remainder of the forward bulkhead is fiberglass with openings provided for venting and for mounting electrical connectors, including several arm plug receptacles.

The aft bulkhead is attached to the aft SES ring. The middle portion is also sheet magnesium and forms the FSE aft end. The remaining portion of this bulkhead consists of the junction box and fiberglass panels. The bulkhead has approximately 97 square inches of screened venting area and additional openings for cable pass-through, ground strap pass-through, film passage to the camera, and accommodation of the viewport door backup motor. The junction box is a fiberglass structure which supports the cabling and provides the connector mountings for interconnection of the electronic control units in the SEM.

1.3.1.3 Film Supply Enclosure. The FSE is a rectangular lighttight and pressure-tight enclosure which provides the environmental protection for the 9 and 5 film supplies (see Figure 3.1-12). The side panels, located

~~TOP SECRET~~ G

Reference Table

No.	Descriptor
1.	Panel No. 32
2.	Panel No. 33
3.	Panel No. 34
4.	Thermistor, IMP 5255 (+Y, Sta 63.5)
5.	Panel No. 35
6.	Panel No. 36
7.	+Z FSE Access Panel
8.	Thermistor, IMP 5254 (+Z, Sta 57.5)
9.	Panel No. 38
10.	+Y FSE Access Panel
11.	Panel No. 39
12.	-Y FSE Access Panel
13.	Panel No. 3
14.	Thermistor, IMP 5257 (-Y, Sta 63.5)
15.	Panel No. 11
16.	-Z FSE Access Panel
17.	Panel No. 30
18.	Panel No. 31
19.	Thermistor, IMP 5256 (-Z, Sta 57.5)
20.	Panel No. 13
21.	Forward Bulkhead

Key: Δ - Electrical Connector
 \square - Low Resistance Modules (LRM)/Arm Plugs
 - Venting Area

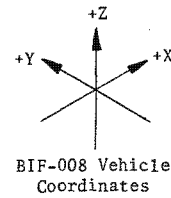
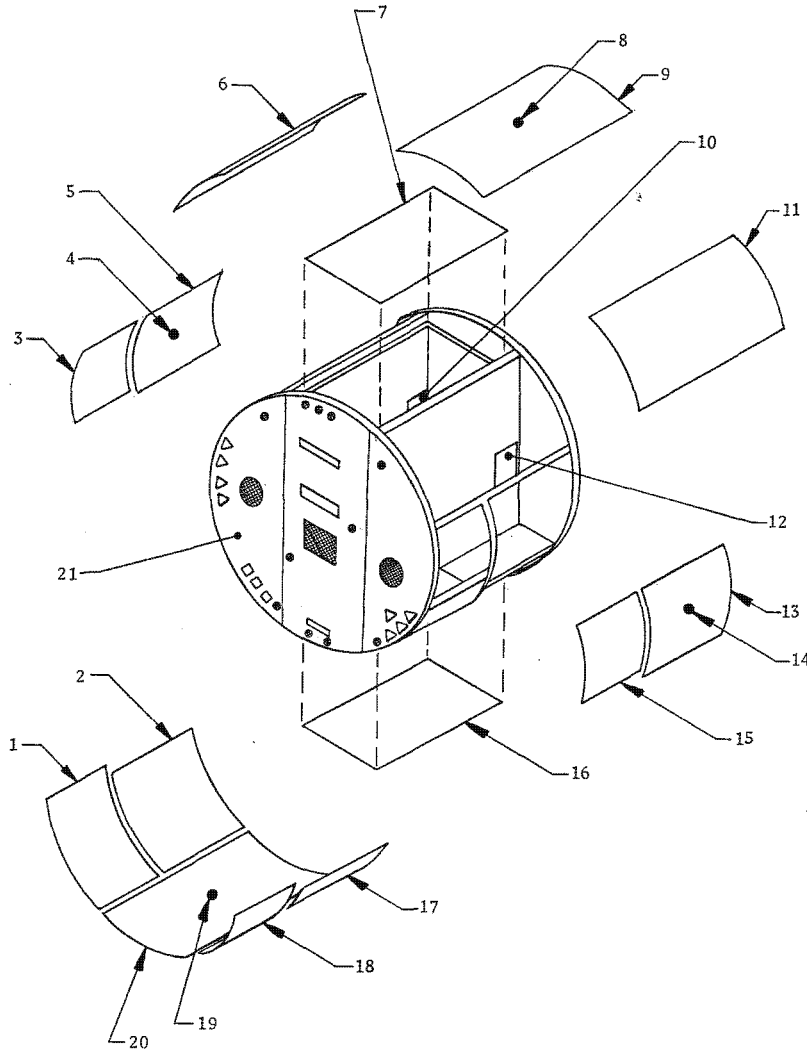


Figure 3.1-11. SEM Access Panels

3.1-29/3.1-30

Handle via BYEMAN
Control System Only

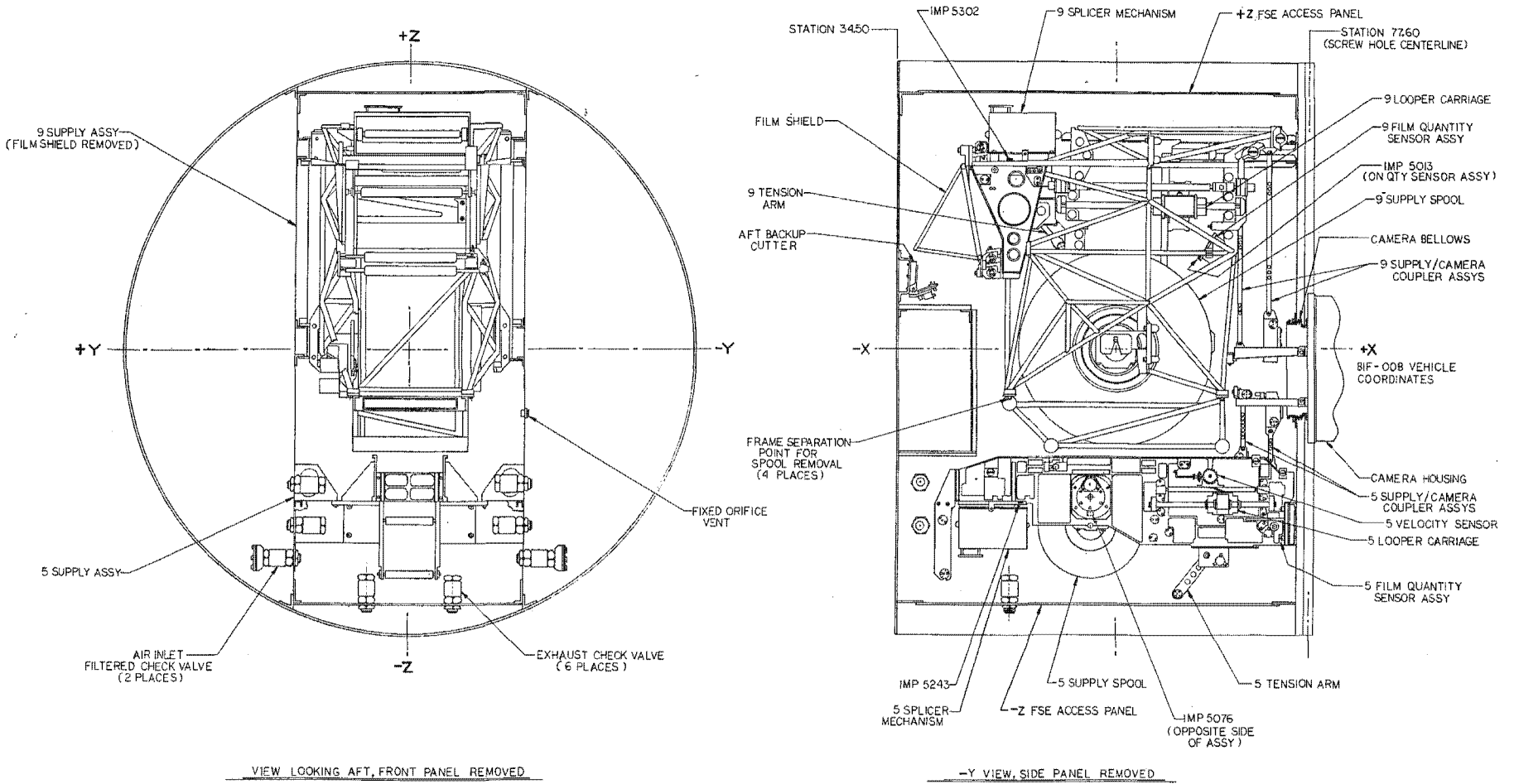


Figure 3.1-12. FSE Internal Components

3.1-31/3.1-32

Handle via BYEMAN
Control System Only

Approved for Release: 2017/02/14 C05097220

Approved for Release: 2017/02/14 C05097220

~~TOP SECRET~~ GBIF-008- W-C-019839-RI-80

12 inches either side of the vehicle centerline, are thin magnesium sheets which extend the full length of the SES, and vertically between radial longerons that also extend the full length of the SES (see Figure 3.1-11). The panels are attached to the longerons by L-shaped fiberglass splices which act as a thermal barrier between the FSE walls and the external shell. Ground straps between the FSE and the external structure maintain the FSE at vehicle ground potential. Removable magnesium panels at the top and bottom (+Z and -Z) complete the enclosure. A sticky coating applied to the inner walls assists in controlling particle contamination.

The forward end of the FSE has three film pass-through openings that interface with the DRM film tunnels. The aft bulkhead has an elliptically shaped opening which interfaces with the dual platen camera bellows. The dual platen camera is mounted at its opposite end to the Ross corrector and field lens assembly (RCFLA) using a gasket seal. The fifth lens element of the RCFLA (nearest the camera) is fully potted on the periphery to complete the pressure-tight seal of the film path. All electrical connections through the FSE walls employ hermetically sealed connectors with "O" rings. An opaque potting is used to maintain lighttightness.

There are four access panels for the FSE. The +Z panel is removed to install the 9 supply unit. The -Z panel is removed to install the 5 supply and to mount both the 9 and 5 film spools. To mount the 9 film spool, the 5 supply unit and the lower portion of the 9 supply unit must be removed. The smaller +Y and -Y access panels, shown in Figure 3.1-11, are used during mating of the SEM and COM to connect the film-handling components (tilt-frame couplers) which direct film into the camera.

The FSE side panels are the principal load-carrying members of the SES. They support the film supplies internally and the electronic units externally. The film supplies are bolted to precisely located mounting pads and aligned by locating pins. The mounting pads are reinforced by beams to distribute the loads into the side panels.

3.1-33

~~TOP SECRET~~ GHandle via **BYEMAN**
Control System Only

~~TOP SECRET~~ GBIF-008- W-C-019839-RI-80

A system of beams and mounting rails attached to the outer surfaces of the FSE side panels supports the following electronic control units:

- (1) camera electronics assemblies (CEAs)
- (2) command processor (CP)
- (3) digital telemetry unit (DTU)
- (4) film control electronics (FCE)
- (5) film handling electronics (FHE)
- (6) frequency phase lock loop electronics (FPLLE)
- (7) initiator electronics unit (IEU)
- (8) instrumentation processor (IP)
- (9) power monitor and control unit (PM and C)
- (10) viewport door electronics (VE)

Except for the command processor (CP), and viewport door electronics (VE), all electronic units are rigidly bolted to the mounting rails. The CP and VE are mounted on special isolators to reduce vibration loading of the units.

Thermistors located on the various mounting rails monitor the internal SEM temperature while on orbit (see Figures 3.1-13 through 3.1-15). All interfaces between box and structure are electrically conductive, presenting a resistance below 2.5 milliohms to control electromagnetic interference effects. A metal strap on one mounting foot provides the necessary electrical and thermal conduction between the CP and SES.

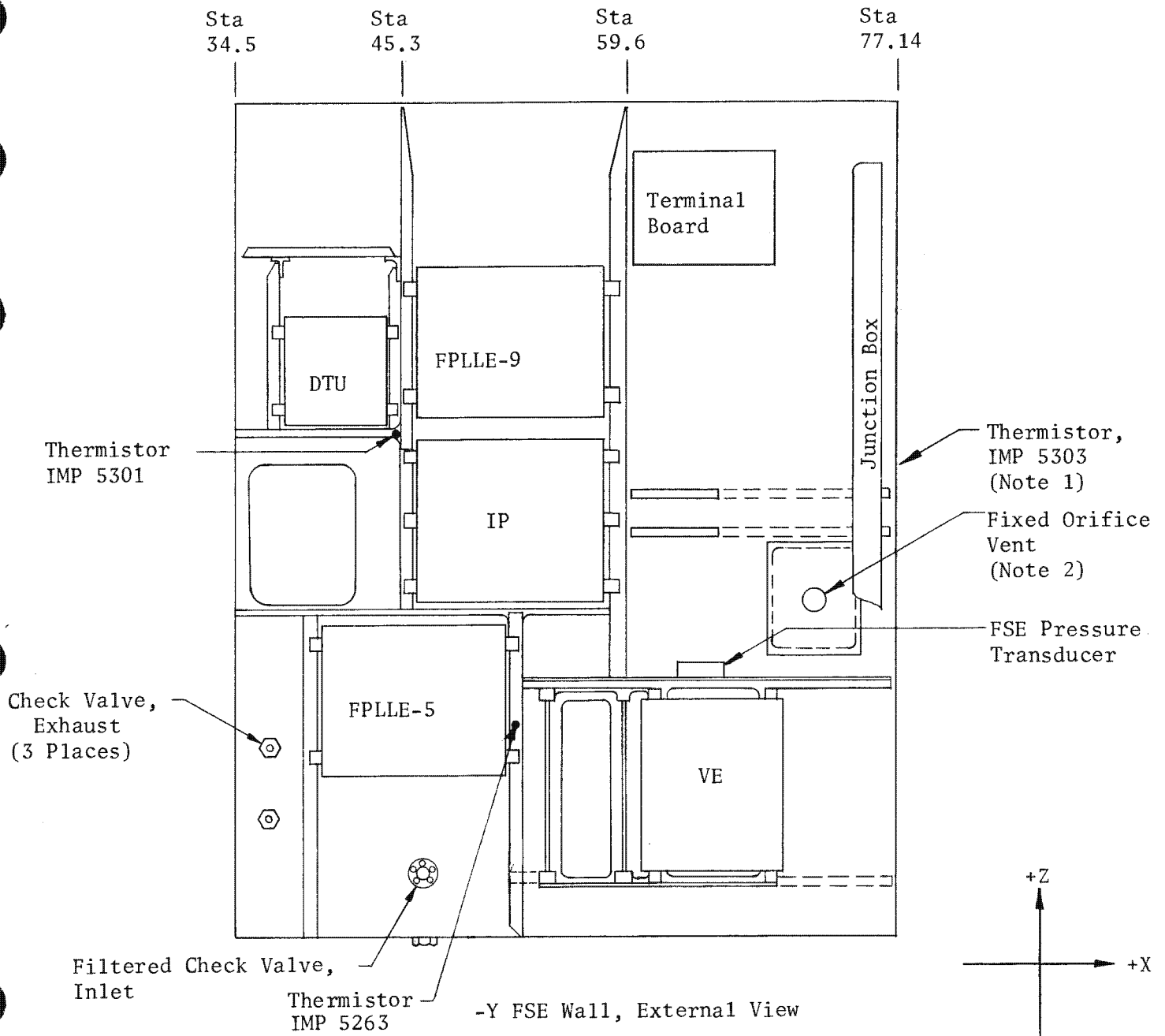
During ascent, air is vented from the FSE and film tunnels by six check valves which open at 0.29 psid. Two similar check valves equipped with filters allow air to reenter the enclosure following vacuum testing or transportation by aircraft. The enclosure also contains a fixed orifice vent on the -Y access panel. The orifice allows water vapor, which results from film being despoiled (film outgassing), to vent during orbital flight. This

3.1-34

~~TOP SECRET~~ GHandle via **BYEMAN**
Control System Only

~~TOP SECRET~~ G

BIF-008- W-C-019839-RI-80



BIF-008 Vehicle Coordinates

Notes:

1. IMP 5303 on aft bulkhead. See Figure 3.1-15.
2. Fixed orifice vent covered by cap until launch.

Figure 3.1-13. SEM Internal Temperature Monitors (-Y Side)

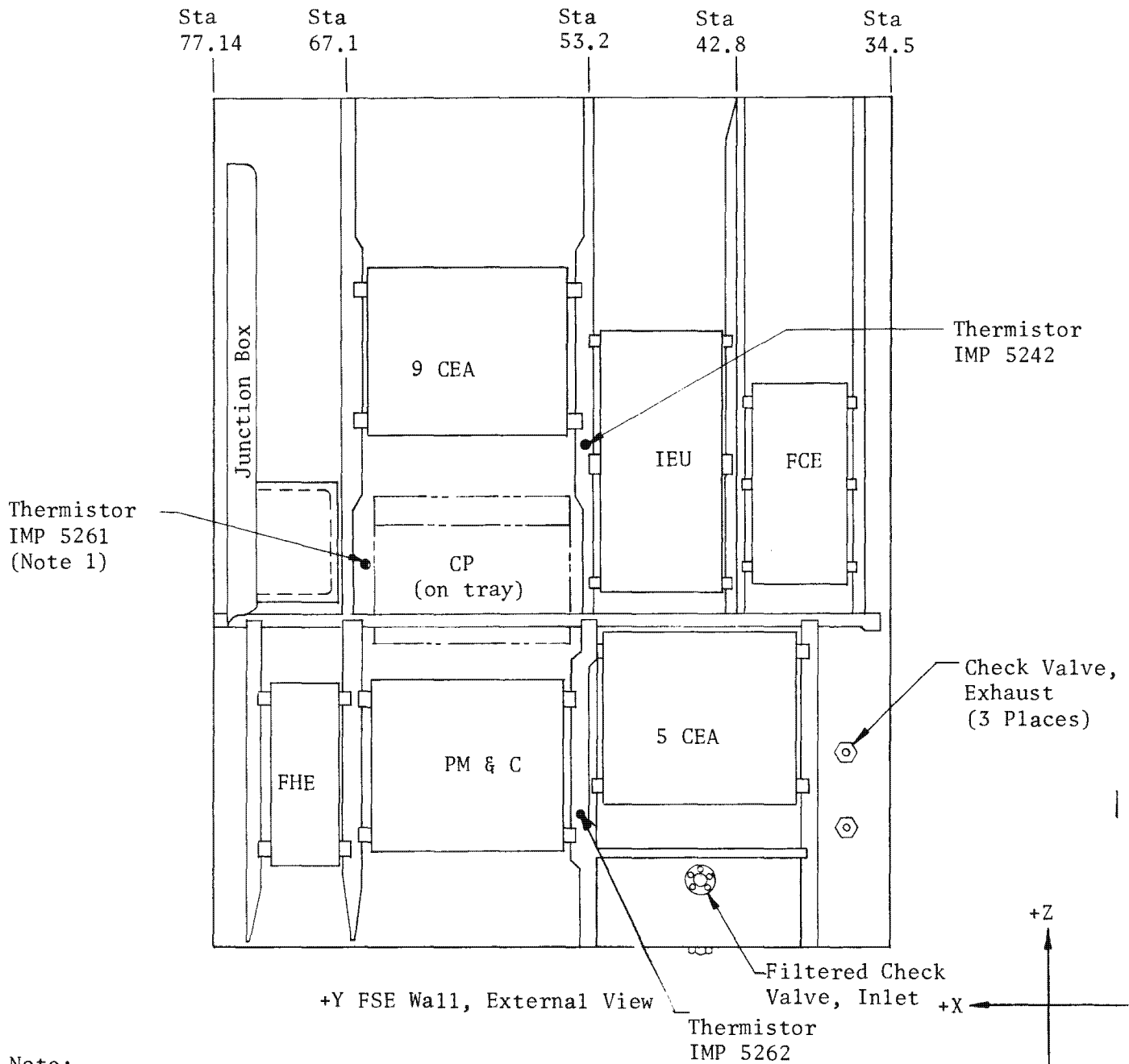
3.1-35

~~TOP SECRET~~ G

Handle via **BYEMAN**
Control System Only

~~TOP SECRET~~ G

BIF-008-W-C-019839-RI-80



Note:
 IMP 5261 on CP mounting tray. See Figure 3.1-15.

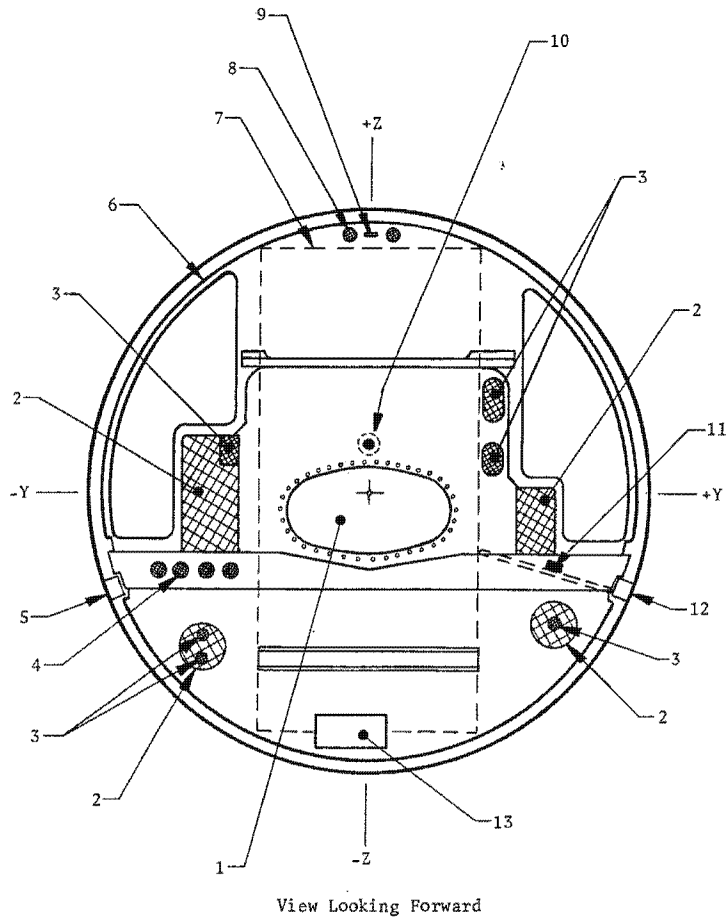
BIF-008 Vehicle
 Coordinates

Figure 3.1-14. SEM Internal Temperature Monitors (+Y Side)

3.1-36

~~TOP SECRET~~ G

Handle via **BYEMAN**
 Control System Only



Note: Coordinates shown are BIF-008 vehicle coordinates.

Reference Table

No.	Descriptor
1.	Camera Pass-through Area
2.	Screened Vent Area
3.	Cable Pass-through Area
4.	Screened Vent Area (4 Places)
5.	Main Vehicle Longeron (-Y)
6.	Junction Box Interface
7.	FSE Boundary
8.	Screened Vent Area (2 Places)
9.	Ground Strap Pass-through Area
10.	Thermistor, IMP 5303 (External To FSE)
11.	Thermistor, IMP 5261 (On CP Mounting Tray)
12.	Main Vehicle Longeron (+Y)
13.	Viewport Door B/U Motor Pass-through Area

Figure 3.1-15. SEM Aft Bulkhead

3.1-37/3.1-38

Handle via BYEMAN
Control System Only

Approved for Release: 2017/02/14 C05097220

Approved for Release: 2017/02/14 C05097220

~~TOP SECRET~~ GBIF-008- W-C-019839-RI-80

orifice is covered by a cap until launch to prevent reverse air flow through the orifice into the FSE. A pressure transducer monitors the positive internal pressure while the vehicle is in orbit.

1.3.2 SEM Components

The following sections describe the form and function of each internal SEM component. The reference following each description indicates where additional information can be found. The physical locations of the units are shown in Figures 3.1-16 and 3.1-17.

1.3.2.1 9 Supply Assembly. The 9 supply assembly provides storage for unexposed 9.5-inch wide film, precisely controlled film transport to and from the camera, and transport to the take-up spools in the satellite reentry vehicles via the DRM film tunnels. (Part 3, Section 2)

1.3.2.2 5 Supply Assembly. The 5 supply assembly functions in a similar fashion to the 9 supply assembly, providing storage for the unexposed 5-inch wide film, and precision handling to and from the camera and to the take-up spools in the SRVs. (Part 3, Section 2)

1.3.2.3 9 Splicer Mechanism. The 9 splicer mechanism provides the capability to transfer the 9 film path from SRV 1 to SRV 2 upon command. (Part 3, Section 11)

1.3.2.4 5 Splicer Mechanism. The 5 splicer mechanism provides the capability to transfer the 5 film path from SRV 1 to SRV 2 upon command. (Part 3, Section 11)

1.3.2.5 Command Processor. The command processor (CP) provides a controlled interface with the satellite control section, processing and distributing all

3.1-39

~~TOP SECRET~~ GHandle via **BYEMAN**
Control System Only

~~TOP SECRET~~ G

BIF-008- W-C-019839-RI-80

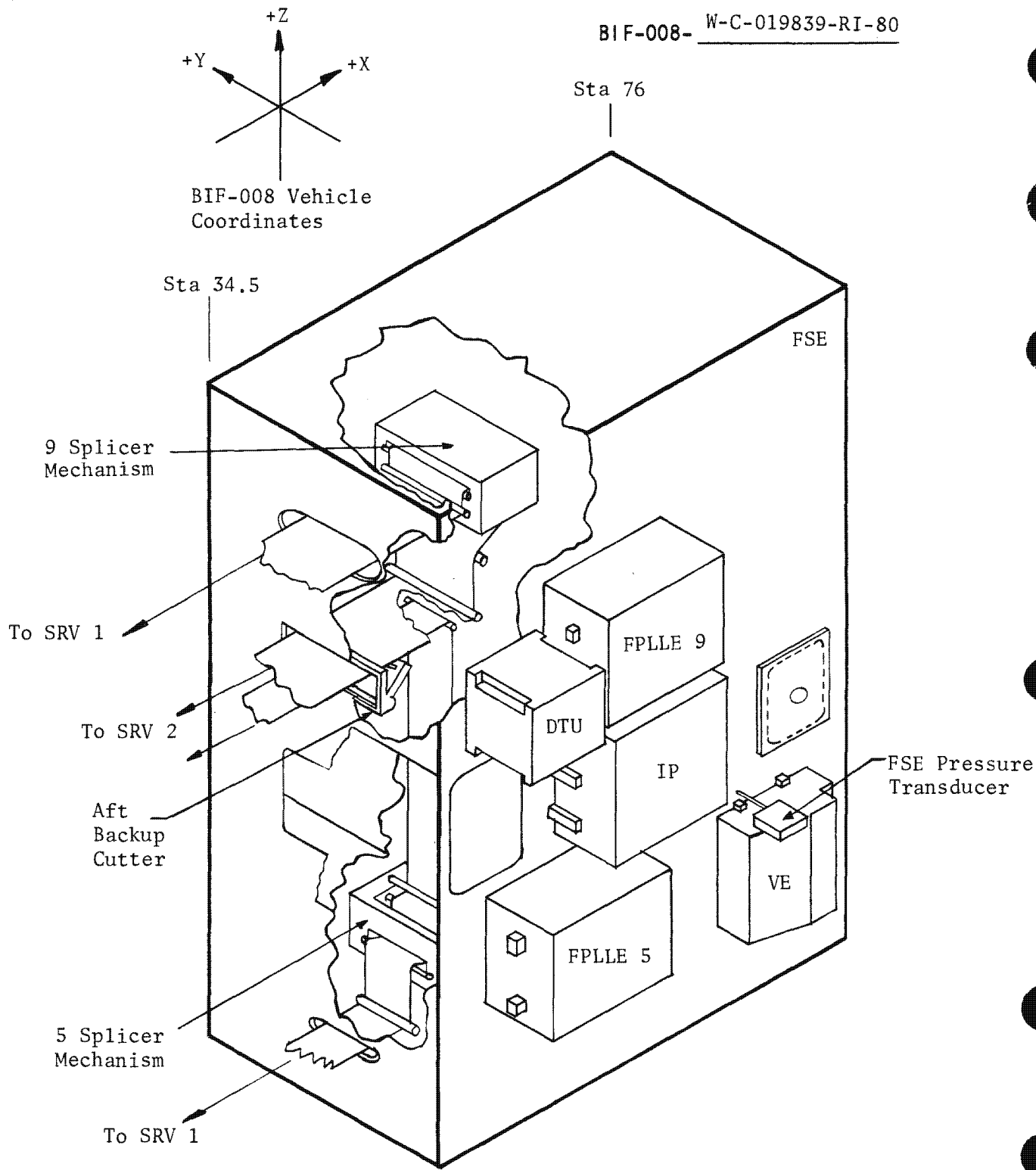


Figure 3.1-16. SEM Electronic Unit Locations (-Y Side)

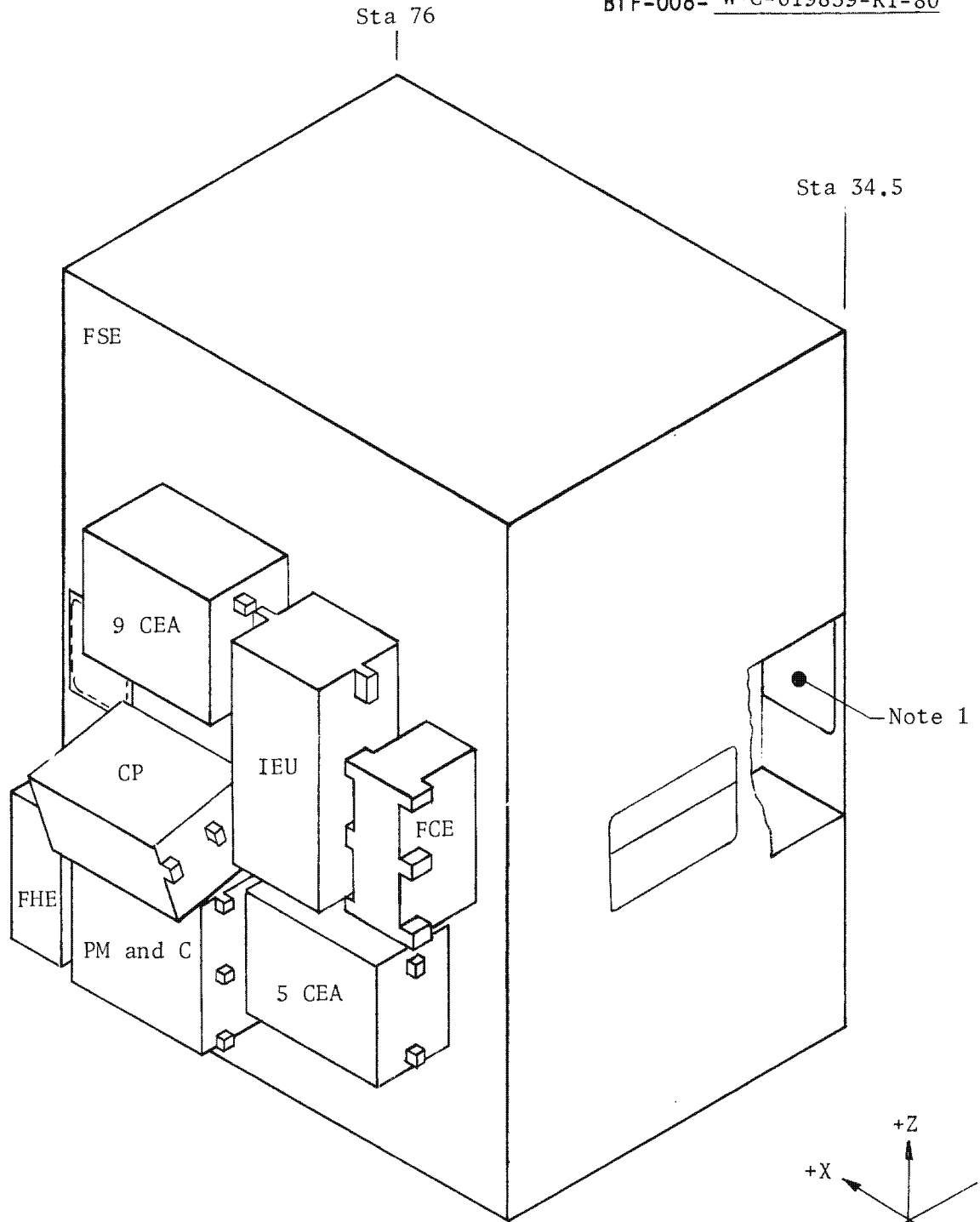
3.1-40

~~TOP SECRET~~ G

Handle via BYEMAN
Control System Only

~~TOP SECRET~~ G

BIF-008- W-C-019839-RI-80



Notes:

1. SRV 2 ignitor access opening (in nozzle access box) and vent opening
2. Coordinates shown are BIF-008 vehicle coordinates.

Figure 3.1-17. SEM Electronic Unit Locations (+Y Side)

3.1-41

~~TOP SECRET~~ G

Handle via **BYEMAN**
Control System Only

~~TOP SECRET~~ GBIF-008- W-C-019839-RI-80

nonpyrotechnic related PPS/DP EAC commands. The CP performs logic operations, and produces signals which control the PPS/DP EAC circuitry. (Part 3, Section 9)

1.3.2.6 Initiator Electronics Unit. The initiator electronics unit (IEU) interfaces with the SCS command lines controlling pyrotechnic related functions. The IEU performs logic operations and processes and distributes signals which fire pyrotechnic devices. In addition, the IEU switches the take-up motor power for the 5 and 9 spool drives from take-up 1 to take-up 2, and generates a switch-over signal for primary to backup viewport door motor drive control. (Part 3, Section 7)

1.3.2.7 Junction Box. The junction box is a removable part of the SES that electrically interconnects components in the PPS/DP EAC, and interfaces with many of the PPS/SCS cable connections, routing power, commands, and signals between the two sections of the vehicle.

1.3.2.8 Power Monitor and Control Unit. The power monitor and control unit (PM and C) distributes power to the PPS/DP EAC and performs limited logical operations in conjunction with the command processor. The PM and C also generates +5 and ± 15 volt instrumentation power, monitors total instantaneous PPS/DP EAC current (excluding pyro firing current) by means of a return-line current sensor, and measures total PPS/DP EAC power consumption using an ampere-hour meter. (Part 3, Section 7)

1.3.2.9 Instrumentation Processor. The instrumentation processor (IP) receives signals from instrumentation transducers in the PPS/DP EAC, conditions them if necessary, and routes them to the digital telemetry unit (DTU). The IP generates internally a limited number of instrumentation signals which are also sent to the DTU. (Part 3, Section 10)

1.3.2.10 Digital Telemetry Unit. The digital telemetry unit (DTU) receives analog and binary signals from the instrumentation processor and other

~~TOP SECRET~~ G

~~TOP SECRET~~ GBIF-008- W-C-019839-RI-80

sources within the PPS/DP EAC samples and encodes them in response to control signals from the SCS master digital telemetry unit (MDTU), and transmits this information to the MDTU. (Part 3, Section 10)

1.3.2.11 9 Camera Electronics Assembly. The 9 camera electronics assembly, usually referred to as the drum recorder electronics assembly (DREA)*, controls slit selection, platen position adjustment, and instrumentation and data recording for the 9 film subsystem. (Part 3, Section 2).

1.3.2.12 5 Camera Electronics Assembly. This unit, a part of the 5 subsystem, functions identically to the 9 camera electronics assembly. (Part 3, Section 2)

1.3.2.13 9 Frequency Phase Lock Loop Electronics. The 9 frequency phase lock loop electronics (FPLLE) is composed of two identical control circuits, either of which provides power and speed control for the 9 film platen drive motor. (Part 3, Section 2)

1.3.2.14 5 Frequency Phase Lock Loop Electronics. The 5 FPLLE is similar to the 9 FPLLE with compensation provided to accommodate the lower inertia of the 5 film platen. (Part 3, Section 2)

1.3.2.15 Film Control Electronics. The film control electronics, usually referred to as the record control electronics (RCE)*, controls the 9 film handling subsystem, processing control signals and switching power to operate the 9 film supply and take-up mechanisms. (Part 3, Section 2)

1.3.2.16 Film Handling Electronics. The film handling electronics, usually referred to as the record handling electronics (RHE)*, controls the 5 film handling subsystem, processing signals and switching power to operate the

* This unit, and several others, are commonly referred to by their unclassified titles to facilitate communication.

~~TOP SECRET~~ G

~~TOP SECRET~~ GBIF-008- W-C-019839-RI-80

5 film supply and take-up mechanisms. (Part 3, Section 2)

1.3.2.17 Viewport Door Electronics. The viewport door electronics module operates the primary and backup door motors in the camera optics module. (Part 3, Section 5)

1.3.2.18 Aft Backup Cutter. The aft backup cutter (ABUC) is a redundant cutter assembly which insures that the film strands entering SRV 2 are severed before SRV separation. (Part 3, Section 11)

1.3.3 SEM/COM Mating

The SEM is connected to the COM by a line of screws around the vehicle circumference which fastens the COM forward barrel shell to the SES aft ring (see Figure 3.1-18). The two principal load-carrying longerons of the COM forward barrel (the main vehicle longerons) are bolted to two structural longerons of the SES located below the vehicle center plane (see Figure 3.1-15). The SEM aft ring is stiffened by the attached bulkhead and a transverse beam across the bulkhead which connects the two bolted longerons.

Additional interfaces include cable routing from the COM through the SEM bulkhead to the SEM internal components, attachment of the bellows to the camera, and connection of the supply and camera tilt-frame couplers.

1.4 Camera Optics Module

The camera optics module (COM) contains the 9x5 dual platen camera and imaging optics of the PPS/DP EAC. The COM extends from the supply electronics module to the SCS payload adapter section (PAS, or roll joint), giving a total length of 211.05 inches (211.03 inches for FM 49 and on). The COM is 60 inches in diameter and weighs approximately 2286 pounds. The major components of the COM include a two part external structure (consisting of the

3.1-44

~~TOP SECRET~~ GHandle via BYEMAN
Control System Only

~~TOP SECRET~~ G

BIF-008- W-C-019839-RI-80

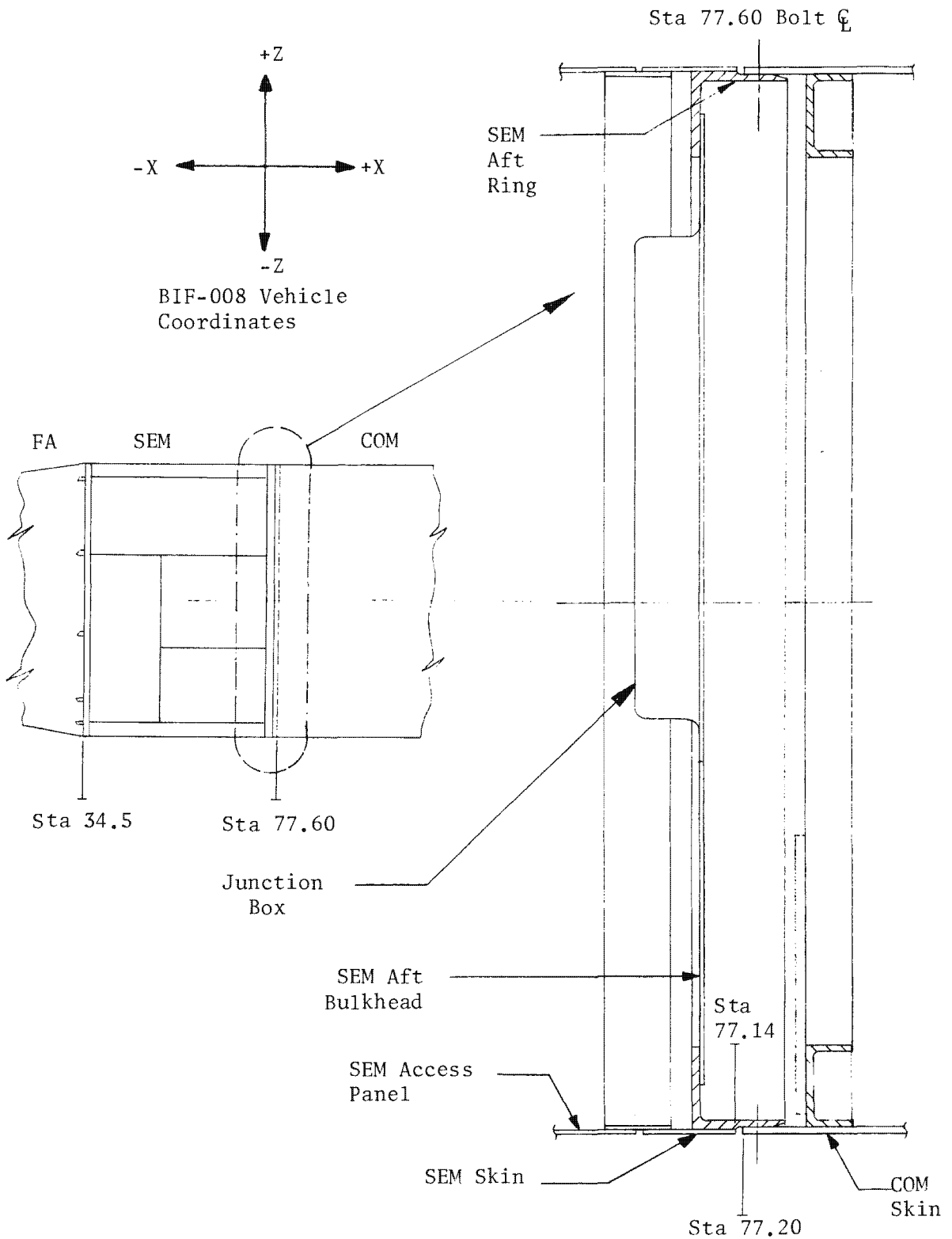


Figure 3.1-18. SEM/COM Interface

3.1-45

~~TOP SECRET~~ G

Handle via BYEMAN
Control System Only

~~TOP SECRET~~ GBIF-008- W-C-019839-RI-80

forward and aft barrels), the camera optics assembly (COA), and the viewport doors.

1.4.1 Camera Optics Module - External Structure

The forward barrel section of the external structure mates to the SEM and to the aft barrel, providing a break in the structure at the forward barrel/aft barrel interface for fabrication and assembly purposes. The aft barrel extends from that interface to the payload adapter section.

1.4.1.1 Access Panels. Like the other modules, the exterior of the COM has several removable structural panels for access to the interior. Table 3.1-2 lists these panels and the components accessible through them. Figure 3.1-19 indicates positions and approximate sizes of the various openings.

Panel 19 is the ejectable hatch covering the viewport doors. It is held in place by six lug/pin-puller assemblies, and, unlike most other panels, is not a true structural member of the COM.

As with the other modules, where a panel must be removed several times during assembly and testing, a shipping panel and a flight panel are provided.

1.4.1.2 Forward Barrel. The forward barrel is a semimonocoque cylindrical structure, 72.2 inches long, reinforced with rings and longerons. The forward barrel components include the viewport doors, the ejectable hatch, electrical wiring and cabling, and the umbilical connection to the ground conditioned air supply. Figures 3.1-20 and 3.1-21 illustrate the structural aspects of the barrel: the magnesium alloy skin, the partial bulkhead supporting the viewport door motors and drive linkage, and the door hinge support structure. Although the barrel forms a portion of the COA housing and

3.1-46

~~TOP SECRET~~ GHandle via BYEMAN
Control System Only

TABLE 3.1-2
COM ACCESS PANELS

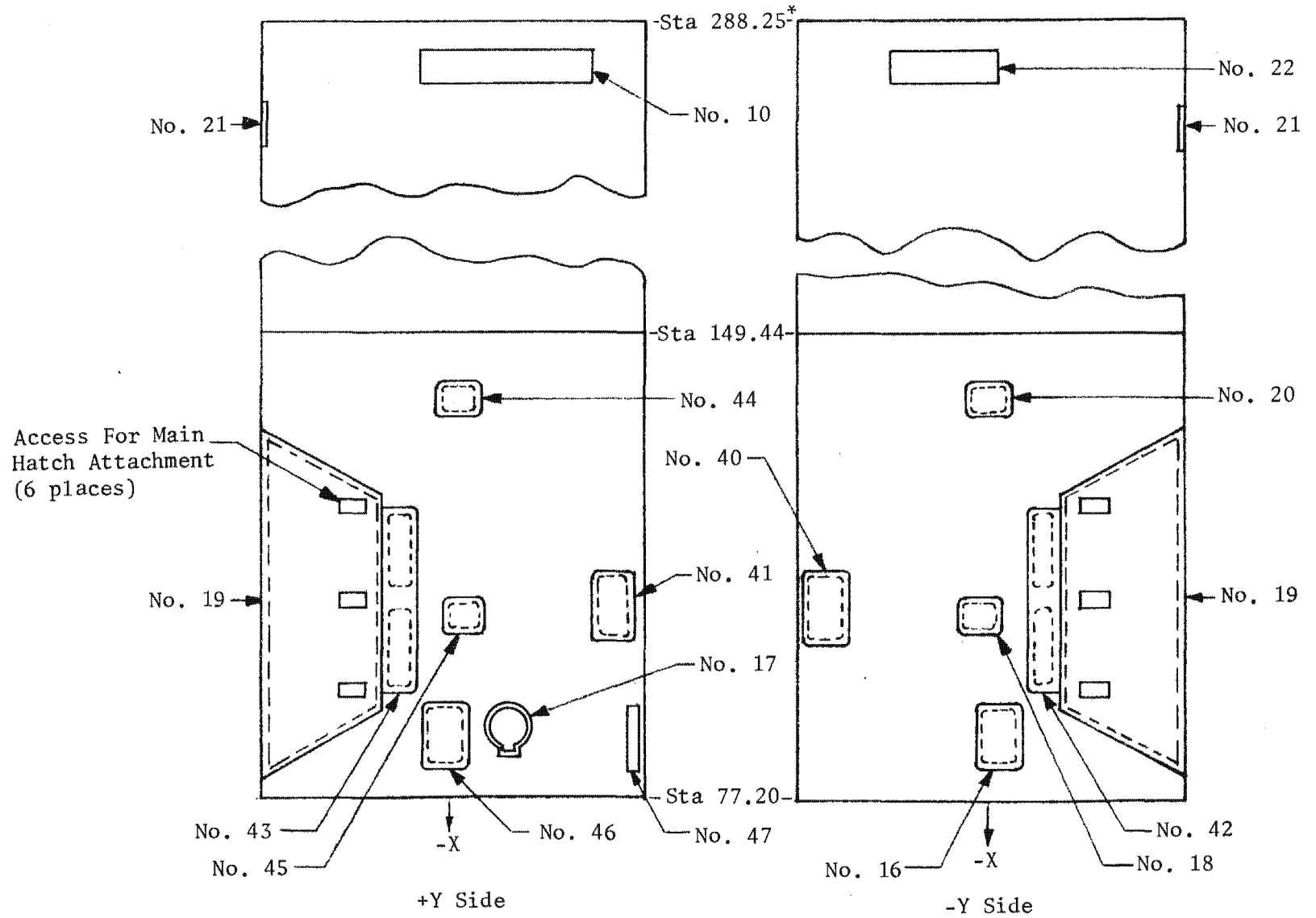
<u>Forward Barrel</u>		<u>Aft Barrel</u>	
<u>Panel Number</u>	<u>Accessible Components</u>	<u>Panel Number</u>	<u>Accessible Components</u>
16	COM Cables (-Y)	10	SCS/PPS Cable Connections (+Y)
17 (Hinged Panel)	Umbilical Conditioned Air Inlet	21	End Bell Mounting (Lollipop)
18	Zero G Support (-Y)	22	SCS/PPS Cable Connections (-Y)
19	Ejectable Hatch		
20	A-Frame Arm, Adjustable (-Y)		
40	Crab Servo		
41	Stereo Servo		
42	Ejectable Hatch Pin-Pullers (-Y)		
43	Ejectable Hatch Pin-Pullers (+Y)		
44	A-Frame Arm (+Y)		
45	Zero G Support (+Y)		
46	COM Cables (+Y)		
47	Camera Cables		

3.1-47

Handle via **BYEMAN**
Control System Only

Approved for Release: 2017/02/14 C05097220

Approved for Release: 2017/02/14 C05097220



3.1-48

* Sta 288.22: FM-49 and on.

Figure 3.1-19. COM Access Panels

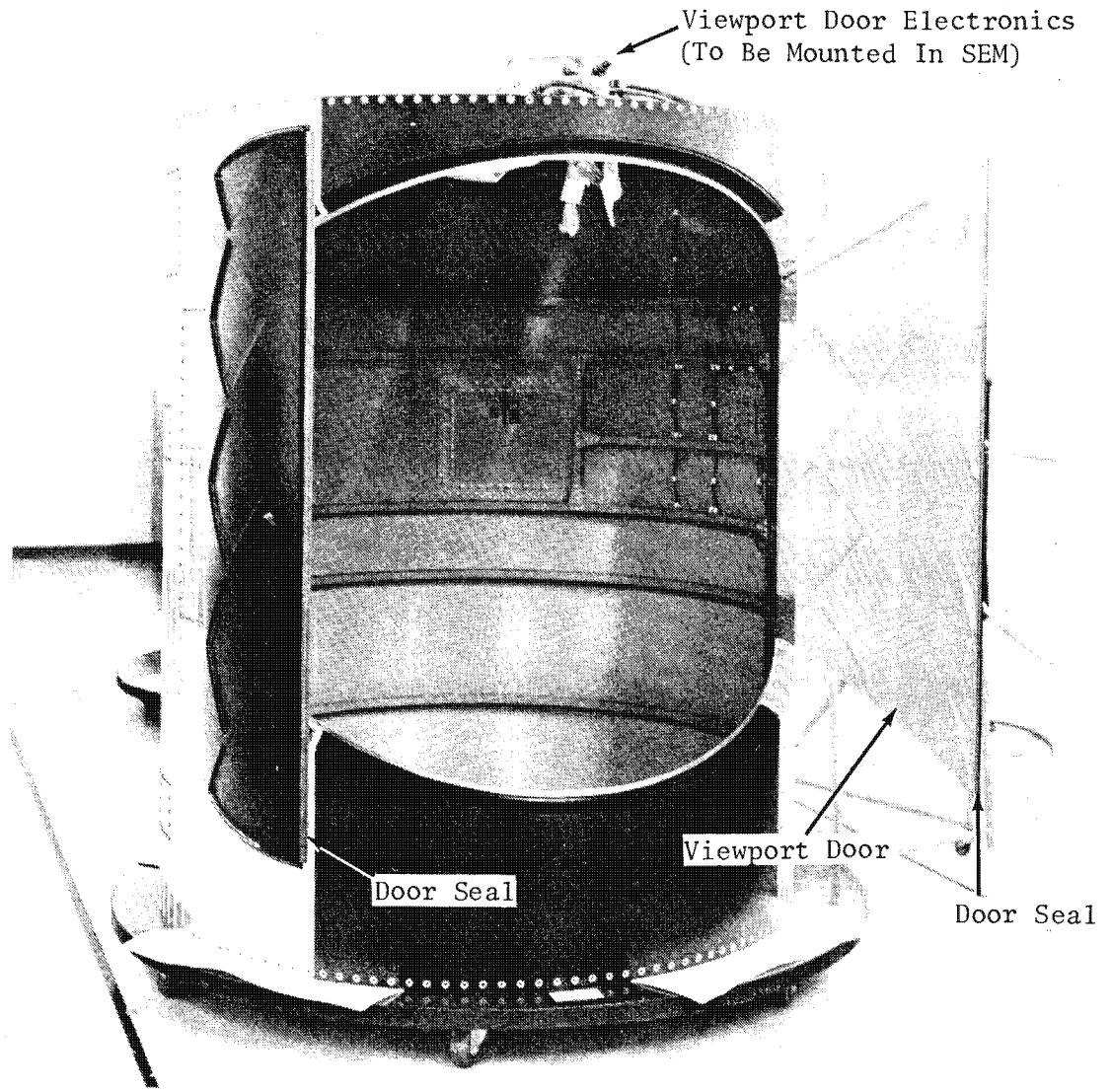
Handle via **BYEMAN**
Control System Only

Approved for Release: 2017/02/14 C05097220

Approved for Release: 2017/02/14 C05097220

~~TOP SECRET~~ G

BIF-008-W-C-019839-RI-80



Notes:

1. Coordinates shown are BIF-008 vehicle coordinates.
2. Insulation blankets and heater tape support screens removed from doors.

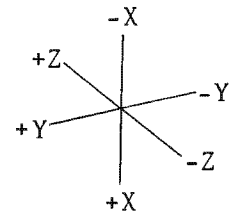


Figure 3.1-20. COM Forward Barrel

3.1-49

~~TOP SECRET~~ G

Handle via **BYEMAN**
Control System Only

~~TOP SECRET~~ G

BIF-008-W-C-019839-RI-80

This page intentionally left blank.

3.1-50

~~TOP SECRET~~ G

Handle via **BYEMAN**
Control System Only

NOTES:

- 1. COORDINATES SHOWN ARE BIF-008 VEHICLE COORDINATES
- 2. VIEW PORT DOOR DRIVE MOTORS REMOVED FOR CLARITY
- 3. VIEW PORT DOORS ROTATE 62° FROM CLOSED TO OPEN

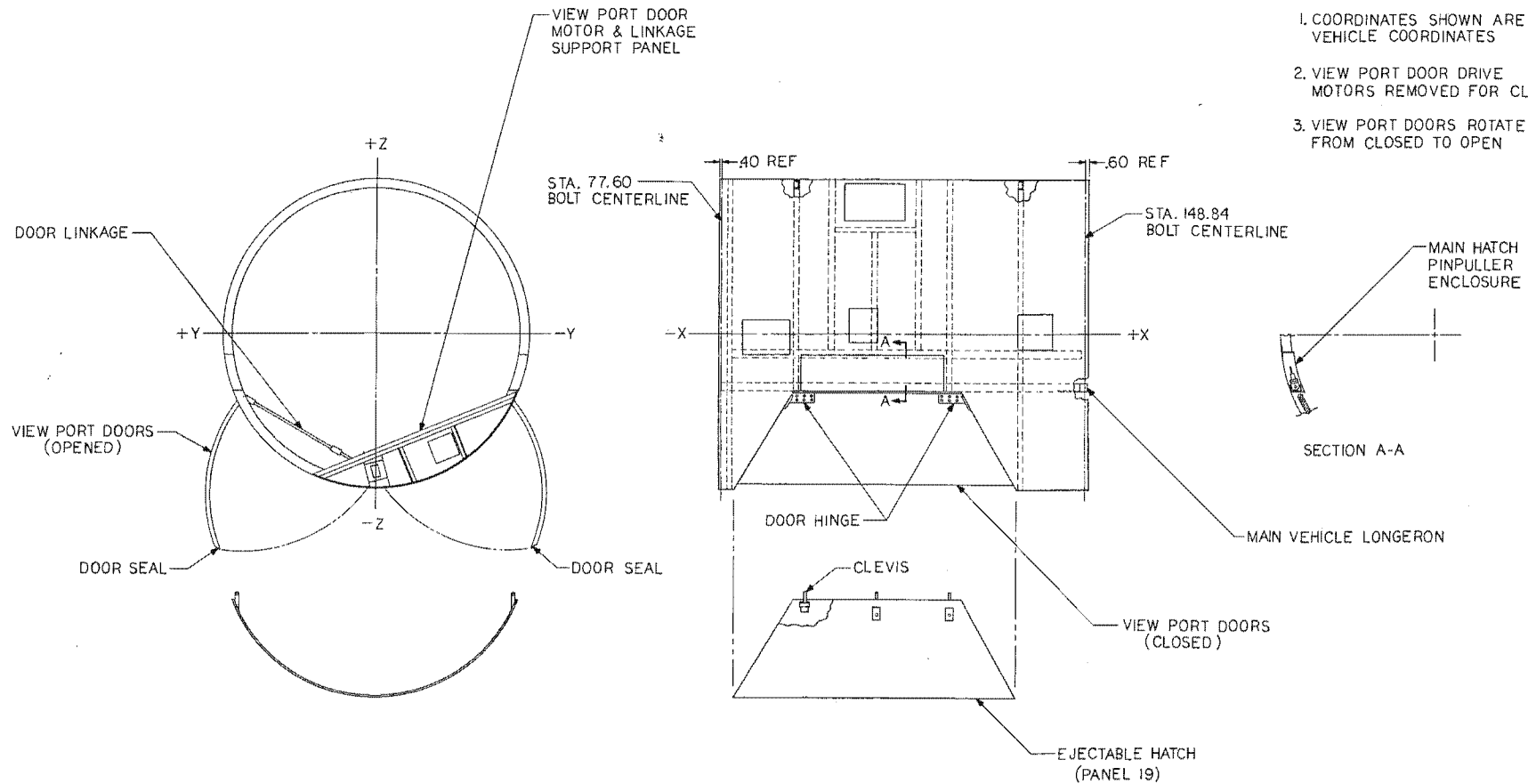


Figure 3.1-21. COM Forward Barrel Structure

3.1-51/3.1-52

Handle via BYEMAN Control System Only

Approved for Release: 2017/02/14 C05097220

Approved for Release: 2017/02/14 C05097220

~~TOP SECRET~~ GBIF-008-W-C-019839-RI-80

contains the opening through which light enters the optical system, it does not support the COA structure at any point.

A single conductive strap is connected to the COA and forward barrel, then continues through the aft SEM bulkhead to the SEM structure for electromagnetic interference control.

The viewport door cutout is the largest discontinuity in the external PPS/DP EAC structure. The doors provide protection for the internal components while on orbit. The ejectable hatch, in place during shipping and launch, is secured by three pin-puller assemblies per side. The hatch is not considered a true structural member, however, whenever the bottom side of the vehicle is in compression, the edge of the hatch butts against the barrel skin and a load transfer takes place. An up-bending condition results in tension on the bottom side of the vehicle and therefore the hatch is structurally less effective.

The forward barrel shell is stiffened circumferentially by continuous and partial rings. Two box-type beams, formed by longerons, stiffeners, and magnesium sheet metal, extend along each door edge to carry axial loads. These beams also provide a housing for the ejectable hatch pin-puller devices.

1.4.1.2.1 Viewport Door Assembly. The viewport door assembly consists of clam-shell type doors and their associated drive linkages and motors, and is controlled by the viewport door electronics module located in the SEM. During launch, the doors are covered by the ejectable hatch (panel 19) which matches the external contour of the forward barrel.

The doors are suspended from the COM structure along an axis parallel to the vehicle X-axis. When the doors are closed, gaskets on the edge of each door overlap to seal the module. The inside surface of each door is faced

3.1-53

~~TOP SECRET~~ GHandle via BYEMAN
Control System Only

~~TOP SECRET~~ GBIF-008- W-C-019839-RI-80

with a thermal insulation blanket and a metal screen that prevents the blanket from billowing during launch. Electrical heater tapes on the support screens form a part of the ground heater system (not powered on-orbit) and will be removed effective with Flight Model 50.

The drive linkage and motors for the doors are supported by the partial bulkhead of the forward barrel. The backup motor is mounted on the forward side of the bulkhead, and extends through an opening in the SEM bulkhead. On the aft side of the partial bulkhead the drive linkage attaches to the door-actuating arms and primary motor.

For additional detail on the viewport door structure and operation, refer to Part 3, Section 5.

1.4.1.2.2 Umbilical Air Supply Connection. The connection for the ground conditioned air is made by means of an umbilical line which disconnects upon lift-off. Panel 17, through which the air enters, consists of a spring-loaded outer coupling assembly that fits flush with the outer skin when closed, and a redundant spring-loaded inner cover. The outer cover is hinged such that the air flow over the skin during launch will tend to close and seal the opening. The redundant inner panel is hinged such that it tends to close when a positive internal pressure is applied to the structure. Air from the ground air conditioner enters through the forward portion of the COM and is vented through four filter assemblies in the aft barrel bulkhead. Structural loads are conducted around the umbilical hole by means of a fitting which frames the opening.

A thermistor located inside the structure near panel 17 monitors the temperature of the incoming ground conditioned air. The output of this sensor is available only through an SCS umbilical line; it is not available for on-orbit use.

3.1-54

~~TOP SECRET~~ GHandle via **BYEMAN**
Control System Only

~~TOP SECRET~~ GBIF-008- W-C-019839-RI-80

1.4.1.3 Aft Barrel. The aft barrel (Figure 3.1-22) is a ring-stiffened, cylindrical shell structure, 139.822 inches long. The forward ring of the aft barrel is attached to the forward barrel by a line of screws and two longeron bolts. These longeron bolts complete the connection of the main vehicle $\pm Y$ longerons which began in the SEM.

The aft barrel supports the COA at the two A-frame arms and at the broomstick (a metal shaft centrally located on the aft end of the COA). The A-frame mounts are attached to the forward ring and support the entire COA X-X axis loading. Directly aft of the A-frame mounts are four longerons (two on each side) which extend to the third aft barrel ring. Between the first two rings the shell is reinforced by short longeron members symmetrically spaced around the entire circumference. An inner skin riveted to each longeron and to the first two rings forms a sturdy box structure. The box ring and the four main longerons redistribute shear loads resulting from discontinuities in the forward barrel, and distribute the loads and torque introduced by the COA supports. The added length of the main longerons is used to distribute the high axial loads imposed by the COA during launch. In addition, the box ring acts as a main vehicle support point during ground handling and shipping.

In-flight altitude changes, made possible with the PPS/DP EAC design, could cause excessive stress on the roll joint since the blow-off ring that normally supported the roll joint during launch is no longer present. Restraint devices were added to support the roll joint during these altitude changes but these restraint devices could cause additional stress in the aft barrel. Therefore, three magnesium doubler plates were added to the aft end of the aft barrel to strengthen the areas placed under additional load. See Figure 3.1-22 for doubler locations.

The aft barrel bulkhead, attached to the last aft barrel ring, consists of a 48-inch diameter magnesium sheet panel and an outer magnesium sheet ring connected by a fiberglass splice. A spherical bearing in an eccentric mount on the aft bulkhead, one inch below the vehicle centerline, provides radial support for the

3.1-55

~~TOP SECRET~~ GHandle via BYEMAN
Control System Only

~~TOP SECRET~~ G

BIF-008- W-C-019839-RI-80

This page intentionally left blank.

3.1-56

~~TOP SECRET~~ G

Handle via BYEMAN
Control System Only

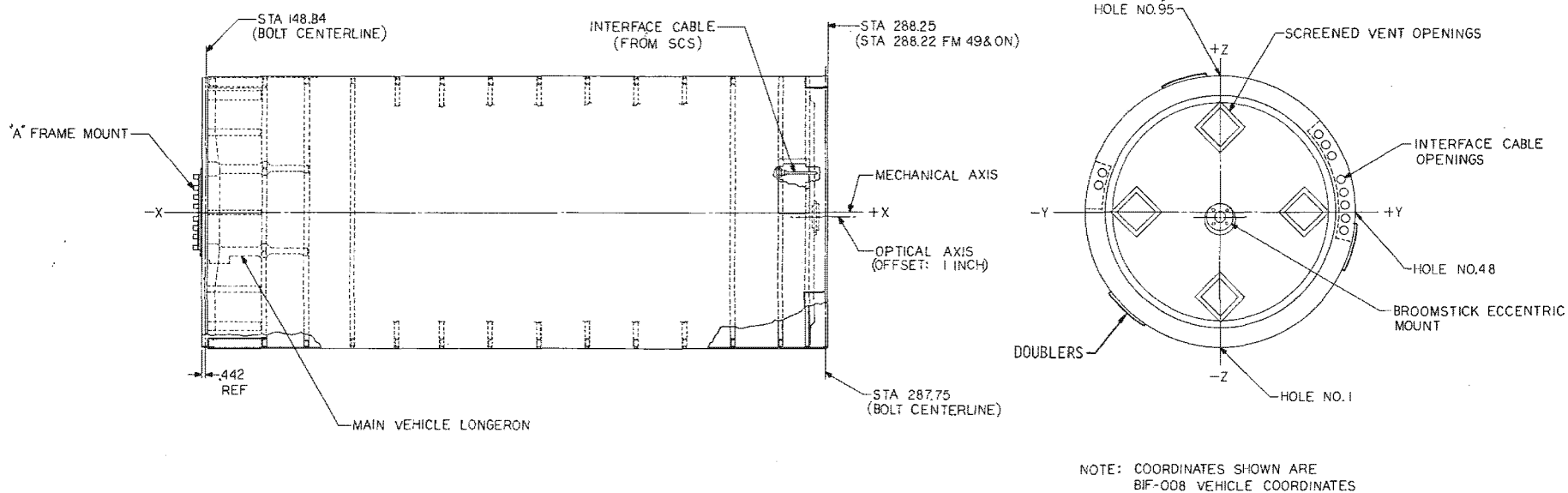


Figure 3.1-22. COM Aft Barrel Structure

3.1-57/3.1-58

Handle via BYEMAN
Control System Only

Approved for Release: 2017/02/14 C05097220

Approved for Release: 2017/02/14 C05097220

~~TOP SECRET~~ GBIF-008- W-C-019839-RI-80

COA through the broomstick. The fiberglass splice in the bulkhead serves as a thermal barrier between the aft barrel and the COA. The bulkhead also contains four 5½-inch-square filtered openings to allow for venting of the PPS/DP EAC through the SCS, and eleven cable pass-through openings for the SCS interface cables. Junction boxes formed between the last two aft barrel rings support the PPS/DP EAC cables and connectors. Access to these boxes for PPS/SCS cable mating is provided by panels 10 and 22.

1.4.2 Camera Optics Assembly (Internal Structure)

The COA (Figures 3.1-23 and 3.1-24) is a welded Invar sheet and stringer cylinder which supports the PPS/DP EAC optics and camera. Thermal control of the assembly is maintained through the use of heater tapes on the structure surface and by high-performance insulation blankets surrounding the structure which isolate it from COM skin temperature variations. Heater tapes on the inner surface of the structure are used only in the ground environmental control system and are powered through an SCS umbilical line. Thermistors on the COA shell and on various components within the COA monitor on-orbit temperature for telemetry purposes (reference Part 3, Section 8).

1.4.2.1 COA Suspension System. The COA is attached to the COM external structure at three points. Two of these points are at the extremities of the Y-Y axis near station 150 where attachment is by two piano-hinged, thermally isolated, titanium links (A-frames), one on each side of the vehicle. The third point is at the aft barrel bulkhead where attachment is by a shaft which mates with the spherical bearing on the bulkhead.

This latter arrangement allows free translation along the COA longitudinal axis to accommodate thermally induced changes in the external shell. The hinge pin of each A-frame is attached to the external structure, parallel to the Z-axis. The apex of each link is secured to the internal structure by a ball joint. The COA is thereby supported by three ball joints, fixing its position and orientation.

3.1-59

~~TOP SECRET~~ GHandle via BYEMAN
Control System Only

~~TOP SECRET~~ G

BIF-008- W-C-019839-RI-80

This page intentionally left blank.

3.1-60

~~TOP SECRET~~ G

Handle via BYEMAN
Control System Only

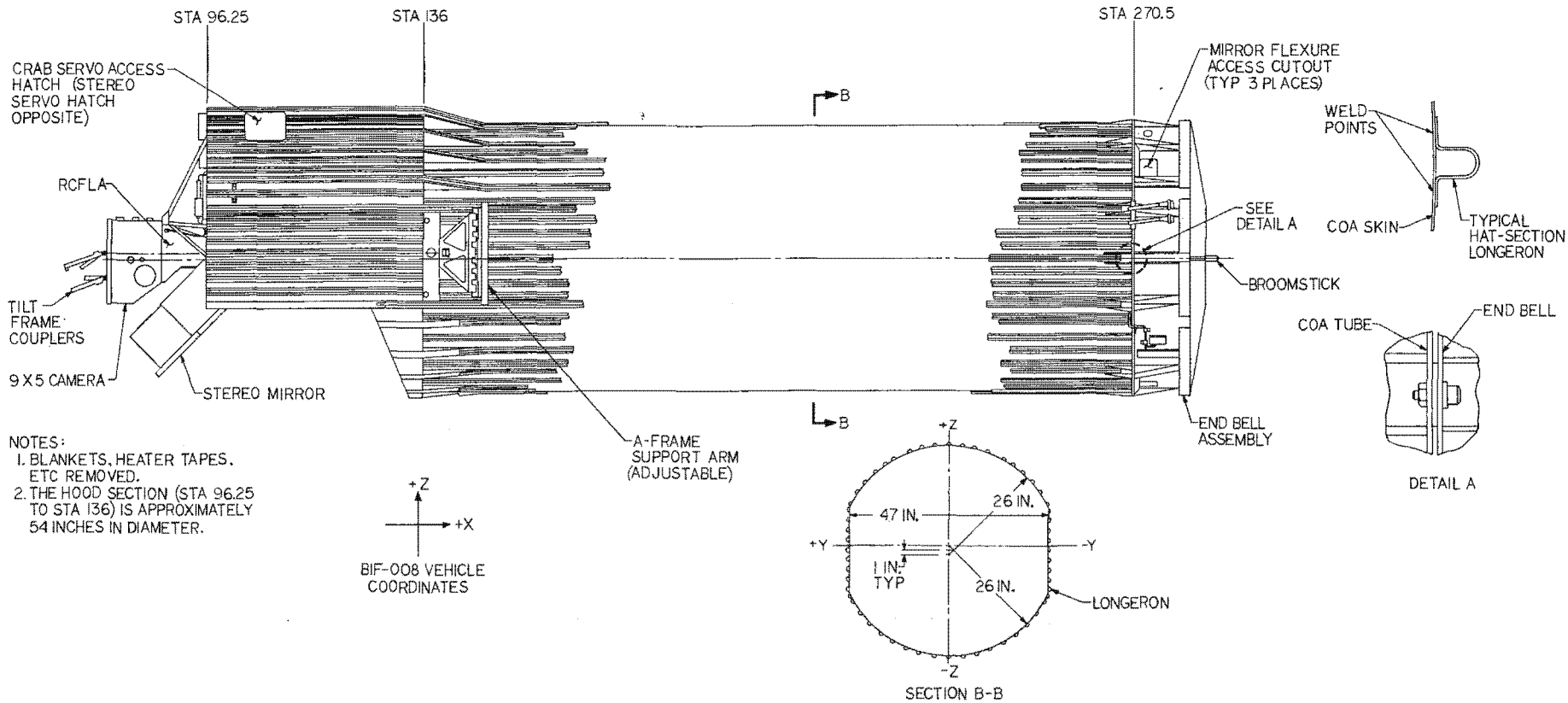


Figure 3.1-23. Camera Optics Assembly

3.1- 61/3.1-62

Handle via BYEMAN Control System Only

Approved for Release: 2017/02/14 C05097220

Approved for Release: 2017/02/14 C05097220

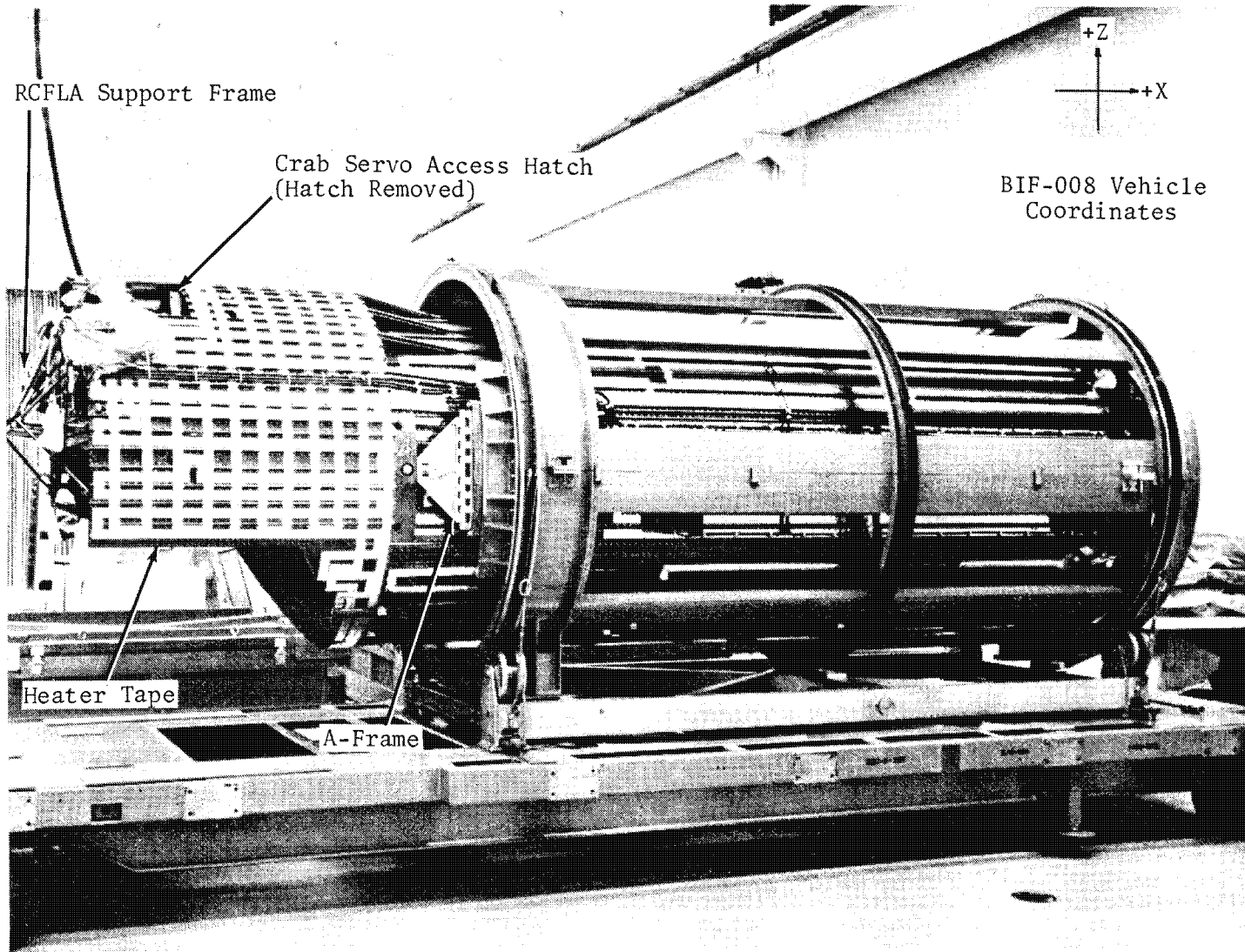


Figure 3.1-24. COA Structural Cylinder (-Y Side)

Handle via BYEMAN
Control System Only

3.1-63

Approved for Release: 2017/02/14 C05097220

Approved for Release: 2017/02/14 C05097220

~~TOP SECRET~~ GBIF-008- W-C-019839-RI-80

The purpose of this mounting design is to prevent generation of stresses on the internal structure which might result from distortion of the external structure caused by thermal gradients, free-beam bending on launch, or ground handling. Such loads will not transmit bending moments to the internal structure through these ball joints. Lateral displacement (in the plane of the film) between the camera and film supply, which results from distortion of the external structural shell, is minimized by the geometry of the A-frame links. Viewed from above (+Z) the vehicle, the links provide a virtual pivot on the X-axis, which is positioned well forward of the actual location of the links.

The A-frame on the -Y side is designed such that the distance between the ball joint and hinge line is adjustable (see Figure 3.1-25). This feature allows easy and rapid alignment of the internal and external structure axes in the X-Y plane. The broomstick-spherical bearing mount features an eccentric type of adjustment to align the vehicle axis and optical axis. The bearing support plate on the aft bulkhead is movable within a small circular area and is then permanently pinned in its final position.

1.4.2.2 COA Structure. The basic internal structure is a stepped cylindrical tube made from Invar sheet metal (reference Figure 3.1-24). The primary mirror mounting cell (the end bell) is bolted to the aft end of the tube at twelve points. The primary mirror is attached within the end bell in a strain-free (kinematic) configuration using axial and tangential flexures as shown in Figure 3.1-26.

The main cylindrical section is reinforced internally by sheet Invar rings to which are attached rubber light baffles (see Figure 3.1-27). The entire interior is painted flat black to further reduce reflections. The cylinder is reinforced externally by hat-section longerons distributed around the circumference.

Forward of the A-frame supports, the Invar cylinder is stepped to a larger diameter to provide clearance for the stereo mirror. This part of the

3.1-64
~~TOP SECRET~~ GHandle via **BYEMAN**
Control System Only

~~TOP SECRET~~ G

BIF-008- W-C-019839-RI-80

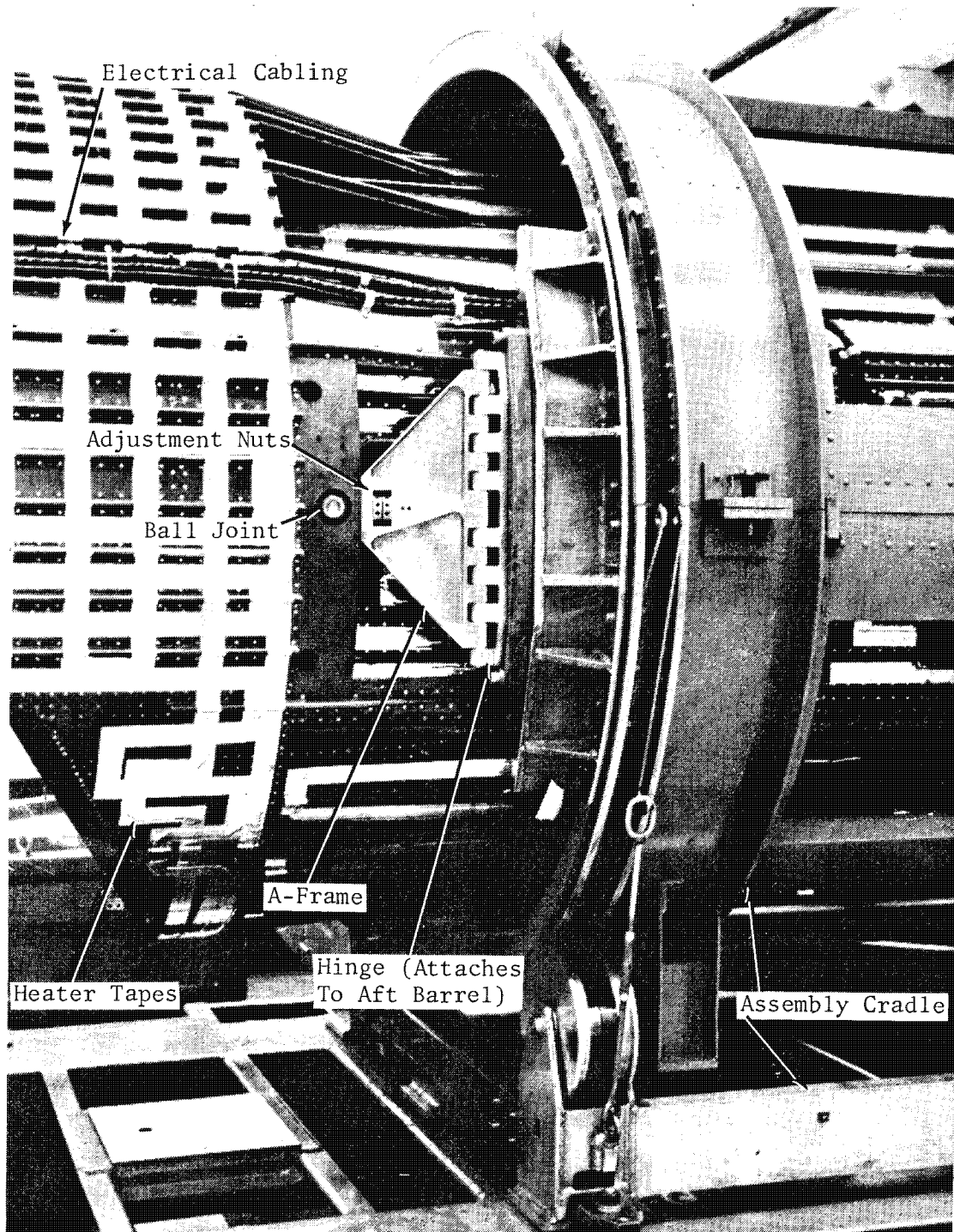


Figure 3.1-25. COA (-Y Side) Showing Adjustable A-Frame

3.1-65

~~TOP SECRET~~ G

Handle via BYEMAN
Control System Only

~~TOP SECRET~~ G

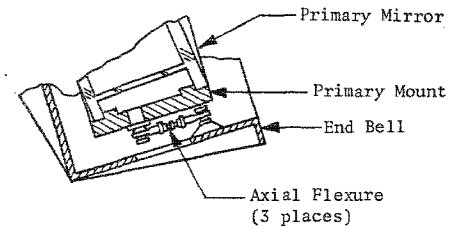
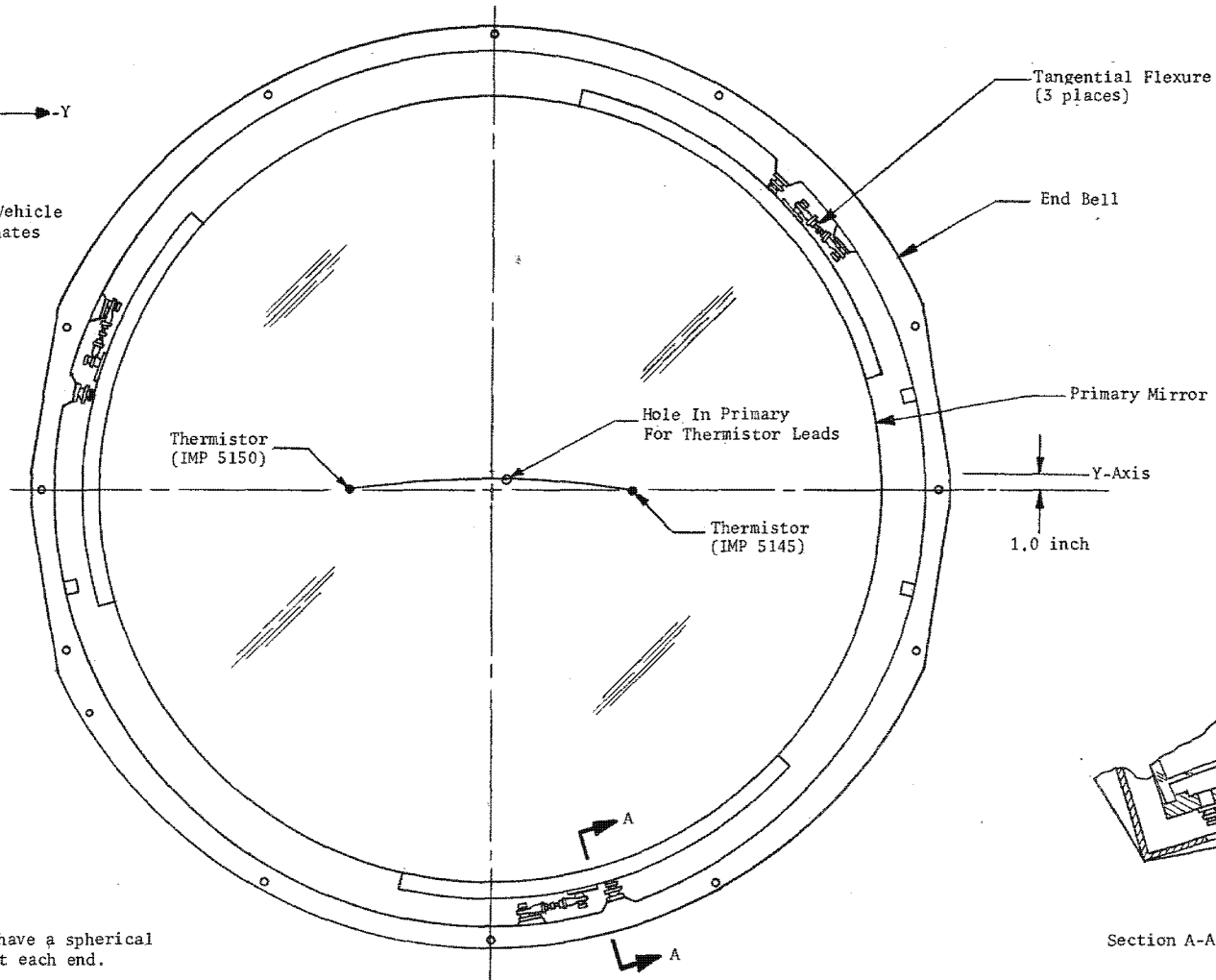
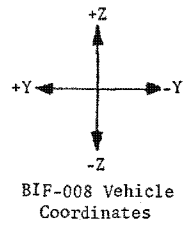
BIF-008-W-C-009888-RH-76

This page intentionally left blank.

3.1-66

~~TOP SECRET~~ G

Handle via **BYEMAN**
Control System Only



Section A-A

Note: Flexures have a spherical bearing at each end.

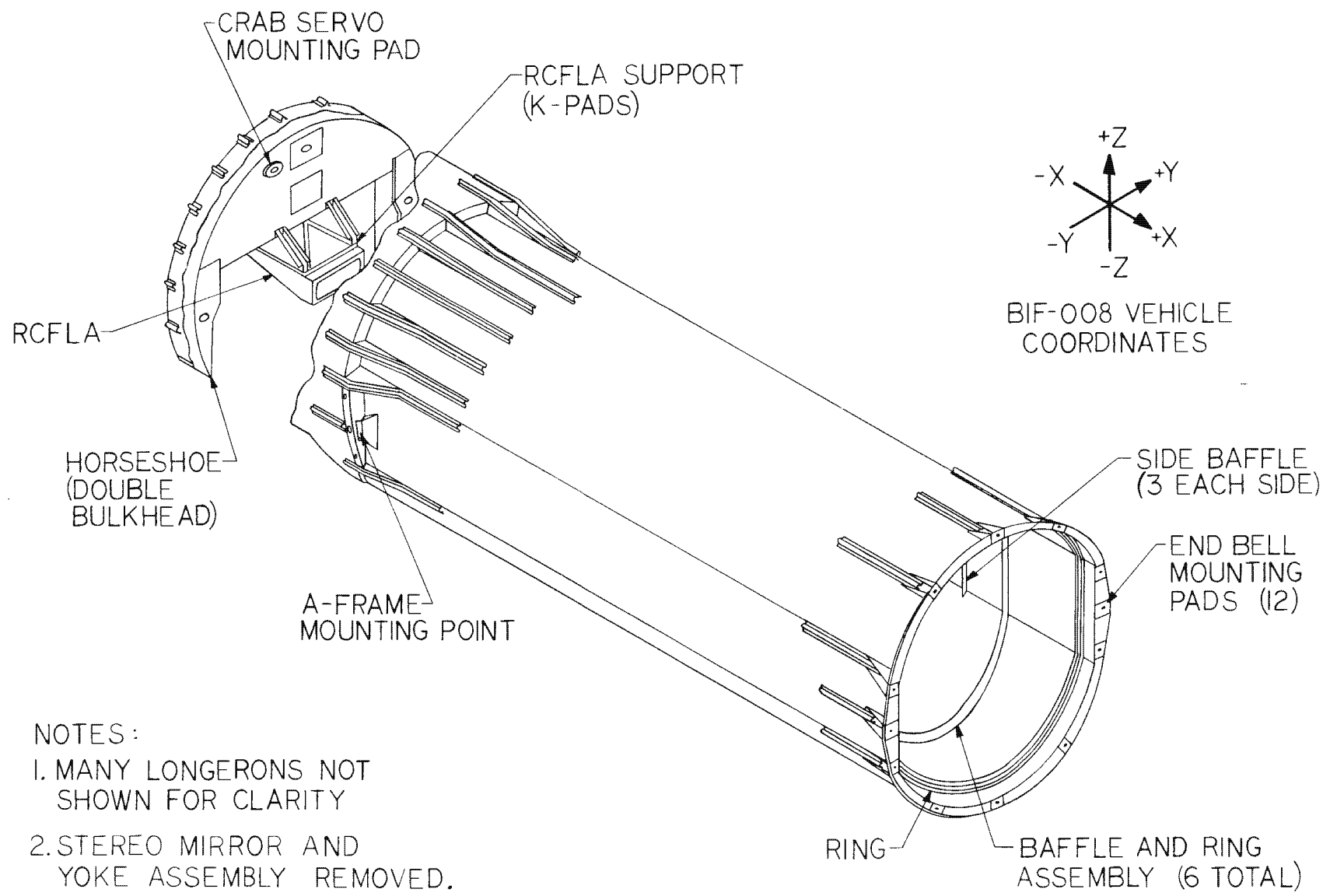
Figure 3.1-26. Primary Mirror Mount (-X View)

3.1-67/3.1-68

Handle via **BYEMAN**
Control System Only

Approved for Release: 2017/02/14 C05097220

Approved for Release: 2017/02/14 C05097220



3.1-69

- NOTES:
1. MANY LONGERONS NOT SHOWN FOR CLARITY
 2. STEREO MIRROR AND YOKE ASSEMBLY REMOVED.

Figure 3.1-27. COA Internal Structure

Handle via **BYEMAN**
Control System Only

Approved for Release: 2017/02/14 C05097220

Approved for Release: 2017/02/14 C05097220

~~TOP SECRET~~ GBIF-008. W-C-019839-RI-80

cylinder is also constructed from Invar sheet, reinforced internally by hat-section rings and externally by hat-section longerons. The forward end of the Invar cylinder terminates in a double bulkhead with internal stiffening webs. Most of the lower half of this forward cylinder and the double bulkhead are cut away to clear the stereo mirror and the optical field of view.

Auxiliary lightweight-alloy frame structures are attached to the structure to support cables, thermal blanketing, and heater tapes (see Part 3, Section 8). Additional components attached to the COA structure such as heater controllers, the S1-PRG encoders, etc., will be addressed in later sections of Part 3.

1.4.2.3 Stereo Mirror Support. The stereo mirror is suspended by two lateral trunnions in spherical bushings attached to the mirror mount. This prevents bending stresses from being introduced into the mirror through the suspension. As seen in Figure 3.1-28, the trunnions are pinned in pillow blocks on the stereo mirror yoke. The opposite end of each trunnion (in the spherical bushing) is teflon coated to reduce friction during mirror movement in the stereo direction. As an additional benefit, this coating provides some thermal isolation between the mirror and yoke.

The mirror support yoke is held in the Y-Z plane on the aft side of the COA double bulkhead, and constrained by rollers and a guide surface so that the yoke can move only in rotation about the crab axis (parallel to the vehicle X-axis). The crab servo, mounted on the aft face of the double bulkhead, is connected to the yoke by a lead-screw and ball nut. Travel of the nut along the screw causes the yoke and mirror to rotate about the crab axis for crab adjustment. In the event of overtravel, a mechanical stop is provided at the end of each yoke-bearing mount.

Rotation of the mirror in stereo is accomplished by a servo motor and hypocycloid mechanism attached to the mirror through a spherical bushing. This

3.1-70

~~TOP SECRET~~ GHandle via **BYEMAN**
Control System Only

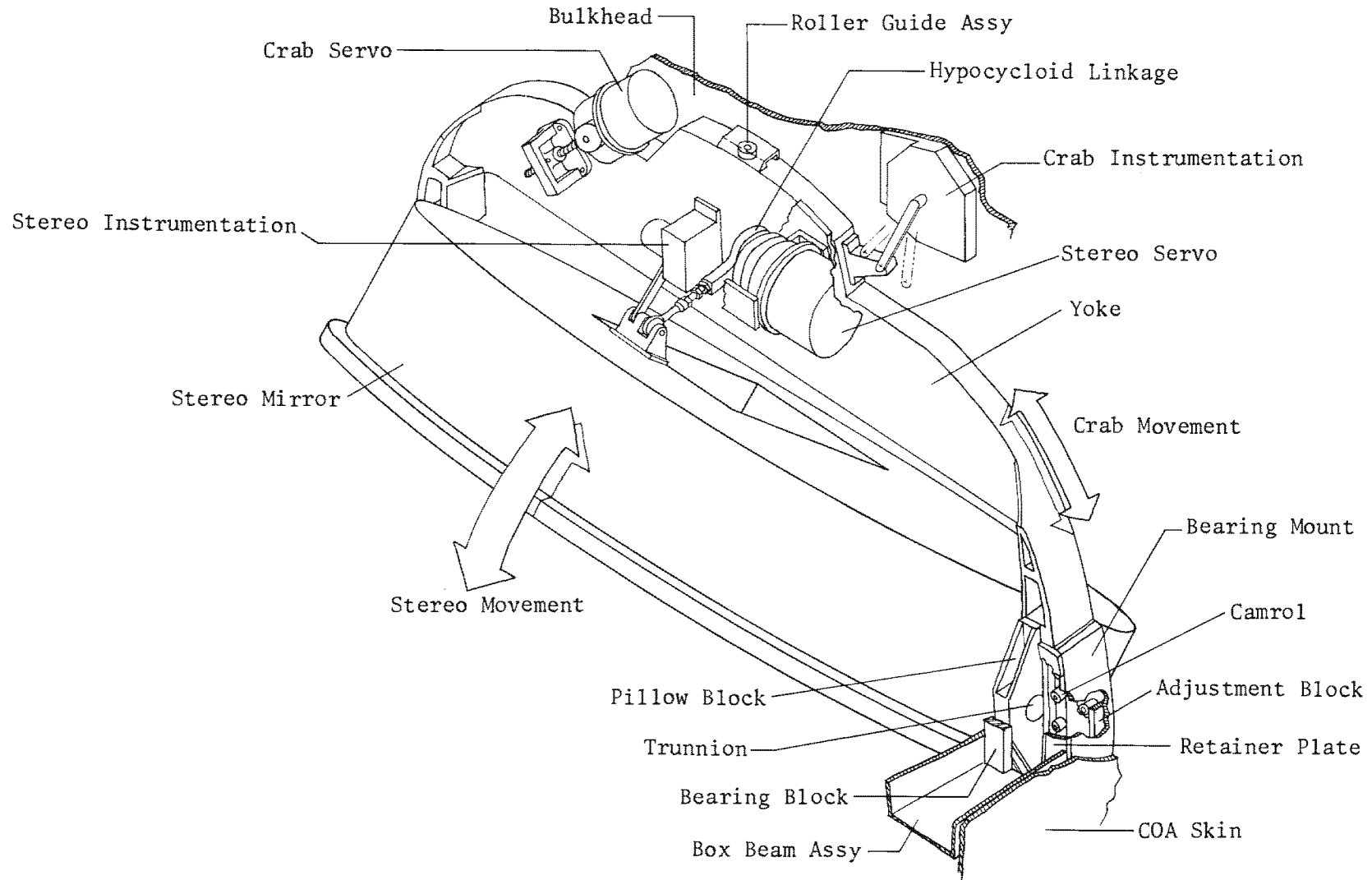


Figure 3.1-28. Stereo Mirror Yoke Assembly

Handle via **BYEMAN**
Control System Only

Approved for Release: 2017/02/14 C05097220

Approved for Release: 2017/02/14 C05097220

3.1-71

~~TOP SECRET~~ GBIF-008- W-C-019839-RI-80

bushing is the third strain-free attachment point to the mirror, with the result that the mirror is kinematically mounted within the internal structure. The hypocycloid drive provides shockless, precise positioning of the mirror at the forward, nadir, and aft stereo positions. The servo is mounted on, and moves in crab with, the yoke.

Removable panels on the upper portion of the COA structure allow access to the crab and stereo servos. Low emittance finishes on the servos reduce thermal effects from the motors.

1.4.2.3.1 Stereo Mirror Load Transfer. The pillow blocks, to which the trunnions are pinned, are attached to the stereo yoke and transfer the mirror load to the yoke during on-orbit operation. The yoke is supported on Camrol bearings running in bearing mounts as shown in Figure 3.1-28. During use, or during ground handling when the vehicle is in a horizontal position, the mirror load is transferred through the yoke to the bearing mounts, where it is carried through the COA skin and box beams to the A-frames. An additional alignment Camrol bearing is located in the +Z area of the yoke and rides on the upper roller and guide assembly that is attached to the aft side of the COA double bulkhead. There are also two Camrol bearings mounted near the center of the yoke which ride on the bearing track attached to the aft side of the double bulkhead.

During launch, or during ground handling when the vehicle is in a vertical position, the mirror X-axis load is transferred from the pillow blocks to two bearing-block assemblies. The bearing-block assemblies are pinned to the two built-up box beams which in turn are pinned to the COA structure. The various components involved are adjusted in assembly so that there is a nominal 0.010-inch clearance between the pillow blocks and bearing blocks with the vehicle horizontal. During ascent, the yoke and mirror loads cause enough structural sagging to eliminate the 0.010-inch clearance, transmitting these loads down the box beams into reinforced sections of the internal

3.1-72

~~TOP SECRET~~ GHandle via BYEMAN
Control System Only

~~TOP SECRET~~ GBIF-008- W-C-019839-RI-80

structure and then in turn to the A-frame mounts.

1.4.2.4 Camera and RCFLA Mounting. The 9x5 camera is three-point mounted on the forward end of an Invar box structure which forms the housing for the Ross corrector and field lens assembly (RCFLA). The RCFLA housing is attached to the internal structure by a supporting framework forward of the double bulkhead, and a double K-pad arrangement on the aft side of the bulkhead (see Figures 3.1-27 and 3.1-29). The five Ross corrector lenses are mounted inside the RCFLA housing with potting compound in order to insure strain-free support of the lenses. The compound is 0.040 inch thick along the $\pm Z$ sides of each lens, with the exception of the number 5 (forward) lens which is potted on all four sides to maintain the pressure seal in the film path.

1.4.3 PPS/DP EAC-SCS Interface

The PPS/DP EAC is attached to the SCS circumferentially by screws which fasten the aft barrel skin to the forward SCS ring. To insure proper orientation, a painted index stripe on both the PPS/DP EAC and SCS marks the screw-hole centered on the -Z axis. In addition, the spacing between the -Z screw-hole and the first screw-hole on the +Y side of the paint stripe is twice as great as the spacing between any other pair of adjacent holes.

Electrical cables provided with the SCS pass through the cable openings in the PPS/DP EAC aft bulkhead and into two electrical junction boxes just forward (-X) of the bulkhead. Panels 10 and 22 provide access to the boxes for connector mating.

Prior to mating (normally, during factory assembly for the PPS/DP EAC section) matched jig gauges are used by Lockheed and BIF-008 to align the reference

3.1-73

~~TOP SECRET~~ GHandle via BYEMAN
Control System Only

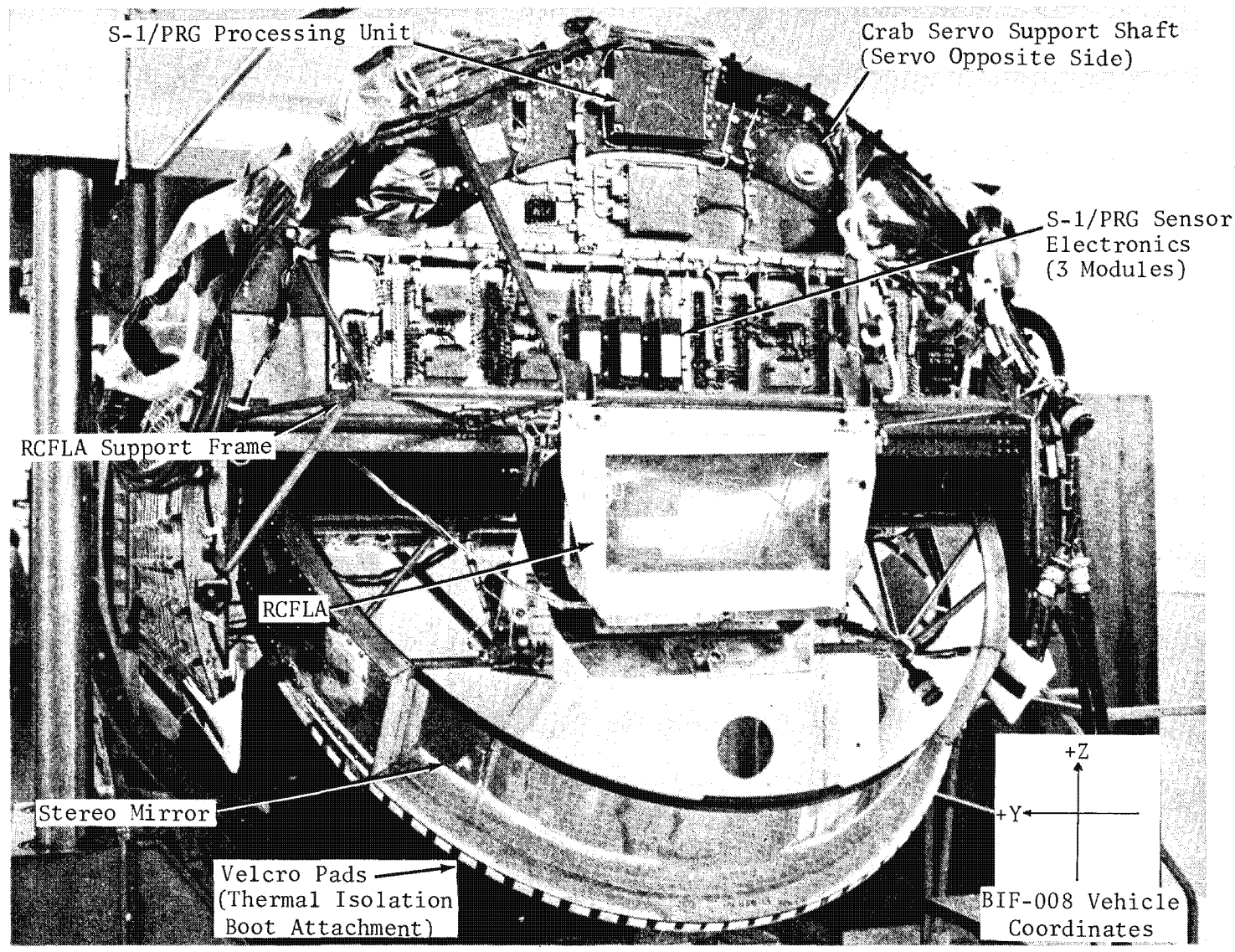


Figure 3.1-29. COA Double Bulkhead (-X View)

3.1-74

Approved for Release: 2017/02/14 C05097220

Approved for Release: 2017/02/14 C05097220

Handle via BYEMAN Control System Only

~~TOP SECRET~~ GBIF-008- W-C-019839-RI-80

optics shown in Figure 3.1-30 with the vehicle axes (refer to Part 4, Section 3 for a more detailed explanation of this procedure.)

Note: The PPS/SCS vehicle and optical axes are defined as follows at the 288 interface:

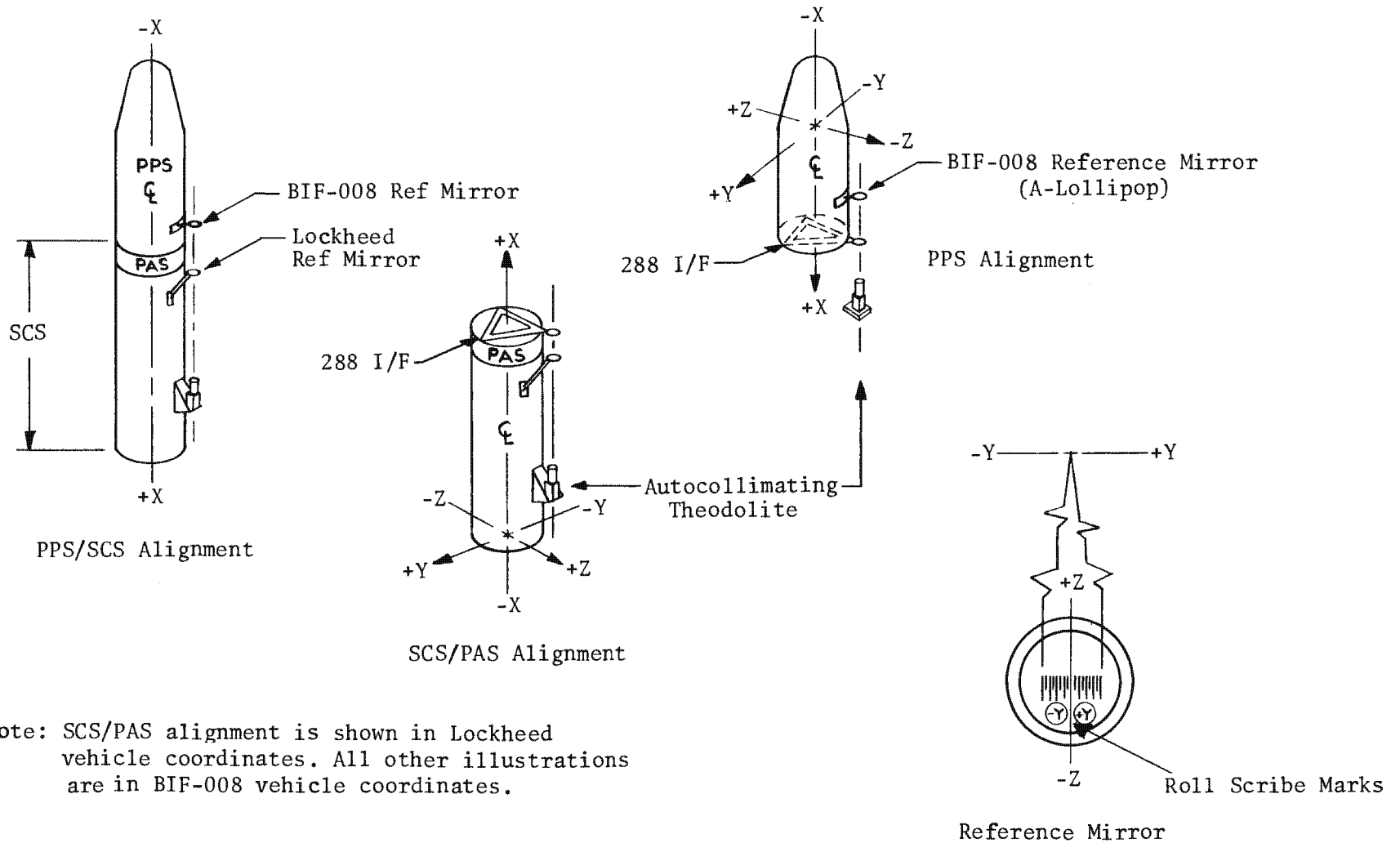
- (1) The mechanical Z-axis is represented by a line through the center of shear-joint holes number 1 and 95 (see Figure 3.1-22).
- (2) The mechanical Y-axis is represented by a line through the center of shear-joint hole number 48 and coplanar and perpendicular to the mechanical Z-axis.
- (3) The mechanical X-axis is represented by a line drawn from the intersection of the Y- and Z-axes and perpendicular to the plane formed by the Y- and Z-axes.
- (4) The optical axis is represented by a line passing perpendicular to the geometric center of the 9 exposure slit in-track and 4.426 ± 0.015 inches from the outside edge of the slit fiducial in cross-track.

Following mating, the alignment between the two sections is measured through the use of special jigs and optical support assemblies. Figure 3.1-30 illustrates this procedure. The PPS/DP EAC reference mirror assembly, known as the "A-lollipop," is attached to the COA through access hatch 21, and a similar reference assembly is mounted on the SCS guidance module. A theodolite is

3.1-75

~~TOP SECRET~~ GHandle via BYEMAN
Control System Only

3.1-76



Note: SCS/PAS alignment is shown in Lockheed vehicle coordinates. All other illustrations are in BIF-008 vehicle coordinates.

Figure 3.1-30. PPS/SCS Alignment Scheme

Handle via **BYEMAN**
Control System Only

Approved for Release: 2017/02/14 C05097220

Approved for Release: 2017/02/14 C05097220

~~TOP SECRET~~ GBIF-008- W-C-019839-RI-80

attached to the SCS and aligned to the SCS reference mirror, roll adjustment being determined by scribe lines on the reference mirror, and pitch and yaw adjustment by autocollimation of the source. The SCS mirror is then removed, and the theodolite is used to measure overall SCS/PPS roll, yaw, and pitch alignments with respect to the PPS/DP EAC A-lollipop, again using scribe lines in the roll direction and autocollimation for pitch and yaw alignment determination.

3.1-77

~~TOP SECRET~~ GHandle via BYEMAN
Control System Only

~~TOP SECRET~~ C

BIF-008- W-C-019839-RI-80

This page intentionally blank

3.1-78

~~TOP SECRET~~ G

Handle via **BYEMAN**
Control System Only